Improving the Theoretical Precision and Looking for New Physics in the Flavour Sector

---

Dissertation
zur
Erlangung der naturwissenschaftlichen Doktorwürde
(Dr. sc. nat.)
vorgelegt der
Mathematisch-naturwissenschaftlichen Fakultät
der
Universität Zürich
von
Sandro Mächler
aus
Altendorf SZ

Promotionskommission
Prof. Dr. Gino Isidori (Vorsitz und Leitung der Dissertation)
Prof. Dr. Paolo Gambino (Leitung der Dissertation)
Prof. Dr. Peter Stoffer
Prof. Dr. Nicola Serra

Zürich, 2023

Abstract

The decays of B mesons exhibit intriguing puzzles. There are departures of experimental measurements from standard model expectation, indicating the presence of new physics, but there is also a persistent discrepancy between the inclusive and exclusive determinations of V_{cb}, the so-called V_{cb} puzzle.

In the first part of this thesis we examine the V_{cb} puzzle. To this end we perform a study of a new method for computing inclusive observables in lattice QCD. Inclusive observables are computed on the lattice at an unphysically low b quark mass and subsequently compared to results of an OPE calculation. We find a generally good agreement between lattice and OPE results despite numerical challenges.

Staying on the topic of inclusive B decays we then study the impact of higher dimensional terms in the weak effective Hamiltonian on inclusive observables. These effects can in principle receive enhancements in the phase space integration and therefore naive estimates are not sufficient to predict their size. Therefore they are computed explicitly and their dependence on lower cuts in the phase space integration is studied.

For the second part of this thesis we shift our focus to the discrepancies between standard model predictions and measured values in branching ratios and angular variables in exclusive $B \to K^{(*)}\mu^+\mu^-$ decays. The SM predictions for these observables receive hadronic long-distance contributions which cannot be quantified within the realm of perturbation theory. We employ a dispersive formulation of intermediate $c\bar{c}$ resonances to determine C_9 from different regions of q^2 and decay channels. The results we find strongly indicate the presence of a missed short-distance contribution in the current standard model analysis of $b \to s\ell\ell$ decays.

To my grandfather. Danke, dass du mich immer dabei unterstützt hast, meinen Träumen zu folgen. Ein Teil von Kapitel 5 ist während der zwei Monate, die wir im Lockdown miteinander verbracht haben, entstanden. Diese Zeit werde ich immer in guter Erinnerung behalten.

To struggle and to understand.
Never this last without the other.
Such is the law.

GEORGE MALLORY

Acknowledgements

There are so many people who have have made the last four years the most fulfilling time of my life so far.

To begin with I want to thank my supervisors Gino and Paolo for your endless patience. Thank you for taking time to discuss physics or life in general with me any time I had a question. Any PhD student would be lucky to have supervisors like you teaching them.

Thank you to Bernat, Chris, Martin and Marzia for making my first year in Turin quite memorable, for countless aperitivos and your invaluable help with my projects.

I want to thank my office mates Darius, Jason and Zach for always keeping the mood light in the office and enduring my bad jokes, Arianna for finding all the bugs in my code for our common project, Marko for winning the poster award with me and everybody else in the Zurich group, Ben, Davide, Felix, Javi, Joe, Julie, Lukas, Noemi, Nudzeim for discussions and beers without number.

I also want to thank all of my climbing friends for keeping me sane and putting things into perspective during stressful times. Thank you to Nico and Marion for making sure I train my weaknesses, climbing high walls with me and showing me that my everyday problems seem rather small from up there. To Lucy, Jens, Nestor, Luca and many others from Minimum, BSide and beyond I want to say thank you for countless trips to Chironico, Fontainebleau, Cadarese, Yosesigo and Magic Wood which allowed me to come back to work with a fresh mind. I would like to thank Eva and Aaron not only for climbing sessions but also for letting me dog sit Kiro when I needed endorphins and to Kiro for being a good boy.

To my parents Catherine and Paul, to Beat, to my brother Claudio, and my grandfather René I want to say thank you for believing in me and supporting me at every step of the way. Without you I would not be where I am today. Thanks to Sally for being such a cute dog that I cannot be unhappy when you are around.

A very special thanks goes to Kathrin. There are so many things I want to thank you for. Thanks for training with me when I injured my knees and enduring by bad mood when I had to stop climbing for half a year. Thank you for being there for me during some of the more stressful phases of my life and for making me smile, no matter how downhearted I was. Thank you for making me a stronger climber and a better person.

Contents

Chapter 1

Introduction

1.1 The Scientific Method

A core principle of scientific theories is falsifiability. They have to admit the possibility of being proven wrong by empirical evidence. Thanks to this they can describe how nature works but not why it works in the way it does. In this sense scientific theories can answer questions starting in with "how", but not those starting with "why".

On the other hand it is utterly impossible to prove any theory right by observations or experiments. It is however possible to improve a theory by empirically testing it and updating it, if it does not survive a test. This is the scientific method.

Thus the basis of scientific progress is constantly scrutinizing the state-of-the-art theories and trying to prove them wrong. As soon as the currently accepted theory can be disproved by an experiment there is a clue potentially leading to a more general one.

How good a theory is can be assessed by the number of tests it survives. Additionally it should make predictions for measurable effects. The more new predictions a theory makes, which are subsequently confirmed experimentally, the better the theory.

By these measures the Standard Model of particle physics (SM) is the best theory ever found by humankind. Its predictions have been tested over an energy range of more than 10 orders of magnitude, most of which have been confirmed to an impressive accuracy. In fact the SM is too good! There is no single significant disagreement between an experimental measurement and the corresponding theory prediction.

This is not to say that there are no discrepancies at all. In decays of B mesons to lighter mesons and two leptons, so–called semileptonic decays, intriguing discrepancies between theory and experiment are observed. As some of the observables in question suffer from large uncertainties and each measurement on its own does not deviate significantly enough from the SM expectation to claim discovery, the path forward is not immediately clear.

In order to scrutinize these discrepancies and make the most of the available data a combined effort on both, the experimental and the theoretical side, is necessary.

To this end a theory program with the goal of

- building new models to explain the discrepancies
- performing independent checks of established computational frameworks
- improving the precision of theory predictions

is being carried out. Here we are concerned with the two latter points.

1.2 Structure of this Thesis

The present thesis is structured in three parts. The first part, consisting of chapters 2 and 3 the SM and concept of Effective Field Theories (EFT's) are introduced.

In the second part, consisting of chapters 4 to 6, we discuss inclusive semileptonic decays of B mesons. chapter 4 serves as a general introduction of the heavy quark expansion for inclusive B decays. After introducing the necessary methods we apply them in chapter 5 to test the heavy quark expansion against a new method for computing inclusive observables in lattice QCD. The second part ends with a study of contributions from higher dimensional operators in the weak effective Hamiltonian to inclusive observables. we derive the leading new physics contribution to the a new method of computing observables in inclusive decays of B mesons is studied and new corrections to them are computed. The following chapter treats exclusive decays of B mesons, scrutinizing the tension between theory prediction and measurement of the differential decay rate in $b \to sll$ processes.

For the third and last part of this thesis, consisting of chapter 7, we turn to the study of exclusive decays of B mesons, where the complete final state is resolved. Unfortunately this additional information comes at a price. Contrary to inclusive observables in $b \to c$ decays, the observables in exclusive $b \to s\ell\ell$ decays suffer from uncertainties originating in our knowledge of form factors and charm-loops. After introducing the problem of these charm-loops we employ a dispersive treatment of intermediate charm resonances to determine the Wilson coefficient C_9 from experimental data in different kinematical regions and from different decay channels.

1.3 Conventions and Abbreviations

Throughout this thesis we will use the following conventions for the Levi-Civita tensor and the Minkowski metric:

- $\epsilon^{0123} = +1$
- $g_{\mu\nu} = \text{diag}\,(1, -1, -1, -1)$

Here we list the abbreviations used in the present thesis in the order of appearance:

- SM: Standard Model of Particle Physics
- EFT: Effective Field Theory
- VEV: Vacuum expectation value
- PT: Perturbation theory
- NLO: Next-To-Leading Order
- OPE: Operator Product Expansion
- HQE: Heavy Quark Expansion
- WC: Wilson Coefficient
- LQCD: Lattice QCD
- FCNC: Flavour Changing Neutral Current

Chapter 2

The Standard Model of Particle Physics

This chapter serves as an introduction of the Standard Model of Particle Physics (SM) [150, 213,220]. As there are many excellent textbook introductions to the SM, for example [209–211], it is by no means meant to be a complete account of this remarkable theory. Instead it serves to introduce the concepts on which the work in chapters 4 and 7 is based.

2.1 Gauge Invariance

The SM is a gauge theory based on the symmetry group

$$\mathcal{G}_{\mathrm{SM}} = \mathrm{SU}(3)_c \times \mathrm{SU}(2)_L \times \mathrm{U}(1)_Y.$$

Its minimal version without right-handed neutrinos and thus without neutrino masses contains 15 fermion fields describing the contents of matter. In table 2.1.1 they are listed together with their transformation properties under the SM gauge group $\mathcal{G}_{\mathrm{SM}}$. In the following we build

Fermion field	$\mathrm{SU}(3)_C$ rep.	$\mathrm{SU}(2)_L$ rep.	$\mathrm{U}(1)_Y$ charge
L_L^f	1	2	$-\frac{1}{2}$
E_R^f	1	1	-1
Q_L^f	3	2	$\frac{1}{6}$
U_R^f	3	1	$\frac{2}{3}$
D_R^f	3	1	$-\frac{1}{3}$

Table 2.1.1: Fermion of content of the Standard Model. The index $f \in \{1, 2, 3\}$ specifies the fermion generation.

the most general renormalizable Lagrangian which is invariant under local transformations of the group $\mathcal{G}_{\mathrm{SM}}$ with the given fermion content, beginning with the kinetic energy terms of the fermion fields.

For a fermion field ψ and defining $\overline{\psi} = \psi^\dagger \gamma^0$ and $\not{\partial} = \gamma^\mu \partial_\mu$, terms of the form $\overline{\psi} \not{\partial} \psi$ are invariant under global transformations the SM group $\mathcal{G}_{\mathrm{SM}}$ but not under local transformations. In order to restore their invariance under local transformations the derivative operator has to be adjusted.

Let us look at the QCD subgroup $\mathrm{SU}(3)_c$ as an example. A global $\mathrm{SU}(3)_c$ transformation of a quark field ψ takes the form

$$\begin{aligned}\psi_i(x) &\to \psi^{'}(x) = e^{i\theta^a T^a_{ij}}\psi_j(x)\\ \overline{\psi}_i(x) &\to \overline{\psi^{'}_i(x)} = \left(e^{i\theta^a T^a_{ji}}\psi_j(x)\right)^\dagger \gamma^0 = \overline{\psi_j(x)}e^{-i\theta^a T^a_{ji}},\end{aligned} \tag{2.1.1}$$

where T^a are the eight generators of SU(3) and the term global refers to the fact that the parameters θ^a are independent of the spacetime coordinate x. If the symmetry is gauged, that is to say it is promoted to a local symmetry, this restriction is not valid anymore. A local $\mathrm{SU}(3)_c$ gauge transformation acts on a fermion field as

$$\psi_i(x) \to \psi^{'}(x) = e^{i\theta^a(x) T^a_{ij}}\psi_j(x). \tag{2.1.2}$$

Due to the explicit dependence of the parameters θ^a on x the term $\overline{\psi}\partial\!\!\!/\psi$ is not invariant under local $\mathrm{SU}(3)_c$ gauge transformations. Explicitly it term transforms as

$$\overline{\psi}(x)\partial\!\!\!/\psi(x) \to \overline{\psi}(x)\partial\!\!\!/\psi(x) + \overline{\psi}(x)e^{-i\theta^a(x)T^a_{ij}}\left(\partial\!\!\!/ e^{i\theta^a(x)T^a_{ij}}\right)\psi(x). \tag{2.1.3}$$

The invariance under gauge transformations can be recovered however by introducing the gauge boson fields G^a_μ. They are added to the derivative, forming the covariant derivative

$$D_\mu = \partial_\mu \mathbb{1} - ig_s G_\mu. \tag{2.1.4}$$

Now the invariance of terms of the form $\overline{\psi}D\!\!\!/\psi$ can be imposed by demanding that the gauge fields transform as

$$G_\mu \to e^{i\theta^a(x)T^a}G_\mu e^{-i\theta^a(x)T^a} + \frac{i}{g_s}e^{i\theta^a(x)T^a}\left(\partial_\mu e^{-i\theta^a(x)T^a}\right) \tag{2.1.5}$$

such that

$$\begin{aligned}D_\mu \to D^{'}_\mu &= \partial_\mu - ig_s G^{'}_\mu\\ &= \partial_\mu + e^{i\theta^a(x)T^a}\left(\partial_\mu e^{-i\theta^a(x)T^a}\right) - ig_s e^{i\theta^a(x)T^a}G_\mu e^{-i\theta^a(x)T^a}\\ &= e^{i\theta^a(x)T^a}\left(\partial_\mu - ig_s G_\mu\right)e^{-i\theta^a(x)T^a}\\ &= e^{i\theta^a(x)T^a}D_\mu e^{-i\theta^a(x)T^a}.\end{aligned} \tag{2.1.6}$$

The covariant derivative has the correct transformation behavior to render the term $\overline{\psi}D\!\!\!/\psi$ invariant under local $\mathrm{SU}(3)_c$ transformations:

$$\begin{aligned}\overline{\psi}_k(x)D\!\!\!/_{kl}\psi_l(x) \to &\overline{\psi}_n(x)e^{-i\theta^a(x)T^a_{nk}}e^{i\theta^a(x)T^a_{kr}}D\!\!\!/_{rs}e^{-i\theta^a(x)T^a_{sl}}e^{i\theta^a(x)T^a_{lm}}\psi_m(x)\\ &= \overline{\psi}_k(x)D\!\!\!/_{kl}\psi_l(x).\end{aligned} \tag{2.1.7}$$

This yields the massless QCD Lagrangian

$$\mathcal{L}_{\text{QCD, massless}} = \sum_{f=1}^{3}\sum_{\psi^f\in\{Q^f_L,U^f_R,D^f_R\}}\overline{\psi}^f_k\left(i\gamma^\mu\left(\partial_\mu\delta_{kl} - ig_s G^a_\mu T^a_{kl}\right)\right)\psi^f_l. \tag{2.1.8}$$

Here the QCD gauge field $G_\mu = G^a_\mu T^a$ is expanded in terms of the SU(3) generators. A mass term of the form $m\overline{\psi}\psi$ would be compatible with the $\mathrm{SU}(3)_c$ symmetry but break the $\mathrm{SU}(2)_L$ symmetry describing weak interactions so it is omitted here.

As can be seen in eq. (2.1.6) the covariant derivative itself is not gauge invariant. But a gauge invariant object can be built out of the gauge field strength

$$G_{\mu\nu} = \frac{i}{g}\left[D_\mu, D_\nu\right] = \partial_\mu G_\nu - \partial_\nu G_\mu - ig\left[G_\mu, G_\nu\right]. \tag{2.1.9}$$

On the r.h.s. we can see that the gauge field strength can be expanded in terms of generators of the gauge group, just like the gauge fields themselves, $G_{\mu\nu} = G^a_{\mu\nu}T^a$. The trace $\mathrm{Tr}\left(G^a_{\mu\nu}G^{\mu\nu}_a\right)$ then is gauge invariant and the kinetic energy of the gauge fields in the Lagrangian can be written as $-1/4\mathrm{Tr}\left(G^a_{\mu\nu}G^{\mu\nu}_a\right)$.

For the electroweak subgroup $\mathrm{SU}(2)_L \times \mathrm{U}(1)$ analogous arguments lead to the covariant derivative

$$D^{\mathrm{EW}}_\mu = \partial_\mu - ig'YB_\mu - ig\sum_{b=1}^{3} W^b_\mu \tau^b, \tag{2.1.10}$$

where B_μ and W_μ gauge field are the $\mathrm{U}(1)_Y$ and $\mathrm{SU}(2)_L$ gauge boson fields, respectively and τ^b denote the generators of SU(2). As in the QCD case one can write gauge invariant kinetic energy terms for the gauge bosons as $-1/4\mathrm{Tr}\left(W^a_{\mu\nu}W^{\mu\nu}_a\right) - 1/4\mathrm{Tr}\left(B_{\mu\nu}B^{\mu\nu}\right)$ with the index a running from 1 to 3.

The interactions between gauge bosons and fermions are completely determined by the Lagrangian

$$\begin{aligned}\mathcal{L}_{\mathrm{matter}} + \mathcal{L}_{\mathrm{gauge}} = &\sum_{f=1}^{3} \sum_{\psi^f \in \{L^f_L, E^f_R, Q^f_L, U^f_R, D^f_R\}} \overline{\psi}^f i \not{D}_\psi \psi^f \\ &-\frac{1}{4}\left(\sum_{a=1}^{8} G^{\mu\nu}_a G^a_{\mu\nu} + \sum_{b=1}^{3} W^{\mu\nu}_b W^b_{\mu\nu} + B^{\mu\nu}B_{\mu\nu}\right).\end{aligned} \tag{2.1.11}$$

Here the covariant derivative carries an index ψ indicating that different fermion fields are acted upon by different covariant derivatives depending on their quantum numbers, explicitly it reads

$$\begin{aligned}
D^\mu_{L_L} &= \partial_\mu + ig'\frac{1}{2}B_\mu - ig\sum_{b=1}^{3} W^b_\mu \tau^b \\
D^\mu_{E_R} &= \partial_\mu + ig'YB_\mu \\
D^\mu_{Q_L} &= \partial_\mu - ig'\frac{1}{6}B_\mu - ig\sum_{b=1}^{3} W^b_\mu \tau^b - ig_s\sum_{a=1}^{8} G^a_\mu T^a \\
D^\mu_{U_R} &= \partial_\mu - ig'\frac{2}{3}B_\mu - ig_s\sum_{a=1}^{8} G^a_\mu T^a \\
D^\mu_{D_R} &= \partial_\mu + ig'\frac{1}{3}B_\mu - ig_s\sum_{a=1}^{8} G^a_\mu T^a.
\end{aligned} \tag{2.1.12}$$

2.2 Spontaneous Symmetry Breaking

So far all particles in the theory, fermions and gauge bosons, are massless. The problem with particle masses is that mass terms couple left - and right-handed fields. This can be seen by

decomposing a fermion field into left- and right-handed components, $\psi = \psi_L + \psi_R = P_L\psi + P_R\psi$, where $P_{L,R}$ are the left- and right handed projectors. They are given by $(1 \mp \gamma^5)/2$ and have the properties $P_{L,R}^2 = \mathrm{Id}$ and $P_{L,R}P_{R,L} = 0$. Then $\overline{\psi_{L,R}} = \psi^\dagger\gamma^0 P_{R,L} = \overline{\psi}P_{R,L}$ and

$$m\overline{\psi}\psi = m\left(\overline{\psi_L} + \overline{\psi_R}\right)(\psi_L + \psi_R) = m\left(\overline{\psi}P_L\psi + \overline{\psi}P_L\psi\right) = m\left(\overline{\psi_R}\psi_L + \overline{\psi_L}\psi_R\right). \tag{2.2.1}$$

A term of this form cannot be invariant under $\mathrm{SU}(2)_L$ because left-handed fields transform under this group while the right-handed ones do not. Therefore in order to account for fermion masses the weak symmetry has to be broken. Explicitly breaking the symmetry would mean giving up on the idea of starting with a gauge symmetry and writing down a Lagrangian density containing all terms which are invariant under the given symmetry group.

Instead the $\mathrm{SU}(2)_L \times \mathrm{U}(1)_Y$ symmetry is broken spontaneously by the vacuum expectation value (VEV) of the scalar Higgs field ϕ. This field is an $\mathrm{SU}(2)_L$ doublet with an assigned hypercharge of $1/2$, so it transforms as

$$\phi \to \phi' = e^{i\theta^b(x)\tau^b}e^{i\frac{\theta(x)}{2}}\phi. \tag{2.2.2}$$

With the covariant derivative $D_\phi^\mu = \partial^\mu - ig'\frac{1}{2}B^\mu - ig\frac{1}{2}\sum_{b=1}^3 W^{\mu,b}\tau^b$ one can write the invariant kinetic energy term $(D_\mu\phi)^\dagger D\mu\phi = |D_\mu\phi|^2$ for the Higgs field. Additional invariant terms can be built out of the product $\phi^\dagger\phi$. At mass dimension four there are two possibilities, $\mu^2(\phi^\dagger\phi)$ and $\lambda(\phi^\dagger\phi)^2$, with a dimension-1 constant μ and a dimensionless constant λ. Both terms can be combined in a Higgs potential

$$V(\phi) = -\mu^2\left(\phi^\dagger\phi\right) - \lambda\left(\phi^\dagger\phi\right)^2. \tag{2.2.3}$$

Writing the Higgs field as

$$\phi(x) = \begin{pmatrix} \frac{1}{\sqrt{2}}\left(\phi_1(x) + i\phi_2(x)\right) \\ \frac{1}{\sqrt{2}}\left(\phi_3(x) + i\phi_4(x)\right) \end{pmatrix} = \begin{pmatrix} \phi^+(x) \\ \phi^0(x) \end{pmatrix}, \tag{2.2.4}$$

where ϕ^+ and ϕ^0 are complex scalar fields. The VEV is found by minimizing the potential in the scenario $\mu^2 < 0$ and $\lambda > 0$, yielding the condition

$$\phi^\dagger\phi = \frac{1}{2}\left(\phi_1^2 + \phi_2^2 + \phi_3^2 + \phi_4^2\right) = -\frac{\mu^2}{2\lambda}. \tag{2.2.5}$$

The vacuum can be fixed to any configuration satisfying this relation. For the choice $\phi_1 = \phi_2 = \phi_4 = 0$ and $\phi_3 = v$, with $v = \sqrt{-\mu^2/(2\lambda)}$, is given by

$$\langle\phi\rangle = \frac{1}{\sqrt{2}}\begin{pmatrix} 0 \\ v \end{pmatrix}. \tag{2.2.6}$$

The action of the generators of $\mathrm{SU}(2)_L \times \mathrm{U}(1)$ on the VEV is given by

$$\begin{aligned}
\tau_1\langle\phi\rangle &= \frac{1}{2\sqrt{2}}\begin{pmatrix} 0 & 1 \\ 1 & 0 \end{pmatrix}\begin{pmatrix} 0 \\ v \end{pmatrix} = \frac{1}{2\sqrt{2}}\begin{pmatrix} v \\ 0 \end{pmatrix} \\
\tau_2\langle\phi\rangle &= \frac{1}{2\sqrt{2}}\begin{pmatrix} 0 & -i \\ i & 0 \end{pmatrix}\begin{pmatrix} 0 \\ v \end{pmatrix} = \frac{1}{2\sqrt{2}}\begin{pmatrix} -iv \\ 0 \end{pmatrix} \\
\tau_3\langle\phi\rangle &= \frac{1}{2\sqrt{2}}\begin{pmatrix} 1 & 0 \\ 0 & -1 \end{pmatrix}\begin{pmatrix} 0 \\ v \end{pmatrix} = -\frac{1}{2}\langle\phi\rangle \\
Y\langle\phi\rangle &= \frac{1}{2}\langle\phi\rangle.
\end{aligned} \tag{2.2.7}$$

As can be seen here, under general $\mathrm{SU}(2)_L \times U(1)_Y$ transformations as given in eq. (2.2.2) the Higgs VEV transforms non-trivially, that is to say it spontaneously breaks the symmetry! The only exception are transformations with $\theta^1(x) \equiv \theta^2(x) \equiv 0$ and $\theta^3(x) = \theta(x)$. Transformation of this form,

$$\langle\phi\rangle \to \left\langle\phi^{'}\right\rangle = e^{i\theta(x)\left(\tau^3+Y\right)}\langle\phi\rangle \tag{2.2.8}$$

make up a U(1) subgroup of $\mathrm{SU}(2)_L \times \mathrm{U}_Y$ identified with the QED group describing electrodynamics. Consequently the combination

$$Q = \tau^3 + Y. \tag{2.2.9}$$

is identified with the electric charge operator.

Mass terms for the gauge bosons are now found by expanding the Higgs field around its VEV as $\phi(x) = \langle\phi\rangle + h(x)$ and plugging it into the Lagrangian. The action of the covariant derivative on the Higgs VEV turns out to be

$$D_\mu\langle\phi\rangle = \frac{-iv}{2\sqrt{2}}\begin{pmatrix} g\left(W_\mu^1 - iW_\mu^2\right) \\ g^{'}B_\mu - gW_\mu^3 \end{pmatrix}. \tag{2.2.10}$$

Thus the kinetic term of the Higgs field evaluated at its VEV is

$$\begin{aligned} \left|D_\mu\langle\phi\rangle\right|^2 &= \frac{v^2}{8}\left(\left(W_\mu^1\right)^2 + \left(W_\mu^2\right)^2 + \left(g^{'}B_\mu - gW_\mu^3\right)^2\right) \\ &= \frac{v^2}{8}\begin{pmatrix} W^{1,\mu} & W^{2,\mu} & W^{3,\mu} & B_\mu \end{pmatrix}\begin{pmatrix} g^2 & 0 & 0 & 0 \\ 0 & g^2 & 0 & 0 \\ 0 & 0 & g^2 & -gg^{'} \\ 0 & 0 & -gg^{'} & g^{'2} \end{pmatrix}\begin{pmatrix} W^{1,\mu} \\ W^{2,\mu} \\ W^{3,\mu} \\ B_\mu \end{pmatrix}. \end{aligned} \tag{2.2.11}$$

This mass matrix is diagonal in the basis $\left(W_\mu^1, W_\mu^2, g^{'}B_\mu - gW_\mu^3, g^{'}B_\mu + gW_\mu^3\right)$ with the corresponding eigenvalues $g^2, g^2, g^2 + g^{'2}, 0$. So there is one massless gauge boson and three massive ones. Not all of these are eigenstates of the electric charge operator however. In order to see this the transformation rule for the gauge bosons under gauge transformations is needed. From eq. (2.1.5) it follows that for an infinitesimal transformation

$$\begin{aligned} W_\mu(x) = W_\mu^b(x)\tau^b \to& \frac{i}{g}\partial_\mu\theta^b(x)\tau^b - \left[W_\mu^a(x)\tau^a, i\theta^c(x)\tau^c\right] \\ =& \frac{i}{g}\partial_\mu\theta^b(x)\tau^b - iW_\mu^a(x)\theta^c(x)\left[\tau^a, \tau^c\right] \\ =& \left(\frac{i}{g}\partial_\mu\theta^b(x) - f^{bac}\theta^a(x)W_\mu^c(x)\right)\tau^b, \end{aligned} \tag{2.2.12}$$

where f^{bac} are the structure functions of SU(2), defined as $\left[\tau^a, \tau^b\right] = if^{abc}\tau^c$. So the gauge fields transform as

$$W_\mu^a(x) \to \frac{i}{g}\partial_\mu\theta^a(x) - f^{abc}\theta^b(x)W_\mu^c(x). \tag{2.2.13}$$

Therefore under global transformations the gauge bosons transform in the adjoint transformation of the $\mathrm{SU}(2)_L$. Note that they do not transform under global $\mathrm{U}(1)_Y$ transformations because $U(1)$ is abelian, i.e. all of its structure functions vanish. Noting that the structure functions of SU(2) are given by $f^{abc} = i\epsilon^{abc}$, where ϵ^{abc} is the totally antisymmetric tensor,

as can be verified by explicit computation and that the generators in the adjoint representation are given by $\left(\tilde{\tau}^b\right)_{ac} = -if^{abc}$, the electric charge operator in the adjoint representation of $\mathrm{SU}(2)_L \times \mathrm{U}(1)_Y$ can be written as

$$Q = \tau^3 + Y = \begin{pmatrix} 0 & i & 0 & 0 \\ -i & 0 & 0 & 0 \\ 0 & 0 & 0 & 0 \\ 0 & 0 & 0 & 0 \end{pmatrix}. \tag{2.2.14}$$

Consequently it is diagonalised by the orthonormal basis

$$\left(\frac{W_\mu^1 + iW_\mu^2}{\sqrt{2}}, \frac{W_\mu^1 - iW_\mu^2}{\sqrt{2}}, \frac{g^{'} B_\mu - gW_\mu^3}{\sqrt{g^{'2} + g^2}}, \frac{g^{'} B_\mu + gW_\mu^3}{\sqrt{g^2 + g^{'2}}} \right) \tag{2.2.15}$$

with respective eigenvalues -1, $+1$, 0 and 0. These are the physical electroweak gauge bosons. Conventionally they are named according to their electric charges. Here we have the charged W bosons

$$W_\mu^{\mp} = \frac{W_\mu^1 \pm iW_\mu^2}{\sqrt{2}}, \tag{2.2.16}$$

the neutral but massive Z boson

$$Z_\mu = \frac{g^{'} B_\mu - gW_\mu^3}{\sqrt{g^{'2} + g^2}} \tag{2.2.17}$$

and the massless and electrically neutral photon

$$A_\mu = \frac{gB_\mu + g^{'} W_\mu^3}{\sqrt{g^{'2} + g^2}}. \tag{2.2.18}$$

In terms of mass and electric charge eigenstates and with the definition $\tau^{\pm} = \tau^1 \mp i\tau^2$ the electroweak covariant derivative from eq. (2.1.10) then reads

$$D_\mu^{\mathrm{EW}} = \partial_\mu - \frac{ig}{\sqrt{2}} \left(W_\mu^- \tau^- + W_\mu^+ \tau^+ \right) - \frac{i}{\sqrt{g^2 + g^{'2}}} Z_\mu \left(g^2 \tau^3 - g^{'2} Y \right) - \frac{igg^{'}}{\sqrt{g^2 + g^{'2}}} A_\mu \left(\tau^3 + Y \right). \tag{2.2.19}$$

From the explicit form of the SU(2) generators in eq. (2.2.7) it is now obvious that the Z boson and photon do not mix upper and lower members of an $\mathrm{SU}(2)_L$ doublet. Upper and lower doublet members are only mixed in interactions with the charged $W^{\mp}$ bosons. As an example the interactions of left-handed quarks and the negative W boson are explicitly given by

$$\begin{aligned} \frac{g}{\sqrt{2}} \overline{Q}_L^f W_\mu^- \tau^- \gamma^\mu Q_L^f &= \frac{g}{\sqrt{2}} W_\mu^- \gamma^\mu \begin{pmatrix} \overline{u}_L^f & \overline{d}_L^f \end{pmatrix} \begin{pmatrix} 0 & 1 \\ 0 & 0 \end{pmatrix} \begin{pmatrix} u_L^f \\ d_L^f \end{pmatrix} \\ &= \frac{g}{\sqrt{2}} W_\mu^- \overline{u}_L^f \gamma^\mu d_L^f. \end{aligned} \tag{2.2.20}$$

The interactions involving leptons and the ones involving the positively charged W boson follow analogously. Note that at this point all interactions are flavour diagonal! So far decays are impossible because the fermions have to be massless. This is going to change in the following section.

2.3 Fermion Masses and Mixing

There is one more kind of term which is invariant under the SM symmetry. From two fermion fields and the Higgs field we can build terms of the form $\overline{\psi}_L \phi \psi_R$. As $\overline{\psi}_L U^\dagger U \phi \psi_R = \overline{\psi}_L U^\dagger U \phi \psi_R$ for any U in $\mathrm{SU}(2)_L$ these terms are clearly SU(2) invariant. To make sure that they are invariant under $\mathrm{U}(1)_Y$ the hypercharges of the involved fields have to add to 0. Looking at table 2.1.1 there are three combinations which achieve this, yielding the Yukawa Lagrangian

$$\mathcal{L}_{\text{Yukawa}} = -\sum_{i,j=1}^{3} Y_d^{ij} \overline{Q}_L^i D_R^j \phi - \sum_{i,j=1}^{3} Y_u^{ij} \overline{Q}_L^j U_R^j \phi^c - \sum_{i,j=1}^{3} Y_\ell^{ij} \overline{L}_L^i E_R^j \phi + \text{h.c.}, \tag{2.3.1}$$

where the indices i and j denote the fermion generation and

$$\phi^c = i\tau_2 \phi^\dagger = \begin{pmatrix} -\overline{\phi}_0 \\ \overline{\phi}_+ \end{pmatrix} \tag{2.3.2}$$

is the charge conjugate Higgs doublet. When the Higgs field acquires a VEV it can be written as

$$\phi^c(x) = \frac{1}{\sqrt{2}} \begin{pmatrix} v + h(x) \\ 0 \end{pmatrix}. \tag{2.3.3}$$

The Yukawa terms are the only terms in the SM Lagrangian which induce interactions between fermions of different generations. Without them all fermions would be stable!

Analogously to the case of the gauge bosons the fermion masses are found by plugging the Higgs field expanded around its VEV into the Yukawa Lagrangian. The terms made up of two fermion fields and one VEV then yield the fermion masses. In order to obtain definite fermion masses the Yukawa couplings have to be diagonalised. In the lepton sector this can be achieved by making use of the global flavour symmetry of the matter part of the SM Lagrangian. The term $\mathcal{L}_{\text{SM}}$ is invariant under global transformations of the form

$$\psi^f \to W_\psi^{fg} e^{i\theta_\psi} \psi^g, \tag{2.3.4}$$

where f is a generation index and $W \in \mathrm{SU}(3)$. For example

$$\begin{aligned} \overline{L}_L^f i\not{D}_{L_L} L_L^f \to & \overline{L}_L^f W_{L_L}^{\dagger fg} e^{-i\theta_{L_L}} i\not{D}_{L_L} e^{i\theta_{L_L}} W_{L_L}^{gh} L_L^h \\ &= \overline{L}_L^f i\not{D}_{L_L} W_{L_L}^{\dagger fg} e^{-i\theta_{L_L}} e^{i\theta_{L_L}} W_{L_L}^{gh} L_L^h \\ &= \overline{L}_L^f i\not{D}_{L_L} W_{L_L}^{\dagger fg} W_{L_L}^{gh} L_L^h \\ &= \overline{L}_L^f i\not{D}_{L_L} \delta^{fh} L_L^h \\ &= \overline{L}_L^f i\not{D}_{L_L} L_L^f. \end{aligned} \tag{2.3.5}$$

The SU(3) flavour transformations W_{L_L} commute with the covariant derivative because the gauge couplings are equal for all generations. These transformations make up the group

$$\mathcal{G}_{\text{flavour}} = \mathrm{U}(1)^5 \times \mathrm{SU}(3)_{L_L} \times \mathrm{SU}(3)_{E_R} \times \mathrm{SU}(3)_{Q_L} \times \mathrm{SU}(3)_{U_R} \times \mathrm{SU}(3)_{D_R} = \mathrm{U}(3)^5. \tag{2.3.6}$$

The lepton Yukawa couplings Y_ℓ can then be diagonalised by applying SU(3) transformations W_{L_L} and W_{E_R} to the left- and right-handed leptons respectively, such that $W_{L_L}^\dagger Y_\ell W_{E_R}$ is diagonal. The diagonal elements of this matrix correspond to the lepton masses.

In the quark sector a complication arises. For the diagonalisation of Y_u and Y_d in general four different unitary matrices are needed. Because $\mathrm{SU}(3)_{Q_L}$ transformations act on the upper and lower members of the left-handed quark doublet in the same way, that is to say only a simultaneous transformation of up-type and down-type quarks leave the matter Lagrangian invariant, only three unitary matrices can be chosen in such a way that they do not change other terms in the Lagrangian.

We can choose W_{Q_L} and W_{U_R} such that the Yukawa couplings to up-type quarks, $W_{Q_L}^\dagger Y_u W_{U_R}$, are diagonal. We can also freely choose W_{D_R} without impacting the rest of the Lagrangian but $W_{Q_L}^\dagger Y_d W_{D_R}$ is not diagonal. This can be corrected by introducing a unitary transformation V rotating the left-handed quark doublets as

$$Q_L^f = \begin{pmatrix} u^f \\ d^f \end{pmatrix} \to V^{fg} Q_L^g = \begin{pmatrix} V_u^{fg} u^g \\ V_d^{fg} d^g \end{pmatrix}. \tag{2.3.7}$$

We choose it in such a way that $V^\dagger W_{Q_L}^\dagger Y_d W_{D_R}$ is diagonal. As V has to transform up- and down-type quarks differently the only terms it impacts in the Lagrangian are the interactions of the charged W bosons with a pair of quarks. The Z boson and photon interactions are unaffected because they do not mix upper and lower members of an $\mathrm{SU}(2)_L$ doublet as was established in the end of section 2.2. The W boson interactions with a pair of quarks from eq. (2.2.20) then become

$$\frac{g}{\sqrt{2}} W_\mu^- \overline{u}_L^f \gamma^\mu d_L^f \to \frac{g}{\sqrt{2}} W_\mu^- \overline{u}_L^f V_u^{\dagger fg} \gamma^\mu V_d^{gh} d_L^h = \frac{g V_{\mathrm{CKM}}^{fh}}{\sqrt{2}} W_\mu^- \overline{u}_L^f \gamma^\mu d_L^h, \tag{2.3.8}$$

where we defined the CKM matrix as $V_{CKM} = V_u^\dagger V_d$. Finally there are couplings between different flavours of quarks. Thanks to the introduction of the Yukawa terms in the Lagrangian the fermions obtain masses and heavy fermions can decay into lighter ones of a different flavour.

In general a unitary 3×3 matrix has 9 parameters, three of which are real rotation angles and 6 are complex phases but we can change the 5 relative phases between the 6 quarks without any effect apart from the Yukawa couplings, or equivalently the CKM matrix. By making use of these, 5 phases can be removed from the CKM matrix. So in the end the CKM matrix contains 3 real mixing angles and one complex phase.

2.4 The Standard Model

In summary, the SM is a gauge theory based on the symmetry $\mathrm{SU}(3)_c \times \mathrm{SU}(2)_L \times \mathrm{U}(1)_Y$ with the Lagrangian

$$\begin{aligned}
\mathcal{L}_{\mathrm{SM}} =& \mathcal{L}_{\mathrm{matter}} + \mathcal{L}_{\mathrm{gauge}} + \mathcal{L}_{\mathrm{Higgs}} + \mathcal{L}_{\mathrm{Yukawa}} \\
=& \sum_{f=1}^{3} \sum_{\psi^f \in \{L_L^f, E_R^f, Q_L^f, U_R^f, D_R^f\}} \overline{\psi}^f i \not{D}_\psi \psi^f \\
& - \frac{1}{4} \left(\sum_{a=1}^{8} G_a^{\mu\nu} G_{\mu\nu}^a + \sum_{a=1}^{3} W_a^{\mu\nu} W_{\mu\nu}^a + B^{\mu\nu} B_{\mu\nu} \right) \\
& + \left| D_\mu^\phi \phi \right|^2 - \mu^2 \left(\phi^* \phi \right) - \lambda \left(\phi^* \phi \right)^2 \\
& - \sum_{i,j=1}^{3} Y_d^{ij} \overline{Q}_L^i D_R^j \phi - \sum_{i,j=1}^{3} Y_u^{ij} \overline{Q}_L^j U_R^j \phi^c - \sum_{i,j=1}^{3} Y_e^{ij} \overline{L}_L^i E_R^j \phi + \mathrm{h.c.}
\end{aligned} \tag{2.4.1}$$

with the covariant derivatives given in eq. (2.1.12). When the Higgs field acquires a VEV the gauge bosons get their masses from the kinetic energy energy term of the Higgs field, while the fermion masses and quark mixing both have their origin in the Yukawa terms. Upon the diagonalisation of the Yukawa couplings the quark mixing is moved to the gauge sector yielding flavour changing charged current interactions. As the Z boson and the photon do not mix upper and lower members of an $SU(2)_L$ doublet, at the tree-level there are no flavour changing neutral currents in the SM.

The Lagrangian above completely fixes the dynamics of all known elementary particles, but it contains 18 input parameters which cannot be predicted from first principles. They are

- 9 Yukawa couplings, or equivalently fermion masses,
- the Higgs self coupling λ,
- the Higgs VEV, or equivalently the constant μ^2,
- the 3 mixing angles and the complex phase of the CKM matrix,
- the gauge couplings $g_s, g, g^{'}$.

Note that, except for the 3 gauge couplings, all a priori unknown input parameters have their origin in the Higgs sector.

Considering the scope of physics it describes the SM is a remarkably simple theory. It is truly impressive how precisely its predictions agree with almost all experiments carried out to test it in the past 50 years.

Still there are big theoretical problems, suggesting that the Standard Model can be generalized to a more complete description of nature. Some of these indications are

- the fact that there are at least 18 constants of nature which have to be plugged in by hand,
- the fact that there is no gravity in the SM,
- the fact that the complex phase of the CKM matrix is the only source of CP violation in the SM and that this is not enough to cause the observed matter/antimatter asymmetry in the universe,
- the fact that the SM in its minimal form does not account for neutrino masses even though there is evidence for neutrino masses from the observation of neutrino oscillations.

The shared property among these issues with the SM is that they are not easily translated into explicit predictions for microscopic processes. Despite it being frustratingly good at predicting the outcome of precision measurements there are some processes in which the SM seems to fail in appropriately describing nature.

Notably in processes which involve the decay of a bottom quark to a strange or a charm quark it seems that the SM fails to describe nature accurately. At this point also the anomalous magnetic moment of the muon should be mentioned for completeness, even though it is not a topic of this thesis. Also in measurements of this constant there seems to be a disagreement between theory prediction and experimental measurement.

In the following we will focus on two current puzzles. The first one is concerned with one of the elements of the CKM matrix, describing the probability of the charged current $b \to c$

decays. This constant can be measured in inclusive and exclusive decays of B mesons and interestingly the results of both determinations disagree with each other. This is known as the V_{cb} puzzle and will be discussed in more detail in chapter 4.

The second one concerns a neutral current flavour changing decay. Being forbidden at tree-level these decays are heavily suppressed in the SM. Explicitly this work deals with the decay rate of a bottom quark decaying to a strange quark and two leptons. The measured decay rate of this process exhibits a departure from the SM expectation which could hint at New Physics (NP), i.e. physics beyond the SM. This is the topic of chapter 7.

Before tackling these problems the necessary theoretical framework is laid out in the following sections and chapter 3.

2.5 The CKM Matrix

The Cabibbo-Kobayashi-Maskawa (CKM) matrix [181] parametrizes the probabilities for flavour changing charged current interactions. It is commonly displayed in the form

$$V = \begin{pmatrix} V_{ud} & V_{us} & V_{ub} \\ V_{cd} & V_{cs} & V_{cb} \\ V_{td} & V_{ts} & V_{tb} \end{pmatrix}. \tag{2.5.1}$$

There are many possible parametrizations of the CKM matrix. The one that is recommended by the PDG is

$$V = \begin{pmatrix} c_{12}c_{13} & s_{12}c_{13} & s_{13}e^{-i\delta} \\ -s_{12}c_{23} - c_{12}s_{23}s_{13}e^{i\delta} & c_{12}c_{23} - s_{12}s_{23}s_{13}e^{i\delta} & s_{23}c_{13} \\ s_{12}s_{23} - c_{12}c_{23}s_{13}e^{i\delta} & -c_{12}s_{23} - s_{12}c_{23}s_{13}e^{i\delta} & c_{23}c_{13} \end{pmatrix}, \tag{2.5.2}$$

where $s_{ij} = \sin\theta_{ij}$ and $c_{ij} = \cos\theta_{ij}$. Unitarity relates its elements to each other. Explicitly the condition $V^\dagger V = \mathbb{1}_{3\times3}$ yields

$$|V_{ud}|^2 + |V_{us}|^2 + |V_{ub}|^2 = |V_{cd}|^2 + |V_{cs}|^2 + |V_{cb}|^2 = |V_{td}|^2 + |V_{ts}|^2 + |V_{tb}|^2 = 1 \tag{2.5.3}$$

and six more relations for the off-diagonal elements of $VV^\dagger$. The relations for the off-diagonal elements define triangles in the complex plane. In depictions usually the relation

$$V_{ub}^* V_{ud} + V_{cb}^* V_{cd} + V_{tb}^* V_{td} = 0 \tag{2.5.4}$$

is shown. Rescaling it the relation becomes

$$1 + \frac{V_{ub}^* V_{ud}}{V_{cb}^* V_{cd}} + \frac{V_{tb}^* V_{td}}{V_{cb}^* V_{cd}} = 0 \tag{2.5.5}$$

and defining

$$R_i = \left| \frac{V_{ib}^* V_{id}}{V_{cb}^* V_{cd}} \right| \tag{2.5.6}$$

for $i \in \{u, t\}$, it is obvious that this relation defines a triangle in the complex plane with sides of length 1, R_u and R_t as depicted in fig. 2.5.1.

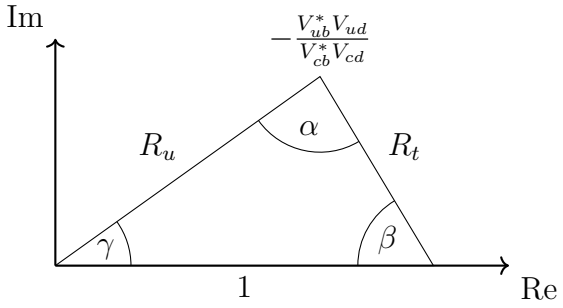

Figure 2.5.1: The unitarity triangle

Experimentally it is observed that the elements of the CKM matrix follow a hierarchical pattern, with the diagonal elements being close to 1, $|V_{us}|$ and $|V_{cd}|$ being close to 0.22, $|V_{cb}|$ and $|V_{ts}|$ being of order 10^{-2} and $|V_{ub}|$ and $|V_{td}|$ being of order 10^{-3}.

2.6 Asymptotic Freedom

At this point we can apply the framework of perturbation theory (PT) to the SM and compute predictions for observables. For hadronic processes, that is to say in processes involving quarks in the initial or final state, these predictions cannot directly be compared to experimental measurements however. This is due to a property of QCD called asymptotic freedom, stating that the QCD coupling constant α_s, decreases when the energy scale of a given process increases and diverges at low energy scales.

This property is intrinsically linked to the renormalization of QCD. In order to make precise predictions in QCD, loop diagrams have to be evaluated. At the Next-To-Leading Order (NLO) we have to evaluate one-loop diagrams with one undetermined momentum which has to be integrated over. These integrals suffer from UV divergences which are dealt with by renormalizing the theory. First the integrals are regularized such that the intermediate results of the computation are formally finite before one takes a certain limit. A commonly used regularization procedure is called dimensional regularization. In dimensional regularization loop integrals are computed in $d = 4 - 2\epsilon$ dimensions. Away from $d = 4$ dimensions the integrals are formally finite and can be computed. The UV singularities then appear as $1/\epsilon$ poles in the result. For obtaining a physical prediction these poles then have to be cancelled before taking the $\epsilon \to 0$ limit. This is achieved through a redefinition of the parameters in the Lagrangian (masses and coupling constants) and of the fields. The singular bare quantities, here denoted by the subscript 0, then relate to their renormalized counterparts as

$$\begin{aligned} \psi_0 &= Z_\psi^{\frac{1}{2}} \psi \\ G_{0,\mu}^a &= Z_G^{\frac{1}{2}} G_\mu^a \end{aligned} \tag{2.6.1}$$

where the renormalization constants Z contain singularities, but the renormalized parameters and fields are finite.

Analogously we introduce a renormalization constant Z_g for the coupling constant to absorb the singularity of the bare coupling $g_{s,0}$. Now we run into a problem if we want the renormalization constant to be dimensionless. The coupling constant $g_{s,0}$ itself is not dimensionless away from $d = 4$. This can be seen from simple dimensional arguments

In d spacetime dimensions we want the action $S = \int \mathcal{L} d^d x$ to be dimensionless so by looking at the fermion kinetic energy terms we see that the fermion fields have mass dimension $(d-1)/2$ and from the kinetic energy terms of the gauge bosons we find that they have mass dimension $(d-2)/2$. Then from the interaction term we find that the coupling constant has mass dimension ϵ. As we would like to keep the coupling constant and thus the renormalization constant associated with it dimensionless, we introduce a new constant μ which absorbs the mass dimension of the coupling. Therefore the relation between the bare coupling $g_{s,0}$ and the renormalized coupling g_s is given by

$$g_{s,0} = Z_g(\mu)\mu^\epsilon g_s(\mu), \tag{2.6.2}$$

where $g_{s,0}$, Z_g and g_s are dimensionless but Z_g and g_s depend on μ.

So the process of renormalization comes at the cost of introducing an artificial energy scale in the theory. The dependence of the coupling constant on μ can be found by noticing that the bare coupling does not scale with μ. Consequently we find

$$\begin{aligned} 0 &= \frac{\mathrm{d}}{\mathrm{d}\mu} g_{s,0} \\ &= \frac{\mathrm{d}}{\mathrm{d}\mu} \left(Z_g \mu^\epsilon g_s(\mu) \right) \\ &= \mu \frac{\mathrm{d}}{\mathrm{d}\mu} \left(Z_g \mu^\epsilon g_s(\mu) \right) \\ &= \mu^\epsilon g_s \frac{\mathrm{d}Z_g}{\mathrm{d}\log\mu} + Z_g \mu^\epsilon \frac{\mathrm{d}g_s}{\mathrm{d}\log\mu} + Z_g g_s \epsilon \mu^\epsilon \end{aligned} \tag{2.6.3}$$

The logarithmic derivative of the coupling constant is called the β function of QCD, $\beta(g_s) = \mathrm{d}\log g_s / \mathrm{d}\log\mu$. The renormalization group equation eq. (2.6.3) lets us write it as

$$\beta(g_s) = \sum_{n=0}^{\infty} \left(\frac{\alpha_s}{4\pi} \right)^{n+1} \beta_n = -\frac{1}{Z_g} \frac{\mathrm{d}Z_g}{\mathrm{d}\log\mu} - \epsilon, \tag{2.6.4}$$

where $\alpha_s = 4\pi g_s^2$ is the fine structure constant of QCD.

Also the constant Z_g has an α_s expansion,

$$Z_g = 1 + \frac{\alpha_s}{4\pi\epsilon} Z_{g,1} + \frac{\alpha_s^2}{16\pi^2\epsilon} Z_{g,2} + \mathcal{O}\left(\alpha_s^3\right) \tag{2.6.5}$$

and only depends on μ through α_s because $Z_{g,n}$ are the singularities of n-loop diagrams and as such μ independent. At the 1-loop level the diagrams in fig. 2.6.1

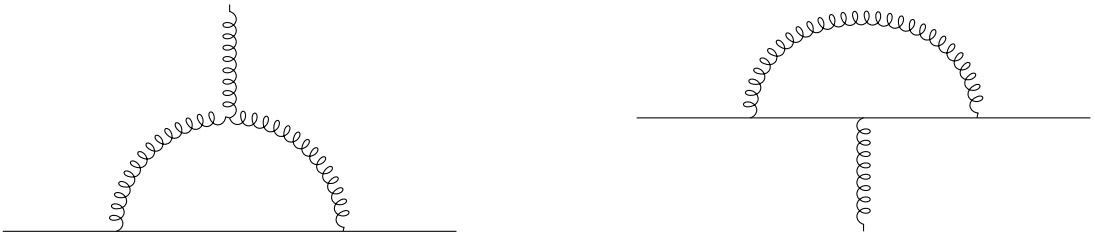

Figure 2.6.1: The diagrams contributing to the renormalization of the QCD coupling constant at 1-loop.

have to be evaluated and yield

$$Z_{g,1} = -\frac{11}{6}C_A + \frac{2}{3}T_F n_F, \tag{2.6.6}$$

where $C_A = 3$ is the number of colors, $T_F = \frac{1}{2}$ and n_F is the number of active quark flavours. While in full QCD this number is 6, in effective low energy theories it can be lower because at energy scales $\Lambda \ll m_t$ for example the top quark does not participate in interactions as a dynamical degree of freedom.

At 1-loop the derivative of Z_g with respect to μ can thus be written as

$$\begin{aligned}
\frac{\mathrm{d}Z_g}{\mathrm{d}\log\mu} &= \frac{\mathrm{d}}{\mathrm{d}\mu}\left(1 + \frac{g_s^2}{16\pi^2\epsilon}Z_{g,1} + \mathcal{O}(g_s^4)\right) \\
&= \frac{Z_{g,1}}{8\pi^2\epsilon}g_s\beta(g_s) + \mathcal{O}\left(g_s^4\right)) \\
&= \frac{g_s Z_{g,1}}{8\pi^2}\left(-g_s\epsilon - \frac{g_s}{Z_g}\frac{\mathrm{d}Z_g}{\mathrm{d}\log\mu} + \mathcal{O}\left(g_s^4\right)\right) \\
&= -\frac{g_s^2 Z_{g,1}}{8\pi^2} + \mathcal{O}\left(g_s^4\right),
\end{aligned} \tag{2.6.7}$$

where we used the fact that $\mathrm{d}Z_g/\mathrm{d}\log\mu$ starts at order g_s^2. Note that the $1/\epsilon$ pole cancels, as it should, so we can take the $\epsilon \to 0$ limit of eq. (2.6.4) and obtain at 1-loop

$$\beta_0 = 2Z_{g,1} = \frac{2}{3}n_F - 11. \tag{2.6.8}$$

As can be seen here, the leading term of the QCD β function is negative as long as $n_F \leq 16$. The scaling of α_s with μ can be found from

$$\begin{aligned}
\frac{\mathrm{d}\alpha_s}{\mathrm{d}\log\mu} &= \left(\frac{\mathrm{d}Z_g}{\mathrm{d}\alpha_s}\right)^{-1}\frac{\mathrm{d}Z_g}{\mathrm{d}\log\mu} \\
&= \left(\frac{Z_{g,1}}{4\pi\epsilon} + \mathcal{O}\left(\alpha_S\right)\right)^{-1}\left(-\frac{\alpha_s Z_{g,1}}{2\pi} + \mathcal{O}\left(\alpha_s^2\right)\right) \\
&= -2\epsilon\alpha_s + \mathcal{O}\left(\alpha_s^2\right) \\
&= \frac{\alpha_s^2\beta_0}{2\pi}
\end{aligned} \tag{2.6.9}$$

at 1-loop. This equation can be solved by separation of variables:

$$\int_{\alpha_s(\mu_1)}^{\alpha_s(\mu_2)}\frac{\mathrm{d}\alpha_s}{\alpha_s^2} = \frac{\beta_0}{2\pi}\int_{\log\mu_1}^{\log\mu_2}\mathrm{d}\log\mu, \tag{2.6.10}$$

yielding

$$\alpha_s(\mu_2) = \frac{\alpha_s(\mu_1)}{1 - \frac{\beta_0}{2\pi}\alpha_s(\mu_1)\log\frac{\mu_2}{\mu_1}}. \tag{2.6.11}$$

For $\mu_2 > \mu_1$ and $\beta_0 < 0$, as indicated in eq. (2.6.8), the denominator of this equation is larger than 1 and thus $\alpha_s(\mu_2) < \alpha_s(\mu_1)$. Therefore the QCD coupling constant decreases if the scale μ is increased. This behavior is linked to QCD being a non-abelian theory. Without the gluon

self interaction we would not get a negative term in eq. (2.6.6) and the strength of the coupling constant would increase with increasing μ, like it does in QED.

If we go in the opposite direction, so to smaller scales μ_2, $\alpha_s(\mu_2)$ increases. At some point the scale is low enough for α_s to grow beyond 4π. Below this scale eq. (2.6.11) is not valid anymore because in its derivation we truncated the perturbation expansion. Even worse, according to eq. (2.6.11) there is a scale at which the denominator of eq. (2.6.11) will vanish and $\alpha_s(\mu_2)$ will diverge. This scale is called Λ_{QCD}. Renaming $\mu_2 \to \mu$ and taking the limit $\mu_1 \to \Lambda_{\text{QCD}}$ we obtain

$$\alpha_s(\mu) = \frac{1}{\frac{1}{\alpha_s(\mu_1)} - \frac{\beta_0}{2\pi}\log\frac{\mu}{\mu_1}} \overset{\mu_1\to\Lambda_{\text{QCD}}}{\longrightarrow} \frac{12\pi}{(33-2n_F)\log\frac{\mu^2}{\Lambda^2_{\text{QCD}}}}. \tag{2.6.12}$$

At energy scales below Λ_{QCD} PT breaks down so it cannot be used to describe bound states in QCD. This is a challenge to experimental tests of QCD because the asymptotic states which are observed are colorless bound states. At high energies this difficulty is mitigated to a degree by the running of the QCD coupling, rendering quarks quasi-free. At low energies, such as m_b however non-perturbative methods have to be used, in order to compute precise predictions. In the following section one of these methods, the Heavy Quark Expansion (HQE) is introduced.

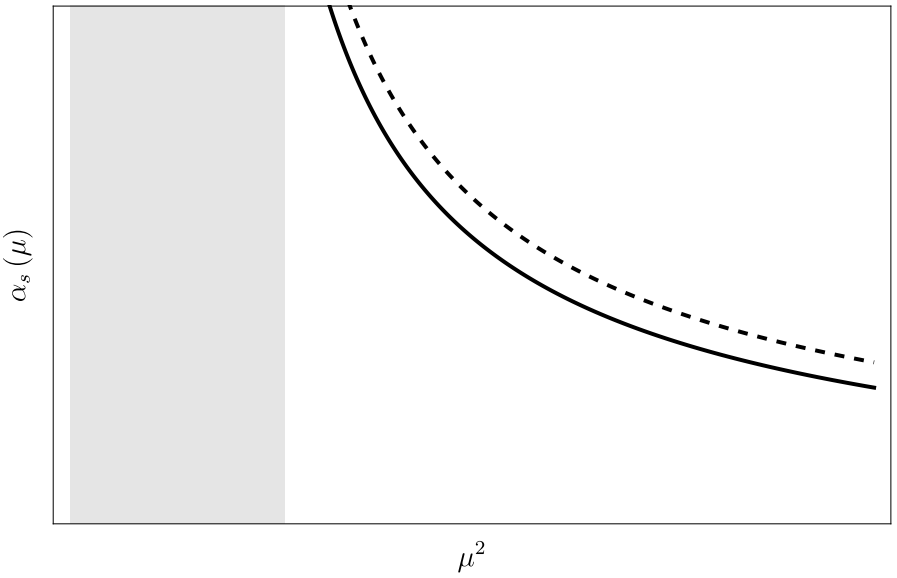

Figure 2.6.2: The running of the QCD coupling constant as a function of the energy scale μ. The dashed line corresponds to a theory with $n_F = 6$ quark flavors, while the solid line corresponds to 5 quark flavors. In the grey shaded region the coupling becomes strong and thus perturbation theory is not valid.

Chapter 3

Effective Field Theories

There are two distinct regions in which the QCD coupling constant behaves very differently. In the high energy region QCD is perturbative and its coupling runs according to eq. (2.6.11). At low energies however the behavior of the coupling constant is not clear a priori and non perturbative methods have to be used for describing processes taking place at these energy scales.

Physical processes like the decays of B mesons depend on very different energy scales. The initial meson has a mass of a few GeV, its decay is mediated by a W boson with a mass of about 80 GeV, while the scale of the kinetic energy of the quarks inside the initial and final state is Λ_{QCD}, which is a few hundred MeV. Therefore calculations are facilitated if the processes happening at the different energy scales can be treated separately from each other and only contributions which matter at a given precision are taken into account.

Such a separation of scales can be achieved by the Operator Product Expansion (OPE) [221, 223, 226]. If it is sandwiched between an initial and a final state, a product of operators $A(x)B(y)$ evaluated at different points in spacetime can be expanded into a sum of local operators $O_n(x)$:

$$\langle f\,|A(x)B(y)|\,i\rangle = \sum_n^\infty C_n\,\langle f\,|O_n(x)|\,i\rangle \tag{3.0.1}$$

As shown explicitly below the Wilson coefficients C_n encode the short distance effects and the matrix element $\langle f\,|O_n(x)|\,i\rangle$ only contains low energy effects.

3.1 The Weak Effective Lagrangian

In order to see the how the scales are separated let us consider the part of the SM Lagrangian describing charged current interactions between bottom and charm quarks,

$$\begin{aligned}\mathcal{L}_{cb} = \bar{c}i\partial\!\!\!/c + \bar{b}i\partial\!\!\!/b + \frac{gV_{cb}}{\sqrt{2}}\bar{b}\gamma_\mu\frac{1-\gamma_5}{2}cW^{+\mu} + \frac{gV_{cb}}{\sqrt{2}}\bar{c}\gamma_\mu\frac{1-\gamma_5}{2}bW^{-\mu}\\ -\frac{1}{2}\left(\partial_\mu W^+_\nu - \partial_\nu W^+_\mu\right)\left(\partial^\mu W^{-\nu} - \partial^\nu W^{+\mu}\right) + m_W^2 W^+_\mu W^{-\mu}.\end{aligned} \tag{3.1.1}$$

Defining

$$\begin{aligned}J^+_\mu &= \bar{b}\gamma_\mu\frac{1-\gamma_5}{2}cW^{+\mu}\\ J^-_\mu &= \bar{c}\gamma_\mu\frac{1-\gamma_5}{2}bW^{-\mu}\end{aligned} \tag{3.1.2}$$

and

$$\begin{aligned}\mathcal{L}_\psi &= \bar{c} i\partial\!\!\!/ c + \bar{b} i\partial\!\!\!/ b \\ \mathcal{L}_{\mathrm{cc}} &= \frac{g V_{cb}}{\sqrt{2}} J_\mu^+ W^{+\mu} + \frac{g V_{cb}}{\sqrt{2}} J_\mu^- W^{-\mu} \\ \mathcal{L}_W &= -\frac{1}{2}\left(\partial_\mu W_\nu^+ - \partial_\nu W_\mu^+\right)\left(\partial^\mu W^{-\nu} - \partial^\nu W^{+\mu}\right) + m_W^2 W_\mu^+ W^{-\mu},\end{aligned} \tag{3.1.3}$$

the generating functional for this theory can be written as

$$Z[J] = \mathcal{N} \int \mathcal{D}\psi \mathcal{D}W \exp\left(i \int \mathrm{d}^4x \mathcal{L}_\psi(x) + \mathcal{L}_{\mathrm{cc}}(x) + \mathcal{L}_W(x) + \mathcal{J}(x)\right), \tag{3.1.4}$$

where $\mathcal{D}\psi = \mathcal{D}c\mathcal{D}\bar{c}\mathcal{D}b\mathcal{D}\bar{b}$ and $\mathcal{D}W = \mathcal{D}W^+\mathcal{D}W^-$ are shorthand notations for the functional integration over the light and heavy degrees of freedom respectively and $\mathcal{J} = J_c c + \overline{J}_c \bar{c} + J_b b + \overline{J}_b \bar{b}$ denotes the source terms. There are no source terms for the W bosons because we are only interested in initial and final states made up of light particles, i.e. particles with mass $m \ll m_W$. The normalization constant $\mathcal{N}$ is given by

$$\frac{1}{\mathcal{N}} = \int \mathcal{D}_\psi \mathcal{D}W \exp\left(i \int \mathrm{d}^4x \mathcal{L}_{cb}\right). \tag{3.1.5}$$

We can separate the terms containing heavy degrees of freedom in eq. (3.1.4) from the rest, obtaining

$$\begin{aligned}Z[J] &= \mathcal{N} \int \mathcal{D}\psi \exp\left(i \int \mathrm{d}^4x \mathcal{L}_\psi(x) + \mathcal{J}(x)\right) \int \mathcal{D}W \exp\left(i \int \mathrm{d}^4x \mathcal{L}_{\mathrm{cc}}(x) + \mathcal{L}_W(x)\right) \\ &= \mathcal{N} \int \mathcal{D}\psi \exp\left(i \int \mathrm{d}^4x \mathcal{L}_\psi(x) + \mathcal{J}(x)\right) I_W.\end{aligned} \tag{3.1.6}$$

The integral over the W bosons can be evaluated explicitly [94]. Integrating $\mathcal{L}_W$ by parts to move the derivatives from the W^+ to the W^- we can write the integral over the heavy degrees of freedom as

$$I_W = \int \mathcal{D}W \exp\left(i \int \mathrm{d}^4x \mathrm{d}^4y W_\mu^+(x) K^{\mu\nu}(x,y) W_\nu^-(y) + \frac{i g V_{cb}}{\sqrt{2}} \int \mathrm{d}^4x J_\mu^+ W^{+\mu} + J_\mu^- W^{-\mu}\right), \tag{3.1.7}$$

with the operator

$$K_{\mu\nu} = \delta^{(4)}(x-y)\left(g_{\mu\nu}\left(\partial^2 + m_W^2\right) - \partial_\mu\partial_\nu\right). \tag{3.1.8}$$

Its inverse is given by the W boson propagator

$$\Delta_{\mu\nu}(x,y) = \int \frac{\mathrm{d}^4q}{(2\pi)^4} \frac{-1}{q^2 - m_W^2}\left(g_{\mu\nu} - \frac{q^\mu q^\nu}{m_W^2}\right) e^{-iq(x-y)}. \tag{3.1.9}$$

Explicitly performing the integration one obtains

$$Z[J] = \mathcal{N} \int \mathcal{D}\psi \exp\left(i \int \mathrm{d}^4x \mathcal{L}_\psi(x) + \mathcal{J}(x) - \frac{i g^2 |V_{cb}|^2}{2} \int \mathrm{d}^4x \mathrm{d}^4y J_\mu^+(x) \Delta^{\mu\nu}(x,y) J_\nu^-(y)\right). \tag{3.1.10}$$

It should be stressed that this relation is exact as long as the full propagator is taken into account. The non-local product of currents can be dealt with by the OPE. In order to perform the OPE, we note that the available energy in the decay of a B meson is the B mass $m_B \approx 5$ GeV so $q^2/m_W^2 \approx 0.004$ is a small parameter. Therefore we can expand the propagator in powers of q^2/m_W^2, finding

$$\Delta_{\mu\nu}(q) = \frac{g_{\mu\nu}}{m_W^2}\delta^{(4)}(x-y) + \frac{q^2}{m_W^2}\frac{q^2 g_{\mu\nu} + q_\mu q_\nu}{m_W^2}\delta^{(4)}(x-y) + \mathcal{O}\left(\frac{q^4}{m_W^4}\right). \tag{3.1.11}$$

Then the generating functional becomes

$$Z[J] = \mathcal{N}\int \mathcal{D}\psi \exp\left(i\int \mathrm{d}^4x \mathcal{L}_\psi(x) + \mathcal{J}(x) - i\frac{4G_\mathrm{F}\left|V_{cb}\right|^2}{\sqrt{2}} J_\mu^+(x)J^{-\mu}(x) + \mathcal{O}\left(\frac{q^4}{m_W^4}\right)\right), \tag{3.1.12}$$

with the Fermi constant $G_\mathrm{F} = \sqrt{2}g^2/(8m_W^2)$.

Therefore, at energies far below the W mass, we get the same physics from the Lagrangian

$$\mathcal{L}_\mathrm{eff} = \mathcal{L}_\psi - \frac{4G_\mathrm{F}\left|V_{cb}\right|^2}{\sqrt{2}}\left[J_\mu^+ J^{-\mu} + \frac{1}{m_W^2}D^2 J_\mu^+ J^{-\mu} - \frac{1}{m_W^2}D_\mu D_\nu J^{+\mu}J^{-\nu} + \mathcal{O}\left(\frac{1}{m_W^4}\right)\right] \tag{3.1.13}$$

as from the Lagrangian $\mathcal{L}_{\psi W} + \mathcal{L}_W$. At energies close to the W mass the effective theory does not reproduce the results of the full SM anymore however because the terms neglected in eq. (3.1.11) become sizeable.

Now we can explicitly see that the high and low energy contributions factorize. As the local operators $J_\mu^+ J^{-\mu}, D^2 J_\mu^+ J^{-\mu}$ and $D_\mu D_\nu J^{+\mu}J^{-\nu}$ only involve the light degrees of freedom we can see that the effects of the heavy particles only appear in the Wilson coefficients. The Wilson coefficients on the other hand are independent of the light degrees of freedom because they only appear in the local operators.

All contributions of the W boson would vanish if we were to send the mass of the W boson to infinity. This is a consequence of the decoupling theorem [48], which states that in a renormalizable quantum field theory with different mass scales, the heavy particles decouple from the theory at low energies, i.e. they do not take part in interactions as dynamical degrees of freedom. Their only contribution to the low energy dynamics is through Wilson coefficients, which in the effective theory are interpreted as effective coupling constants. One has to be careful here though. One of the particles integrated out in the effective Lagrangian for weak B decays is the top quark. Since the bottom quark is obviously left in the theory, this violates gauge symmetry and thus renormalizability. So in this case the decoupling theorem is not valid and amplitudes can for example scale with the top quark mass.

A quick dimensional analysis of eq. (3.1.13) shows that this effective Lagrangian contains one operator with mass dimension 6 followed by two operators at dimension 8, which are accompanied by appropriate powers of the scale m_W so the terms have dimension 4. This pattern generalizes.

In general an effective Lagrangian is given by all terms invariant under a given gauge symmetry, accompanied by appropriate powers of a high scale Λ,

$$\mathcal{L}_\mathrm{eff} = \mathcal{L}_0 + \sum_{i=1}^{n}\frac{1}{\Lambda^i}C_i(\mu)O_i \tag{3.1.14}$$

up to a fixed dimension $n+4$, determined by the desired precision of the computation. If a more complete theory exists, the effective theory correctly reproduces its physics at energies

far below Λ. In this context more complete means that this theory is still valid at energies above Λ.

Intuitively going from an effective theory to a more complete theory can be pictured as observing nature and zooming in, resolving more and more details of the processes happening. At everyday distances in the meter range, classical mechanics is an adequate description of nature, but when we zoom in and start resolving atoms, classical mechanics does not appropriately describe natural processes anymore. We need a more complete theory, quantum mechanics, which extends classical mechanics and yields the same predictions in the limit of large distances. Therefore classical mechanics is an effective theory of non relativistic quantum mechanics. Non relativistic quantum mechanics itself is an effective theory of the SM. Following this logic, it seems likely that the SM is an effective theory of a yet unknown more general theory. There has been a lot of effort spent on exploring this idea of a Standard Model Effective Field Theory, or SMEFT [176].

In the study of B decays in chapters 4 and 7 the inclusion of dimension 6 operators is sufficient to reach the desired precision, with the exception of chapter 6, where the effects of dimension 8 operators in the weak effective Lagrangian on inclusive observables are studied.

When loop effects are taken into account the Wilson coefficients $C_i(\mu)$ are renormalized. Just like in the case of the QCD coupling constant in section 2.6 there is a renormalization group equation for the Wilson coefficients, obtained by demanding that physical observables are independent of this scale, which yields μ dependent Wilson coefficients. In case the full theory is known, we can demand that the matrix elements computed in the effective theory are equal to their counterparts in the full theory at the heavy scale, in our case m_W. This procedure is known as matching. After matching one uses the renormalization group running to determine the Wilson coefficients at the scale of the processes of interest, in our case m_b. Since matching computations are not a subject of this work, in the following we will focus on the last step of an EFT computation. This step is concerned with the computation of the matrix elements of effective operators between given initial B meson states and final states composed of hadrons and leptons.

3.2 Heavy Quark Effective Theory

The main complication which arises in this last step lies in the fact that the asymptotic (initial and final) hadronic states we observe are mesons and baryons instead of single quarks. The structure of these composite objects is governed by long distance QCD effects. This statement begs the question of what exactly "short" and "long" distances in this context are. Looking back at eq. (2.6.12) one can see that the distance separating the non-perturbative from the perturbative regime is $1/\Lambda_{\text{QCD}}$ so a sensible definition of a long distance is any distance $l \gg 1/\Lambda_{\text{QCD}}$. Analogously we define short distances as distances $l \ll 1/\Lambda_{\text{QCD}}$. Consequently we need a non-perturbative framework if we want to treat these hadronic states consistently.

Similarly we call quarks with masses $m_q \gg \Lambda_{\text{QCD}}$ heavy and the others light. In this sense the charm, bottom and top quarks are heavy, while the up, down and strange are light. The top quark will be excluded in the following because of its short lifetime. In the following sections we briefly discuss the strict heavy quark limit $m_q \to \infty$, followed by an introduction of HQET which takes into account corrections to the heavy quark limit in a systematic way. A textbook treatise of HQET can be found in [198].

3.2.1 Heavy Quark Symmetry

Following [129] let us consider a hadron H_Q containing a heavy quark Q and light degrees of freedom, consisting of light quarks, light antiquarks and gluons in the strict heavy quark limit $m_Q \to \infty$. Because the momenta of the light degrees of freedom are of the order of Λ_{QCD} and thus small compared to m_Q, the interactions between them and the heavy quark do not change the kinematical state of the heavy quark. In this limit the heavy quark can be seen as a static source of an electric and a chromoelectric (or color) field which holds the hadron together, similar to the proton in the hydrogen atom. Additionally the Compton wavelength of the heavy quark scales with its inverse mass $\lambda_Q \sim 1/m_Q$ and since the Compton wavelength of the light degrees of freedom is of order $\lambda_l \sim 1/\Lambda_{\mathrm{QCD}}$, we have $\lambda_Q \ll \lambda_l$. So the light degrees of freedom cannot probe the exact value of m_Q, they are independent of the actual heavy quark mass. There is also another simplification in the heavy quark limit. As quarks carry spin, the heavy quark carries a chromomagnetic moment $\mu_Q = g/(2m_Q)$ which vanishes in the heavy quark limit. From these simple arguments we can see that the light degrees of freedom are oblivious to the heavy quark mass and spin. For N_h heavy quark flavours (in nature $N_h = 2$) this results in an $SU(2N_h)$ symmetry of our theory. This symmetry relates different hadrons $H_1(v)$ and $H_2(v)$ with the same velocity $v = p/m_H$ but different momenta, as opposed to other symmetries of QCD which relate states of the same momentum. Therefore we will label hadrons with their velocity from now on.

We can use the heavy quark symmetry to relate different hadronic matrix elements. For instance if we consider the decay $b \to c\ell\overline{\nu}$ in the heavy quark limit for the b and c quarks. Before the decay we have a hadron $H_b(v)$ consisting of a b quark dressed with light degrees of freedom. After the decay we have a pair of leptons carrying away momentum and a hadron $H'_c(v')$ containing a c quark dressed with light degrees of freedom as well.

From the point of view of the light degrees of freedom the only change which occurs at the time of the decay is that the color source instantly ($\delta t \sim 1/m_W \ll 1/\Lambda_{\mathrm{QCD}}$) changes its velocity from v to v'. In general they then build an excited state of the final state meson or additional color neutral particles. But there is also a probability for them to build another ground state meson. For example we can consider $H_b(v) = B(v)$ and $H_c(v') = D(v')$. In this case the amplitude for the final state to be a ground state D meson only depends on $v \cdot v' = w$ and is called $\xi(w)$, known as the Isgur-Wise function.

At the kinematic point $w = 1$, or $v = v'$, nothing changes for the light degrees of freedom, since the only property which changes during the decay at this kinematic point is the mass of the heavy quark, to which the light degrees of freedom are blind. Consequently we have [174]

$$\xi(1) = 1. \tag{3.2.1}$$

The heavy quark limit is useful for finding relations among different hadronic matrix elements but still we cannot use it directly for doing precise phenomenology. This is because even though we know that it is an approximation, at this point we have no idea of how good it is. In other words, to make precise statements we have to quantify the effects we neglect. This is important because for example $\Lambda_{\mathrm{QCD}}/m_c \sim 0.15$, so corrections of this order could be important.

We want a theory which provides a systematic expansion about the heavy quark limit. In the following section we will find such an expansion in terms of powers of $\Lambda_{\mathrm{QCD}}/m_Q$, m_Q being the mass of the heavy quark. The first term in this expansion corresponds to the strict heavy quark limit and the subleading terms correspond to corrections arising from the fact that the bottom and charm quarks are, in fact, not infinitely heavy. The full result of an

HQET computation then is a double expansion in terms of powers of $\Lambda_{\mathrm{QCD}}/m_Q$ and powers of α_s. The former are commonly called power corrections while the latter are known as radiative corrections.

3.2.2 The HQET Lagrangian

Let us consider a hadron containing one heavy quark, denoted by Q. As we noted before the typical momenta it exchanges with the light degrees of freedom are of the order of Λ_{QCD}. Since $\Lambda_{\mathrm{QCD}} \ll m_Q$, the heavy quark is always close to its mass shell, where $p_Q^2 = m_Q^2$. So it is natural to decompose its momentum into a large on–shell part $m_Q v$ and a small deviation from its mass shell, k. We write it as

$$p_Q^\mu = m_Q v^\mu + k^\mu, \tag{3.2.2}$$

where v^μ denotes the heavy quark's four velocity. Now noting that $k^\mu = \mathcal{O}(\Lambda_{\mathrm{QCD}})$ is small compared to m_Q let us take a look at what happens to the heavy quark propagator in this limit. It becomes

$$\begin{aligned} \frac{i}{\not{p} - m_Q + i\epsilon} &= \frac{i\left(\not{p} + m_Q\right)}{p^2 - m_Q^2 + i\epsilon} = \frac{i\left[m_Q\left(1 + \not{v}\right) + \not{k}\right]}{k^2 + 2m_Q v\cdot k + i\epsilon} \\ &\to \frac{1+\not{v}}{2}\frac{i}{v\cdot k + i\epsilon} \quad (m_Q \gg k)\,. \end{aligned} \tag{3.2.3}$$

We notice that the heavy quark propagator becomes independent of the heavy quark mass. Additionally it contains a factor of $P_+ = (1+\not{v})/2$ which projects onto the positive frequency parts of a Dirac spinor. This can be seen in the rest frame of the heavy quark, where it becomes $(1+\gamma^0)/2$ and projects onto the two upper components of the heavy quark field Q. Therefore in the limit of a heavy quark only the upper components of the field Q propagate. Then the action of the projectors $P_\pm = (1 \pm \not{v})/2$ on the heavy quark field $Q(x)$ is given by

$$P_+ Q(x) = Q(x) + \mathcal{O}\left(\frac{1}{m_Q}\right), \qquad P_- Q(x) = 0 + \mathcal{O}\left(\frac{1}{m_Q}\right). \tag{3.2.4}$$

The action of the heavy quark field on a heavy quark state is given by

$$Q(x)\,|Q(p)\rangle = e^{-ip\cdot x}\,|0\rangle\,. \tag{3.2.5}$$

If we multiply both sides of this equation by the phase $e^{im_Q v\cdot x}$, we obtain

$$e^{im_Q v\cdot x} Q(x)\,|Q(p)\rangle = e^{-ik\cdot x}\,|0\rangle\,. \tag{3.2.6}$$

The right-hand-side of this equation is independent of m_Q and consequently the left-hand-side as well. We just removed the dependence on the heavy quark mass by the multiplication with a phase. We already established that in the heavy quark limit only the upper components of the heavy quark field propagate so we can define a heavy quark field

$$h_v(x) = e^{im_Q v\cdot x} P_+ Q(x), \tag{3.2.7}$$

where $Q(x)$ denotes the heavy quark field defined in full QCD.

The field $h_v(x)$ is independent of m_Q, which was to be expected by heavy quark symmetry. We define a second field containing the small components of the heavy quark field as

$$H_v(x) = e^{im_Q v\cdot x} P_- Q(x). \tag{3.2.8}$$

This field becomes necessary as soon as we want to consider effects of order $1/m_Q$. It is straightforward to find the HQET Lagrangian at the leading order in $1/m_Q$. We take the QCD Lagrangian

$$\mathcal{L}_{\text{QCD}} = \overline{Q}(x)\left(i\not{D} - m_Q\right)Q(x), \tag{3.2.9}$$

where $D_\mu = \partial_\mu - igA^a_\mu T^a$ is the covariant derivative of QCD, and plug in

$$Q(x) = e^{-im_Q v\cdot x}h_v(x) + \mathcal{O}\left(\frac{1}{m_Q}\right) \tag{3.2.10}$$

to find

$$\begin{aligned}
\mathcal{L}_{\text{QCD}} &= \left(e^{im_Q v\cdot x}\overline{h}_v(x) + \mathcal{O}\left(\frac{1}{m_Q}\right)\right)(i\gamma_\mu D^\mu - m_Q)\left(e^{-im_Q v\cdot x}h_v(x) + \mathcal{O}\left(\frac{1}{m_Q}\right)\right)\\
&= \overline{h}_v(x)i\gamma_\mu D^\mu h_v(x) + \mathcal{O}\left(\frac{1}{m_Q}\right)\\
&= \overline{h}_v(x)P_+ i\gamma_\mu D^\mu P_+ h_v(x) + \mathcal{O}\left(\frac{1}{m_Q}\right)\\
&= \overline{h}_v(x)iv\cdot Dh(x) + \mathcal{O}\left(\frac{1}{m_Q}\right).
\end{aligned} \tag{3.2.11}$$

Here we used that fact that $P_+h_v = h_v$, which entails $\not{v}h_v = h_v$ and $P_+\gamma_\mu P_+ = v^\mu$. Then we can read off the HQET Lagrangian at LO,

$$\mathcal{L}^{\text{LO}}_{\text{HQET}} = \overline{h}_v(x)iv\cdot Dh_v(x). \tag{3.2.12}$$

This Lagrangian leads to the propagator $i/(v\cdot k + i\epsilon)$ we already derived in the heavy quark limit and the quark gluon vertex $igT^a v^\mu A^a_\mu$. Its classical equation of motion is given by

$$iv\cdot Dh_v(x) = 0, \tag{3.2.13}$$

which is often useful in the simplification of matrix elements, even though at higher orders subtleties may arise.
In order to include the $1/m_Q$ corrections we have to include the small components of the heavy quark field as well. So we plug

$$Q(x) = e^{-im_Q v\cdot x}\left(h_v(x) + H_v(x)\right) \tag{3.2.14}$$

into the QCD Lagrangian to find

$$\begin{aligned}
\mathcal{L}_{\text{QCD}} &= e^{im_Q v\cdot x}\left(\overline{h}_v(x) + \overline{H}_v(x)\right)(i\gamma_\mu D^\mu - m_Q)\,e^{-im_Q v\cdot x}\left(h_v(x) + H_v(x)\right)\\
&= \overline{h}_v(x)iv\cdot Dh_v(x) - \overline{H}_v(x)\left(iv\cdot D + 2m_Q\right)H_v(x)\\
&\quad + \overline{h}_v(x)i\not{D}H_v(x) + \overline{H}_v(x)i\not{D}h_v(x).
\end{aligned} \tag{3.2.15}$$

It is convenient to project four vectors into components parallel and perpendicular to the velocity v. To this end we can replace the factors $i\not{D}$ by $i\not{D}_\perp$, where $D^\mu_\perp = D^\mu - v\cdot Dv^\mu$ is perpendicular to v. Then

$$\begin{aligned}
\mathcal{L}_{\text{QCD}} &= \overline{h}_v(x)iv\cdot Dh_v(x) - \overline{H}_v(x)\left(iv\cdot D + 2m_Q\right)H_v(x)\\
&\quad + \overline{h}_v(x)i\not{D}_\perp H_v(x) + \overline{H}_v(x)i\not{D}_\perp h_v(x).
\end{aligned} \tag{3.2.16}$$

We can eliminate the field H_v at the classical level by making use of its equation of motion,

$$(iv \cdot D + 2m_Q)\, H_v = i\not{D}_\perp h_v. \tag{3.2.17}$$

Then

$$H_v = \frac{1}{iv \cdot D + 2m_Q} i\not{D}_\perp h_v, \tag{3.2.18}$$

where we explicitly see that H_v is of order $1/m_Q$. We can insert this into the Lagrangian to find

$$\begin{aligned}\mathcal{L}_{\text{HQET}} &= \overline{h}_v iv \cdot D h_v + \overline{h}_v i\not{D}_\perp \frac{1}{iv \cdot D + 2m_Q} i\not{D}_\perp h_v \\ &= \overline{h}_v iv \cdot D h_v - \frac{1}{2m_Q} \overline{h}_v \not{D}_\perp \not{D}_\perp h_v + \mathcal{O}\left(\frac{1}{m_Q^2}\right).\end{aligned} \tag{3.2.19}$$

In the second line we expanded in $1/m_Q$. We can simplify this expression by using

$$\not{D}_\perp \not{D}_\perp = \gamma_\mu \gamma_\nu D_\perp^\mu D_\perp^\nu = D_\perp^2 + \frac{1}{2}\left[\gamma_\mu, \gamma_\nu\right] D_\perp^\mu D_\perp^\nu, \tag{3.2.20}$$

the identity $[D^\mu, D^\nu] = igG^{\mu\nu}$ and $\sigma_{\mu\nu} = i\left[\gamma_\mu, \gamma_\nu\right]/2$. Then

$$\not{D}_\perp \not{D}_\perp = D_\perp^2 + \frac{g}{2}\sigma_{\mu\nu} G^{\mu\nu}. \tag{3.2.21}$$

In the second term we do not have to include the $\perp$ labels because $\overline{h}_v \sigma_{\mu\nu} v^\mu h_v = 0$. By inserting the above relation into our Lagrangian eq. (3.2.19) it takes the form

$$\mathcal{L}_{\text{HQET}} = \mathcal{L}^{\text{LO}}_{\text{HQET}} + \mathcal{L}^{1}_{\text{HQET}} + \cdots \tag{3.2.22}$$

with

$$\begin{aligned}\mathcal{L}^1_{HQET} &= \frac{1}{2m_Q}\left(\mathcal{O}_K + \mathcal{O}_G\right) \\ &= -\overline{h}_v \frac{D_\perp^2}{2m_Q} h_v - g\overline{h}_v \frac{\sigma_{\mu\nu} G^{\mu\nu}}{4m_Q} h_v.\end{aligned} \tag{3.2.23}$$

The leading order Lagrangian corresponds to the heavy quark limit and respects the heavy quark symmetry.

This Lagrangian has the form of an effective Lagrangian we postulated in eq. (3.1.14). It is interesting to note now that the terms of order $1/m_Q$ explicitly violate the heavy quark symmetry of the leading order term. The operator $\mathcal{O}_K$ is independent of the heavy quark spin but explicitly depends on the heavy quark mass. The operator $\mathcal{O}_G$ depends on the heavy quark mass and has a Dirac structure so it also violates the heavy quark spin symmetry.

3.2.3 Effective States and Currents

It is convenient to have states independent of m_Q, since in the end we want to make the dependence of the matrix elements on m_Q explicit. To this end we define the states in the HQET to be eigenstates of the lowest order Hamiltonian and thus independent of m_Q. Note

that now the HQET states are not the same as the full QCD states anymore. They differ by $1/m_Q$ corrections and a normalization factor.

In full QCD the hadronic state $H(p)$ is normalized as

$$\langle H(p') \, | H(p) \rangle = 2E_p (2\pi)^3 \delta^3 \left(\boldsymbol{p} - \boldsymbol{p'} \right). \tag{3.2.24}$$

On the right–hand–side we see that the states depend on m_Q through $\boldsymbol{p} = m_Q \boldsymbol{v} + \boldsymbol{k}$. Since the lowest order in the HQET corresponds to the heavy quark limit, HQET states can be labeled with a four velocity v and a residual momentum k, which satisfies $v \cdot k = 0$ because in the heavy quark limit the on–shell condition for the heavy quark is given by

$$m_Q^2 = \left(m_Q v^\mu + k^\mu \right)^2 = m_Q^2 + 2 m_Q v \cdot k + k^2 \tag{3.2.25}$$

and we can neglect the last term. The normalization convention for HQET then is

$$\langle H(v', k') \, | H(v, k) \rangle = 2 v^0 \delta_{vv'} (2\pi)^3 \delta^3 (\boldsymbol{k} - \boldsymbol{k'}). \tag{3.2.26}$$

The r.h.s. of this equation is independent of m_Q and thus the l.h.s. must be as well. The states of QCD and HQET are then related by

$$|H(p)\rangle = \sqrt{m_H} \left(|H(v)\rangle + \mathcal{O}\left(\frac{1}{m_Q} \right) \right), \tag{3.2.27}$$

where m_H denotes the hadron mass.

In order to find the $1/m_Q$ expansion of flavour changing currents like $\bar{c}(1-\gamma^5)b$ we note that now we have to introduce two effective fields

$$b \to h_v^b, \qquad c \to h_{v'}^c. \tag{3.2.28}$$

The relation between the QCD fields and the effective ones is found by inserting eq. (3.2.18) into eq. (3.2.14), which yields

$$\begin{aligned} Q(x) &= e^{-i m_Q v \cdot x} \left(1 + \frac{1}{iv \cdot D + 2m_Q} i \not{D}_\perp \right) h_v(x) \\ &= e^{-i m_Q v \cdot x} \left(1 + \frac{i \not{D}_\perp}{2m_Q} + \mathcal{O}\left(\frac{1}{m_b^2} \right) \right) h_v(x). \end{aligned} \tag{3.2.29}$$

By plugging this relation into the current $\bar{c} \Gamma b$ at NLO in the power corrections we find HQET current

$$h_{v'}^c \Gamma h_v^b + \frac{1}{2m_b} \overline{h}_{v'}^c \Gamma \left(i \not{D}_\perp \right) h_v^b + \frac{1}{2m_c} \overline{h}_{v'}^c \left(-i \overleftarrow{\not{D}}_\perp \right) \Gamma h_v^b + \mathcal{O}\left(\frac{1}{m_c^2}, \frac{1}{m_b^2} \right). \tag{3.2.30}$$

The arrow denotes that the derivative acts on the factor to its left. This notation is convenient because moving the Dirac matrix contained in $\not{D}$ around in general entails the appearance of extra terms.

Chapter 4

Inclusive Decays of B Mesons

In the study of semileptonic decays of B mesons one distinguishes decays in which all particles of the final state are resolved, i.e. exclusive decays, from decays in which only partial information on the final state is available, so-called inclusive decays.

In this chapter we focus on inclusive semileptonic $b \to c\ell\nu$ decays. This is to say that the only information we have about the identity of the hadronic part of the final state is that it contains a charm quark.

4.1 Why Study Inclusive B Decays?

At tree level in the SM the decay $b \to c\ell\nu$ is mediated by the flavour changing charged current Lagrangian in eq. (2.3.8). We can integrate out the W boson by faithfully repeating the steps in section 3.1 with the Lagrangian

$$\begin{aligned}\mathcal{L}_{b\to c\ell\nu} = \bar{c}i\not{\partial}c + \bar{b}i\not{\partial}b + \frac{g}{\sqrt{2}}\bar{\ell}\gamma_\mu\frac{1-\gamma_5}{2}\nu W^{+\mu} + \frac{gV_{cb}}{\sqrt{2}}\bar{c}\gamma_\mu\frac{1-\gamma_5}{2}bW^{-\mu} \\ - \frac{1}{2}\left(\partial_\mu W^+_\nu - \partial_\nu W^+_\mu\right)\left(\partial^\mu W^{-\nu} - \partial^\nu W^{+\mu}\right) + m_W^2 W^+_\mu W^{-\mu}. \end{aligned} \tag{4.1.1}$$

At dimension 6 we obtain the effective Hamiltonian

$$\mathcal{H}^{\text{eff}}_{\text{b}\to\text{c}\ell\nu} = \frac{4G_\text{F}V_{cb}}{\sqrt{2}}\left[\bar{c}\frac{1-\gamma_5}{2}\gamma_\mu b\right]\left[\bar{\ell}\frac{1-\gamma^5}{2}\gamma^\mu\nu\right], \tag{4.1.2}$$

which is related to the effective Lagrangian as $\mathcal{H}_{\text{eff}} = -\mathcal{L}_{\text{eff}}$. From this effective Hamiltonian we find the total inclusive $B(p) \to X_c(p-q)\ell(p_\ell)\nu(p_\nu)$ decay rate

$$\frac{\text{d}^3\Gamma}{\text{d}q^2\text{d}E_\ell dE_\nu} = \frac{G_\text{F}^2\left|V_{\text{cb}}\right|^2}{8\pi^3}W_{\mu\nu}L^{\mu\nu}\Theta\left(4E_\ell E_\nu - q^2\right)\Theta\left(q^2\right)\Theta\left(E_\ell\right)\Theta\left(E_\nu\right), \tag{4.1.3}$$

where $q = p_\ell + p_\nu$ is the four momentum of the lepton pair and E_ℓ and E_ν are the energies of the charged lepton and the neutrino, respectively. A detailed derivation of this expression can be found in appendix A.1.

Here we can see that the inclusive B meson decay rate is proportional to the squared modulus of the CKM matrix element V_{cb}. Thus $|V_{cb}|$ can be extracted from measurements of the inclusive B meson decay rate. The main challenge in this endeavor is the computation of the hadronic tensor $W^{\mu\nu}$, which describes the non-perturbative dynamics. It can be computed

in an OPE framework [83, 105, 197]. The OPE allows for a parametrization of the inclusive decay rate in terms of hadronic matrix elements which are then determined by fitting moments of kinematical distributions to experimental measurements.

Similarly $|V_{cb}|$ can be measured in exclusive decays, in which the full final state is known. Interestingly the value which are obtained from the inclusive and exclusive determinations of V_{cb} are not compatible. Indeed recent determinations found

$$\begin{aligned} \left|V_{cb}^{\text{incl}}\right| &= (42.16 \pm 0.51) \times 10^{-3} \quad [88] \\ \left|V_{cb}^{\text{excl}}\right| &= (39.36 \pm 0.68) \times 10^{-3} \quad [47] \end{aligned} \tag{4.1.4}$$

so there is a $\sim 3\sigma$ discrepancy. The situation is summarized in fig. 4.1.1.

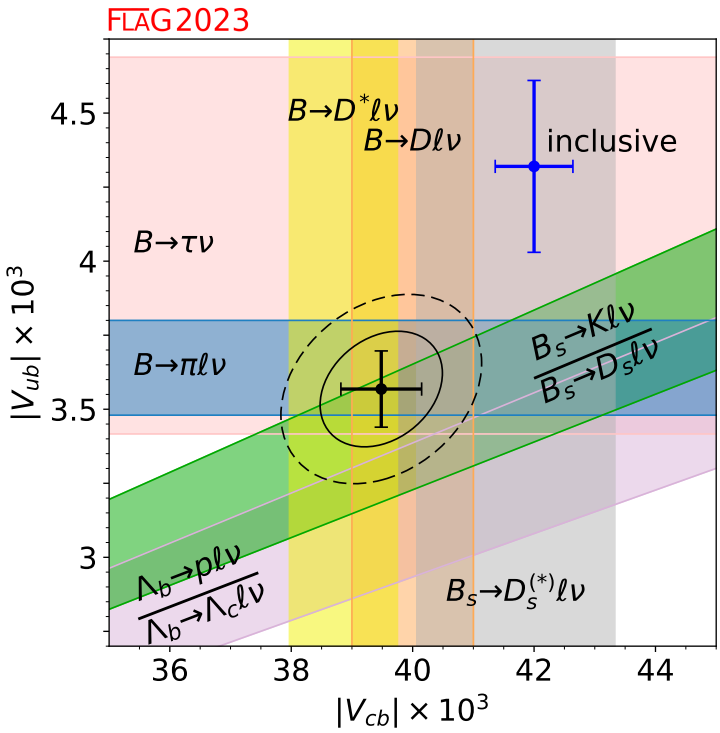

Figure 4.1.1: Overview plot of the inclusive and exclusive determinations of V_{cb} and V_{ub} from the FLAG review 2021 [47].

This V_{cb} puzzle has received a lot of attention over the last decade, recent reviews can be found in [43, 141, 146, 225]. Nevertheless it has not been resolved so far. Since it is unlikely that this tension is due to NP [111], improving the precision of V_{cb} necessitates independent checks of the methods used in the exclusive and inclusive determination of V_{cb}.

After a general introduction of the inclusive observables and their computation within the OPE framework its predictions are tested against new lattice QCD predictions in chapter 5 and in chapter 6 we compute the effects of dimension 8 operators in the weak Lagrangian of eq. (4.1.2).

4.2 Generalities

4.2.1 Inclusive Observables

As stated in the last section the observables in inclusive semileptonic decays of B mesons are the total decay rate

$$\Gamma = \int \mathrm{d}E_\ell \mathrm{d}q^2 \mathrm{d}E_\nu \frac{\mathrm{d}^3\Gamma}{\mathrm{d}E_\ell \mathrm{d}q^2 \mathrm{d}E_\nu} \tag{4.2.1}$$

and the spectra of the charged lepton energy E_ℓ, the hadronic invariant mass m_X^2 and the invariant mass of the lepton pair q^2. The shape of the spectra is parametrized by the moments

$$\langle x^n \rangle = \frac{1}{\Gamma} \int \mathrm{d}E_\ell \mathrm{d}q^2 \mathrm{d}E_\nu x^n \frac{\mathrm{d}^3\Gamma}{\mathrm{d}E_\ell \mathrm{d}q^2 \mathrm{d}E_\nu}, \tag{4.2.2}$$

where $x \in \{E_\ell, m_X^2, q^2\}$. From these one builds the central moments

$$\mathcal{X}_n = \begin{cases} \langle x \rangle \,, \text{ for } n = 1 \\ \langle (x - \langle x \rangle)^n \rangle \,, \text{ for } n > 1 \end{cases} \tag{4.2.3}$$

the first of which corresponds to the mean value of the spectrum, the second corresponds to its variance and the third one corresponds to its skewness.

The moments of E_ℓ and q^2 can be evaluated directly. For the hadronic invariant mass moments we have to relate hadronic variables to parton-level variables because the B meson and the b quark have different momenta. We relate the hadronic quantity m_X to the parton-level quantities $\hat{u} = \left((p-q)^2 - m_c^2\right)^2 / m_b^2$ and $\hat{\omega} = 1 - q_0/m_b$, where $q = (q_0, \boldsymbol{q})$, by the fact that in the HQE the B meson and the b quark have the same four-velocity v. From now on all quantities with a hat are made dimensionless by dividing by an appropriate power of m_b, e.g. $\boldsymbol{q}^2 = m_b^2 \hat{\boldsymbol{q}}^2$. In terms of its velocity the hadronic final state mass is given by

$$m_X^2 = (p_B - q)^2 = m_B^2 - 2 m_B v \cdot q + q^2. \tag{4.2.4}$$

For the parton-level quantities we have

$$\begin{aligned} \hat{u} &= 1 - 2v \cdot \hat{q} + \hat{q}^2 - \rho \\ \hat{\omega} &= 1 - v \cdot \hat{q}, \end{aligned} \tag{4.2.5}$$

where we defined $\rho = m_c^2/m_b^2$. We use eq. (4.2.5) to replace q^2 and $v \cdot q$ in eq. (4.2.4) by parton-level quantities and obtain

$$m_X^2 = m_c^2 + \Lambda^2 + 2\Lambda m_b \hat{\omega} + m_b^2 \hat{u} \tag{4.2.6}$$

where $\Lambda = m_B - m_b$ is the mass difference between the B meson and the b quark mass. Therefore we obtain the hadronic invariant mass moments from the relation

$$\left\langle m_X^2 \right\rangle = m_c^2 + \Lambda^2 + 2\Lambda m_b \left\langle \hat{\omega} \right\rangle + m_b^2 \left\langle \hat{u} \right\rangle \tag{4.2.7}$$

after computing the moments of $\hat{u}$ and $\hat{\omega}$.

Because the moments are normalized to the decay rate they are independent of V_{cb}. In practice they are used to extract non-perturbative matrix elements which appear in the OPE for inclusive B decays from experimental data. As we will see explicitly in the following sections

the OPE for inclusive B decays results in a double expansion of observables in terms of powers of $\Lambda_{\rm QCD}/m_b$ and α_s. Any given inclusive observable M, that is to say the total decay rate or one of the moments defined above, then takes the form

$$\begin{aligned} M_i = M_i^{(0,0)} + \frac{\alpha_s}{\pi} M_i^{(1)} + \frac{\mu_\pi^2}{m_b^2}\left(M_i^{(\pi,0)} + \frac{\alpha_s}{\pi} M_i^{(\pi,1)}\right) \\ + \frac{\mu_G^2}{m_b^2}\left(M_i^{(G,0)} + \frac{\alpha_s}{\pi} M_i^{(G,1)}\right) + \frac{\rho_D^3}{m_b^3} M_i^{(D,0)} + \frac{\rho_{LS}^3}{m_b^3} M_i^{(LS,0)} + \cdots , \end{aligned} \tag{4.2.8}$$

where μ_π^2, μ_G^2, ρ_D^3 and ρ_{LS}^3 are non-perturbative matrix elements which will be properly defined in section 4.2.4. An overview of all available corrections of this expansion, their size and where to find them can be found in table A.8.1.

There have been many experimental studies of the inclusive observables introduced above. The charged lepton energy moments have been measured by the DELPHI [24], BaBar [51] and Belle [217] collaborations, the hadronic invariant mass moments have been measured by the BaBar [53,54], Belle [214], Belle II [28], CDF [29], CLEO [112] and DELPHI [24] collaborations and the q^2 moments have been measured by the Belle [218], Belle II [2] and CLEO [112] collaborations.

In the following sections we turn to the theoretical description of inclusive B decays before confronting them with experimental data.

4.2.2 The Triple Differential Decay Rate

In order to accommodate for general NP we generalize eq. (4.1.2) to

$$\mathcal{H}_{\rm eff}^{b\to c\ell\nu_{\ell'}} = \frac{4G_{\rm F}}{\sqrt{2}} V_{\rm cb} \sum_\Gamma \left[\bar{c}\left(c_\Gamma \Gamma + d_\Gamma \Gamma\gamma_5\right) b\right]\left[\bar{\ell}\left(a_\Gamma \Gamma + b_\Gamma \Gamma\gamma_5\right)\nu_{\ell'}\right], \tag{4.2.9}$$

allowing for all possible Dirac structures $\Gamma \in \{\mathbb{1}, \gamma_\mu, \sigma_{\mu\nu} = i\left[\gamma_\mu, \gamma_\nu\right]/2\}$. As the matrices $\mathbb{1}$, γ_μ, $\gamma_\mu\gamma_5$ and $\sigma_{\mu\nu}$ span the space of 4×4 matrices the product $\sigma_{\mu\nu}\gamma_5$ is redundant. We keep the corresponding terms to facilitate a comparison of our result with [107].

By following the steps from appendix A.1 we obtain the triple differential decay rate

$$\frac{d\Gamma\left(\overline{B}\to X_c \ell \overline{\nu}_\ell\right)}{dq^2 dE_\ell dE_\nu} = \frac{G_{\rm F}^2 \left|V_{cb}\right|^2}{8\pi^3} L_{\Gamma\Gamma'} W_{\Gamma\Gamma'} \tag{4.2.10}$$

with the hadronic and leptonic tensors

$$\begin{aligned} L_{\Gamma\Gamma'} &= \frac{1}{8}\sum_{s,s'} \left\langle \overline{\nu}_{s'} \ell_s^- \left| a_\Gamma \overline{\ell}\Gamma\nu + b_\Gamma \overline{\ell}\Gamma\gamma_5\nu \right| 0\right\rangle \left\langle \overline{\nu}_{s'} \ell_s^- \left| a_\Gamma \overline{\ell}\Gamma'\nu + b_\Gamma \overline{\ell}\Gamma'\gamma_5\nu \right| 0\right\rangle^\dagger \\ W_{\Gamma\Gamma'} &= \frac{(2\pi)^3}{2m_{\rm B}} \sum_{X_{\rm c}} \delta^4\left(p_{\rm B} - p_{X_{\rm c}} - p_\ell - p_{\nu_\ell}\right) \left\langle X_{\rm c}\left| c_\Gamma \overline{c}\Gamma b + d_\Gamma \overline{c}\Gamma\gamma_5 b\right| \overline{B}\right\rangle \left\langle X_{\rm c}\left| c_\Gamma \overline{c}\Gamma' b + d_\Gamma \overline{c}\Gamma'\gamma_5 b\right| \overline{B}\right\rangle^\dagger . \end{aligned} \tag{4.2.11}$$

We can compute the leptonic tensor directly by evaluating the spin sums. This computation

is straightforward and can be found in full in appendix A.2. We obtain

$$
\begin{aligned}
L_{1,1} &= 2\left(|a_{\mathrm{S}}|^2+|b_{\mathrm{P}}|^2\right)\left(q^2-m_\ell^2\right)\\
L_{\gamma^\mu\gamma^\nu} &= 2\left(|a_{\mathrm{V}}|^2+|b_{\mathrm{A}}|^2\right)\left(-g^{\mu\nu}\left(q^2-m_\ell^2\right)-4p_\ell^\mu p_\ell^\nu+4\left(p_\ell^\mu q^\nu+p_\ell^\nu q^\mu\right)\right)\\
&\quad+4i\mathrm{Re}\left(a_{\mathrm{V}}b_{\mathrm{A}}^*\right)\epsilon^{\mu\nu\alpha\beta}p_{\ell,\alpha}q_\beta\\
L_{\sigma^{\kappa\lambda}\sigma\rho\tau} &= \left(|a_{\mathrm{T}}|^2+|b_{\mathrm{T}_5}|^2\right)\Big(\left(g^{\kappa\tau}g^{\lambda\rho}-g^{\kappa\rho}g^{\lambda\tau}\right)\left(m_\ell^2+q^2\right)\\
&\qquad+4\left(p_\ell^\kappa\left(p_\ell^\rho g^{\lambda\tau}-p_\ell^\tau g^\lambda\rho\right)+p_\ell^\lambda\left(p_\ell^\tau g^{\kappa\rho}-p_\ell^\rho g^{\kappa\tau}\right)\right)\\
&\qquad+2g^{\kappa\tau}\left(p_\ell^\kappa q^\rho+p_\ell^\rho q^\lambda\right)-2g^{\lambda\tau}\left(p_\ell^\kappa q^\rho+p_\ell^\rho q^\kappa\right)\\
&\qquad-2g^{\kappa\rho}\left(p_\ell^\lambda q^\tau+p_\ell^\tau q^\lambda\right)+2g^{\lambda\rho}\left(p_\ell^\kappa q^\tau+p_\ell^\tau q^\kappa\right)\Big)\\
&\quad-4i\mathrm{Re}\left(a_{\mathrm{T}}b_{\mathrm{T}_5}^*\right)\Big(\left(p_\ell^\lambda\epsilon^{\kappa\rho\tau\alpha}-p_\ell^\kappa\epsilon^{\lambda\rho\tau\alpha}+p_\ell^\rho\epsilon^{\kappa\lambda\tau\alpha}-p_\ell^\tau\epsilon^{\kappa\lambda\rho\alpha}\right)p_{\ell,\alpha}\\
&\qquad+\left(q^\tau\epsilon^{\kappa\lambda\rho\alpha}-q^\rho\epsilon^{\kappa\lambda\tau\alpha}\right)p_{\ell,\alpha}+\left(p_\ell^\kappa\epsilon^{\lambda\rho\tau\alpha}-p_\ell^\lambda\epsilon^{\kappa\rho\tau\alpha}\right)q_\alpha\Big)\\
L_{1,\gamma^\mu} &= 2m_\ell\left(a_{\mathrm{S}}a_{\mathrm{V}}^*+b_{\mathrm{P}}b_{\mathrm{A}}^*\right)\left(q^\mu-p_\ell^\mu\right)\\
L_{\gamma^\mu,1} &= L_{1,\gamma^\mu}^*\\
L_{1,\sigma\kappa\lambda} &= 2i\left(a_{\mathrm{S}}a_{\mathrm{T}}^*+b_{\mathrm{P}}b_{\mathrm{T}_5}^*\right)\left(p_\ell^\lambda q^\kappa-p_\ell^\kappa q^\lambda\right)-2\left(a_{\mathrm{S}}b_{\mathrm{T}_5}^*+b_{\mathrm{P}}a_{\mathrm{T}}^*\right)\epsilon^{\kappa\lambda\alpha\beta}p_{\ell,\alpha}q_\beta\\
L_{\sigma^{\kappa\lambda},1} &= L_{1,\sigma^{\kappa\lambda}}^*\\
L_{\gamma^\mu,\sigma^{\kappa\lambda}} &= 2m_\ell\Big(i\left(a_{\mathrm{V}}a_{\mathrm{T}}^*+b_{\mathrm{A}}b_{\mathrm{T}_5}^*\right)\left(g^{\mu\kappa}p_\ell^\lambda-g^{\mu\lambda}p_\ell^\kappa+g^{\mu\lambda}q^\kappa-g^{\mu\kappa}q^\lambda\right)\\
&\qquad+\left(a_{\mathrm{V}}b_{\mathrm{T}_5}^*+b_{\mathrm{A}}a_{\mathrm{T}}^*\right)\left(\epsilon^{\kappa\lambda\mu\alpha}p_{\ell,\alpha}-\epsilon^{\kappa\lambda\mu\alpha}q_\alpha\right)\Big)\\
L_{\sigma^{\kappa\lambda},\gamma^\mu} &= L_{\gamma^\mu,\sigma^{\kappa\lambda}}^*.
\end{aligned}
\tag{4.2.12}
$$

The SM can be found from this general expression by setting $a_V = -b_A = 1/2$ and $a_i = b_i = 0$ for all the other Wilson coefficients, yielding the well known result

$$
L_{\mathrm{SM}} = -g^{\mu\nu}\left(q^2-m_\ell^2\right)-4p_\ell^\mu p_\ell^\nu+4\left(p_\ell^\mu q^\nu+p_\ell^\nu q^\mu\right)-i\epsilon^{\mu\nu\alpha\beta}p_{\ell,\alpha}q_\beta. \tag{4.2.13}
$$

As the hadronic tensor cannot be computed directly, we start by parametrizing it in terms of Lorentz invariant structure functions and deal with the problem of finding the structure functions subsequently. We can decompose the hadronic tensor as

$$
\begin{aligned}
W_{1,1} &= w_0\\
W_{\gamma^\mu\gamma^\nu} &= -g^{\mu\nu}w_1+v^\mu v^\nu w_2+i\epsilon^{\mu\nu\alpha\beta}v_\alpha\hat{q}_\beta w_3+\hat{q}^\mu\hat{q}^\nu w_4+\left(v^\mu\hat{q}^\nu+v^\nu\hat{q}^\mu\right)w_5\\
W_{\sigma^{\kappa\lambda}\sigma^{\rho\tau}} &= \left(v^\kappa\hat{q}^\lambda-v^\lambda\hat{q}^\kappa\right)\left(v^\rho\hat{q}^\tau-v^\tau\hat{q}^\rho\right)w_6+\left(g^{\kappa\rho}g^{\lambda\tau}-g^{\kappa\tau}g^{\lambda\rho}\right)w_7\\
&\quad+\left(v^\kappa\left(v^\tau g^{\lambda\rho}-v^\rho g^{\lambda\tau}\right)-v^\lambda\left(v^\tau g^{\kappa\rho}-v^\rho g^{\kappa\tau}\right)\right)w_8\\
&\quad+\left(\hat{q}^\kappa\left(\hat{q}^\tau g^{\lambda\rho}-\hat{q}^\rho g^{\lambda\tau}\right)-\hat{q}^\lambda\left(\hat{q}^\tau g^{\kappa\rho}-\hat{q}^\rho g^{\kappa\tau}\right)\right)w_9\\
&\quad+\left(g^{\kappa\tau}\left(v^\lambda\hat{q}^\rho+v^\rho\hat{q}^\lambda\right)-g^{\lambda\tau}\left(v^\kappa\hat{q}^\rho+v^\rho\hat{q}^\kappa\right)-g^{\kappa\rho}\left(v^\lambda\hat{q}^\tau+v^\tau\hat{q}^\lambda\right)+g^{\lambda\rho}\left(v^\kappa\hat{q}^\tau+v^\tau\hat{q}^\kappa\right)\right)w_{10}\\
&\quad+i\left(v^\kappa\epsilon^{\lambda\rho\tau\alpha}-v^\lambda\epsilon^{\kappa\rho\tau\alpha}-v^\rho\epsilon^{\kappa\lambda\tau\alpha}+v^\tau\epsilon^{\kappa\lambda\rho\alpha}\right)\left(v_\alpha w_{11}+\hat{q}_\alpha w_{12}\right)\\
&\quad+i\left(\hat{q}^\kappa\epsilon^{\lambda\rho\tau\alpha}-\hat{q}^\lambda\epsilon^{\kappa\rho\tau\alpha}-\hat{q}^\rho\epsilon^{\kappa\lambda\tau\alpha}+\hat{q}^\tau\epsilon^{\kappa\lambda\rho\alpha}\right)\left(v_\alpha w_{13}+\hat{q}_\alpha w_{14}\right)\\
&\quad+\epsilon^{\kappa\lambda\rho\tau}w_{15}\\
W_{1\gamma^\mu} &= \hat{q}^\mu w_{16}+v^\mu w_{17}
\end{aligned}
$$

$$
\begin{aligned}
W_{1\sigma^{\kappa\lambda}} &= i\left(v^\kappa \hat{q}^\lambda - v^\lambda \hat{q}^\kappa\right) w_{18} + \epsilon^{\kappa\lambda\alpha\beta} v_\alpha \hat{q}_\beta w_{19} \\
W_{\gamma^\mu \sigma^{\kappa\lambda}} &= i\left(g^{\mu\kappa} v^\lambda - g^{\mu\lambda} v^\kappa\right) w_{20} + i\left(g^{\mu\kappa}\hat{q}^\lambda - g^{\mu\lambda}\hat{q}^\kappa\right) w_{21} \\
&\quad + i\left(v^\kappa \hat{q}^\lambda - v^\lambda \hat{q}^\kappa\right)\left(v^\mu w_{22} + \hat{q}^\mu w_{23}\right) + \epsilon^{\mu\kappa\lambda\alpha}\left(v_\alpha w_{24} + \hat{q}_\alpha w_{25}\right)
\end{aligned} \tag{4.2.14}
$$

We can easily find a general expression for the differential decay rate by plugging the leptonic and hadronic tensors into eq. (4.2.10) but we have to be careful about how the Lorentz indices are contracted. In the effective Hamiltonian the Lorentz indices of the Dirac matrix Γ appearing in the hadronic current are contracted with the ones of the matrix Γ appearing in the leptonic current. Consequently in the differential decay rate the Lorentz indices of the matrix Γ appearing in the leptonic tensor are contracted with the ones of the matrix Γ in the hadronic tensor and analogously for Γ'. As an example the differential decay rate contains terms of the form $W_{\gamma^\mu\sigma^{\kappa\lambda}} L_{\gamma_\mu \sigma_{\kappa\lambda}}$ but no terms of the form $W_{\gamma^\mu\sigma^{\kappa\lambda}} L_{\sigma_{\mu\kappa}\gamma_\lambda}$. Keeping this in mind we contract the hadronic and leptonic tensors, finding

$$
\begin{aligned}
WL|_{S,S} &= \left(|a_S|^2 + |b_P|^2\right)\left(q^2 - m_\ell^2\right) w_0 \\
WL|_{V,V} &= \left(|a_V|^2 + |b_A|^2\right)\left[2\left(q^2 - m_\ell^2\right) w_1 + \left(m_\ell^2 - q^2 + 4E_\ell E_\nu\right) w_2\right. \\
&\qquad \left. + \frac{m_\ell^2\left(q^2 - m_\ell^2\right)}{m_b^2} w_4 + \frac{4 m_\ell^2 E_\nu}{m_b} w_5\right] \\
&\quad + 4\mathrm{Re}\left(a_V b_A^*\right) \frac{q^2\left(E_\ell - E_\nu\right) - m_\ell^2\left(E_\ell + E_\nu\right)}{m_b} w_3 \\
WL|_{T,T} &= 4\left(|a_T|^2 + |b_{T_5}|^2\right)\left[\left(\frac{q^2\left(E_\ell - E_\nu\right)^2 + m_\ell^4 - m_\ell^2\left(\left(E_\ell - E_\nu\right)^2 - 4E_\nu^2 + q^2\right)}{m_b^2}\right) w_6\right. \\
&\quad + \left(m_\ell^2 - q^2 + 8E_\ell E_\nu\right) w_8 + \frac{q^2 m_\ell^2 - 2m_\ell^4 + q^4}{m_b^2} w_9 \\
&\quad \left. + \frac{2\left(\left(q^2 - m_\ell^2\right)\left(E_\ell + E_\nu\right) + 4m_\ell^2 E_\nu\right)}{m_b} w_{10}\right] \\
&\quad - 16\mathrm{Re}\left(a_T b_{T_5}^*\right)\left[+ \left(m_\ell^2 - q^2 + 8E_\ell E_\nu\right) w_{11}\right. \\
&\quad \left. + \frac{\left(q^2 - m_\ell^2\right)\left(E_\ell + E_\nu\right) + 4m_\ell^2 E_\nu}{m_b}\left(w_{12} + w_{13}\right) + \frac{q^2 m_\ell^2 - 2m_\ell^4 + q^4}{m_b^2} w_{14}\right] \\
WL|_{S,V} &= 2m_\ell \mathrm{Re}\left(a_S a_V^* + b_P b_A^*\right)\left[\frac{q^2 - m_\ell^2}{m_b} w_{16} + 2E_\nu w_{17}\right] \\
WL|_{S,T} &= \frac{4\left(E_\ell\left(q^2 - m_\ell^2\right) - E_\nu\left(q^2 + m_\ell^2\right)\right)}{m_b}\left[\mathrm{Re}\left(\left(a_S a_T^* + b_P b_{T_5}^*\right) w_{18}\right)\right. \\
&\qquad \left. + \mathrm{Re}\left(\left(a_S b_{T_5}^* + b_P a_T^*\right) w_{19}\right)\right] \\
WL|_{V,T} &= 4m_\ell \mathrm{Re}\left(a_V a_T^* + b_A b_{T_5}^*\right)\left[6E_\nu w_{20} + \frac{3\left(q^2 - m_\ell^2\right)}{m_b} w_{21}\right. \\
&\qquad \left. - \frac{m_\ell^2 - q^2 + 2E_\nu\left(E_\ell + E_\nu\right)}{m_b} w_{22}\right.
\end{aligned}
$$

$$+\frac{E_\ell\left(q^2-m_\ell^2\right)-E_\nu\left(q^2+m_\ell^2\right)}{m_b^2}w_{23}\Bigg]$$
$$+12m_\ell\mathrm{Re}\left(a_V b_{T_5}^*+b_A a_T^*\right)\left[2E_\nu w_{24}+\frac{q^2-m_\ell^2}{m_b}w_{25}\right]., \tag{4.2.15}$$

where we denote the scalar and pseudoscalar WC by a_S and b_P, the vector and axial vector WC as a_V and b_A and the tensor WC as a_T and b_{T_5}, respectively.

Again we can set $a_V=-b_A=1/2$ and $a_i=b_i=0$ for all the other cases to recover the SM expression

$$W_{\mu\nu}L^{\mu\nu}=\left(q^2-m_\ell^2\right)w_1+\frac{\left(m_\ell^2-q^2+4E_\ell E_\nu\right)}{2}w_2+\frac{m_\ell^2\left(q^2-m_\ell^2\right)}{m_b^2}w_4$$
$$+\frac{4m_\ell^2E_\nu}{m_b}w_5+\frac{q^2\left(E_\ell-E_\nu\right)-m_\ell^2\left(E_\ell+E_\nu\right)}{m_b}w_3. \tag{4.2.16}$$

4.2.3 Operator Product Expansion

So far we have avoided the main complication in the computation of the inclusive B meson decay rate, namely the fact that the hadronic tensor contains long distance QCD effects. This problem can be dealt with by studying the forward scattering amplitude

$$T_{\Gamma\Gamma'}=-\frac{1}{m_B}i\int \mathrm{d}^4x e^{-iq\cdot x}\left\langle\overline{B}\left|T\left\{J_\Gamma^\dagger(x)J_{\Gamma'}(0)\right\}\right|\overline{B}\right\rangle, \tag{4.2.17}$$

where $J_\Gamma(x)=\overline{c}(x)\left(c_\Gamma\Gamma+d_\Gamma\Gamma\gamma_5\right)b(x)$.

This amplitude has the same Lorentz structure as the hadronic tensor, hence it has a decomposition into Lorentz invariant structure functions t_i analogous to eq. (4.2.14). The structure functions t_i are related to the functions w_i by the optical theorem [105,215], yielding

$$w_i=-\frac{1}{\pi}\mathrm{Im}\left(t_i\right). \tag{4.2.18}$$

In order to evaluate the imaginary part we note that at the leading order in α_s the matrix element of the forward scattering amplitude between two b quark states with momentum $m_b v+k$ is given by [197]

$$\overline{u}\frac{\left(c_\Gamma^*-d_\Gamma^*\gamma_5\right)\Gamma\left(m_b\not{v}-\not{q}+\not{k}+m_c\right)\Gamma'\left(c_{\Gamma'}+d_{\Gamma'}\gamma_5\right)}{\left(m_b v-q+k\right)^2-m_c^2+i\epsilon}u \tag{4.2.19}$$

where u is a quark spinor. In fig. 4.2.1 the corresponding Feynman diagram is shown. The

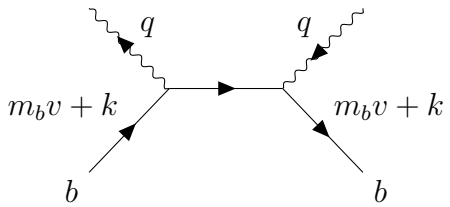

Figure 4.2.1: Forward scattering amplitude

momentum k is of order $\Lambda_{\mathrm{QCD}}\ll m_b$. Therefore we can expand the matrix element eq. (4.2.19)

in powers of k. This way we obtain an expansion in powers of $\Lambda_{\rm QCD}/m_b$ because operators of higher mass dimension are suppressed by powers of m_b.

At the leading order in k the amplitude is given by

$$\begin{aligned}&\frac{1}{\Delta_0}\left(m_b v-q\right)_\alpha \overline{u}\left(c_\Gamma^*-d_\Gamma^*\gamma_5\right)\Gamma\gamma^\alpha\Gamma'\left(c_{\Gamma'}+d_{\Gamma'}\gamma_5\right)u\\&+\frac{m_c}{\Delta_0}\overline{u}\left(c_\Gamma^*-d_\Gamma^*\gamma_5\right)\Gamma\Gamma'\left(c_{\Gamma'}+d_{\Gamma'}\gamma_5\right)u\end{aligned}\tag{4.2.20}$$

where we defined

$$\Delta_0=m_b^2v^2+q^2-2m_bv\cdot q-m_c^2+i\epsilon.\tag{4.2.21}$$

We then get the OPE by replacing the quark spinor u with the field b. This is because at the LO we only have terms of the form $\overline{u}\gamma^\mu u=\langle b|\bar{b}\gamma^\mu b|b\rangle$ and $\overline{u}\gamma^\mu\gamma_5 u=\langle b|\bar{b}\gamma^\mu\gamma_5 b|b\rangle$. Consequently the forward scattering amplitude defined in eq. (4.2.17) is given by

$$\begin{aligned}T_{\Gamma\Gamma'}=&\frac{\left(m_bv-q\right)_\alpha}{2m_B\Delta_0}\left\langle\overline{B}\left|\bar{b}\left(c_\Gamma^*-d_\Gamma^*\gamma_5\right)\Gamma\gamma^\alpha\Gamma'\left(c_{\Gamma'}+d_{\Gamma'}\gamma_5\right)b\right|\overline{B}\right\rangle\\&+\frac{m_c}{2m_B\Delta_0}\left\langle\overline{B}\left|\bar{b}\left(c_\Gamma^*-d_\Gamma^*\gamma_5\right)\Gamma\Gamma'\left(c_{\Gamma'}+d_{\Gamma'}\gamma_5\right)b\right|\overline{B}\right\rangle+\mathcal{O}\left(\frac{\Lambda_{\rm QCD}}{m_b}\right).\end{aligned}\tag{4.2.22}$$

The hadronic matrix elements appearing in this expression can be computed in HQET. We find for the matrix elements without γ_5

$$\begin{aligned}\left\langle\overline{B}\left|\bar{b}b\right|\overline{B}\right\rangle&=2m_B\\\left\langle\overline{B}\left|\bar{b}\gamma^\mu b\right|\overline{B}\right\rangle&=2p_B^\mu=2m_Bv^\mu\\\left\langle\overline{B}\left|\bar{b}\gamma^\mu\gamma^\nu b\right|\overline{B}\right\rangle&=2m_Bg^{\mu\nu},\end{aligned}\tag{4.2.23}$$

while the others vanish. Using eq. (4.2.23) it is then straightforward to compute the t_i functions. As the full computation is a bit lengthy it can be found in appendices A.5 and A.6.

It turns out that all the functions t_i get an imaginary part from the factor Δ_0^{-1} they are proportional to. Their imaginary parts can be computed by making use of the relation

$$\frac{1}{\omega+i\varepsilon}=\mathrm{P}\frac{1}{\omega}-i\pi\delta\left(\omega\right),\tag{4.2.24}$$

where P denotes the Cauchy principal value. Using this relation we find

$$\begin{aligned}\mathrm{Im}\frac{1}{\Delta_0}&=-\pi\delta\left(\left(p_b-q\right)^2-m_c^2\right)\\&=-\pi\delta\left(-2m_b\left(v\cdot q-\frac{m_b^2+q^2-m_c^2}{2m_b}\right)\right)\\&=-\frac{\pi}{2m_b}\delta\left(v\cdot q-\frac{m_b^2+q^2-m_c^2}{2m_b}\right)\\&=-\frac{\pi}{2m_b}\delta\left(E_\nu+E_\ell-\frac{m_b^2+q^2-m_c^2}{2m_b}\right).\end{aligned}\tag{4.2.25}$$

Therefore the structure functions w_i are given by eq. (A.6.22) with the replacement

$$\Delta_0^{-1}\to\frac{1}{2m_b}\delta\left(E_\nu+E_\ell-\frac{m_b^2+q^2-m_c^2}{2m_b}\right).\tag{4.2.26}$$

We can plug them into eq. (4.2.10), with $W_{\Gamma\Gamma'}L_{\Gamma\Gamma'}$ from eq. (4.2.15) to obtain the full triple differential decay rate.

Observables can then be calculated by integrating the triple differential decay rate over the kinematical variables. In appendix A.7 the complete double differential decay rate including general NP can be found. In the following we restrict ourselves to the SM case and finish developing the OPE framework by going beyond the leading order, before applying it in a study of a new method for computing inclusive observables on the lattice.

4.2.4 Higher Order Corrections

In eq. (4.2.20) we expanded eq. (4.2.19) to the order k^0. In this section we will see that at this order the Heavy Quark Expansion (HQE) exactly reproduces the decay of a free b quark. If we want to take non-perturbative effects, originating in the confinement of the heavy quark inside the meson, into account, we have to go to higher orders in this expansion. In order to facilitate the treatment of the higher order corrections from now on we will restrict ourselves to the SM case with light leptons, i.e. $\ell \in \{e, \mu\}$, in the final state. In this case the triple differential decay rate from eqs. (4.2.10) and (4.2.16) simplifies to

$$\frac{8\pi^3}{G_F^2 \left|V_{cb}\right|^2} \frac{\mathrm{d}^3\Gamma}{\mathrm{d}E_\ell \mathrm{d}q^2 \mathrm{d}E_\nu} = q^2 w_1 + \frac{(4E_\ell E_\nu - q^2)}{2} w_2 + \frac{q^2\,(E_\ell - E_\nu)}{m_b} w_3 \tag{4.2.27}$$

A useful property of the HQE is that there are no terms which are suppressed by only one power of the heavy quark mass m_b [189]. In our case this can be seen by expanding eq. (4.2.19) to linear order in k. Then one obtains the operators $\bar{b}\gamma_\mu i D_\nu b$ and $\bar{b}\gamma_\mu\gamma_5 i D_\nu b$ in the OPE. When the b fields are replaced by their leading order HQET counterparts the matrix elements of the latter vanish by the parity conservation of QCD while the former operator will have a vanishing matrix element by the HQET equation of motion eq. (3.2.13).

There are only non-vanishing contributions from these operators when the relation between QCD and HQET fields at order $1/m_b$ is used or, in other words, when they are suppressed by an additional power of the heavy quark mass.

The matrix elements of the higher dimensional operators cannot be computed from first principles like the ones appearing at the leading order because they contain non-perturbative dynamics. They can be parametrized in a minimal number of non-perturbative matrix elements however. At the order $\Lambda_{\mathrm{QCD}}^2/m_b^2$ one finds two matrix elements [83, 191, 197]

$$\begin{aligned} \mu_\pi^2 &= -\frac{1}{2m_B} \left\langle B \left| \bar{b}_v \left(i\vec{D}\right)^2 b_v \right| B \right\rangle \\ \mu_G^2 &= \frac{1}{2m_B} \left\langle B \left| \bar{b}_v \frac{i}{2} \sigma_{\mu\nu} G^{\mu\nu} b_v \right| B \right\rangle, \end{aligned} \tag{4.2.28}$$

where $b_v(x) = e^{i m_b v\cdot x} b(x)$ is the QCD b field without its high energy modes, D^μ is the covariant derivative and $G^{\mu\nu}$ is the gluon field strength tensor. At order $\Lambda_{\mathrm{QCD}}^3/m_b^3$ two more matrix elements,

$$\begin{aligned} \rho_D^3 &= \frac{1}{2m_B} \left\langle B \left| \bar{b}_v \left(iD_\mu\right) \left(iv\cdot D\right) \left(iD^\mu\right) b_v \right| B \right\rangle \\ \rho_{LS}^3 &= \frac{1}{2m_B} \left\langle B \left| \bar{b}_v \left(iD_\mu\right) \left(iv\cdot D\right) \left(iD_\nu\right) \left(-i\sigma^{\mu\nu}\right) b_v \right| B \right\rangle \end{aligned} \tag{4.2.29}$$

appear [78, 156].

As these matrix elements cannot be computed from first principles, with the notable exception of lattice QCD methods which are the topic of chapter 5, they are usually treated as free parameters and extracted from experimental data. This has been done for the above matrix elements [88]. But at order $\Lambda^4_{\text{QCD}}/m_b^4$ there are 9 new matrix elements and at order $\Lambda^5_{\text{QCD}}/m_b^5$ 18 new matrix elements appear [196]. This proliferation of non-perturbative matrix elements renders their extraction from data impossible.

One way to deal with this problem is the usage of a framework which allows one to find relations between the WC of matrix elements appearing at different orders in the HQE, such as Reparametrization Invariance (RPI) with which fits at order $\Lambda^4_{\text{QCD}}/m_b^4$ become possible [68,123] or the Lowest-Lying-State-Approximation (LLSA) [165, 196] which allows for an estimation of the matrix elements at $\Lambda^5_{\text{QCD}}/m_b^5$. Ultimately the sheer number of non-perturbative matrix elements at higher orders in the HQE will remain a challenge however.

To get more acquainted with the power correction up to $\mathcal{O}(\Lambda^3_{\text{QCD}}/m_b^3)$ we now compute the total tree-level $B \to X_c \ell \nu_\ell$ decay rate at this order using the structure functions at $\mathcal{O}(\Lambda^2_{\text{QCD}}/m_b^2)$ from [83] and at $\mathcal{O}(\Lambda^3_{\text{QCD}}/m_b^3)$ from [156].

In order to facilitate a comparison with lattice results later on we change variables from (E_ℓ, q^2, E_ν) to $(E_\ell, \hat{\boldsymbol{q}}^2, \hat{\omega})$, where $\hat{\boldsymbol{q}}^2 = (E_\ell + E_\nu)^2 - q^2$, $\omega = m_b - (E_\ell + E_\nu)$, before explicitly performing the phase space integration. Because the hadronic tensor is independent of the leptonic dynamics we can integrate eq. (4.2.27) over the charged lepton energy without any knowledge of the structure functions w_i. By doing this we obtain the double differential decay rate

$$m_b^3 \hat{X}\left(\hat{\omega}, \hat{\boldsymbol{q}}^2\right) = \frac{\mathrm{d}^2\Gamma}{\mathrm{d}\hat{\omega}\mathrm{d}\hat{\boldsymbol{q}}^2} = \frac{G_{\text{F}}^2 \left|V_{cb}\right|^2 m_b^3}{24\pi^3} \sqrt{\hat{\boldsymbol{q}}^2} \left(-3\left(\hat{\boldsymbol{q}}^2 - (1-\hat{\omega})^2\right) w_1 + \hat{\boldsymbol{q}}^2 w_2\right). \tag{4.2.30}$$

We write the inclusive decay rate as

$$\Gamma = \frac{G_{\text{F}}^2 \left|V_{cb}\right|^2 m_b^5}{24\pi^3} \int_0^{\hat{\boldsymbol{q}}^2_{\text{max}}} \mathrm{d}\hat{\boldsymbol{q}}^2 \sqrt{\hat{\boldsymbol{q}}^2}\, \overline{X}(\hat{\boldsymbol{q}}^2), \tag{4.2.31}$$

where $\hat{\boldsymbol{q}}^2_{\text{max}} = (1-\rho)^2/4$, $\rho = m_c^2/m_b^2$ and

$$\overline{X}(\hat{\boldsymbol{q}}^2) = \int_{\sqrt{\rho+\hat{\boldsymbol{q}}^2}}^{1-\sqrt{\hat{\boldsymbol{q}}^2}} \mathrm{d}\hat{\omega} \hat{X}\left(\hat{\omega}, \hat{\boldsymbol{q}}^2\right). \tag{4.2.32}$$

In the literature the differential decay rate is usually studied as a function of q_0 and q^2. We use different variables here because in our study of inclusive decays in Lattice QCD in chapter 5 we need the differential spectrum of $\boldsymbol{q}^2$.

NLO Power Corrections

Starting from the NLO in $1/m_b$ the structure functions t_i contain terms proportional to $1/u^2$ and $1/u^3$, where $u = \omega^2 - (\boldsymbol{q}^2 + m_c^2)$. Their imaginary parts are found by employing the identity

$$-\frac{1}{\pi}\mathrm{Im}\frac{1}{(u+i\epsilon)^n} = \frac{(-1)^{n-1}}{(n-1)!}\frac{\mathrm{d}^{n-1}}{\mathrm{d}u^{n-1}}\delta(u). \tag{4.2.33}$$

By integrating over $\hat{\omega}$ we find the $\boldsymbol{q}^2$-distribution

$$\begin{aligned}
\overline{\hat{X}}\left(\hat{\boldsymbol{q}}^2\right) &= \int_{\sqrt{\rho+\hat{\boldsymbol{q}}^2}}^{1-\sqrt{\hat{\boldsymbol{q}}^2}} \mathrm{d}\hat{\omega}\hat{X}\left(\hat{\omega},\hat{\boldsymbol{q}}^2\right) \\
&= \int_{-\infty}^{\infty}\mathrm{d}\hat{u}\frac{1}{2\sqrt{\hat{u}+\hat{\boldsymbol{q}}^2+\rho}}\Big[f^{(0)}\left(\hat{\omega}\left(\hat{u}\right),\hat{\boldsymbol{q}}^2\right)\delta\left(\hat{u}\right) \\
&\qquad - f^{(1)}\left(\hat{\omega}\left(\hat{u}\right),\hat{\boldsymbol{q}}^2\right)\delta'\left(\hat{u}\right)+\frac{1}{2}f^{(2)}\left(\hat{\omega}\left(\hat{u}\right),\hat{\boldsymbol{q}}^2\right)\delta''\left(\hat{u}\right)\Big] \\
&\qquad \times\Theta\left(\hat{q}^2\left(\hat{u}\right)\right) \\
&= \frac{1}{2}\int_{-\infty}^{\infty}\mathrm{d}\hat{u}\sum_{n=0}^{2}\frac{(-1)^n}{(n-1)!}\frac{\mathrm{d}^{(n)}}{\mathrm{d}\hat{u}^{(n)}}\left[\frac{f^{(n)}\left(\hat{\omega}\left(\hat{u}\right),\hat{\boldsymbol{q}}^2\right)}{\sqrt{\hat{u}+\hat{\boldsymbol{q}}^2+\rho}}\Theta\left(\hat{q}^2\left(\hat{u}\right)\right)\right]\delta\left(\hat{u}\right) \\
&= \frac{1}{2}\sum_{n=0}^{2}\frac{(-1)^n}{(n-1)!}\frac{\mathrm{d}^{(n)}}{\mathrm{d}\hat{u}^{(n)}}\left[\frac{f^{(n)}\left(\hat{\omega}\left(\hat{u}\right),\hat{\boldsymbol{q}}^2\right)}{\sqrt{\hat{u}+\hat{\boldsymbol{q}}^2+\rho}}\Theta\left(\hat{q}^2\left(\hat{u}\right)\right)\right]\Bigg|_{\hat{u}=0} \qquad (4.2.34)
\end{aligned}$$

where $\hat{q}^2\left(\hat{u}\right)=1+\rho+\hat{u}-2\sqrt{\hat{u}+\hat{\boldsymbol{q}}^2+\rho}$ and we decomposed $X=\sum_{l=0}^{2}X^{(l)}$ into terms proportional to $\delta(u)$, $\delta'(u)$ and $\delta''(u)$,

$$\begin{aligned}
\hat{X} =& f^{(0)}\left(\hat{\omega},\hat{\boldsymbol{q}}^2\right)\delta\left(\hat{u}\right)-f^{(1)}\left(\omega,\hat{\boldsymbol{q}}^2\right)\frac{\mathrm{d}}{\mathrm{d}\hat{u}}\delta\left(\hat{u}\right) \\
&+\frac{1}{2}f^{(2)}\left(\hat{\omega},\hat{\boldsymbol{q}}^2\right)\frac{\mathrm{d}^2}{\mathrm{d}\hat{u}^2}\delta\left(\hat{u}\right). \qquad (4.2.35)
\end{aligned}$$

Now the $\boldsymbol{q}^2$-spectrum contains terms proportional to the first second derivative of $\Theta\left(\hat{q}^2\left(\hat{u}\right)\right)$ with respect to $\hat{u}$. These are given by

$$\begin{aligned}
&\frac{\mathrm{d}}{\mathrm{d}\hat{u}}\Theta\left(1+\rho+\hat{u}-2\sqrt{\rho+\hat{\boldsymbol{q}}^2+\hat{u}}\right)\Big|_{\hat{u}=0} \\
&=\left(1-\frac{1}{\sqrt{\rho+\hat{\boldsymbol{q}}^2}}\right)\delta\left(1+\rho-2\sqrt{\rho+\hat{\boldsymbol{q}}^2}\right) \\
&=\left(1-\frac{1}{\sqrt{\rho+\hat{\boldsymbol{q}}^2}}\right)\frac{1+\rho}{2}\delta\left(\hat{\boldsymbol{q}}^2-\left(\frac{1-\rho}{2}\right)^2\right) \\
&=\frac{\rho-1}{2}\delta\left(\hat{\boldsymbol{q}}^2-\hat{\boldsymbol{q}}^2_{\max}\right) \qquad (4.2.36)
\end{aligned}$$

and

$$\begin{aligned}
&\frac{\mathrm{d}^2}{\mathrm{d}\hat{u}^2}\Theta\left(1+\rho+\hat{u}-2\sqrt{\rho+\hat{\boldsymbol{q}}^2+\hat{u}}\right)\Big|_{\hat{u}=0} \\
&=\frac{\delta\left(1+\rho-2\sqrt{\rho+\hat{\boldsymbol{q}}^2}\right)}{2\left(\rho+\hat{\boldsymbol{q}}^2\right)^{\frac{3}{2}}} \\
&\quad+\left(1-\frac{1}{\sqrt{\rho+\hat{\boldsymbol{q}}^2+\hat{u}}}\right)\frac{\mathrm{d}}{\mathrm{d}\hat{u}}\delta\left(1+\rho+\hat{u}-2\sqrt{\rho+\hat{\boldsymbol{q}}^2+\hat{u}}\right)\Big|_{\hat{u}=0}
\end{aligned}$$

$$= \frac{2\delta\left(\hat{\boldsymbol{q}}^2 - \hat{\boldsymbol{q}}^2_{\max}\right)}{(1+\rho)^2} + \frac{\left(\sqrt{\rho+\hat{\boldsymbol{q}}^2}-1\right)^2}{\rho+\hat{\boldsymbol{q}}^2}\delta'\left(1+\rho-2\sqrt{\rho+\hat{\boldsymbol{q}}^2}\right). \tag{4.2.37}$$

When integrated together with a test function g the last term yields

$$\begin{aligned}
&\int_0^{\frac{(1-\rho)^2}{4}} \mathrm{d}\hat{\boldsymbol{q}}^2 \frac{\left(\sqrt{\rho+\hat{\boldsymbol{q}}^2}-1\right)^2}{\rho+\hat{\boldsymbol{q}}^2} g\left(\hat{\boldsymbol{q}}^2\right)\delta'\left(1+\rho-2\sqrt{\rho+\hat{\boldsymbol{q}}^2}\right) \\
&= \int_{\left(1-\sqrt{\rho}\right)^2}^{0} \mathrm{d}x \frac{\mathrm{d}\hat{\boldsymbol{q}}^2}{\mathrm{d}x} \frac{\left(\sqrt{\rho+\hat{\boldsymbol{q}}^2(x)}-1\right)^2}{\rho+\hat{\boldsymbol{q}}^2(x)} g\left(\hat{\boldsymbol{q}}^2(x)\right)\delta'(x) \\
&= -\int_0^{\left(1-\sqrt{\rho}\right)^2} \mathrm{d}x \frac{\mathrm{d}\hat{\boldsymbol{q}}^2}{\mathrm{d}x} \frac{\left(\sqrt{\rho+\hat{\boldsymbol{q}}^2(x)}-1\right)^2}{\rho+\hat{\boldsymbol{q}}^2(x)} g\left(\hat{\boldsymbol{q}}^2(x)\right)\delta'(x) \\
&= \frac{\mathrm{d}}{\mathrm{d}x}\left[\frac{\mathrm{d}\hat{\boldsymbol{q}}^2}{\mathrm{d}x}\frac{\left(\sqrt{\rho+\hat{\boldsymbol{q}}^2(x)}-1\right)^2}{\rho+\hat{\boldsymbol{q}}^2(x)} g\left(\hat{\boldsymbol{q}}^2(x)\right)\right]_{x=0} \\
&= -\sqrt{\rho+\hat{\boldsymbol{q}}^2}\frac{\mathrm{d}}{\mathrm{d}\hat{\boldsymbol{q}}^2}\left[\frac{\mathrm{d}\hat{\boldsymbol{q}}^2}{\mathrm{d}x}\frac{\left(\sqrt{\rho+\hat{\boldsymbol{q}}^2}-1\right)^2}{\rho+\hat{\boldsymbol{q}}^2} g\left(\hat{\boldsymbol{q}}^2\right)\right]_{\hat{\boldsymbol{q}}^2=\hat{\boldsymbol{q}}^2_{\max}},
\end{aligned} \tag{4.2.38}$$

where $x = 1+\rho-2\sqrt{\rho+\hat{\boldsymbol{q}}^2}$ is the argument of the δ' function. After decomposing the $\hat{\boldsymbol{q}}^2$-distribution as

$$\hat{\overline{X}}\left(\hat{\boldsymbol{q}}^2\right) = \sum_{n=0}^{2} g^{(n)}\left(\hat{\boldsymbol{q}}^2\right)\left(\frac{\mathrm{d}}{\mathrm{d}\hat{u}}\right)^n \Theta\left(1+\rho+\hat{u}-2\sqrt{\rho+\hat{\boldsymbol{q}}^2+\hat{u}}\right)\Big|_{\hat{u}=0} \tag{4.2.39}$$

the total decay rate is given by

$$\begin{aligned}
\frac{\Gamma}{\Gamma_0} &= 8\int_0^{\hat{\boldsymbol{q}}^2_{\max}} \mathrm{d}\hat{\boldsymbol{q}}^2\sqrt{\hat{\boldsymbol{q}}^2}\sum_{n=0}^{2} g^{(n)}\left(\hat{\boldsymbol{q}}^2\right)\left(\frac{\mathrm{d}}{\mathrm{d}\hat{u}}\right)^n \Theta\left(1+\rho+\hat{u}-2\sqrt{\rho+\hat{\boldsymbol{q}}^2+\hat{u}}\right)\Big|_{\hat{u}=0} \\
&= 8\int_0^{\hat{\boldsymbol{q}}^2_{\max}} \mathrm{d}\hat{\boldsymbol{q}}^2\sqrt{\hat{\boldsymbol{q}}^2} g^{(0)}\left(\hat{\boldsymbol{q}}^2\right) + \left[\frac{\rho-1}{2}\sqrt{\hat{\boldsymbol{q}}^2} g^{(1)}\left(\hat{\boldsymbol{q}}^2\right) + \frac{2\sqrt{\hat{\boldsymbol{q}}^2} g^{(2)}\left(\hat{\boldsymbol{q}}^2\right)}{(1+\rho)^2}\right]\Big|_{\hat{\boldsymbol{q}}^2=\hat{\boldsymbol{q}}^2_{\max}} \\
&\quad - \sqrt{\rho+\hat{\boldsymbol{q}}^2}\frac{\mathrm{d}}{\mathrm{d}\hat{\boldsymbol{q}}^2}\left[\frac{\mathrm{d}\hat{\boldsymbol{q}}^2}{\mathrm{d}x}\frac{\left(\sqrt{\rho+\hat{\boldsymbol{q}}^2}-1\right)^2}{\rho+\hat{\boldsymbol{q}}^2} g^{(2)}\left(\hat{\boldsymbol{q}}^2\right)\right]_{\hat{\boldsymbol{q}}^2=\hat{\boldsymbol{q}}^2_{\max}} \\
&= f(\rho)\left(1+\frac{1}{2}\left(\mu_G^2-\mu_\pi^2\right)\right) - 2(1-\rho)^4\mu_G^2,
\end{aligned} \tag{4.2.40}$$

where $\Gamma_0 = G_{\mathrm{F}}^2\left|V_{cb}\right|^2 m_b^5/(192\pi^3)$ and $f(\rho) = (1-8\rho+8\rho^3-\rho^4-12\rho^2\log(\rho))$. This result coincides with the literature [83, 197].

NNLO Power Corrections

At $\mathcal{O}(1/m_b^3)$ the total decay rate is given by

$$\frac{\Gamma}{\Gamma_0} = 8\int_0^{\hat{\boldsymbol{q}}^2_{\max}} \mathrm{d}\hat{\boldsymbol{q}}^2 \sqrt{\hat{\boldsymbol{q}}^2} \sum_{n=0}^{3} g^{(n)}\left(\hat{\boldsymbol{q}}^2\right) \left(\frac{\mathrm{d}}{\mathrm{d}\hat{u}}\right)^n \Theta\left(1+\rho+\hat{u}-2\sqrt{\rho+\hat{\boldsymbol{q}}^2+\hat{u}}\right)\Bigg|_{\hat{u}=0}, \tag{4.2.41}$$

the difference to the first line of eq. (4.2.40) being that the sum over n now runs from 0 to 3 because at this order in the power expansion the structure functions t_i contain terms proportional to $1/(u+i\epsilon)^4$ which translate to terms proportional to the third derivative of a δ-function of u after taking the imaginary part. Once we move the derivatives away from the δ-functions by integrating by parts we encounter terms proportional to

$$\begin{aligned}\frac{\mathrm{d}^3}{\mathrm{d}\hat{u}^3}\Theta\left(1+\rho+\hat{u}-2\sqrt{\hat{u}+\hat{\boldsymbol{q}}^2+\rho}\right)\Big|_{\hat{u}=0} =& -\frac{12}{(\rho+1)^4}\delta\left(\hat{\boldsymbol{q}}^2-\hat{\boldsymbol{q}}^2_{\max}\right)\\ &+\frac{3\left(\sqrt{\hat{\boldsymbol{q}}^2+\rho}-1\right)}{2\left(\hat{\boldsymbol{q}}^2+\rho\right)^2}\delta'\left(1+\rho-2\sqrt{\hat{\boldsymbol{q}}^2+\rho}\right)\\ &+\left(\frac{\left(\sqrt{\hat{\boldsymbol{q}}^2+\rho}-1\right)}{\sqrt{\hat{\boldsymbol{q}}^2+\rho}}\right)^3\delta''\left(1+\rho-2\sqrt{\hat{\boldsymbol{q}}^2+\rho}\right).\end{aligned} \tag{4.2.42}$$

The integration of the second term together with a test function $g\left(\hat{\boldsymbol{q}}^2\right)$ is analogous to eq. (4.2.38),

$$\begin{aligned}&\frac{3}{2}\int_0^{\hat{\boldsymbol{q}}^2_{\max}}\mathrm{d}\hat{\boldsymbol{q}}^2\frac{\sqrt{\hat{\boldsymbol{q}}^2+\rho}-1}{\left(\hat{\boldsymbol{q}}^2+\rho\right)^2}g\left(\hat{\boldsymbol{q}}^2\right)\delta'\left(1+\rho-2\sqrt{\hat{\boldsymbol{q}}^2+\rho}\right)\\ &=-\frac{3}{2}\int_0^{\left(1-\sqrt{\rho}\right)^2}\mathrm{d}x\frac{\mathrm{d}\hat{\boldsymbol{q}}^2}{\mathrm{d}x}\frac{\sqrt{\hat{\boldsymbol{q}}\left(x\right)^2+\rho}-1}{\left(\hat{\boldsymbol{q}}\left(x\right)^2+\rho\right)^2}g\left(\hat{\boldsymbol{q}}\left(x\right)^2\right)\delta'\left(x\right)\\ &=-\frac{3}{2}\sqrt{\hat{\boldsymbol{q}}^2+\rho}\frac{\mathrm{d}}{\mathrm{d}\hat{\boldsymbol{q}}^2}\left[\frac{\mathrm{d}\hat{\boldsymbol{q}}^2}{\mathrm{d}x}\frac{\sqrt{\hat{\boldsymbol{q}}^2+\rho}-1}{\left(\hat{\boldsymbol{q}}^2+\rho\right)^2}g\left(\hat{\boldsymbol{q}}^2\right)\right]_{\hat{\boldsymbol{q}}^2=\hat{\boldsymbol{q}}^2_{\max}}.\end{aligned} \tag{4.2.43}$$

When we integrate the last term of eq. (4.2.42) together with a test function we obtain

$$\begin{aligned}&\int_0^{\hat{\boldsymbol{q}}_{\max}}\mathrm{d}\hat{\boldsymbol{q}}^2\left(\frac{\sqrt{\hat{\boldsymbol{q}}^2+\rho}-1}{\sqrt{\hat{\boldsymbol{q}}^2+\rho}}\right)^3 g\left(\hat{\boldsymbol{q}}^2\right)\delta''\left(1+\rho-1\sqrt{\hat{\boldsymbol{q}}^2+\rho}\right)\\ &=-\int_0^{\left(1-\sqrt{\rho}\right)^2}\mathrm{d}x\frac{\mathrm{d}\hat{\boldsymbol{q}}\left(x\right)^2}{\mathrm{d}x}\left(\frac{\sqrt{\hat{\boldsymbol{q}}\left(x\right)^2+\rho}-1}{\sqrt{\hat{\boldsymbol{q}}\left(x\right)^2+\rho}}\right)^3 g\left(\hat{\boldsymbol{q}}^2(x)\right)\delta''\left(x\right)\\ &=-\frac{\mathrm{d}^2}{\mathrm{d}x^2}\left[\frac{\mathrm{d}\hat{\boldsymbol{q}}\left(x\right)^2}{\mathrm{d}x}\left(\frac{\sqrt{\hat{\boldsymbol{q}}\left(x\right)^2+\rho}-1}{\sqrt{\hat{\boldsymbol{q}}\left(x\right)^2+\rho}}\right)^3 g\left(\hat{\boldsymbol{q}}^2(x)\right)\right]_{x=0}\\ &=-\left[\left(\frac{\mathrm{d}^2\hat{\boldsymbol{q}}^2}{\mathrm{d}x^2}\frac{\mathrm{d}}{\mathrm{d}\hat{\boldsymbol{q}}^2}+\left(\frac{\mathrm{d}\hat{\boldsymbol{q}}^2}{\mathrm{d}x}\right)^2\frac{\mathrm{d}^2}{\left(\mathrm{d}\hat{\boldsymbol{q}}^2\right)^2}\right)\left(\frac{\mathrm{d}\hat{\boldsymbol{q}}\left(x\right)^2}{\mathrm{d}x}\left(\frac{\sqrt{\hat{\boldsymbol{q}}\left(x\right)^2+\rho}-1}{\sqrt{\hat{\boldsymbol{q}}\left(x\right)^2+\rho}}\right)^3 g\left(\hat{\boldsymbol{q}}^2\right)\right)\right]_{\hat{\boldsymbol{q}}^2=\hat{\boldsymbol{q}}^2_{\max}}\end{aligned}$$

$$= \left[\left(\frac{1}{2} \frac{\mathrm{d}}{\mathrm{d}\hat{\boldsymbol{q}}^2} + \left(\hat{\boldsymbol{q}}^2 + \rho\right) \frac{\mathrm{d}^2}{\left(\mathrm{d}\hat{\boldsymbol{q}}^2\right)^2} \right) \left(\frac{\left(\sqrt{\hat{\boldsymbol{q}}\left(x\right)^2 + \rho} - 1 \right)^3}{\hat{\boldsymbol{q}}^2 + \rho} g\left(\hat{\boldsymbol{q}}^2\right) \right) \right]_{\hat{\boldsymbol{q}}^2 = \hat{\boldsymbol{q}}^2_{\mathrm{max}}} \tag{4.2.44}$$

Using this result we obtain

$$\begin{aligned}
\frac{\Gamma}{\Gamma_0} =& 8 \int_0^{\hat{\boldsymbol{q}}^2_{\mathrm{max}}} \mathrm{d}\hat{\boldsymbol{q}}^2 \sqrt{\hat{\boldsymbol{q}}^2} g^{(0)}\left(\hat{\boldsymbol{q}}^2\right) \\
&+ \left[\frac{\rho - 1}{2} \sqrt{\hat{\boldsymbol{q}}^2} g^{(1)}\left(\hat{\boldsymbol{q}}^2\right) + \frac{2\sqrt{\hat{\boldsymbol{q}}^2} g^{(2)}\left(\hat{\boldsymbol{q}}^2\right)}{(1+\rho)^2} - \frac{12}{(\rho+1)^4} g^{(3)}\left(\hat{\boldsymbol{q}}^2\right) \right] \Bigg|_{\hat{\boldsymbol{q}}^2 = \hat{\boldsymbol{q}}^2_{\mathrm{max}}} \\
&+ \sqrt{\rho + \hat{\boldsymbol{q}}^2} \frac{\mathrm{d}}{\mathrm{d}\hat{\boldsymbol{q}}^2} \left[\frac{\left(\sqrt{\rho + \hat{\boldsymbol{q}}^2} - 1 \right)^2}{\sqrt{\rho + \hat{\boldsymbol{q}}^2}} g^{(2)}\left(\hat{\boldsymbol{q}}^2\right) + \frac{3}{2} \frac{\sqrt{\hat{\boldsymbol{q}}^2 + \rho} - 1}{\left(\hat{\boldsymbol{q}}^2 + \rho\right)^{\frac{3}{2}}} g^{(3)}\left(\hat{\boldsymbol{q}}^2\right) \right]_{\hat{\boldsymbol{q}}^2 = \hat{\boldsymbol{q}}^2_{\mathrm{max}}} \\
&+ \left[\left(\frac{1}{2} \frac{\mathrm{d}}{\mathrm{d}\hat{\boldsymbol{q}}^2} + \left(\hat{\boldsymbol{q}}^2 + \rho\right) \frac{\mathrm{d}^2}{\left(\mathrm{d}\hat{\boldsymbol{q}}^2\right)^2} \right) \left(\frac{\left(\sqrt{\hat{\boldsymbol{q}}\left(x\right)^2 + \rho} - 1 \right)^3}{\hat{\boldsymbol{q}}^2 + \rho} g^{(3)}\left(\hat{\boldsymbol{q}}^2\right) \right) \right]_{\hat{\boldsymbol{q}}^2 = \hat{\boldsymbol{q}}^2_{\mathrm{max}}} \\
=& f(\rho) \left(1 + \frac{1}{2} \left(\left(\mu_G^2 + \frac{\rho_{\mathrm{LS}}^3}{3} \right) - \mu_\pi^2 \right) \right) - 2\left(1-\rho\right)^4 \left(\mu_G^2 + \frac{\rho_{\mathrm{LS}}^3}{3} \right) \\
&+ \frac{1}{6} \left(77 - 88\rho + 24\rho^2 - 8\rho^3 - 5\rho^4 + \left(48 + 36\rho^2\right) \log\left(\rho\right) \right) \rho_{\mathrm{D}}^3,
\end{aligned} \tag{4.2.45}$$

which agrees with [156].

The moments introduced in eq. (4.2.2) can be computed by weighting the triple differential decay rate with powers of the kinematical variable in question and faithfully repeating the steps above.

Radiative Corrections and Quark Masses

As we have seen before the OPE lets us separate long distance effects happening over distances $l \gg \Lambda_{\mathrm{QCD}}^{-1}$ from short distance effects. The long distance effects are encoded in the matrix elements of higher dimensional operators while the short distance effects are described by their Wilson Coefficients (WC). Being of a short distance nature, the WC have a perturbative expansion.

Analytical results for the one-loop corrections to the structure functions w_i, i.e. to the triple differential decay rate, have been computed a while ago [49]. At one-loop they take the form

$$w_i^{(1)} = w_{i,v}^{(1)} \delta\left(\hat{u}\right) + w_{i,+}^{(1)} \left[\frac{1}{\hat{u}} \right]_+ + w_{i,r}^{(1)}. \tag{4.2.46}$$

Here we distinguish the contributions of virtual gluons proportional to a delta function from the part of the real gluon emission which is proportional to a plus distribution defined by

$$\int_0^{\hat{u}} \mathrm{d}\hat{u} \left[\frac{1}{\hat{u}} \right]_+ f(\hat{u}) = \int_0^{\hat{u}} \mathrm{d}\hat{u} \frac{f\left(\hat{u}\right) - f(0)}{\hat{u}}, \tag{4.2.47}$$

where f is a test function, and the part of the real gluon emission contribution which contains neither a delta nor a plus distribution.

We find $\overline{X}(\hat{u}, \hat{\boldsymbol{q}}^2)$ at order α_s by plugging the results from [49] into eq. (4.2.30) and replacing $q^2 = 1 + \hat{u} + \rho - 2\sqrt{\hat{\boldsymbol{q}}^2 + \hat{u} + \rho}$ and $\hat{\omega} = \sqrt{\hat{u} + \hat{\boldsymbol{q}}^2 + \rho}$. The total decay rate is then found by integrating over $\hat{u}$ and $\hat{q}^2$:

$$\begin{aligned}
\frac{24\pi^3}{G_F \left|V_{cb}\right|^2 m_b^5}\Gamma &= \int_0^{\frac{(1-\rho)^2}{4}} \mathrm{d}\hat{\boldsymbol{q}}^2 \int_0^{1-2\sqrt{\hat{\boldsymbol{q}}^2}-\rho} \mathrm{d}\hat{u} \frac{\sqrt{\hat{\boldsymbol{q}}^2}}{\sqrt{\hat{u} + \hat{\boldsymbol{q}}^2 + \rho}} \hat{X}\left(\hat{u}, \hat{\boldsymbol{q}}^2\right) \\
&= \int_0^{\frac{(1-\rho)^2}{4}} \mathrm{d}\hat{\boldsymbol{q}}^2 \int_0^{1-2\sqrt{\hat{\boldsymbol{q}}^2}-\rho} \mathrm{d}\hat{u} \frac{\sqrt{\hat{\boldsymbol{q}}^2}}{\sqrt{\hat{u} + \hat{\boldsymbol{q}}^2 + \rho}} \Bigg[\hat{X}_{\mathrm{v}}\left(\hat{u}, \hat{\boldsymbol{q}}^2\right) \delta\left(\hat{u}\right) \\
&\qquad + \hat{X}_{+}\left(\hat{u}, \hat{\boldsymbol{q}}^2\right) \left[\frac{1}{\hat{u}}\right]_{+} + \hat{X}_{\mathrm{r}}\left(\hat{u}, \hat{\boldsymbol{q}}^2\right) \Bigg] \\
&= \int_0^{\frac{(1-\rho)^2}{4}} \mathrm{d}\hat{\boldsymbol{q}}^2 \frac{\sqrt{\hat{\boldsymbol{q}}^2}}{\sqrt{\hat{\boldsymbol{q}}^2 + \rho}} \hat{X}_{\mathrm{v}}\left(0, \hat{\boldsymbol{q}}^2\right) \\
&+ \int_0^{\frac{(1-\rho)^2}{4}} \mathrm{d}\hat{\boldsymbol{q}}^2 \int_0^{1-2\sqrt{\hat{\boldsymbol{q}}^2}-\rho} \mathrm{d}\hat{u} \frac{\sqrt{\hat{\boldsymbol{q}}^2}}{\hat{u}} \left[\frac{\hat{X}_{+}\left(\hat{u}, \hat{\boldsymbol{q}}^2\right)}{\sqrt{\hat{\boldsymbol{q}}^2 + \hat{u} + \rho}} - \frac{\hat{X}_{+}\left(0, \hat{\boldsymbol{q}}^2\right)}{\sqrt{\hat{\boldsymbol{q}}^2 + \rho}} \right] \\
&+ \int_0^{\frac{(1-\rho)^2}{4}} \mathrm{d}\hat{\boldsymbol{q}}^2 \int_0^{1-2\sqrt{\hat{\boldsymbol{q}}^2}-\rho} \mathrm{d}\hat{u} \frac{\sqrt{\hat{\boldsymbol{q}}^2}}{\sqrt{\hat{\boldsymbol{q}}^2 + \hat{u} + \rho}} \hat{X}_{\mathrm{r}}\left(\hat{u}, \hat{\boldsymbol{q}}^2\right). \qquad (4.2.48)
\end{aligned}$$

After numerically evaluating the last three integrals we recover the literature result [49]

$$\frac{\Gamma_{\mathcal{O}(\alpha_s)}}{\Gamma_0 f(\rho)} = -1.778. \qquad (4.2.49)$$

As the heavy quark masses get renormalized it is important to fix the scheme in which they are defined when radiative corrections are taken into account. A natural definition of the heavy quark masses is provided by the pole mass. It is defined as the zero of the inverse propagator at every order in perturbation theory. But this definition of the heavy quark mass suffers from an ambiguity of order Λ_{QCD}, a so-called renormalon ambiguity, which hampers the convergence of the perturbative series. Indeed in the relation between the pole mass and the $\overline{\mathrm{MS}}$ mass of the b quark the four-loop term still amounts to about 100 MeV [199]. The modified minimal subtraction, or $\overline{\mathrm{MS}}$ scheme, in which one absorbs the divergence plus a constant term appearing along with it into the counterterms, is commonly used in high energy computations. But because of the low energy scale of B meson decays, the energy of the final hadronic state is limited by $m_b - m_c$ and significantly reduced by the momentum carried away by the lepton pair, also this scheme is not ideal in this case. In fact we saw above that the total decay rate is proportional to m_b^5, which introduces large corrections in the conversion from the pole mass to the $\overline{\mathrm{MS}}$ mass.

Instead in inclusive calculations one usually defines the b quark mass in the kinetic scheme [76, 78]. The heavy quark mass is defined by its relation to the meson mass [125]:

$$m_Q(\mu) = M_H - \overline{\Lambda} - \frac{\mu_\pi^2}{2m_Q(\mu)} + \cdots \qquad (4.2.50)$$

The quantities $\overline{\Lambda}$ and μ_π^2 are related to the double differential decay rate by Small Velocity (SV) sum rules. These rules are obtained from moments of the hadronic final state energy in the limit where $|\boldsymbol{q}| \ll m_c \sim m_b$, additional to $\Lambda_{\rm QCD} \ll m_c \sim m_b$. The conversion between the kinetic scheme and the pole and $\overline{\rm MS}$ schemes has been computed at the three-loop level [124, 125].

For the charm quark the situation is different. Because of the lower charm mass the HQE is worse behaved than in the bottom case, which renders the definition of a kinetic m_c difficult. But as the scale of B decays is above the charm mass we can use the $\overline{\rm MS}$ mass scheme for m_c. At one-loop the relations between the pole mass scheme and the kinetic scheme for m_b are given by [142]

$$\begin{aligned} m_b^{\rm pole} &\equiv m_b^{\rm kin}(0) = m_b^{\rm kin}(\mu_b) + \frac{\alpha_s(\mu_b)}{\pi} C_F \mu_b \left(\frac{4}{3} + \frac{\mu_b}{2m_b^{\rm kin}}\right) \\ \mu_{\pi,\rm pole}^2 &= \mu_{\pi,\rm kin}^2(\mu_b) - C_F \mu_b^2 \frac{\alpha_s}{\pi} \\ \rho_{D,\rm pole}^3 &= \rho_{D,\rm kin}^3(\mu_b) - \frac{2}{3} C_F \mu_b^3 \frac{\alpha_s}{\pi}. \end{aligned} \tag{4.2.51}$$

while the relation between the pole mass and $\overline{\rm MS}$ mass for the charm quark is [124]

$$m_c^{\rm pole} = \left(1 + \frac{\alpha_s(\mu_c)}{\pi}\left(\frac{4}{3} + \ln\frac{\mu_c^2}{\overline{m}_c(\mu_c)^2}\right)\right)\overline{m}_c(\mu_c)\,, \tag{4.2.52}$$

where $C_F = \frac{4}{3}$.

4.3 Inclusive Decays in Lattice QCD

As mentioned above, non-perturbative effects in QCD, such as the HQE matrix elements, cannot be computed analytically from first principles. Numerically however it is possible to compute them by making use of Lattice QCD (LQCD) [222] simulations. Lattice computations provide a way of computing inclusive observables without relying on the HQE and can serve as an important check of the established HQE framework.

LQCD provides a regularization of QCD by discretizing Euclidean spacetime, related to Minkowski space by a Wick rotation, which is equivalent to introducing a momentum cutoff in the UV. In discrete spacetime formerly continuous momentum integrals are replaced by finite sums, rendering their values finite. Processes can be simulated on a lattice with a given spacing a and a volume $V = L^3 \times T$, where L corresponds to the spatial extent and T corresponds to the time extent of the lattice. Here a complication arises. Once the simulation is performed its results cannot directly be linked to physical observables. First their dependence on the lattice volume has to be studied, such that one can take their limit when $V \to \infty$. Secondly one also has to study their dependence on the lattice spacing in order to take the continuum limit $a \to 0$. These difficulties can be dealt with and lattice computations have become crucial in accessing non-perturbative objects like quark masses, form factors and decay constants. For a review on lattice results for flavour physics one may consult [45].

Most lattice computations concern exclusive processes, in which the exact final state is known as well as the initial state. Simulations of inclusive processes are more complicated because of the large number of possible intermediate states.

For inclusive decays of heavy mesons however a method of directly computing observables which circumvents this problem has been found recently [143, 164].

It is based on the observation that the hadronic matrix element

$$C_{\mu\nu}\left(\boldsymbol{q},t\right)=\frac{1}{2m_{B_s}}\left\langle B_s\left|\tilde{J}_\mu^\dagger\left(\boldsymbol{q},t\right)e^{-\hat{H}t}\tilde{J}_\nu\left(\boldsymbol{q},t\right)\right|B_s\right\rangle, \tag{4.3.1}$$

which can be computed on the lattice from four-point correlators, is related to the hadronic tensor through a Laplace transform:

$$C_{\mu\nu}\left(\boldsymbol{q},t\right)=\int_0^\infty \mathrm{d}\omega W_{\mu\nu}\left(\boldsymbol{q},\omega\right)e^{-\omega t} \tag{4.3.2}$$

Here the hadronic tensor is expressed in terms of the three-momentum $\boldsymbol{q}$ of the lepton pair and the energy ω energy of the hadronic final state X_c,

$$W_{\mu\nu}=\frac{1}{2m_{B_s}}\sum_{X_c}\delta\left(\omega-E_{X_c}\right)\left\langle B_s\left|\tilde{J}_\mu^\dagger\left(\boldsymbol{q},0\right)\right|X_c\right\rangle\left\langle X_c\left|\tilde{J}_\nu\left(\boldsymbol{q},0\right)\right|B_s\right\rangle. \tag{4.3.3}$$

Now inverting the integral on the r.h.s. of eq. (4.3.2) is an ill-posed problem so the hadronic tensor cannot be computed directly. But this is not necessary either if we are interested in inclusive observables. As the quantity $\overline{X}$ defined in eq. (4.2.32) is nothing else but the $\boldsymbol{q}^2$ spectrum we can write it in the form

$$\overline{X}\left(\boldsymbol{q}^2\right)=\int_{\omega_{\min}}^{\omega_{\max}}\mathrm{d}\omega k_{\mu\nu}\left(\boldsymbol{q},\omega\right)W^{\mu\nu}\left(\boldsymbol{q},\omega\right), \tag{4.3.4}$$

where $k_{\mu\nu}$ is a kinematical factor determined by the E_ℓ integral of the leptonic tensor. We can exchange the upper integration by a Heaviside function $\theta\left(\omega_{\max}-\omega\right)$ and the lower integration limit can be exchanged with any $0\leq\omega_0\leq\omega_{\min}$ thanks to the δ function in eq. (4.3.3). After doing this and defining $K_{\mu\nu}=\theta\left(\omega_{\max}-\omega\right)k_{\mu\nu}$ we obtain

$$\overline{X}\left(\boldsymbol{q}^2\right)=\int_{\omega_0}^{\infty}\mathrm{d}\omega K_{\mu\nu}\left(\boldsymbol{q},\omega\right)W^{\mu\nu}\left(\boldsymbol{q},\omega\right) \tag{4.3.5}$$

which looks very similar to eq. (4.3.2). Making use of the fact that we can approximate any smooth function $f\left(\omega\right)$ as

$$f\left(\omega\right)=\sum_\tau g_\tau e^{-\omega\tau} \tag{4.3.6}$$

we can write eq. (4.3.5) as a sum of terms equal to eq. (4.3.2) times a coefficient $g_\tau^{\mu\nu}$. But we are not done just yet. The last problem is that the integrand of eq. (4.3.5) is cut off sharply at $\omega_{\max}$ while the integrand of eq. (4.3.2) dies off smoothly. this problem can be solved by replacing the Heaviside function in eq. (4.3.5) with a smooth function which tends to the Heaviside function in a well defined limit. Such a function is given by the sigmoid

$$\theta_\sigma(x)=\frac{1}{1+e^{-\frac{x}{\sigma}}} \tag{4.3.7}$$

which satisfies $\lim_{\sigma\to0}\theta_\sigma(x)=\theta(x)$. Combining this with the approximation of the kernel function in eq. (4.3.6) we obtain

$$\lim_{\sigma\to0}\sum_\tau g_\tau^{\mu\nu}C_{\mu\nu}\left(\boldsymbol{q},t\right)=\lim_{\sigma\to0}\int_{\omega_0}^{\infty}\mathrm{d}\omega\theta_\sigma\left(\omega_{\max}-\omega\right)k_{\mu\nu}\left(\boldsymbol{q},\omega\right)W^{\mu\nu}\left(\boldsymbol{q},\omega\right)=\overline{X}\left(\boldsymbol{q}^2\right). \tag{4.3.8}$$

In chapter 5 the l.h.s. of this equation is computed on the lattice and confronted with an OPE calculation of the r.h.s. This serves as an independent check of the OPE framework commonly used to extract $|V_{cb}|$ from inclusive B meson decays. Furthermore in the future it could be used to access hadronic matrix elements which are difficult to extract from experimental data.

Afterwards the part on inclusive decays of B mesons will conclude with chapter 6 in which the tools developed in this chapter will be applied to study the effects of dimension 8 operators in the weak effective theory to inclusive observables.

Chapter 5

Lattice QCD Study of Inclusive Semileptonic Decays of Heavy Mesons

This chapter presents the work published in [144].

5.1 Introduction

The theoretical study of semileptonic decays of B mesons continues to be an important and very active area of research in high-energy physics: this interest is mainly driven by the fact that these decays encode direct information on the modulus of two of the elements of the Cabibbo-Kobayashi-Maskawa (CKM) quark mixing matrix [100, 181], namely $|V_{ub}|$ and $|V_{cb}|$, and may be a sensitive probe to new physics beyond the Standard Model (SM). As a matter of fact, many different types of extensions of the SM are expected to affect flavour physics, inducing new flavour-changing interactions, complex phases in the CKM matrix, possible violations of lepton-flavour universality, etc. Even if the mass scales of new particles beyond the SM turned out to be very high, quantum effects of the associated fields could leave detectable imprints onto the physics of bottom and charm quarks.

On the experimental side, recent results from B factories reveal some tension with SM predictions, but also exhibit puzzling discrepancies between exclusive and inclusive channels [43, 141, 146, 228]. For theorists, this provides further motivation to improve the understanding of these decays and to refine their predictions. Currently, the most powerful tool to obtain theoretical predictions from the first principles of QCD is the one based on numerical simulations in the lattice regularisation of the theory [222]. It is an intrinsically non-perturbative approach, that allows one to obtain accurate and systematically improvable predictions for a variety of quantities, including those relevant for decays of heavy mesons: for an up-to-date world review of lattice results relevant to flavour physics, see ref. [45]. It should be emphasized, however, that most lattice calculations focus on *exclusive* decays: in a nutshell, this is due to the fact that inclusive processes consist of a potentially very large number of physical states—including states featuring multiple hadrons, which pose their own challenges—and their systematic analysis in numerical calculations is very impractical, if possible at all.

Recently, however, novel approaches have been put forward, that allow one to address inclusive decays in lattice QCD. As an example, in ref. [164] it was pointed out that the differential rate for inclusive decays of the type $B \to X\ell\nu$ (where X denotes all hadronic states that are compatible with the semileptonic decay of the bottom quark) could be evaluated by

relating the hadronic tensor

$$W_{\mu\nu}(p,q) = \frac{4\pi^3}{E_B} \sum_X \delta^4(p-q-p_X) \langle B(p)|J_\mu^\dagger|X(p_X)\rangle\langle X(p_X)|J_\nu|B(p)\rangle \tag{5.1.1}$$

(where J_μ is the weak current associated with the b quark decay, p and p_X respectively denote the four-momenta of the B meson and of the X state, while q is the transferred four-momentum) to the forward scattering matrix element $T_{\mu\nu}(p,q)$ [83,197], and by extracting the latter through an analytical continuation of lattice results obtained for this quantity in an unphysical region, where the decay is forbidden by kinematics.

In ref. [163], on the other hand, it was proposed to study decay and transition rates into final states with an arbitrary number of hadrons by reconstructing the spectral function associated with a Euclidean four-point function in a finite volume from lattice correlators, with an appropriate smoothing protocol. A closely related approach was discussed in ref. [162] (see also refs. [95, 96]).

Finally, in ref. [143] it was suggested to study inclusive decays on the lattice by computing a suitable "smeared" spectral density $\rho(w)$ of hadron correlators, where the smearing is defined by the integration over the allowed phase-space region. Also in this case, the strategy involves the lattice determination of a class of four-point correlation functions. This technique allows one to bypass the need for analytical continuation, and, at least in principle, paves the way for the determination of the total semileptonic width as well as of the moments of any kinematic distribution associated with general $B \to X\ell\nu$ decays.

In the present work, we focus on the method proposed in ref. [143], presenting the results of explicit lattice calculations based upon this framework. We discuss results from two different types of ensembles of lattice QCD configurations, and we also compare them with an analytical calculation based on the operator-product expansion (OPE) [178, 221] within the framework of an expansion in inverse powers of the heavy-quark mass [77, 79, 83].

The structure of this article is the following. In section 5.2, we recapitulate the formulation of the method, extending the presentation in ref. [143] with additional remarks, and commenting on its application to observables of particular interest (including differential distributions and moments). In section 5.3, we present an explicit implementation of the method in lattice QCD calculations, using two different ensembles of configurations, generated by the JLQCD collaboration and by the ETM collaboration; the final part of the section is devoted to a technical discussion about the extrapolation to the limit in which the smearing parameter σ tends to zero. The following section 5.4 presents the analytical calculation based on the OPE, and compares its predictions with the results from lattice QCD. Finally, in section 5.5 we summarize our results and discuss future prospects.

5.2 Formulation of the method and application to observables

5.2.1 Spectral representation of the inclusive decay rate

Here we review the formalism to calculate the inclusive semileptonic decay rate in lattice QCD [143]. To be specific, we consider the semileptonic decay of a B meson to charmed final states X_c with a pair of massless leptons $(\ell\bar{\nu})$ through the flavour-changing current $J_\mu = V_\mu - A_\mu = \bar{c}\gamma_\mu(1-\gamma_5)b$.

We start from the differential decay rate

$$\frac{d\Gamma}{dq^2 dq^0 dE_\ell} = \frac{G_F^2 |V_{cb}|^2}{8\pi^3} L_{\mu\nu} W^{\mu\nu} \,, \tag{5.2.1}$$

where G_F is the Fermi constant and $|V_{cb}|$ is the relevant CKM matrix element. Here we work in the rest frame of the initial B meson, so that

$$p = (m_B, \mathbf{0}) \,, \qquad q = p_\ell + p_{\bar\nu} = (q_0, \boldsymbol{q}) \,, \qquad r = p - q = (\omega, -\boldsymbol{q}) \,, \tag{5.2.2}$$

where the differential decay rate is a function of the three kinematical variables q^2, q_0 and the lepton energy E_ℓ, and is given by the product of the leptonic tensor,

$$L^{\mu\nu} = p_\ell^\mu p_{\bar\nu}^\nu - p_\ell \cdot p_{\bar\nu} g^{\mu\nu} + p_\ell^\nu p_{\bar\nu}^\mu - i\epsilon^{\mu\alpha\nu\beta} p_{\ell,\alpha} p_{\bar\nu,\beta} \,, \tag{5.2.3}$$

and the hadronic tensor,

$$W^{\mu\nu}(p,q) = \sum_{X_c} (2\pi)^3 \delta^{(4)}(p - q - r) \frac{1}{2E_B(\boldsymbol{p})} \langle \bar B(\boldsymbol{p}) | J^{\mu\dagger}(0) | X_c(\boldsymbol{r}) \rangle \langle X_c(\boldsymbol{r}) | J^\nu(0) | \bar B(\boldsymbol{p}) \rangle . \tag{5.2.4}$$

The sum over the charmed states $X_c(\boldsymbol{r})$ actually includes an integral over $\boldsymbol{r}$.[1]

Performing the integral over the lepton energy E_ℓ in its kinematical range, i.e. from $(q_0 - \sqrt{\boldsymbol{q}^2})/2$ to $(q_0 + \sqrt{\boldsymbol{q}^2})/2$, and changing the remaining kinematical variables from (q_0, q^2) to $(\omega, \boldsymbol{q}^2)$, the total rate can be written as

$$\Gamma = \frac{G_F^2 |V_{cb}|^2}{24\pi^3} \int_0^{\boldsymbol{q}^2_{\rm max}} d\boldsymbol{q}^2 \sqrt{\boldsymbol{q}^2} \bar X(\boldsymbol{q}^2) \,, \qquad \bar X(\boldsymbol{q}^2) \equiv \int_{\omega_{\rm min}}^{\omega_{\rm max}} d\omega \, X(\omega, \boldsymbol{q}^2) \,, \tag{5.2.5}$$

where

$$\boldsymbol{q}^2_{\rm max} = \frac{(m_B^2 - m_D^2)^2}{4m_B^2} \,, \qquad \omega_{\rm min} = \sqrt{m_D^2 + \boldsymbol{q}^2} \,, \qquad \omega_{\rm max} = m_B - \sqrt{\boldsymbol{q}^2} \,. \tag{5.2.6}$$

The quantity $X(\omega, \boldsymbol{q}^2)$ appearing above is a linear combination, with coefficients depending on the kinematical variables, of the different components of the hadronic tensor. Indeed, Lorentz invariance and time-reversal symmetry allow one to decompose $W^{\mu\nu}$ into invariant structure functions according to

$$\begin{aligned} W^{\mu\nu}(p,q) = &- g^{\mu\nu} W_1(\omega, \boldsymbol{q}^2) + \frac{p^\mu p^\nu}{m_B^2} W_2(\omega, \boldsymbol{q}^2) - i\epsilon^{\mu\nu\alpha\beta} \frac{p_\alpha q_\beta}{m_B^2} W_3(\omega, \boldsymbol{q}^2) \\ &+ \frac{q^\mu q^\nu}{m_B^2} W_4(\omega, \boldsymbol{q}^2) + \frac{p^\mu q^\nu + p^\nu q^\mu}{m_B^2} W_5(\omega, \boldsymbol{q}^2) \,. \end{aligned} \tag{5.2.7}$$

By introducing the following basis for three-dimensional space,

$$\hat{\boldsymbol{n}} = \frac{\boldsymbol{q}}{\sqrt{\boldsymbol{q}^2}} \,, \qquad \boldsymbol{\epsilon}^{(a)} \cdot \hat{\boldsymbol{n}} = 0 \,, \qquad \boldsymbol{\epsilon}^{(a)} \cdot \boldsymbol{\epsilon}^{(b)} = \delta^{ab} \,, \qquad \{a, b\} = \{1, 2\} \,, \tag{5.2.8}$$

[1] More precisely, the sum over the charmed states $X_c(\boldsymbol{r})$ should be written as

$$\sum_{X_c} |X_c(\boldsymbol{r})\rangle\langle X_c(\boldsymbol{r})| \to \sum_{X_c} \int \frac{d^3\boldsymbol{r}}{(2\pi)^3} \frac{1}{2E_{X_c(\boldsymbol{r})}} |X_c(\boldsymbol{r})\rangle\langle X_c(\boldsymbol{r})|$$

when the standard relativistic normalization for a single-particle state is employed for X_c.

and the hadronic quantities

$$Y^{(1)} = -\sum_{a=1}^{2}\sum_{i,j=1}^{3}\epsilon_i^{(a)}\epsilon_j^{(a)}W^{ij}\;, \qquad Y^{(2)} = W^{00}\;, \qquad Y^{(3)} = \sum_{i,j=1}^{3}\hat{n}^i\hat{n}^j W^{ij}\;,$$
$$Y^{(4)} = \sum_{i=1}^{3}\hat{n}^i(W^{0i}+W^{i0})\;, \qquad Y^{(5)} = \frac{i}{2}\sum_{i,j,k=1}^{3}\varepsilon^{ijk}\hat{n}^k W^{ij}\;, \tag{5.2.9}$$

it is easy to see that, in the rest frame of the B meson, the information contained in $W^{\mu\nu}$ can be equivalently parametrized in terms of $Y^{(i)} \equiv Y^{(i)}(\omega, \boldsymbol{q}^2)$. A convenient representation of $X(\omega, \boldsymbol{q}^2)$ is then given by

$$X(\omega,\boldsymbol{q}^2) = \sum_{l=0}^{2}(\sqrt{\boldsymbol{q}^2})^{2-l}(m_B-\omega)^l X^{(l)}(\omega,\boldsymbol{q}^2)\;,$$
$$X^{(0)} = Y^{(1)}+Y^{(2)}\;, \qquad X^{(1)} = -Y^{(4)}\;, \qquad X^{(2)} = Y^{(3)}-Y^{(1)}\;. \tag{5.2.10}$$

At this point, some observations are in order. First, we notice that the parity-violating structure function W_3 (or equivalently $Y^{(5)}$) does not contribute to the differential decay rate after the integral over E_ℓ has been performed (this will not be the case for the moments considered below). Then, by rewriting eq. (5.2.4) as

$$W_{\mu\nu}(\omega,\boldsymbol{q}) = \frac{(2\pi)^3}{2m_B}\langle\bar{B}(\mathbf{0})|J_\mu^\dagger(0)\delta(\hat{H}-\omega)\delta^3(\hat{\boldsymbol{P}}+\boldsymbol{q})J_\nu(0)|\bar{B}(\mathbf{0})\rangle\;, \tag{5.2.11}$$

where $\hat{H}$ and $\hat{\boldsymbol{P}}$ are the QCD Hamiltonian and momentum operators, we explicitly see that in the rest frame of the B meson the different components of the hadronic tensor are functions of ω and $\boldsymbol{q}$ (we already used this information in changing the integration variables from (q_0, q^2) to $(\omega, \boldsymbol{q}^2)$). In the following we refer to eq. (5.2.11) as the *spectral* representation of the hadronic tensor. Flavour and momentum conservation imply that the hadronic tensor vanishes identically for energies $\omega < \omega_{\rm min}$. From this observation one obtains $\omega_{\rm min} = \sqrt{m_D^2+\boldsymbol{q}^2}$. This means that by introducing the kernels

$$K^{(l)}(\omega,\boldsymbol{q}^2) = (m_B-\omega)^l\theta(\omega_{\rm max}-\omega)\;, \tag{5.2.12}$$

the ω integral in eq. (5.2.5) can be rewritten as

$$\bar{X}(\boldsymbol{q}^2) = \sum_{l=0}^{2}(\sqrt{\boldsymbol{q}^2})^{2-l}\int_0^\infty d\omega\, K^{(l)}(\omega,\boldsymbol{q}^2)\,X^{(l)}(\omega,\boldsymbol{q}^2)\;. \tag{5.2.13}$$

We close this subsection by providing an equivalent representation of $X(\omega, \boldsymbol{q}^2)$ which will be useful later. It is given by

$$X(\omega,\boldsymbol{q}^2) = \sum_{l=0}^{2}(\sqrt{\boldsymbol{q}^2})^{2-l}(\omega_{\rm max}-\omega)^l Z^{(l)}(\omega,\boldsymbol{q}^2)\;, \tag{5.2.14}$$

where the $Z^{(l)}(\omega, \boldsymbol{q}^2)$ are again linear combinations of the $Y^{(l)}$,

$$Z^{(0)} = Y^{(2)}+Y^{(3)}-Y^{(4)}\;, \qquad Z^{(1)} = 2Y^{(3)}-2Y^{(1)}-Y^{(4)}\;, \qquad Z^{(2)} = Y^{(3)}-Y^{(1)}\;. \tag{5.2.15}$$

By introducing the kernels

$$\Theta^{(l)}(x) = x^l \theta(x) \,, \tag{5.2.16}$$

that are functions of the single variable $x = \omega_{\max} - \omega$, we thus have

$$\bar{X}(\boldsymbol{q}^2) = \sum_{l=0}^{2} (\sqrt{\boldsymbol{q}^2})^{2-l} \, Z^{(l)}(\boldsymbol{q}^2) \,, \qquad Z^{(l)}(\boldsymbol{q}^2) = \int_0^\infty d\omega \, \Theta^{(l)}(\omega_{\max} - \omega) \, Z^{(l)}(\omega, \boldsymbol{q}^2) \,. \tag{5.2.17}$$

5.2.2 Decay rate from Euclidean correlators

In order to calculate $\bar{X}(\boldsymbol{q}^2)$, as given in eq. (5.2.13) or eq. (5.2.17), we need to evaluate the integral over ω of the different components of the hadronic spectral density (5.2.11) with the kernels $K^{(l)}(\omega, \boldsymbol{q}^2)$ or $\Theta^{(l)}(\omega_{\max} - \omega)$. To this end, following ref. [164], we first establish the connection between suitably chosen correlation functions that can be calculated on the lattice, and $W_{\mu\nu}$.

We start by considering the Euclidean correlator

$$C_{\mu\nu}(t_{\text{snk}}, t_2, t_1, t_{\text{src}}; \boldsymbol{q}) = \int d^3x \, e^{i\boldsymbol{q}\cdot\boldsymbol{x}} \, T\langle 0| \, \tilde{\phi}_B(\mathbf{0}; t_{\text{snk}}) J_\mu^\dagger(\boldsymbol{x}; t_2) J_\nu(\mathbf{0}; t_1) \tilde{\phi}_B^\dagger(\mathbf{0}; t_{\text{src}}) \, |0\rangle \,, \tag{5.2.18}$$

where $\tilde{\phi}_B(\mathbf{0}; t)$ is a B-meson creation/annihilation operator projected onto zero spatial momentum by integrating over space at a time t. A zero-momentum B meson is thus created at time t_{src} and annihilated at t_{snk}. The two currents are inserted in between, at times t_2 and t_1. The charmed hadrons are created at time t_1 with a momentum insertion $-\boldsymbol{q}$ and propagate until they are transformed back to the B-meson state at time t_2.

The four-point function $C_{\mu\nu}$ is saturated by the B-meson non-local matrix element

$$M_{\mu\nu}(t; \boldsymbol{q}) = e^{-m_B t} \int d^3x \, \frac{e^{i\boldsymbol{q}\cdot\boldsymbol{x}}}{2m_B} \langle \bar{B}(\mathbf{0}) | J_\mu^\dagger(\boldsymbol{x}, t) J_\nu(\mathbf{0}, 0) | \bar{B}(\mathbf{0}) \rangle \,, \tag{5.2.19}$$

when the double limit $t_{\text{src}} \to -\infty$, $t_{\text{snk}} \to \infty$ is taken. To include a proper normalization, one can analyse

$$M_{\mu\nu}(t_2 - t_1; \boldsymbol{q}) = Z_B \lim_{\substack{t_{\text{snk}} \to +\infty \\ t_{\text{src}} \to -\infty}} \frac{C_{\mu\nu}(t_{\text{snk}}, t_2, t_1, t_{\text{src}}; \boldsymbol{q})}{C(t_{\text{snk}} - t_2) C(t_1 - t_{\text{src}})} \,, \tag{5.2.20}$$

where $C(t)$ is the B-meson two-point function

$$C(t) = T\langle 0| \, \tilde{\phi}_B(\mathbf{0}; t) \tilde{\phi}_B^\dagger(\mathbf{0}; 0) |0\rangle \tag{5.2.21}$$

and Z_B is its residue when a large time separation is taken, $C(t) \to Z_B e^{-m_B t}$.

Starting from eq. (5.2.19) we can establish the connection between $M_{\mu\nu}(t; \boldsymbol{q})$ and the hadronic tensor given in eq. (5.2.11). We have

$$\begin{aligned} M_{\mu\nu}(t; \boldsymbol{q}) &= \int d^3x \, \frac{e^{i\boldsymbol{q}\cdot\boldsymbol{x}}}{2m_B} \langle \bar{B}(\mathbf{0}) | J_\mu^\dagger(\mathbf{0}, 0) e^{-t\hat{H} + i\hat{\boldsymbol{P}}\cdot\boldsymbol{x}} J_\nu(\mathbf{0}, 0) | \bar{B}(\mathbf{0}) \rangle \\ &= \frac{(2\pi)^3}{2m_B} \langle \bar{B}(\mathbf{0}) | J_\mu^\dagger(\mathbf{0}, 0) e^{-t\hat{H}} \delta^3(\hat{\boldsymbol{P}} + \boldsymbol{q}) J_\nu(\mathbf{0}, 0) | \bar{B}(\mathbf{0}) \rangle \\ &= \int_0^\infty d\omega \, W_{\mu\nu}(\omega, \boldsymbol{q}) \, e^{-\omega t} \,. \end{aligned} \tag{5.2.22}$$

The problem of the calculation of $\bar{X}(\boldsymbol{q}^2)$ is now reduced to that of trading the integral of $W_{\mu\nu}(\omega, \boldsymbol{q})$ with the kernels $e^{-t\omega}$ for the integral with the kernels $\Theta^{(l)}(\omega_{\rm max} - \omega)$ (or $K^{(l)}(\omega, \boldsymbol{q}^2)$).

The general inverse problem represented by the extraction of hadronic spectral densities from Euclidean correlators is notoriously ill-posed. Recently, methods to cope with these problems have been proposed, and they treat the above mentioned integrals with some kernels. In this paper we use two approaches proposed in refs. [55, 162]. The differences between the two methods will be discussed in detail in the following sections. Here we concentrate on the common starting point of the two approaches, which are actually closely related to each other.

We start by introducing an arbitrary length scale a. On the lattice this will be identified with the lattice spacing. The correlators $M_{\mu\nu}(t; \boldsymbol{q})$ will be computed at times $t = a\tau$ where $\tau \geq 0$ is an integer. By introducing the variable $x = e^{-a\omega}$ (and its inverse mapping $\omega = -\log(x)/a$), standard theorems of numerical analysis guarantee that any C_∞ function $f(\omega) \equiv g(x)$ in the interval $\omega \in [0, \infty]$ (corresponding to $x \in [0, 1]$), vanishing at $\omega = \infty$ ($x = 0$), can be approximated with arbitrary precision in terms of polynomials in x according to

$$f(\omega) = \sum_{\tau=1}^{\infty} g_\tau \, x^\tau \equiv \sum_{\tau=1}^{\infty} g_\tau \, e^{-a\omega\tau} \; . \tag{5.2.23}$$

This implies that the integral of the product of $W_{\mu\nu}(\omega, \boldsymbol{q})$ with $f(\omega)$ can be computed, once the coefficients g_τ are known, by using the linear relation

$$\int_0^\infty d\omega \, W_{\mu\nu}(\omega, \boldsymbol{q}) \, f(\omega) = \sum_{\tau=1}^{\infty} g_\tau \, M_{\mu\nu}(a\tau; \boldsymbol{q}) \; . \tag{5.2.24}$$

This procedure cannot be applied straightforwardly to the calculation of $X(\boldsymbol{q}^2)$ because the kernels $\Theta^{(l)}(\omega_{\rm max} - \omega)$ (or $K^{(l)}(\omega, \boldsymbol{q}^2)$) are not smooth, i.e. they contain a discontinuity due to the θ-function. In this case, a sequence of polynomials can still converge to the kernels *in mean*, which would be sufficient for our purposes, but a reasonable approximation would imply a very large number of terms. However, the problem can be solved by introducing smeared C_∞ versions of the θ-function, θ_σ, such that the sharp step-function is recovered in the limit in which the smearing parameter σ is sent to zero, $\lim_{\sigma\to 0} \theta_\sigma(x) = \theta(x)$.

By considering, as suggested in ref. [143], the corresponding smeared versions of the kernels entering the definition of $\bar{X}(\boldsymbol{q}^2)$, that we call $\Theta^{(l)}_\sigma(\omega_{\rm max} - \omega)$ and $K^{(l)}_\sigma(\omega, \boldsymbol{q})$, we then have

$$\Theta^{(l)}_\sigma(\omega_{\rm max} - \omega) = m_B^l \sum_{\tau=1}^{\infty} g^{(l)}_\tau(\omega_{\rm max}, \sigma) \, e^{-a\omega\tau} \; , \tag{5.2.25}$$

and

$$\int_0^\infty d\omega \, W_{\mu\nu}(\omega, \boldsymbol{q}) \, \Theta^{(l)}(\omega_{\rm max} - \omega) = \lim_{\sigma\to 0} m_B^l \sum_{\tau=1}^{\infty} g^{(l)}_\tau(\omega_{\rm max}, \sigma) \, M_{\mu\nu}(a\tau; \boldsymbol{q}) \; , \tag{5.2.26}$$

as well as similar relations in the case of the kernels $K^{(l)}(\omega, \boldsymbol{q}^2)$.

A few observations are now in order. The first concerns a subtle theoretical issue. The smearing procedure, which is algorithmically required to implement the procedure just outlined, is also necessary for theoretical reasons. Hadronic spectral densities, and therefore also $W_{\mu\nu}(\omega, \boldsymbol{q})$, are elements in the space of distributions and their product with another distribution, such as the θ-function, can only be defined through a regularization procedure (when it

exists). The issue is particularly important in the case of lattice simulations because they are necessarily performed on a finite volume. Finite-volume spectral functions, due to the quantization of the energy spectrum, are sums of isolated δ-function singularities and their connection with the corresponding physical quantities requires an ordered double-limit procedure: first the infinite volume limit has to be taken and only *after* that, if the quantity is non-singular, can one take the $\sigma \to 0$ limit.

The second observation is related to the fact that the problem we are addressing is particularly hard from the computational point of view. In the limit of very small σ the coefficients $g_\tau^{(l)}(\omega_{\rm max}, \sigma)$ of eq. (5.2.25) tend to become arbitrarily large in modulus and oscillate in sign. Since lattice correlators are unavoidably affected by statistical and systematic errors, in these cases the resulting uncertainties on the sums on the left-hand side of eq. (5.2.26) tend to explode. The two approaches of refs. [55, 162] differ for the procedures used to determine the coefficients $g_\tau^{(l)}(\omega_{\rm max}, \sigma)$, once the series is truncated at $\tau = \tau_{\rm max}$, in such a way to keep both statistical and systematic errors under control.

5.2.3 Kernel approximation

In this subsection we review the methods of refs. [55, 162] by highlighting the differences in the procedures used to approximate the smearing kernels. To simplify the formulae, we shall consider a generic kernel $f(\omega)$, that will then be identified with the kernels $\Theta^{(l)}(\omega_{\rm max} - \omega)/m_B^l$ or $K^{(l)}(\omega, \boldsymbol{q})/m_B^l$, and a generic correlator

$$C(t) = \int_0^\infty d\omega\, \rho(\omega)\, e^{-\omega t}\,, \tag{5.2.27}$$

to be identified with $M_{\mu\nu}(t; \boldsymbol{q})$, so that $\rho(\omega)$ will correspond to $W_{\mu\nu}(\omega, \boldsymbol{q})$. In this work we shall not address the systematics associated with the finiteness of the extent of the lattice in the temporal direction, see refs. [96, 162] for an extended discussion of this issue and, in general, for more details concerning the algorithm and its applications.

In the method of ref. [162] the coefficients g_τ corresponding to the approximation of $f(\omega)$ are determined by minimizing the functional

$$W_\lambda[g] = (1-\lambda)\frac{A[g]}{A[0]} + \lambda B[g]\,, \tag{5.2.28}$$

where $\lambda \in [0,1]$ is the so-called "trade-off parameter" (see below) and the functionals $A[g]$ and $B[g]$ are given by

$$A[g] = a\int_{E_0}^\infty d\omega \left\{ f(\omega) - \sum_{\tau=1}^{\tau_{\rm max}} g_\tau\, e^{-a\omega\tau} \right\}^2, \qquad B[g] = \sum_{\tau,\tau'=1}^{\tau_{\rm max}} g_\tau g_{\tau'}\, \frac{{\rm Cov}\,[C(a\tau), C(a\tau')]}{[C(0)]^2}\,. \tag{5.2.29}$$

Here ${\rm Cov}\,[C(t), C(t')]$ is the statistical covariance of the correlator $C(t)$ and, consequently, the functional $B[g]$ is positive definite. The functional $A[g]$ is also a positive definite quadratic form in the coefficients g_τ. Therefore, the minimum conditions

$$\left.\frac{\partial W_\lambda[g]}{\partial g_\tau}\right|_{g_\tau = g_\tau^\lambda} = 0 \tag{5.2.30}$$

are a linear system of equations to be solved for the coefficients g_τ^λ. These coefficients define the approximation of $f(\omega)$ and the associated estimator for the integral of $\rho(\omega)$ with $f(\omega)$ according to

$$f^\lambda(\omega) = \sum_{\tau=1}^{\tau_{\max}} g_\tau^\lambda \, e^{-a\omega\tau} \;, \qquad \rho^\lambda[f] = \sum_{\tau=1}^{\tau_{\max}} g_\tau^\lambda C(a\tau) = \int_0^\infty d\omega \, f^\lambda(\omega) \, \rho(\omega) \;. \tag{5.2.31}$$

The functional $B[g^\lambda]$ is the statistical variance of $\rho^\lambda[f]$ normalized with the square of the correlator in zero and, therefore, vanishes in the ideal case of infinitely precise input data. On the other hand, $A[g^\lambda]$ measures the distance between the target kernel $f(\omega)$ and its approximation $f^\lambda(\omega)$ in the range[2] $\omega \in [E_0, \infty]$. In fact $A[g^\lambda]$ is the squared L_2-norm in function space of the difference $f^\lambda(\omega) - f(\omega)$ and can only vanish in the limit $t_{\max} \to \infty$.

In the absence of errors, the coefficients g_τ^λ that minimize $A[g]$ provide the best polynomial approximation of $f(\omega)$ with respect to the L_2-norm. This has to be compared with the method of ref. [55] that provides the best polynomial approximation of $f(\omega)$ with respect to the L_∞-norm (see below). In the presence of errors, the coefficients g_τ^λ that minimize $W_\lambda[g]$ represent a particular balance between statistical and systematic errors, as dictated by the λ parameter. For small λ the estimator $\rho^\lambda[f]$ is close to $\rho[f]$ but with a large statistical uncertainty. Conversely, for large λ the estimator $\rho^\lambda[f]$ has a small statistical error but differs significantly from $\rho[f]$. When evaluated at the minimum, the functional $W_\lambda[g]$ is a function of λ only, thus defining $W(\lambda) \equiv W_\lambda[g^\lambda]$. The prescription suggested in ref. [162] to choose the optimal value of the trade-off parameter defines $\lambda_\star$ such that

$$\left. \frac{\partial W(\lambda)}{\partial \lambda} \right|_{\lambda=\lambda_\star} = 0 \;. \tag{5.2.32}$$

From eq. (5.2.30) it follows that at $\lambda_\star$ (the maximum of $W(\lambda)$ where $g_\tau^\lambda = g_\tau^\star$) one has $A[g^\star] = A[0]B[g^\star]$. This can be understood as the condition of "optimal balance" between statistical and systematic errors. The numerical results discussed in subsection 5.3.2 have been obtained using this method, also monitoring the stability of the results with respect to $\lambda \leq \lambda_\star$.

In ref. [55], on the other hand, the function $f(\omega)$ is approximated using the Chebyshev approximation as

$$f(\omega) \simeq \frac{c_0^*}{2} + \sum_{j=1}^{N} c_j^* T_j^*(e^{-a\omega}) \;, \tag{5.2.33}$$

where $T_j^*(x)$ is a (shifted) Chebyshev polynomial of the j-th order. The coefficients c_j^* are determined only by the function $f(\omega)$:

$$c_j^* = \frac{2}{\pi} \int_0^\pi d\theta \, f\left(-\ln \frac{1+\cos\theta}{2} \right) \cos(j\theta) \;. \tag{5.2.34}$$

This yields the best approximation in the sense of the L_∞-norm[3]. The approximation of the

[2]The parameter E_0 can be adjusted by exploiting the fact that $\rho(\omega)$ has support only for $\omega > \omega_{\min}$, so that $\rho[f]$ is insensitive to $f(\omega)$ for $\omega < \omega_{\min}$. The same holds for $\rho^\lambda[f]$ so that the functional form of $f^\lambda(\omega)$ can be left unconstrained for $\omega < \omega_{\min}$. Any $E_0 < \omega_{\min}$ is therefore a viable choice in determining the coefficients g_t^λ so E_0 can be chosen to improve the numerical stability of the minimization procedure.

[3]More precisely, the Chebyshev approximation of a generic function $f(y)$ for $y \in [-1, 1]$ is in practice equivalent, although not identical, to the optimal polynomial approximation of $f(\vec{g}; y) = \sum_{\tau=0}^{N} g_\tau y^\tau$ obtained

ω-integral is then constructed as

$$\int d\omega f(\omega)\rho(\omega) = \frac{\langle\psi_\mu|f(\hat{H})|\psi_\nu\rangle}{\langle\psi_\mu|\psi_\nu\rangle} \simeq \frac{c_0^*}{2} + \sum_{j=1}^{N} c_j^* \frac{\langle\psi_\mu|T_j^*(e^{-a\hat{H}})|\psi_\nu\rangle}{\langle\psi_\mu|\psi_\nu\rangle} \,, \tag{5.2.35}$$

where $|\psi_\mu\rangle \equiv e^{-\hat{H}t_0}J_\mu|B\rangle$ is defined such that the state is evolved for some small time t_0 after applying the current insertion: this allows one to avoid any ultraviolet divergence due to contact terms of two currents. To reflect this change, the kernel $f(\omega)$ is multiplied by $e^{2\omega t_0}$ to cancel the time evolution. The right-hand side of eq. (5.2.35) can be reconstructed from the matrix elements (5.2.19) using $M_{\mu\nu}(t+2t_0)/M_{\mu\nu}(2t_0)$.

An advantage of this construction is that the matrix element appearing on the right-hand side of eq. (5.2.35), $\langle\psi_\mu|T_j^*(e^{-a\hat{H}})|\psi_\nu\rangle/\langle\psi_\mu|\psi_\nu\rangle$, is strictly bound between -1 and $+1$, by construction of the Chebyshev polynomial. This corresponds to the condition that the eigenvalues of $e^{-\hat{H}}$ lie between 0 and 1, or equivalently that the eigenvalues of $\hat{H}$ are positive semi-definite. Then, the convergence of the series appearing in eq. (5.2.35) is dictated by that of the coefficients c_j^*. Since c_j^* can be easily calculated for arbitrarily large j's, the error due to the truncation in (5.2.35) can be rigorously estimated.

The constraint $|\langle\psi_\mu|T_j^*(e^{-a\hat{H}})|\psi_\nu\rangle/\langle\psi_\mu|\psi_\nu\rangle| \leq 1$ is not automatically satisfied in the presence of statistical errors. Since the Chebyshev polynomial $T_j^*(x)$ is a sign-alternating series of growing powers of x with (exponentially) large coefficients, this constraint is satisfied after huge cancellations for large j. Therefore, even a small statistical error of the lattice correlator can easily violate the constraint. In the numerical analysis, one should add the constraint when the Chebyshev matrix elements are determined by a fit, see ref. [55] for details. The higher-order terms are then masked by the statistical uncertainties and become basically undetermined within ± 1, so that they only contribute to the truncation error.

In both methods, a good approximation is obtained only when the kernel function is sufficiently smooth. If this is not the case, the truncation error becomes significant, e.g. due to unsuppressed higher-order coefficients c_j^* in the case of the Chebyshev approximation. Unfortunately, the kernel functions $K^{(l)}(\omega, \boldsymbol{q})$ or $\Theta^{(l)}(\omega_{\rm max}-\omega)$ are not smooth, because they contain the Heaviside function $\theta(\omega_{\rm max}-\omega)$. We therefore introduce smeared versions of the θ-function and then we take the limit of $\sigma \to 0$ to recover the unsmeared kernel. This has been done by considering three different smeared θ-functions,

$$\theta_\sigma^{\mathtt{s}}(x) = \frac{1}{1+e^{-\frac{x}{\sigma}}} \,, \qquad \theta_\sigma^{\mathtt{s1}}(x) = \frac{1}{1+e^{-\sinh\left(\frac{x}{r^{\mathtt{s1}}\sigma}\right)}} \,, \qquad \theta_\sigma^{\mathtt{e}}(x) = \frac{1+\mathrm{erf}\left(\frac{x}{r^{\mathtt{e}}\sigma}\right)}{2} \,, \tag{5.2.36}$$

and by extrapolating the numerical data to the $\sigma \to 0$ limit. In the following we shall refer to $\theta_\sigma^{\mathtt{s}}(x)$ as the "sigmoid function", to $\theta_\sigma^{\mathtt{s1}}(x)$ as the "modified sigmoid function" and to $\theta_\sigma^{\mathtt{e}}(x)$ as the "error function". Any choice of the parameters $r^{\mathtt{s1}}$ and $r^{\mathtt{e}}$ appearing in the previous formulae corresponds to a legitimate definition of the smearing kernels that approach the same $\sigma \to 0$ limit, i.e. the θ-function. By adjusting the values of these parameters one can change the rate of convergence to the θ-function and balance between statistical and systematic errors. In the following we set $r^{\mathtt{s1}} = 2.2$ and $r^{\mathtt{e}} = 2.0$. This (empirical) choice gives statistical errors of

by minimizing the L_∞-norm $\|f(y) - f(\vec{g};y)\|_\infty = \max_{y\in[-1,1]}|f(y) - f(\vec{g};y)|$ with respect to the coefficients $\vec{g}$. In fact, the Chebyshev approximation is obtained by minimizing the *weighted* squared L_2-norm given by $\int_{-1}^{1} dy\, w(y)|f(y) - f(\vec{g};y)|^2$ with $w(y) = 1/\sqrt{1-y^2}$. By setting instead $w(y) = 1$, as done in the case of the method of ref. [162], one gets the Legendre polynomial approximation.

the same order of magnitude for the three kernels at fixed σ and similar (although not identical) shapes for $\theta^{\mathtt{s}}_\sigma(x)$ and $\theta^{\mathtt{e}}_\sigma(x)$ while $\theta^{\mathtt{s1}}_\sigma(x)$ results into a smoother approximation of the θ-function. A combined analysis of smearing kernels that have rather different shapes at fixed σ is in fact helpful in order to quantify the systematics associated with the $\sigma \to 0$ extrapolations (see also ref. [96]).

5.2.4 Decomposition of the total rate

The expression of the total rate in eq. (5.2.5) can also be used to compute the differential decay rate in $\boldsymbol{q}^2$, i.e. $d\Gamma/d\boldsymbol{q}^2 = G_F^2|V_{cb}|^2/(24\pi^3)|\boldsymbol{q}|\bar{X}(\boldsymbol{q}^2)$. This can be further decomposed into its contributions from parallel ($\|$) and perpendicular ($\perp$) components, where the $\perp$ components are defined as those involving the polarization vector $\epsilon^{*(\alpha)}$, while the $\|$ ones are the rest. In addition, we also separate the contributions from vector (V) and axial-vector (A) current insertions. Since two currents are inserted, we have VV, AA, as well as VA and AV contributions. Among them, VA and AV do not contribute to the differential rate after integrating over E_ℓ, and thus to the total decay rate. We therefore analyze four components: $VV_\|$, $VV_\perp$, $AA_\|$, $AA_\perp$. For the lepton energy moments, the VA and AV insertions can also appear (see below).

5.2.5 Moments

It is also interesting to consider the moments of various kinematical quantities. In particular, two types of moments have been studied experimentally: the hadronic mass moments $\langle (M_X^2)^n \rangle$ and the lepton energy moments $\langle E_\ell^{n_\ell} \rangle$. They are defined as

$$\langle (M_X^2)^n \rangle = \frac{\displaystyle\int d\boldsymbol{q}^2 dq_0 dE_\ell \, (\omega^2 - \boldsymbol{q}^2)^n \left[\frac{d\Gamma}{d\boldsymbol{q}^2 dq_0 dE_\ell}\right]}{\displaystyle\int d\boldsymbol{q}^2 dq_0 dE_\ell \left[\frac{d\Gamma}{d\boldsymbol{q}^2 dq_0 dE_\ell}\right]} \,, \tag{5.2.37}$$

$$\langle E_\ell^{n_\ell} \rangle = \frac{\displaystyle\int d\boldsymbol{q}^2 dq_0 dE_\ell \, E_\ell^{n_\ell} \left[\frac{d\Gamma}{d\boldsymbol{q}^2 dq_0 dE_\ell}\right]}{\displaystyle\int d\boldsymbol{q}^2 dq_0 dE_\ell \left[\frac{d\Gamma}{d\boldsymbol{q}^2 dq_0 dE_\ell}\right]} \,. \tag{5.2.38}$$

The strategy to compute these moments on the lattice is the same as in the method described above. For the hadronic mass moments defined in eq. (5.2.37), the numerator contains extra powers of $\omega^2 - \boldsymbol{q}^2$, with which the ω-dependence of $X^{(0)}$, $X^{(1)}$, $X^{(2)}$ is modified. Otherwise, the basic procedure remains the same. Beside these quantities which require an integration over the whole $\boldsymbol{q}^2$ range, we will also consider moments at fixed values of $\boldsymbol{q}^2$, i.e. *differential moments*:

$$H_n(\boldsymbol{q}^2) \equiv \langle (M_X^2)^n \rangle_{\boldsymbol{q}^2} = \frac{\displaystyle\int dq_0 dE_\ell \, (\omega^2 - \boldsymbol{q}^2)^n \left[\frac{d\Gamma}{d\boldsymbol{q}^2 dq_0 dE_\ell}\right]}{\displaystyle\int dq_0 dE_\ell \left[\frac{d\Gamma}{d\boldsymbol{q}^2 dq_0 dE_\ell}\right]} \,, \tag{5.2.39}$$

$$L_{n_\ell}(\boldsymbol{q}^2) \equiv \langle E_\ell^{n_\ell} \rangle_{\boldsymbol{q}^2} = \frac{\displaystyle\int dq_0 dE_\ell \, E_\ell^{n_\ell} \left[\frac{d\Gamma}{d\boldsymbol{q}^2 dq_0 dE_\ell}\right]}{\displaystyle\int dq_0 dE_\ell \left[\frac{d\Gamma}{d\boldsymbol{q}^2 dq_0 dE_\ell}\right]} \,, \tag{5.2.40}$$

and the second central moment or variance of the lepton energy distribution

$$L_{2c}(\boldsymbol{q}^2) = L_2(\boldsymbol{q}^2) - \Big(L_1(\boldsymbol{q}^2)\Big)^2 \,.$$

In the case of leptonic moments, the E_ℓ integral is modified with respect to (5.2.5). The integrand in the denominator is the same as in (5.2.10); if we set the $\boldsymbol{q}$ momentum direction $\boldsymbol{n}$ along the k-th axis, the two vectors $\boldsymbol{\epsilon}^a$ can be chosen in the perpendicular directions of the i-th and j-th axes, and we can re-express $X(\omega, \boldsymbol{q}^2)$ as

$$X_{n_\ell=0} = \boldsymbol{q}^2(W^{00} - W^{ii} - W^{jj}) - q_0 q_k(W^{0k} + W^{k0}) + q_0^2(W^{kk} + W^{ii} + W^{jj}) \,, \tag{5.2.41}$$

where repeated indices are not summed. The integrand in the numerators of eq. (5.2.38) and eq, (5.2.40) depends on the exponent n_ℓ. For $n_\ell = 1$, it reads

$$\begin{aligned} X_{n_\ell=1} \;=\; & \frac{q_0}{2}\left[\boldsymbol{q}^2(W^{00} - W^{ii} - W^{jj}) - q_0 q_k(W^{0k} + W^{k0}) + q_0^2(W^{kk} + W^{ii} + W^{jj})\right] \\ & + \frac{i}{2} q_k(q_0^2 - \boldsymbol{q}^2) W^{ij} \,, \end{aligned} \tag{5.2.42}$$

where the last term corresponds to the insertion of VA or AV. The other terms are the same as $X_{n_\ell=0}$, up to a factor $q_0/2$. The next orders are more involved:

$$\begin{aligned} X_{n_\ell=2} \;=\; & \frac{1}{4}\left\{\left(q_0^2\boldsymbol{q}^2 + \frac{1}{5}|\boldsymbol{q}|^4\right) W^{00} + \left(2q_0^4 - \frac{6}{5}q_0^2\boldsymbol{q}^2 - \frac{4}{5}|\boldsymbol{q}|^4\right) W^{ii} + \left(q_0^4 + \frac{1}{5}q_0^2\boldsymbol{q}^2\right) W^{kk} \right. \\ & \left. - \left(q_0^3|\boldsymbol{q}| + \frac{1}{5}q_0|\boldsymbol{q}|^3\right)(W^{0k} + W^{k0}) + \frac{i}{2}q_0|\boldsymbol{q}|(q_0^2 - \boldsymbol{q}^2) W^{ij}\right\} \,, \end{aligned} \tag{5.2.43}$$

$$\begin{aligned} X_{n_\ell=3} \;=\; & \frac{1}{8}\left\{\left(q_0^3\boldsymbol{q}^2 + \frac{3}{5}q_0|\boldsymbol{q}|^4\right) W^{00} + \left(q_0^5 + \frac{3}{5}q_0^3\boldsymbol{q}^2\right) W^{kk} + \left(2q_0^5 + \frac{2}{5}q_0^3\boldsymbol{q}^2 - \frac{12}{5}q_0|\boldsymbol{q}|^4\right) W^{ii} \right. \\ & \left. - \left(q_0^4|\boldsymbol{q}| + \frac{3}{5}q_0^2|\boldsymbol{q}|^3\right)(W^{0k} + W^{k0}) + i\left(3q_0^2|\boldsymbol{q}| + \frac{3}{5}|\boldsymbol{q}|^3\right)(q_0^2 - \boldsymbol{q}^2) W^{ij}\right\} \,. \end{aligned} \tag{5.2.44}$$

Again, the term with W^{ij} survives for VA and AV insertions, while the others are from VV or AA.

The contributions in eq. (5.2.42) can be rearranged in such a way that the ω-integral contributing to the numerator of eq. (5.2.40) takes the form

$$\begin{aligned} \bar{X}_{n_\ell=1}(\boldsymbol{q}^2) &= \sum_{l=0}^{3} (\sqrt{\boldsymbol{q}^2})^{3-l}\, Z^{(l)}_{n_\ell=1}(\boldsymbol{q}^2) \,, \\ Z^{(l)}_{n_\ell=1}(\boldsymbol{q}^2) &= \int_0^\infty d\omega\, \Theta^{(l)}(\omega_{\max} - \omega)\, Z^{(l)}_{n_\ell=1}(\omega, \boldsymbol{q}^2) \,, \end{aligned} \tag{5.2.45}$$

where the $Z^{(l)}_{n_\ell=1}(\omega, \boldsymbol{q}^2)$ are given by

$$\begin{aligned} Z^{(0)}_{n_\ell=1} &= \frac{Y^{(2)} + Y^{(3)} - Y^{(4)}}{2} \,, \qquad Z^{(1)}_{n_\ell=1} = \frac{-2Y^{(1)} + Y^{(2)} + 3Y^{(3)} - 2Y^{(4)} + 2Y^{(5)}}{2} \,, \\ Z^{(2)}_{n_\ell=1} &= \frac{-3Y^{(1)} + 3Y^{(3)} - Y^{(4)} + Y^{(5)}}{2} \,, \qquad Z^{(3)}_{n_\ell=1} = \frac{-Y^{(1)} + Y^{(3)}}{2} \,. \end{aligned} \tag{5.2.46}$$

The previous expressions are analogous to the corresponding expressions for the differential decay rate, eq. (5.2.17) and eq. (5.2.15), but include the sum of four terms with the one corresponding to $l = 3$ that involves the kernel $\Theta^{(3)}(\omega_{\rm max} - \omega)$. In this basis the second leptonic moment is given by

$$\begin{aligned}
\bar{X}_{n_\ell=2}(\boldsymbol{q}^2) &= \sum_{l=0}^{4} (\sqrt{\boldsymbol{q}^2})^{4-l}\, Z^{(l)}_{n_\ell=2}(\boldsymbol{q}^2)\,, \\
Z^{(l)}_{n_\ell=2}(\boldsymbol{q}^2) &= \int_0^\infty d\omega\, \Theta^{(l)}(\omega_{\rm max} - \omega)\, Z^{(l)}_{n_\ell=2}(\omega, \boldsymbol{q}^2)\,,
\end{aligned} \tag{5.2.47}$$

where

$$\begin{aligned}
Z^{(0)}_{n_\ell=2} &= 3\frac{Y^{(2)} + Y^{(3)} - Y^{(4)}}{10}\,, \\
Z^{(1)}_{n_\ell=2} &= \frac{7Y^{(1)} - 5Y^{(2)} - 11Y^{(3)} + 8Y^{(4)} - 10Y^{(10)}}{10}\,, \\
Z^{(2)}_{n_\ell=2} &= \frac{-27Y^{(1)} + 5Y^{(2)} + 31Y^{(3)} - 15Y^{(4)} + 30Y^{(5)}}{20}\,, \\
Z^{(3)}_{n_\ell=2} &= \frac{4Y^{(1)} - 4Y^{(3)} + Y^{(4)} - 2Y^{(5)}}{4}\,, \\
Z^{(4)}_{n_\ell=2} &= \frac{-Y^{(1)} + Y^{(3)}}{4}\,,
\end{aligned} \tag{5.2.48}$$

and the first hadronic moment is

$$\bar{X}_{n=1}(\boldsymbol{q}^2) = \sum_{l=0}^{4} Z^{(l)}_{n=1}(\boldsymbol{q}^2)\,, \qquad Z^{(l)}_{n=1}(\boldsymbol{q}^2) = \int_0^\infty d\omega\, \Theta^{(l)}(\omega_{\rm max} - \omega)\, Z^{(l)}_{n=1}(\omega, \boldsymbol{q}^2)\,, \tag{5.2.49}$$

where the $Z^{(l)}_{n=1}(\omega, \boldsymbol{q}^2)$ are given by

$$\begin{aligned}
Z^{(0)}_{n=1} &= m_B|\boldsymbol{q}|^3(m_B - 2|\boldsymbol{q}|)\left(Y^{(2)} + Y^{(3)} - Y^{(4)}\right)\,, \\
Z^{(1)}_{n=1} &= 2|\boldsymbol{q}|^4\left(Y^{(2)} + Y^{(3)} - Y^{(4)}\right) + m_B^2|\boldsymbol{q}|^2\left(-2Y^{(1)} + 2Y^{(3)} - Y^{(4)}\right) \\
&\quad + m_B|\boldsymbol{q}|^3\left[-2\left(Y^{(2)} + Y^{(3)} - Y^{(4)}\right) + 2\left(2Y^{(1)} - 2Y^{(3)} + Y^{(4)}\right)\right]\,, \\
Z^{(2)}_{n=1} &= m_B^2|\boldsymbol{q}|\left(-Y^{(1)} + Y^{(3)}\right) + |\boldsymbol{q}|^3\left[Y^{(2)} + Y^{(3)} - Y^{(4)} - 2\left(2Y^{(1)} - 2Y^{(3)} + Y^{(4)}\right)\right] \\
&\quad + m_b|\boldsymbol{q}|^2\left[-2\left(-Y^{(1)} + Y^{(3)}\right) + 2\left(2Y^{(1)} - 2Y^{(3)} + Y^{(4)}\right)\right]\,, \\
Z^{(3)}_{n=1} &= -2m_B|\boldsymbol{q}|\left(-Y^{(1)} + Y^{(3)}\right) + |\boldsymbol{q}|^2\left[-2Y^{(1)} + 2Y^{(3)} + 2\left(-Y^{(1)} + Y^{(3)}\right) - Y^{(4)}\right]\,, \\
Z^{(4)}_{n=1} &= |\boldsymbol{q}|\left(-Y^{(1)} + Y^{(3)}\right)\,.
\end{aligned} \tag{5.2.50}$$

5.3 Numerical implementation in lattice QCD

In this section, we discuss in detail two different implementations of the method in lattice QCD calculations. First, in subsection 5.3.1 we present an implementation based on configurations

generated within the JLQCD collaboration. Then, in subsection 5.3.2 we discuss an analogous calculation based on an ensemble generated by the ETM collaboration (ETMC). In both cases, we specify the technical details of the lattice calculations, and discuss the different types of uncertainties affecting the results. Finally, in subsection 5.3.3, we discuss a few technical aspects related to the extrapolation to the $\sigma \to 0$ limit.

5.3.1 Lattice implementation with JLQCD configurations

One dataset used to demonstrate the lattice computation of the inclusive semileptonic decay rate is based on the ensemble generated by the JLQCD collaboration. See the supplementary materials of [108] for details of the gauge configurations. It employs Möbius domain-wall fermions for both valence and sea quarks. In the sea, 2+1 flavors of light and strange quarks are included. The light quark mass corresponds to a pion of mass around 300 MeV; the strange quark mass is slightly heavier than its physical value. The gauge action is the tree-level $O(a^2)$-improved Symanzik at $\beta = 4.35$. The corresponding lattice spacing is $a \simeq 0.055$ fm, corresponding to inverse lattice spacing $1/a = 3.610(9)$ GeV. The lattice volume is $48^3 \times 96$, so that the spatial volume is about $L^3 = (2.6 \text{ fm})^3$. This ensemble corresponds to "M-ud3-sa" of [108]. (See also [202].)

The valence quarks are also described by Möbius domain-wall fermions. The charm quark mass is tuned to its physical value (see ref. [202] for details), while the bottom quark mass is set at $1.25^4 \simeq 2.44$ times the charm quark mass. The spectator quark is a strange quark, so the process corresponds to the inclusive semileptonic decay of a B_s meson, albeit with a light B_s meson mass of $\simeq 3.45$ GeV.

The measurement is carried out on 100 gauge configurations and is replicated four times on each configuration with shifted position of the initial source. The B_s meson is created by a interpolating pseudoscalar operator, which is spatially smeared by a gauge-invariant operator $(1 - (\alpha/N)\Delta)^N$ with a discretized Laplacian Δ and parameters $\alpha = 20$ and $N = 200$. The source points are spread over the source time slice $t_{\text{src}} = 0$ with $\mathbb{Z}_2$ noises to improve statistics. The initial B_s meson is thus projected to zero spatial momentum. The B_s meson on the other end is created by another pseudoscalar operator of the same type placed at the time slice $t_{\text{snk}} = 42$ using a sequential source from the spectator strange quark propagator. The bottom quark propagates from there to a time slice t_2, where the first $b \to c$ current is inserted with momentum $\boldsymbol{q}$ and is fixed at $t_2 = 26$. The charm quark propagator then connects the time slice t_2 to t_1 where the other $b \to c$ current is contracted with momentum insertion $-\boldsymbol{q}$. The charm quark propagator is computed repeatedly for each choice of the current operator and momentum insertion at t_1. We fix the time separation between t_{src} and t_{snk} under an assumption that the ground-state B_s meson state dominates the signal between t_{src} and t_1 or between t_2 and t_{snk}. This separation is at least 16 in the lattice unit, which corresponds to 0.9 fm. The saturation is confirmed in [164].

The matrix element (5.2.19) is then constructed as in eq. (5.2.20). For the analysis of this ensemble we applied the Chebyshev polynomial approximation, following [143]. The polynomial order is set to $N = 15$, but the results are unchanged within the statistical error with other choices beyond $N = 12$. The $\sigma \to 0$ limit is taken for each point assuming a polynomial in σ with data points at $\sigma a = 0.02$, 0.05, 0.10 and 0.20. For all the cases, the extrapolation is small compared to the statistical error on the finite values of σ.

The results are shown in Figure 5.3.1. The left panel is $\bar{X}$ as a function of $\boldsymbol{q}^2$, while the integrand to produce the numerator of $\langle E_\ell \rangle$ is shown in the right panel. The lattice data are

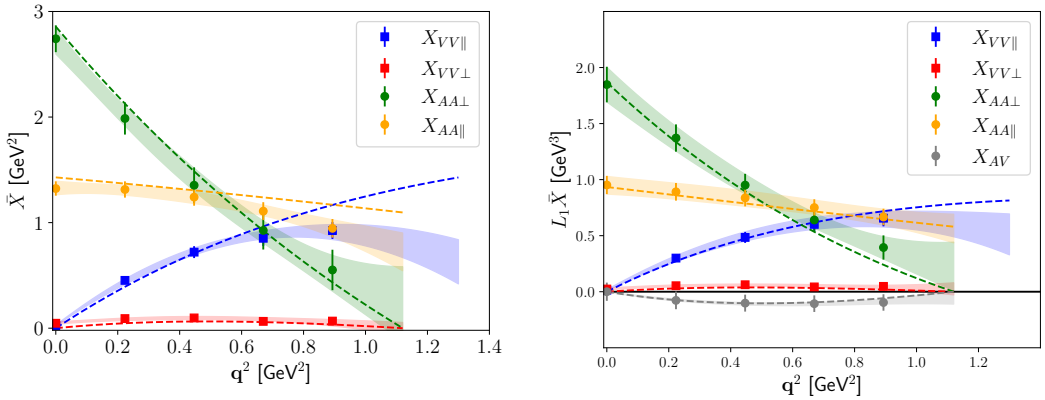

Figure 5.3.1: $\bar{X}$ (left panel) and $L_1\bar{X}$ (right panel, corresponding to the numerator of eq. (5.2.38)) as functions of $\boldsymbol{q}^2$. The results are shown for each channel. X^{AV} is non-vanishing only for $L_1\bar{X}$. The dashed curves are the estimated contributions from the ground states of D_s and D_s^*.

obtained at momentum transfer $\boldsymbol{q}$ at (0,0,0), (0,0,1), (0,1,1), (1,1,1), (0,0,2) in units of $2\pi/L$. Data points represent different channels as discussed in section 5.2.4.

Also shown in figure 5.3.1 are dashed curves which represent the contributions from the ground-states, i.e. D_s and D_s^* mesons. They are computed using the form factors obtained by JLQCD for the same quark mass parameters. The necessary formulae and the lattice data are presented in the appendix A.9.

The lattice data with different momentum insertion $\boldsymbol{q}$ are analyzed together to account for the statistical correlations among them. We then fit $\bar{X}$ in a polynomial of $\boldsymbol{q}^2$ including terms up to $(\boldsymbol{q}^2)^2$.

We observe that the inclusive results for each channel are consistent with the expected ground-state contributions. This means that the excited-state contributions are small, which is consistent with our expectation from the $B \to D^{**}\ell\nu$ form factors based on heavy-quark effective theory (HQET) [188]. Also phenomenologically, it is plausible because the mass of the initial bottom quark is smaller than its physical value. The heavy quark symmetry predicts that the wave-function overlap is 1 at zero recoil when the initial and final masses are degenerate.

We also calculate the differential moments. The numerators for the hadronic mass moments $\langle M_X^2 \rangle$ and $\langle (M_X^2)^2 \rangle$ are shown in figure 5.3.2, while that for $\langle E_\ell \rangle$ is in figure 5.3.1 (right panel). The corresponding differential moments, evaluated for each channel at individual momentum $\boldsymbol{q}^2$, are shown in figure 5.3.3 and in figure 5.3.4.

5.3.2 Lattice implementation with ETMC configurations

The ETMC gauge ensemble used in this work is the one named B55.32, generated by ETMC together with other 14 ensembles with $N_f = 2+1+1$ dynamical quarks in refs. [60, 61] for determining the average up/down, strange and charm quark masses. The Iwasaki action [177] and the Wilson twisted-mass action [132, 134, 136] were used for gluons and sea quarks, respectively. Using the mass renormalization constants determined in ref. [104] the physical light, strange, and charm quark masses were found to be $m_{ud}^{\rm phys}(\overline{\rm MS}, 2\,{\rm GeV}) = 3.70(17)$ MeV, $m_s^{\rm phys}(\overline{\rm MS}, 2\,{\rm GeV}) = 99.6(4.3)$ MeV, and $m_c^{\rm phys}(\overline{\rm MS}, 2\,{\rm GeV}) = 1176(39)$ MeV, respectively.

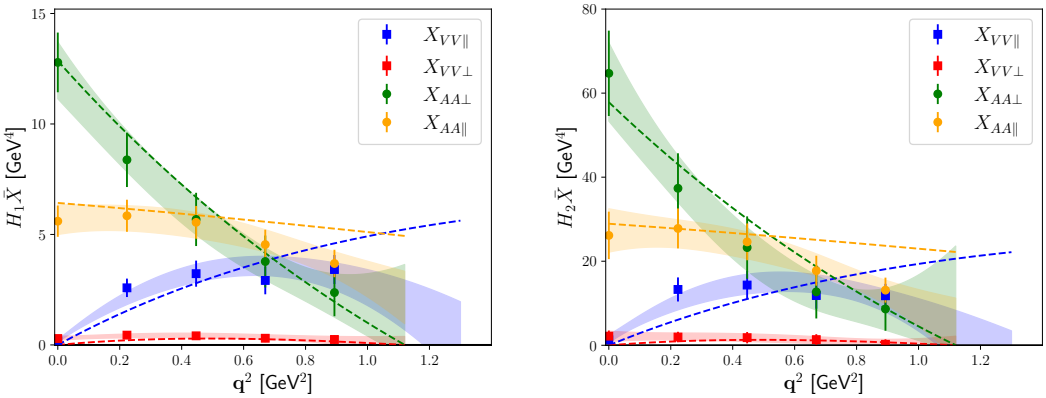

Figure 5.3.2: $H_1\bar{X}$ (left panel) and $H_2\bar{X}$ (right panel), which are numerators of eq. (5.2.37), as a function of $\boldsymbol{q}^2$. The results are shown for each channel. The dashed curves are estimated contributions from the ground state of D and D^*.

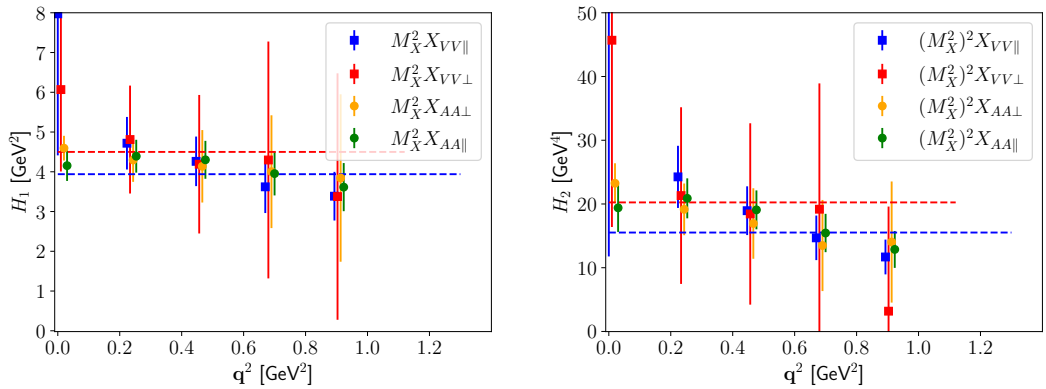

Figure 5.3.3: $\langle H_1 \rangle_{\boldsymbol{q}^2}$ (left panel) and $\langle H_2 \rangle_{\boldsymbol{q}^2}$ (right panel) for each channel. The dashed lines are those of the expected contribution from the ground state.

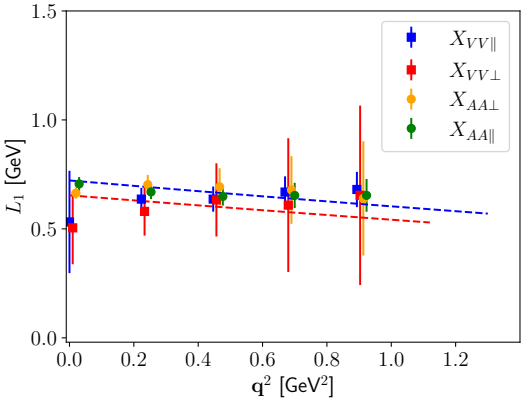

Figure 5.3.4: $\langle L_1 \rangle_{\boldsymbol{q}^2}$ for each channel. The dashed lines are those of the expected contribution from the ground state.

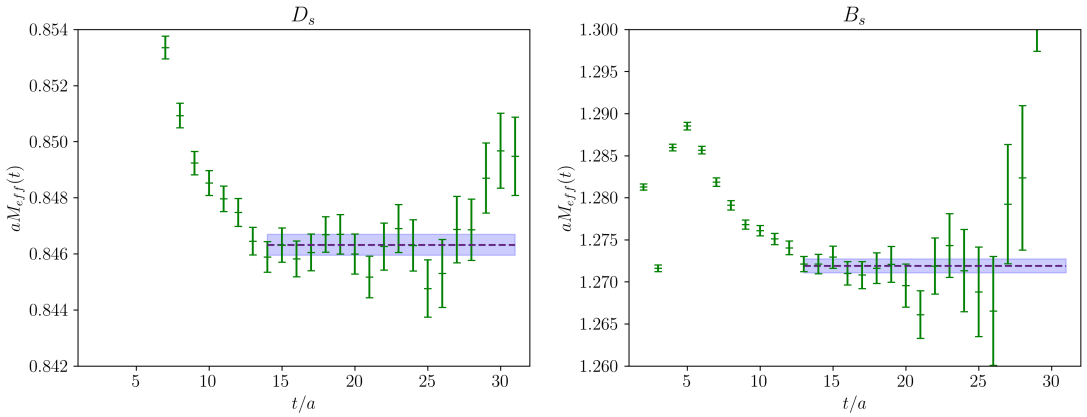

Figure 5.3.5: Effective mass $aM_{\rm eff}(t) \equiv \log\left(C(t)/C(t+a)\right)$ in lattice units for the D_s-meson (left panel) and the B_s-meson (right panel) correlation function (5.2.21), evaluated using the ETMC gauge ensemble B55.32 for bare quark masses equal to $a\mu_b = 0.50$, $a\mu_c = 0.25$ and $a\mu_s = 0.021$, corresponding to renormalised quark masses $m_b(\overline{\rm MS}, 2\,{\rm GeV}) \simeq 2.4$ GeV, $m_c(\overline{\rm MS}, 2\,{\rm GeV}) \simeq 1.2$ GeV and $m_s(\overline{\rm MS}, 2\,{\rm GeV}) \simeq 100$ MeV. The values of the Wilson r-parameter of the two valence quarks are opposite, i.e. $r_c = -r_s$ in the D_s meson and $r_b = -r_s$ in the B_s meson.

In order to avoid the mixing of K- and D-meson states in the correlation functions a non-unitary setup [135] is used in the valence sectors: the strange and the charm valence quarks are regularised as Osterwalder-Seiler fermions [204], while the up and down valence quarks have the same action as the sea. Working at maximal twist, such a setup guarantees an automatic $\mathcal{O}(a)$-improvement [134, 135].

The ensemble B55.32 has a lattice volume $L^3 \times T = (32^3 \times 64)\ a^4$ with a lattice spacing equal to $a = 0.0815(30)$ fm and a bare light-quark mass equal to $a\mu_\ell = 0.0055$, corresponding to a simulated pion mass $m_\pi = 375(13)$ MeV [104] with $m_\pi L \simeq 5.0$. The number of analyzed gauge configurations, separated by 20 trajectories, is 150. We have carried out our simulations using the values $a\mu_s = 0.021$ and $a\mu_c = 0.25$ for the bare valence strange and charm quark masses, which correspond to renormalised strange and charm quark masses very close to their physical values.

We have calculated the two-point function $C(t)$, defined in eq. (5.2.21), using the interpolating operator $\bar{b}(x)\gamma_5 s(x)$ with a simulated b-quark mass equal to twice the physical charm mass, i.e. $m_b(\overline{\rm MS}, 2\,{\rm GeV}) \simeq 2.4$ GeV, and a physical strange quark. We set opposite Wilson parameters for the two valence quarks in order to guarantee that cutoff effects on the pseudoscalar mass are $O(a^2\mu_f)$ [122, 133, 134]. To improve the statistical precision we have made use of the "one-end trick" stochastic method [131, 200] and employed 10 spatial stochastic sources at a randomly chosen time-slice per gauge configuration. Moreover, in order to suppress contributions of the excited states in the B_s-meson correlation function, we have used Gaussian smeared interpolating quark fields [160] both at the source and at the sink. For the values of the smearing parameters we set $k_G = 4$ and $N_G = 30$. In addition, we apply APE smearing to the gauge links [31] in the interpolating fields with parameters $\alpha_{\rm APE} = 0.5$ and $N_{\rm APE} = 20$.

Smearing leads to improved projection onto the lowest-energy eigenstate at smaller Euclidean time separations. As shown by the effective mass $aM_{\rm eff}(t) \equiv \log\left(C(t)/C(t+a)\right)$ in fig. 5.3.5, the dominance of the ground-state signal starts around $t/a \simeq 13$ for both the D_s and B_s mesons. By averaging over the plateau regions shown in fig. 5.3.5 the ground-state masses

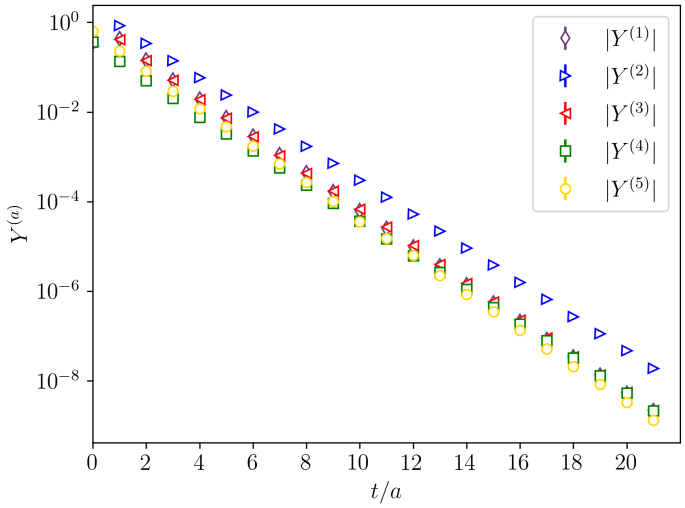

Figure 5.3.6: Time dependence of the correlators $Y^{(a)}(t;\boldsymbol{q})$ for $|\boldsymbol{q}| \simeq 0.5$ GeV calculated on the ETMC ensemble B55.32. The error bars are smaller than the point markers on this scale and a similar quality of the numerical signal is observed for the other momentum values considered in this work.

are respectively found to be $m_{D_s} = 2.05(8)$ GeV and $m_{B_s} = 3.08(11)$ GeV.

We have calculated the four-point function $C_{\mu\nu}(t_{\rm snk}, t_2, t_1, t_{\rm src}; \boldsymbol{q})$, given by eq. (5.2.18), as a function of t_1, the time at which the first weak current is inserted with momentum $\boldsymbol{q}$, for fixed values of t_2, where the second weak current is contracted with momentum insertion $-\boldsymbol{q}$, fixing $t_{\rm src} = 0$ and $t_{\rm snk} = T/2 = 32a$. The momentum $\boldsymbol{q}$ is inserted along one spatial direction, namely $\boldsymbol{q} = (0, 0, q)$ and we have considered eleven values for q ranging from $q = 0$ up to $q = q_{\rm max} \simeq 0.9$ GeV. On the lattice these values are injected through the use of twisted boundary conditions (BC's) [64,115,157] in the spatial directions and anti-periodic BC's in time. The sea dynamical quarks, on the contrary, are simulated with periodic BC's in the spatial directions and anti-periodic ones in time. The twisted BC's for the valence quark fields lift the severe limitations, arising from the use of periodic BC's, on the accessible kinematical regions of momentum-dependent quantities. Furthermore we remark that, as shown in refs. [65, 212], for physical quantities which do not involve final-state interactions (like, e.g., meson masses, decay constants and form factors), the use of different BC's for valence and sea quarks produces only finite-size effects that are exponentially small.

For the $b \to c$ weak current we use the local vector and axial-vector quark currents, $\overline{b}(x)\gamma_\mu c(x)$ and $\overline{b}(x)\gamma_\mu\gamma_5 c(x)$. The value of the Wilson r-parameter for the charm quark is chosen to be opposite to that of the b quark, i.e. $r_c = -r_b$, and therefore in our maximally twisted setup the vector and axial-vector currents renormalise respectively with the axial and vector renormalization constants, Z_A and Z_V, determined in ref. [104].

We extract the matrix elements $M_{\mu\nu}(t_2 - t_1; \boldsymbol{q})$ using eq. (5.2.20). In order to calculate $\bar{X}(\boldsymbol{q}^2)$, as defined in eq. (5.2.17), we apply the smearing kernel $\Theta^{(l)}(\omega_{\rm max} - \omega)$ to the quantities $Z^{(l)}(\omega, \boldsymbol{q}^2)$. These in turn are defined in terms of the quantities $Y^{(a)}(\omega, \boldsymbol{q})$ in eq. (5.2.15). To this end we start from the linear combinations of the correlators $M_{\mu\nu}(t; \boldsymbol{q})$ with the kinematical

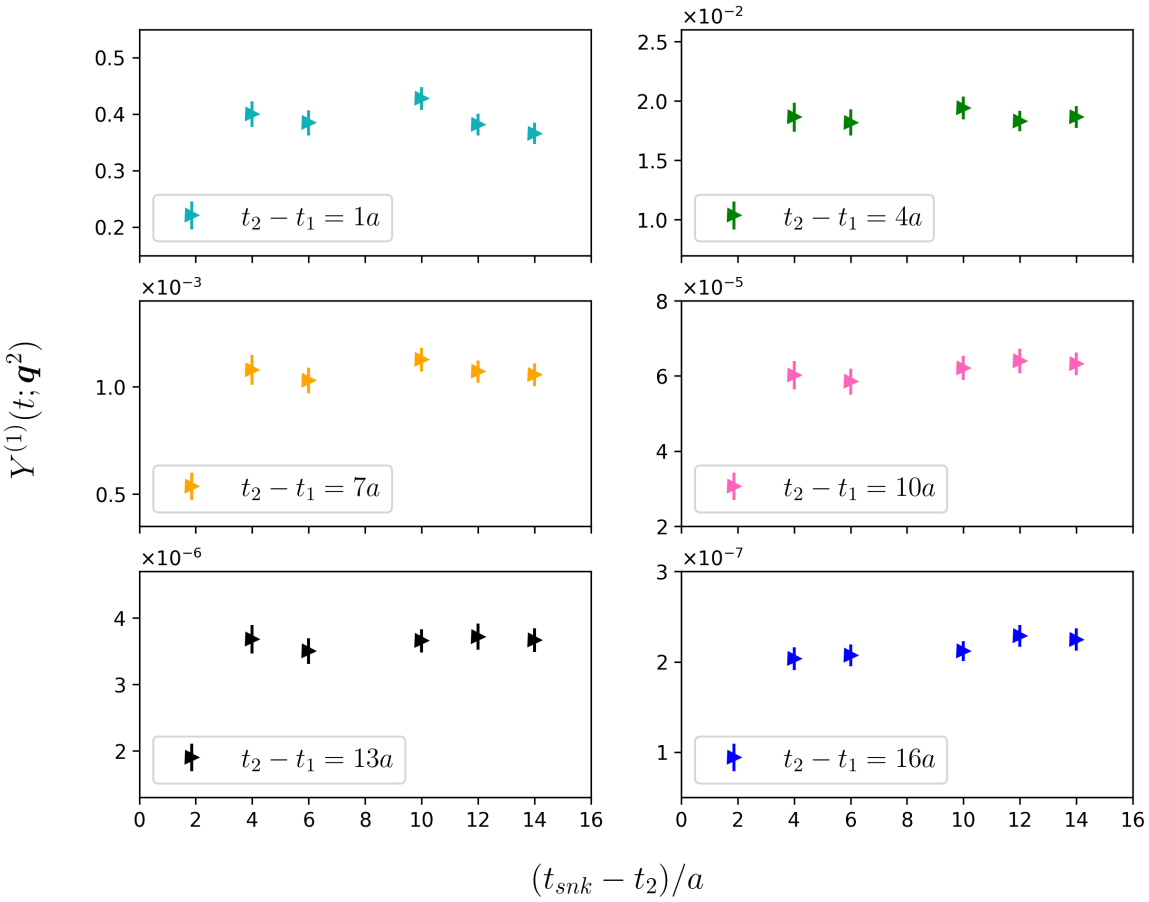

Figure 5.3.7: Correlator $Y^{(1)}(t, \boldsymbol{q}^2)$ at various time separations $t_2 - t_1$ for $|\boldsymbol{q}| \simeq 0.5$ GeV. The points in each subplot are obtained for different values of t_2, with the x-axis showing the distance between $t_{\rm snk}$ and the time t_2 at which the current is inserted.

coefficients of eqs. (5.2.9). We call these objects

$$Y^{(a)}(t;\boldsymbol{q}^2) = \int_0^\infty d\omega\, Y^{(a)}(\omega,\boldsymbol{q}^2)\, e^{-\omega t}\,, \qquad a = 1,\cdots,5\,,$$
$$Z^{(l)}(t;\boldsymbol{q}^2) = \int_0^\infty d\omega\, Z^{(l)}(\omega,\boldsymbol{q}^2)\, e^{-\omega t}\,, \qquad l = 0,1,2\,. \tag{5.3.1}$$

To show the quality of the numerical data, in fig. 5.3.6 we plot the correlators $Y^{(a)}(t;\boldsymbol{q}^2)$ corresponding to $|\boldsymbol{q}| \simeq 0.5$ GeV. Notice that the correlators $Z^{(l)}(t;\boldsymbol{q}^2)$ are linear combinations of the $Y^{(a)}(t;\boldsymbol{q}^2)$'s, see eq. (5.2.15). Similar results are obtained for the other momenta considered in this work.

The central values for all the physical quantities extracted from the $Y^{(a)}(t,\boldsymbol{q})$ correlators have been extracted by setting $t_2 = 22a$ in eq. (5.2.20) and by using the data up to $t = 18a$, which corresponds to $t_1 - t_{\rm src} = 4a$. To check the approach to the $t_{\rm src} \to -\infty$ and $t_{\rm snk} \to \infty$ limits we have repeated the analysis by setting $t_2 = \{18a, 20a, 22a, 26a, 28a\}$ and by varying the maximum value of t used to reconstruct the smearing kernels. Figure 5.3.7 shows the comparison of the correlator $Y^{(1)}(t,\boldsymbol{q})$ at $|\boldsymbol{q}| \simeq 0.5$ GeV for different values of $t = t_2 - t_1$ and

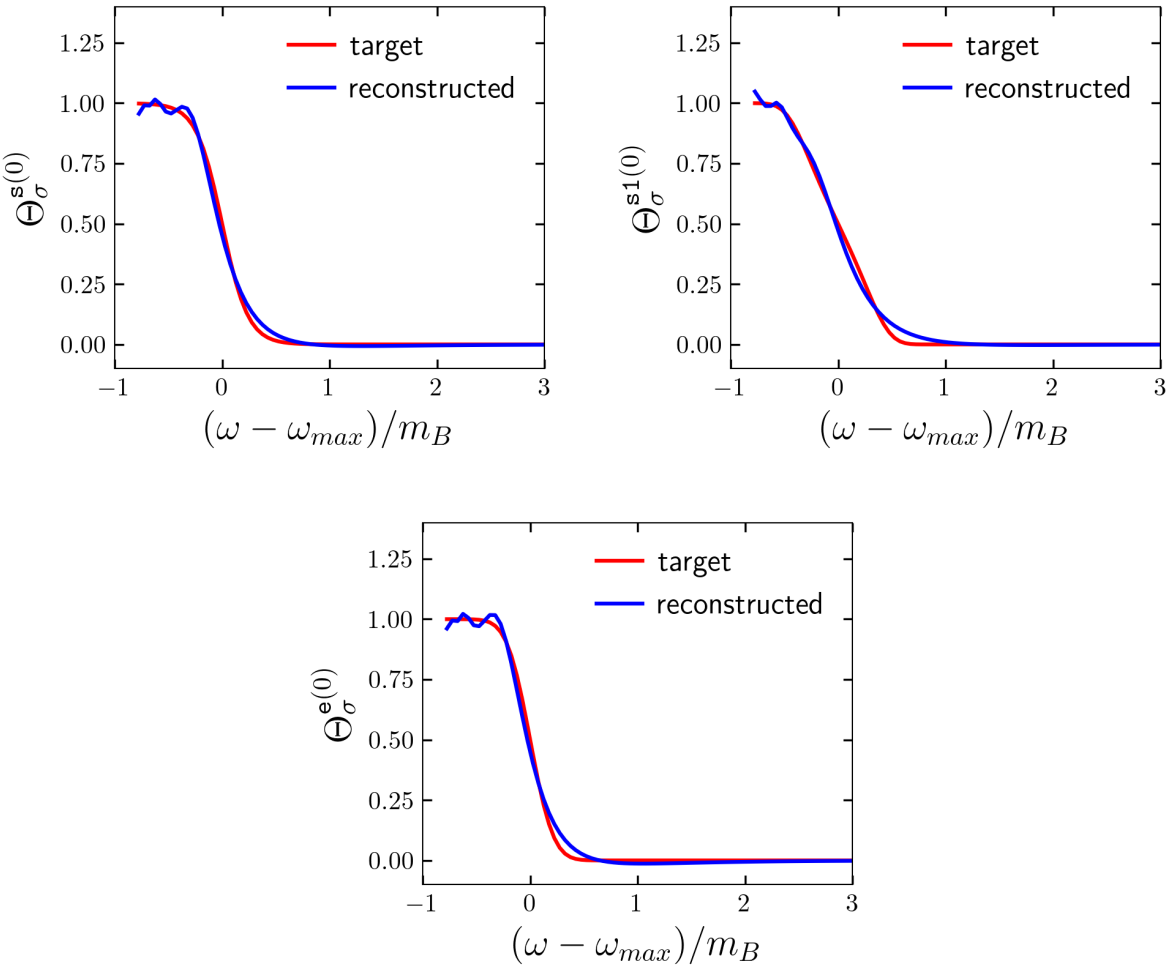

Figure 5.3.8: Reconstruction of the kernels $\Theta^{(0)}_\sigma(\omega_{\rm max} - \omega)$ defined with the three smearing types `s`, `s1` and `e`, see eq. (5.2.36), at $\lambda = \lambda_\star$. The data correspond to $|\boldsymbol{q}| \simeq 0.7$ GeV and $\sigma = 0.12 m_{B_s}$, the smallest value of the smearing parameter that we used.

t_2. In the following analysis, we chose the value $(t_{\rm snk} - t_2) = 10a$, corresponding to $t_2 = 22a$. Similar results are obtained for the other correlators ($Y^{(2)}$, $Y^{(3)}$, $Y^{(4)}$ and $Y^{(5)}$), and, in all cases, we observe that the onset of the $t_{\rm snk} \to \infty$ limit is reached within the uncertainties already for $t_{\rm snk} - t_2 = 4a$.

We now turn to the discussion of the systematics associated with the approximation of the kernels of eq. (5.2.36) by using the method of ref. [162]. This is an important issue because, on the one hand, the reconstruction of a given kernel can never be exact with a finite number of time-slices and in the presence of errors. On the other hand, one can (and must) quantify the systematic error associated with an approximate reconstruction.

In order to illustrate this point we consider the quantity $Z^{(0)}_\sigma(\boldsymbol{q}^2)$ (see eq. (5.2.17)) for three smooth approximations of the θ-function given in eq. (5.2.36). The kernels are approximated as described in section 5.2, see in particular eq. (5.2.31), with $\tau_{\rm max} = 18$. The quantity $Z^{(0)}_\sigma(\boldsymbol{q}^2)$ is then obtained by applying the coefficients g^λ_τ that represent the approximated kernel at a fixed value of λ to the correlator $Z^{(0)}(t; \boldsymbol{q}^2)$. Figure 5.3.8 shows the comparison of the reconstructed kernels with the target ones for $|\boldsymbol{q}| \simeq 0.7$ GeV and $\sigma = 0.12 m_{B_s}$ at the values $\lambda = \lambda_\star$ determined

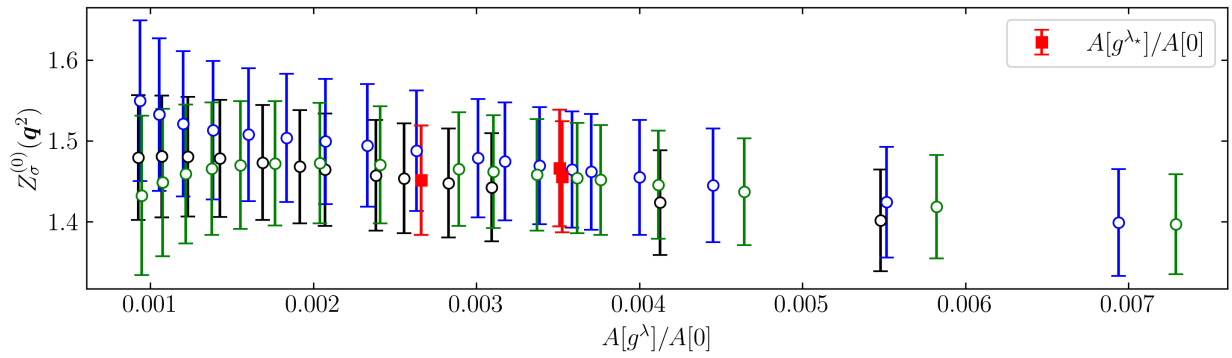

Figure 5.3.9: Integral $\bar{Z}_\sigma^{(0)}(\boldsymbol{q})$ of the hadronic correlator with three kernels, plotted as a function of $A[g^\lambda]/A[0]$. No significant difference is observed within the statistical errors for values $A[g^\lambda]/A[0]$ smaller than $A[g^{\lambda_\star}]/A[0]$.

independently for each kernel. The values of $\lambda_\star$ are marked with red points in fig. 5.3.9, where we show the dependence of $Z_\sigma^{(0)}(\boldsymbol{q}^2)$ on the normalised L_2-norm $A[g^\lambda]/A[0]$. As explained in section 5.2, for smaller values of λ one obtains a more accurate reconstruction of the kernels and thus smaller $A[g^\lambda]/A[0]$ values. There is no significant difference on the final results for $Z_\sigma^{(0)}(\boldsymbol{q})$ by decreasing λ with respect to $\lambda_\star$.

By implementing this strategy, proposed in ref. [96], we have checked that the estimated errors on the different quantities that enter our determinations of the physical observables discussed below properly take into account the systematics associated with the kernel approximation.

In fig. 5.3.10 we show our results for the total decay rate, with the different points corresponding to different input parameters used in the analysis, as described in the figure's caption. The plot shows clearly that all results are compatible with each other. In order to take into account all the results showed in the figure, we use eq. (28) of ref. [104] to get an estimate of the central value and its standard deviation, corresponding to the filled red dots in the plot, and we quote that value as our final result for the total decay rate. This procedure is repeated for all other observables considered in this work.

The final ETMC results for all the physical observables, divided into four different channels, are shown together with the OPE results in figures 5.4.1, 5.4.4, 5.4.6, and 5.4.7.

5.3.3 Extrapolation to $\sigma = 0$

The ETMC data are produced at several values of the smearing parameter σ and, for each of the target kernels $\Theta^{(l)}(x)$ with three different smeared versions of the θ-function in eq. (5.2.36). These are used in a combined $\sigma \to 0$ extrapolation for each contribution to the differential decay rate and to the leptonic and hadronic moments.

Before presenting the results of the $\sigma \to 0$ extrapolation an important remark is needed. As discussed in section 5.2 the limits of zero smearing radius and of infinite volume do *not* commute. Because of the quantized energy spectrum on a finite volume, the $\sigma \to 0$ extrapolation must be performed only after the infinite-volume limit. Under the reasonable assumption that smeared QCD spectral densities are affected by exponentially suppressed finite-volume effects, and given the exploratory nature of the present work, we shall assume below that finite-volume effects are negligible with respect to our statistical uncertainties. This assumption can only be verified with simulations on larger volumes, a task that we leave for future work on the

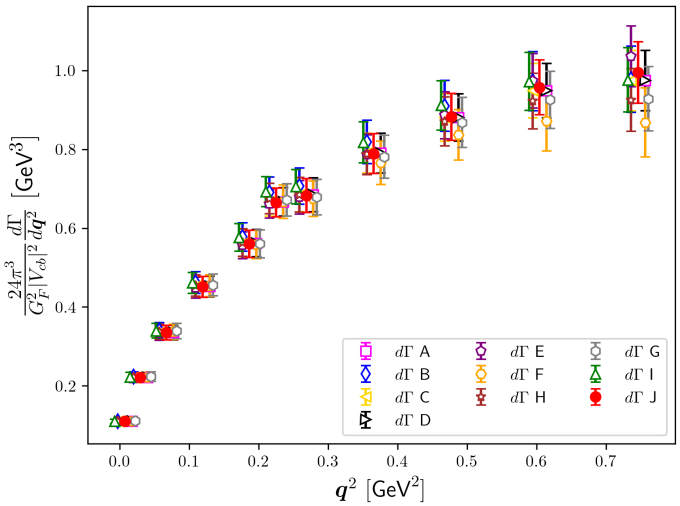

Figure 5.3.10: Results for $\frac{24\pi^3}{G_F^2|V_{cb}|^2}\frac{d\Gamma}{dq^2}$, obtained changing the parameters given as input to our analysis. The default values are: $A_{tr} = 1 \times 10^{-3}$, $\tau_{max} = 18$, extrapolations to $\sigma = 0$ using 5 values of σ. The letters in the legend stand for: **A)** All parameter equal to default, the final result is given by extrapolating to $\sigma = 0$ the single components $X^{(i)}$ and then summing the extrapolations together. **B)** The same as case **(A)** but with extrapolations done employing all 10 values of σ, as quoted in the caption of fig. 5.3.11. **C)** A threshold changed to $A_{tr} = 1 \times 10^{-2}$. **D)** A threshold changed to $A_{tr} = 5 \times 10^{-3}$. **E)** All parameters equal to default, final result given by summing all the single contributions $X^{(i)}$ together and then extrapolation the sum to $\sigma = 0$. **F)** τ_{max} changed to $\tau_{max} = 15$. **G)** τ_{max} changed to $\tau_{max} = 16$. **H)** τ_{max} changed to $\tau_{max} = 17$. **I)** Same as default, analysis performed using the bootstrap method. **J)** Final results obtained considering all previous results listed here. Central value and standard deviation are calculated using the average procedure given by eq. (28) of ref. [104]. It is important to note that the analysis of all the cases listed above is performed taking the result corresponding to $\lambda = \lambda_\star$ as discussed in subsection 5.3.2, the only exception being when we change the A_{tr} parameter. In these two cases we take the results corresponding to values of $A[g^\lambda]/A[0]$ smaller than A_{tr}.

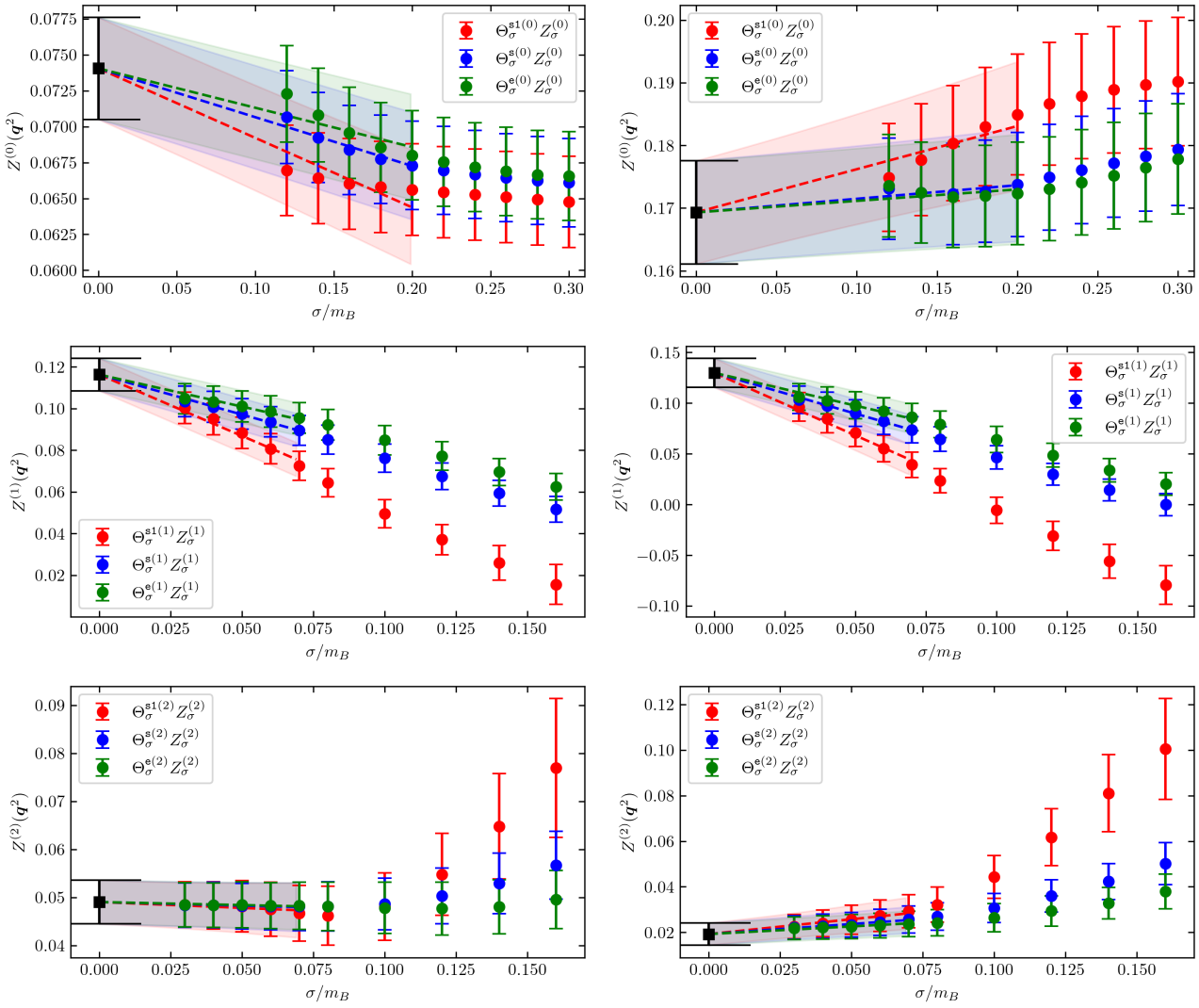

Figure 5.3.11: Combined $\sigma \to 0$ extrapolations of three contributions $Z^{(l)}(\boldsymbol{q}^2)$ to the differential decay rate, see eq. (5.2.17). The plots on the left correspond to $|\boldsymbol{q}| \simeq 0.5$ GeV while those on the right to $|\boldsymbol{q}| \simeq 0.7$ GeV. The reconstruction of the kernels $\Theta_\sigma^{(0)}(\omega_{\rm max} - \omega)$ is more difficult from the numerical point of view w.r.t. the case of the kernels $\Theta_\sigma^{(l)}(\omega_{\rm max} - \omega)$ with $l = 1, 2$. In all cases we have obtained results at 10 different values of σ that, in the case of $\Theta_\sigma^{(0)}(\omega_{\rm max} - \omega)$ span the region $\sigma \in [0.12 m_{B_s}, 0.3 m_{B_s}]$ while in the other case we have $\sigma \in [0.03 m_{B_s}, 0.16 m_{B_s}]$. In all cases we include the five smallest values of σ into a combined linear extrapolation to quote our results at $\sigma = 0$.

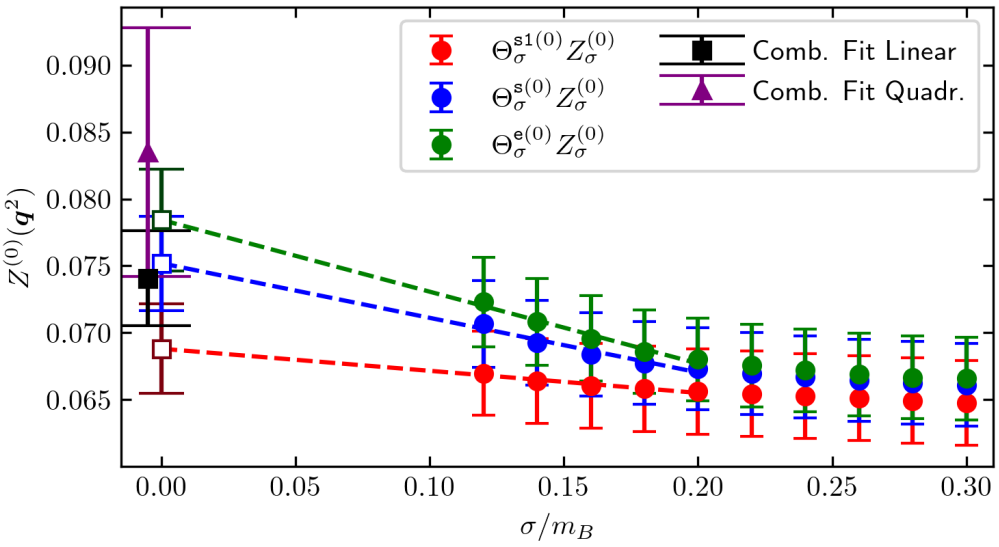

Figure 5.3.12: Systematics associated with the $\sigma \to 0$ extrapolation of $Z^{(0)}(\boldsymbol{q}^2)$ at $|\boldsymbol{q}| \simeq 0.5$ GeV, the same set of data shown in the top–left panel of fig. 5.3.11. The unconstrained linear extrapolations of the different sets of data, corresponding to the three different smearing kernels, are shown together with the results of the combined linear extrapolation of the five points at the smaller values of σ (black point) and of the combined quadratic extrapolation including all ten values of σ (violet point). The black and violet points have been slightly displaced on the horizontal axis to help the eye.

subject. Taking this issue into account, the $\sigma \to 0$ extrapolation discussed below has to be considered as a feasibility study that, as we work at unphysical meson masses and fixed cutoff, we consider interesting and promising.

In fig. 5.3.11 we show the $\sigma \to 0$ extrapolations of the three contributions $Z_\sigma^{(l)}(\boldsymbol{q}^2)$ to the differential decay rate for $|\boldsymbol{q}| \simeq 0.5$ GeV (plots on the left) and $|\boldsymbol{q}| \simeq 0.7$ GeV (plots on the right). The reconstruction of the kernels $\Theta_\sigma^{(0)}(\omega_{\rm max} - \omega)$ is more challenging from the numerical point of view with respect to the case of the kernels $\Theta_\sigma^{(l)}(\omega_{\rm max} - \omega)$ with $l = 1, 2$. In all cases studied in this work we have obtained results at 10 different values of σ that, for the kernel $\Theta_\sigma^{(0)}(\omega_{\rm max} - \omega)$ span the region $\sigma \in [0.12 m_{B_s}, 0.3 m_{B_s}]$ while for the other kernels we have $\sigma \in [0.03 m_{B_s}, 0.16 m_{B_s}]$. For all the values of $\boldsymbol{q}^2$ we have included the five smallest σ values into a combined linear extrapolation to obtain the central values and statistical errors that we quote for our results at $\sigma = 0$. As evident from the plots in fig. 5.3.11 there is a reassuring convergence of the results corresponding to the different kernels for small values of σ. The five points included in the fit are always in the linear regime and the χ^2/d.o.f. for all the combined $\sigma \to 0$ linear extrapolations performed in this work never exceed 1.

The systematics associated with the $\sigma \to 0$ extrapolations has been quantified (see also the caption of fig. 5.3.10) by performing unconstrained linear extrapolations of the five points at the smaller values of σ and combined quadratic extrapolations of all points, i.e. with ten values of σ. This procedure is illustrated in fig. 5.3.12 where we show, for the same set of data appearing in the top–left panel of fig. 5.3.11, the unconstrained linear extrapolations and the result of the combined quadratic extrapolation (violet point). As can be seen in this plot, the results of the three different unconstrained extrapolations are compatible within the quoted errors and also compatible with our central value result (black point). Following the procedure explained

in the caption of fig. 5.3.10, i.e. estimating the systematics associated with the extrapolation by adding in quadrature the statistical error of the black point and the difference between the central values of the black and violet points, largely takes into account the spread of the results coming from the different extrapolations, including the unconstrained ones. The same procedure has been repeated for all the sets of data analyzed in this work and similar plots can be shown in all cases.

In fig. 5.3.13 we show the $\sigma \to 0$ extrapolations of the four different terms that enter the calculation of the leptonic moment $L_1(\boldsymbol{q}^2)$.

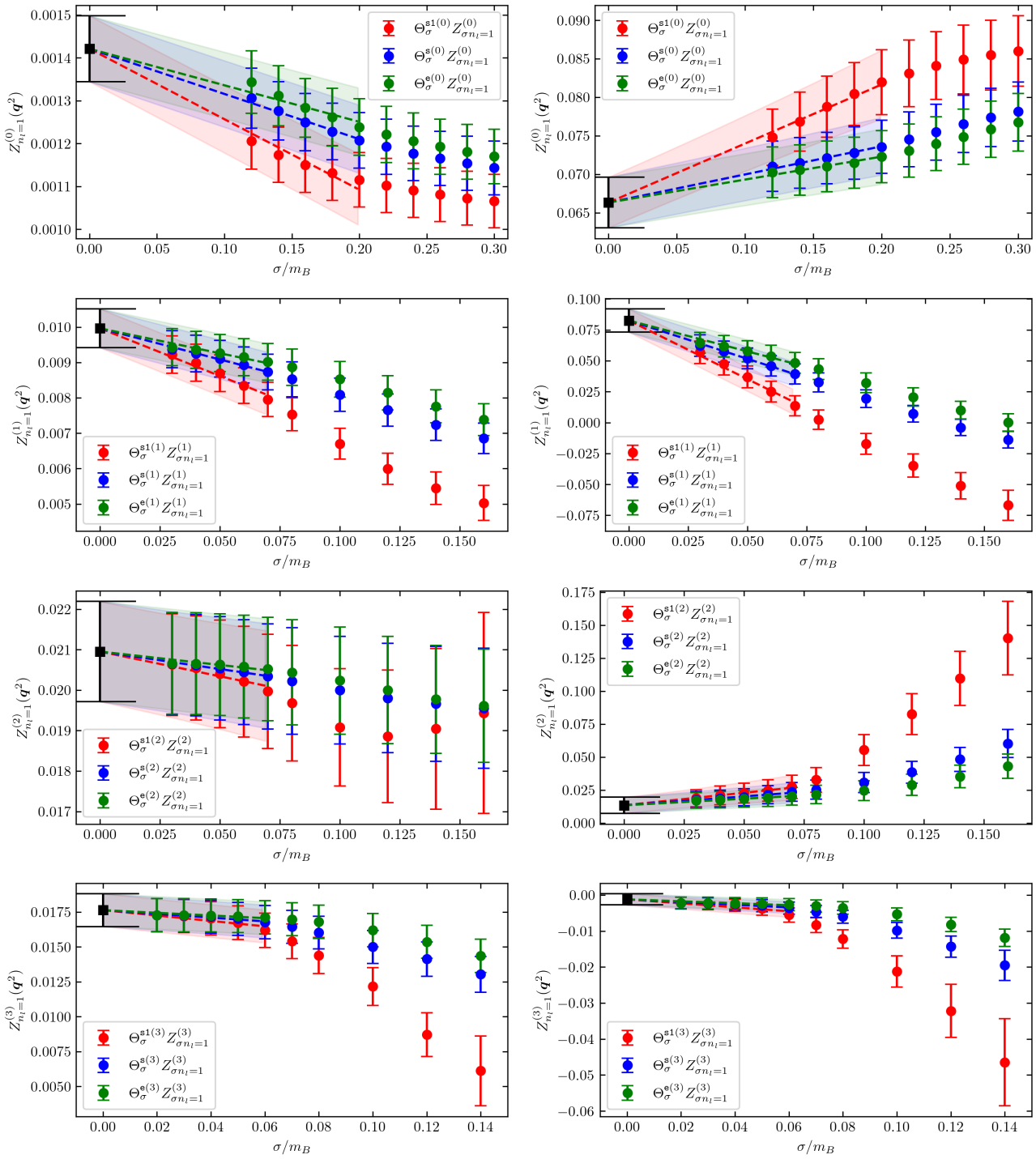

Figure 5.3.13: Combined $\sigma \to 0$ extrapolations of the four contributions $Z^{(l)}_{n_\ell=1}(\boldsymbol{q}^2)$ to the first leptonic moment, see eq. (5.2.45). The plots on the left correspond to $|\boldsymbol{q}| \simeq 0.26$ GeV while those on the right to $|\boldsymbol{q}| \simeq 0.78$ GeV.

5.4 Operator-product expansion and comparison with lattice results

As inclusive semileptonic B decays are described by an OPE, observables which are sufficiently inclusive admit a double expansion in α_s and in inverse powers of m_b [77, 79, 83, 105, 197], or more precisely of the energy release, which is of the order of $m_b - m_c$. Schematically, for an observable M we have

$$\begin{aligned} M =& M^{(0)} + M^{(1)} a_s + M^{(2)} a_s^2 + \left(M_\pi^{(0)} + M_\pi^{(1)} a_s \right) \frac{\mu_\pi^2}{m_b^2} \\ &+ \left(M_G^{(0)} + M_G^{(1)} a_s \right) \frac{\mu_G^2}{m_b^2} + M_D^{(0)} \frac{\rho_D^3}{m_b^3} + M_{LS}^{(0)} \frac{\rho_{LS}^3}{m_b^3} + \dots \end{aligned} \tag{5.4.1}$$

where $a_s = \alpha_s(\mu)/\pi$ is the QCD coupling evaluated at a scale $\mu \sim m_b$ and the ellipsis represents higher-order terms in a_s and in $1/m_b$. The parameters μ_π^2, μ_G^2, ρ_D^3, ρ_{LS}^3 are expectation values of dimension-5 and dimension-6 local operators in the physical B meson. For instance,

$$\mu_\pi^2(\mu_k) = \frac{1}{2M_B} \langle B | \bar{b}_v \, \vec{\pi}^2 \, b_v | B \rangle_{\mu_k}, \qquad \mu_G^2(\mu_k) = \frac{1}{2M_B} \langle B | \bar{b}_v \frac{i}{2} \sigma_{\mu\nu} G^{\mu\nu} b_v | B \rangle_{\mu_k} \tag{5.4.2}$$

where $\vec{\pi} = -i\vec{D}$, while D^μ is the covariant derivative, $b_v(x) = e^{-i m_b v \cdot x} b(x)$ is the b field deprived of its high-frequency modes, and $G^{\mu\nu}$ is the gluon-field tensor. In the so-called kinetic scheme [76,113,125], the Wilsonian cutoff $\mu_k \sim 1$ GeV is introduced to factorise long- and short-distance contributions. Indeed, the OPE disentangles the physics associated with *soft* scales of order $\Lambda_{\rm QCD}$ (described by the above parameters) from that associated with *hard* scales $\sim m_b$, which determine the Wilson coefficients M_i that admit an expansion in α_s. Quite importantly, the power corrections start at $O(\Lambda_{\rm QCD}^2/m_b^2)$ and are therefore comparatively suppressed. The kinetic scheme provides a short-distance, renormalon-free definition of m_b and of the OPE parameters by introducing the cutoff μ_k to factor out the infrared contributions from the perturbative calculation.

The smearing provided by the phase-space integration, discussed in section 5.2, is in general sufficient to guarantee the convergence of the OPE for the quantities introduced in eqs. (5.2.6) and (5.2.37)–(5.2.40), which can then be expressed in the form (5.4.1). The OPE calculation proceeds therefore as in refs. [83, 149, 197]. There are however two specific points related to the kinematics chosen in the lattice calculation that need to be mentioned. First, while the hard scale that governs the OPE is generally $m_b - m_c$, there are regions of the phase space, e.g. at small recoil $|\boldsymbol{q}| \sim 0$, where it is rather m_c, possibly implying a slower convergence of the expansion. Second, near the maximum value of $\boldsymbol{q}^2$ the smearing interval in ω closes up and one cannot expect the OPE to provide reliable results.

5.4.1 Details of the OPE calculation and related uncertainties

From a technical point of view, the OPE provides a double expansion like the one in eq. (5.4.1) for the hadronic tensor $W^{\mu\nu}$ defined in eq. (5.2.4) that can be used to compute the total rate, the moments, and any sufficiently inclusive quantity. The coefficients of the expansion involve the Dirac delta $\delta(r^2 - m_c^2)$ and its derivatives, which upon integration over the *quark* (partonic) phase space lead to results valid for sufficiently inclusive observables. It is customary to use the decomposition of $W^{\mu\nu}$ into Lorentz-invariant form factors as in eq. (5.2.7) and to identify

the four-velocities of the B meson and of the b quark, $v = p/m_B = p_b/m_b$. In this section we will use eq. (5.2.7) replacing m_B with the b quark mass m_b and employing a hat for quantities that are normalised to m_b. In the case of massless leptons considered in this work, the form factors $W_{4,5}$ do not contribute to the decay amplitude.

The lowest order of the expansion for the relevant W_i and the $1/m_b^2$ corrections can be found in refs. [83,197], while analytic expressions for the $O(\alpha_s)$ terms are given in refs. [33,49]. The $O(1/m_b^3)$ corrections have been first computed in ref. [156]. Higher power corrections have been investigated in ref. [196], but involve a large number of new and poorly known parameters. They appear to be sufficiently suppressed at the physical m_b [145]; we will not consider them but they represent an important source of theoretical uncertainty in our low m_b setup. The $O(\alpha_s/m_b^2)$ corrections to the W_i are also known [33,34], while for the total rate we also have $O(\alpha_s/m_b^3)$ corrections [193,195]. Numerical results for the $O(\alpha_s^2\beta_0)$ contributions are also available [49], while the complete $O(\alpha_s^2)$ are available only for the total rate and for a few moments [80,201,205,206]. Finally, the $O(\alpha_s^3)$ correction to the total rate has been recently computed in ref. [126].

While these corrections have generally been computed in the $V-A$ case realised in the SM, the decomposition in VV, AA and $AV = VA$ components is potentially useful in our case, and has been made manifest for the $O(1/m_b^{2,3})$ and $O(\alpha_s)$ corrections, see refs. [32,83,107]. In the calculation of the $\boldsymbol{q}^2$ spectrum and of the differential moments we will therefore consider only power corrections up to and including $O(1/m_b^3)$ and the $O(\alpha_s)$ perturbative corrections. However in the calculation of the total width and of the total moments we will restrict to the SM case and will employ all the known corrections.

Following section 5.2, we take the three-momentum $\boldsymbol{q}$ to point along the k direction and the i and j directions to be perpendicular to that. The components of the hadronic tensor along these directions are given by

$$\begin{aligned}
W^{00} &= -W_1 + W_2 + \hat{q}_0^2 W_4 + 2\hat{q}_0 W_5 \,, \\
W^{ii} &= W^{jj} = W_1 \,, \\
W^{kk} &= W_1 + \hat{q}_k^2 W_4 \,, \\
W^{0i} &= W^{i0} = W^{ik} = W^{ki} = W^{jk} = W^{kj} = 0 \,, \\
W^{0k} &= W^{k0} = \hat{q}_0 \hat{q}_k W_4 + \hat{q}_k W_5 \,, \\
W^{ij} &= -W^{ji} = -i\epsilon^{ij0k}\hat{q}_k W_3 \,.
\end{aligned}$$

In the OPE the decay occurs at the quark level: $p_b = p' + p_\ell + p_\nu$, where p_b and p' are the momenta of the initial b quark and of a final hadronic state made of a c quark and $n \geq 0$ perturbative gluons. At the leading order in α_s and in $1/m_b$, this is a free-quark decay into an on-shell c quark, which implies that the W_i are proportional to $\delta(p'^2 - m_c^2) = \delta(\hat{u})/m_b^2$, where $\hat{u} = (p'^2 - m_c^2)/m_b^2$. We can rewrite this δ function in terms of the energy of the final c quark,

$$\delta(\hat{u}) = \frac{1}{2\sqrt{\hat{\boldsymbol{q}}^2 + \rho}} \left[\delta\left(\hat{\chi} - \sqrt{\hat{\boldsymbol{q}}^2 + \rho}\right) + \delta\left(\hat{\chi} + \sqrt{\hat{\boldsymbol{q}}^2 + \rho}\right) \right] \,, \tag{5.4.3}$$

where $\rho = m_c^2/m_b^2$ and $\hat{\chi}$ is the parton-level energy of the final hadronic state in units of m_b, which is related to the total hadronic energy ω by $\omega = m_b\hat{\chi} + \Lambda$, with $\Lambda = M_B - m_b$. Similarly, the invariant hadronic mass M_X^2 is related to the partonic variables by

$$M_X^2 = (p_B - q)^2 = (p_b + \Lambda v - q)^2 = m_b^2\hat{u} + 2m_b\Lambda\hat{\chi} + \Lambda^2 + m_c^2 \,.$$

Only the first term of eq. (5.4.3) contributes to the physical process of interest and can be readily integrated over $\hat{\chi}$. At $O(1/m_b^{2,3})$ one has to deal with $\delta'(\hat{u})$, $\delta''(\hat{u})$ and $\delta'''(\hat{u})$ that upon integration subject to kinematic constraints lead to new singularities. A typical case is provided by the interplay between the δ' and the requirement that $q^2 \geq 0$:

$$\begin{aligned}\int f(\hat{u})\,\theta\left(q^2\right)\,\delta'(\hat{u})\,d\hat{u} &= \int f(\hat{u})\,\theta(1+\rho+\hat{u}-2\sqrt{\rho+\hat{\boldsymbol{q}}^2+\hat{u}})\,\delta'(\hat{u})\,d\hat{u} \\ &= -f'(0)\theta(1+\rho-2\sqrt{\rho+\hat{\boldsymbol{q}}^2}) + f(0)\frac{1+\rho}{2}\delta(\hat{\boldsymbol{q}}^2-\hat{\boldsymbol{q}}^2_{\rm max})\,. \quad (5.4.4)\end{aligned}$$

The singularity at the partonic endpoint of the $\boldsymbol{q}^2$ spectrum, $\hat{\boldsymbol{q}}^2_{\rm max} = (1-\rho)^2/4$, appears because one reaches the maximum energy exactly on the mass-shell of the charm quark.

We apply exactly the same setup to compare with both JLQCD and ETMC data, adjusting only the heavy-quark masses to the two cases. The unphysically light b quark mass and the OPE parameters are expressed in the kinetic scheme with $\mu_k = 1$ GeV, while the c quark mass is expressed in the $\overline{\rm MS}$ scheme at 2 GeV. In the case of the JLQCD data we employ $m_b(1\text{ GeV}) = 2.70(4)$ GeV, obtained from matching the observed m_{B_s} with the results of [147, 148], and $\overline{m_c}^{(4)}(2\text{ GeV}) = 1.10(2)$ GeV. In the case of the ETMC data we employ $\overline{m_c}^{(4)}(2\text{ GeV}) = 1.186(41)$ GeV and $\overline{m_b}^{(4)}(2\text{ GeV}) = 2.372(82)$ GeV (with 100% correlated uncertainties), and translate the latter into the kinetic scheme using the three-loop conversion formula [125] implemented in version 3.1 of *RunDec* [166] obtaining $m_b(1\text{ GeV}) = 2.39(8)$ GeV. The strong coupling employed in the conversion and elsewhere is $\alpha_s^{(4)}(2\text{ GeV}) = 0.301$.

For the OPE parameters that appear in eq. (5.4.1) we start from the results of the most recent fit to the semileptonic moments [88], which refer to the physical B meson, with a much heavier b quark and without a strange spectator. The difference induced in these parameters by the strange spectator at the physical point has been investigated in [75, 91, 147], where it was found that spectroscopic and lattice data approximately suggest a 20% upward shift in μ_π^2 and μ_G^2, while heavy-quark sum rules hint at a similar or even stronger SU(3) flavour-symmetry breaking in ρ_D^3. The dependence on the mass of the heavy quark, on the other hand, can be analysed by observing that μ_π^2 and μ_G^2 satisfy a heavy-quark expansion

$$\mu_\pi^2 = \mu_\pi^2|_\infty - \frac{\rho^3_{\pi\pi}+\frac{1}{2}\rho^3_{\pi G}}{m_b} + \ldots, \qquad \mu_G^2 = \mu_G^2|_\infty + \frac{\rho_S^3+\rho_A^3+\frac{1}{2}\rho^3_{\pi G}}{m_b} + \ldots \quad (5.4.5)$$

where $\rho^3_{\pi\pi}$, $\rho^3_{\pi G}$, ρ^3_S, ρ^3_A are expectation values of non-local operators, of which little is known, see ref. [148]. If they were of the same order of magnitude of ρ_D^3 and ρ^3_{LS}, i.e. about 0.1–0.2 GeV^3, they could shift μ_π^2 and μ_G^2 by 0.02–0.1 GeV in going from the physical value of m_b to $m_b \sim 2.5$ GeV, which amounts to a 5–25% shift. We show the inputs of our calculation in table 5.4.1. While the heavy-quark masses are slightly different between the two setups, we adopt the same expectation values in both cases. Their central values take into account the shift related to the strange spectator, while the uncertainties follow from the uncertainty of the fit of ref. [88], the SU(3) symmetry breaking, and the lower b mass.

Beside the parametric uncertainty of the inputs, our results are subject to an uncertainty due the truncation of the expansion in eq. (5.4.1) and to possible violations of quark-hadron duality. We estimate the former by varying the OPE parameters, the heavy-quark masses, and α_s in an uncorrelated way and adding the relative uncertainties in quadrature. In particular, we shift $m_{b,c}$ by 6 MeV, $\mu^2_{\pi,G}$ by 15%, and $\rho^3_{D,LS}$ by 25%. These corrections should mimic the effect of higher-power corrections. Since in the case of the $\boldsymbol{q}^2$ spectrum and differential moments we restrict ourselves to $O(\alpha_s)$ corrections, we include the relative uncertainty in

m_b^{kin} (JLQCD)	2.70 ± 0.04
$\overline{m}_c(2\text{ GeV})$ (JLQCD)	1.10 ± 0.02
m_b^{kin} (ETMC)	2.39 ± 0.08
$\overline{m}_c(2\text{ GeV})$ (ETMC)	1.19 ± 0.04
μ_π^2	0.57 ± 0.15
ρ_D^3	0.22 ± 0.06
$\mu_G^2(m_b)$	0.37 ± 0.10
ρ_{LS}^3	-0.13 ± 0.10
$\alpha_s^{(4)}(2\text{ GeV})$	0.301 ± 0.006

Table 5.4.1: Inputs for our OPE calculation. All parameters are in GeV at the appropriate power and all, except m_c, in the kinetic scheme at $\mu = 1$ GeV. The heavy-quark masses for the ETMC setup are 100% correlated. As a remnant of the semileptonic fit, we include a 50% correlation between μ_π^2 and ρ_D^3.

the same way, shifting α_s by 0.15, which corresponds to a 50% uncertainty. In the case of the total width and total moments, higher-order perturbative corrections are known and the perturbative uncertainty can be reduced, as discussed below.

5.4.2 Comparison with lattice results

q^2 spectrum and differential moments

We start our comparison of lattice and OPE results with the $\boldsymbol{q}^2$ spectrum and the differential moments introduced in eq. (5.2.39) and in eq. (5.2.40). Only the $O(\alpha_s)$ perturbative corrections are included in this case. Figure 5.4.1 shows the $\boldsymbol{q}^2$ spectrum in the SM, namely with a $V-A$ current. Despite the large uncertainty of the OPE prediction, about 30% in the JLQCD case and 50% in the ETMC case, the overall agreement is good. The OPE uncertainty is dominated by the power corrections. We also stress that close to the partonic endpoint, corresponding to 1.27 GeV^2 and 0.82 GeV^2 in the two cases, we do not expect the OPE calculation to be reliable, as discussed above. The corresponding hadronic endpoints are 1.35 GeV^2 and 0.75 GeV^2, respectively.

The uncertainties affecting both calculations can be greatly reduced by considering the differential moments. In particular, the OPE uncertainty becomes smaller because of the cancellations between power corrections to the numerator and to the denominator. To expose the cancellations we expand the ratios in powers of α_s and $1/m_b$. In figure 5.4.2 we show the first differential lepton energy moment, $L_1(\boldsymbol{q}^2)$, in the SM, comparing the OPE with ETMC data. As expected, the relative uncertainty of both the OPE calculation and of the lattice data is much smaller than in the bottom panel of figure 5.4.1 and we observe good agreement at low and moderate $\boldsymbol{q}^2$.

Figs. 5.4.3 and 5.4.4 show the $\boldsymbol{q}^2$ spectrum in the individual channels. Comparing them with figure 5.4.1 we see that in the individual channels the agreement between OPE and lattice results is poorer than in their sum, especially at large $\boldsymbol{q}^2$. This is to be expected and (unless discretisation and/or finite-volume effects turn out to have a sizeable impact on the lattice results) is likely to be a manifestation of duality violations. Notice that the OPE central predictions for the $AA_\perp$ and $VV_\perp$ channels turn negative at large and moderate $\boldsymbol{q}^2$, respectively,

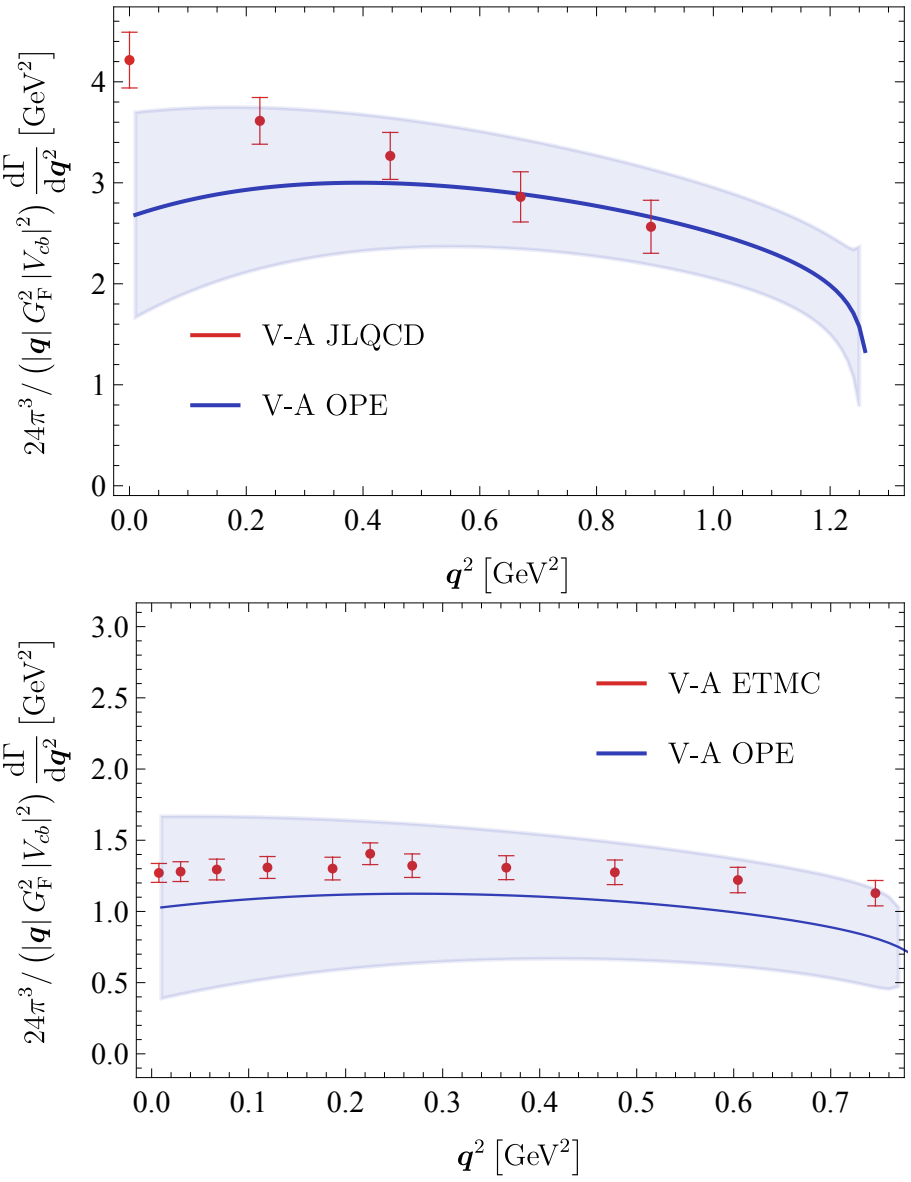

Figure 5.4.1: Differential $\boldsymbol{q}^2$ spectrum, divided by $|\boldsymbol{q}|$, in the SM. Comparison of OPE with JLQCD (top panel) and ETMC (bottom panel) data are shown.

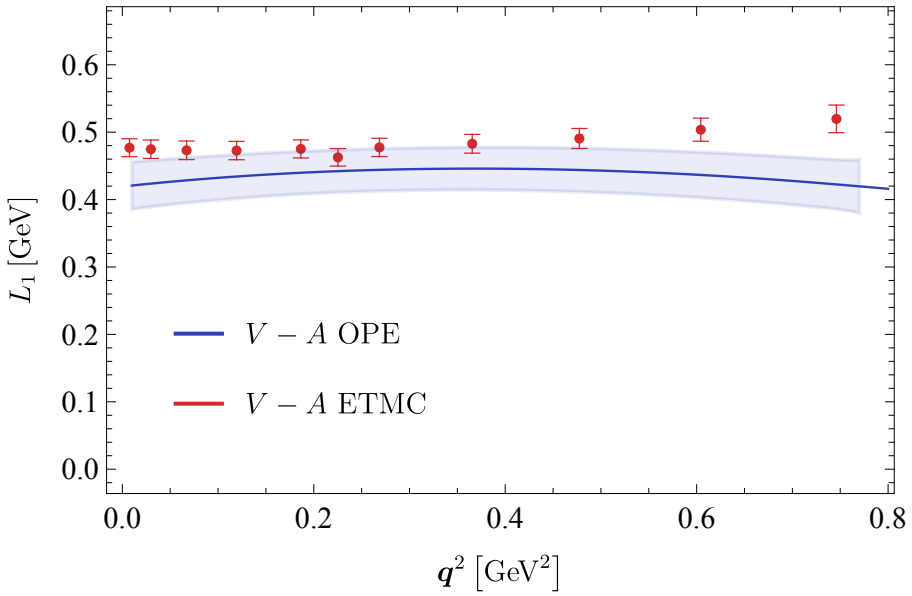

Figure 5.4.2: Differential lepton energy mean value, $L_1(\boldsymbol{q}^2)$, in the SM. The comparison of OPE with ETMC data is shown.

and that for $\boldsymbol{q}^2 > 0.6$ GeV^2 the spectrum is always negative within errors. This unphysical feature suggests that our error estimates are not adequate at large $\boldsymbol{q}^2$. The contribution to the $VV_\perp$ channel, moreover, is particularly small and very sensitive to large power corrections.

Figs. 5.4.5 and 5.4.6 show $L_1(\boldsymbol{q}^2)$ in the individual channels, for the JLQCD and ETMC cases. In general, we observe good agreement with the lattice data, especially at low $\boldsymbol{q}^2$. However, the expansion in powers of α_s and $1/m_b$ of the denominator is not justified when the lowest-order contribution to the denominator becomes particularly small or has a zero, like in the $VV_\parallel$ and $VV_\perp$ channels. In these cases we also show the unexpanded version of the ratio, whose uncertainty is much larger, but we stress that away from the singularities the expanded form is preferable, and this appears to be confirmed by better agreement with the lattice data.

Figure 5.4.7 shows the second central moment computed at different values of $\boldsymbol{q}^2$ in the ETMC case. We do not display the $VV_\perp$ channel, for which the OPE result would have a very large uncertainty. In the case of $L_{2c}(\boldsymbol{q}^2)$ the OPE does not reproduce the lattice results within uncertainties, except for very small $\boldsymbol{q}^2$. It is certainly possible that our method to estimate the OPE uncertainty fails here as a result of multiple cancellations between large contributions to L_2 and L_1^2 which are not necessarily replicated by higher-order contributions. On the other hand, it has not yet been possible to estimate discretisation and finite volume effects on our lattice results, and the additional systematics could affect this particular quantity in a relevant way. For this quantity we do not display the comparison with the JLQCD data, which agree with the OPE but have very large uncertainties.

We also looked at the moments of the hadronic invariant mass. In figure 5.4.8 we show the mean hadronic mass $\langle M_X^2 \rangle$ as a function of $\boldsymbol{q}^2$ computed from JLQCD configurations in comparison with the OPE predictions. Again, we do not display the $VV_\perp$ channel because of the large OPE uncertainty. We observe excellent agreement except at large $\boldsymbol{q}^2$, but the lattice uncertainty is larger here than in the case of the leptonic moments. Analogous plots for the ETMC calculation are shown in fig. 5.4.9. In figure 5.4.10 we also show $\langle M_X^4 \rangle$ as a function of $\boldsymbol{q}^2$ with JLQCD data.

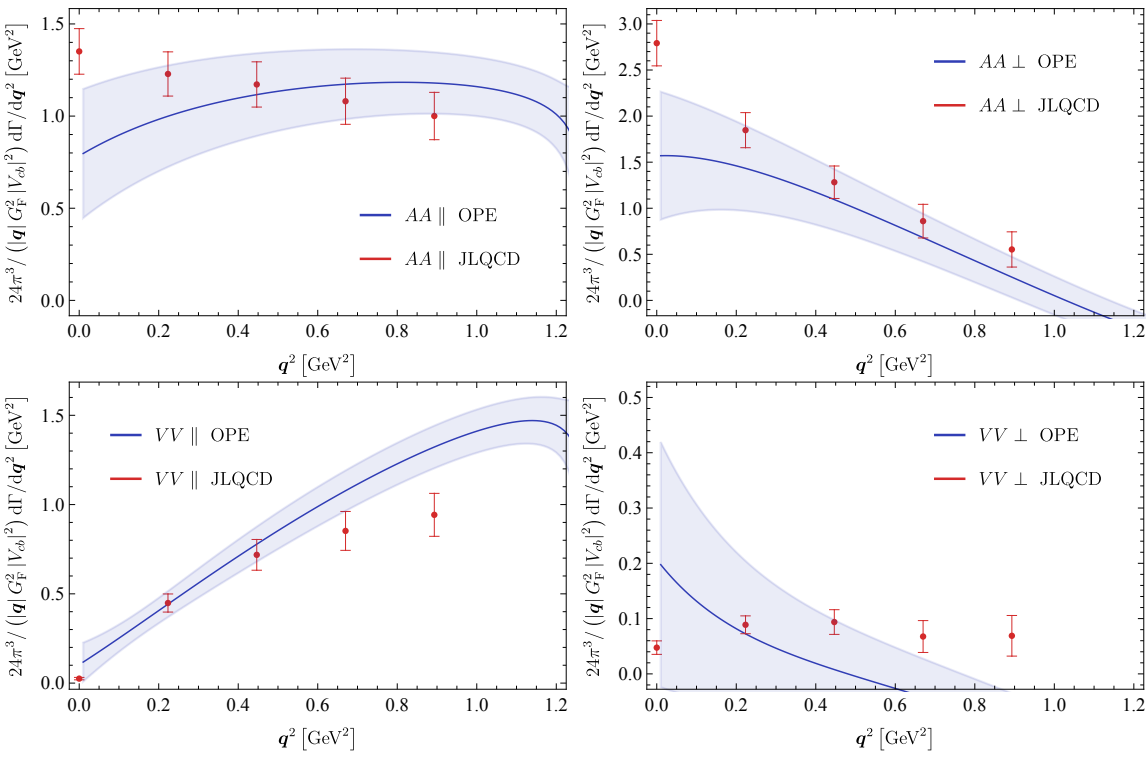

Figure 5.4.3: Differential $\boldsymbol{q}^2$ spectrum, divided by $|\boldsymbol{q}|$, in the various channels. The plots show the comparison between OPE and JLQCD data.

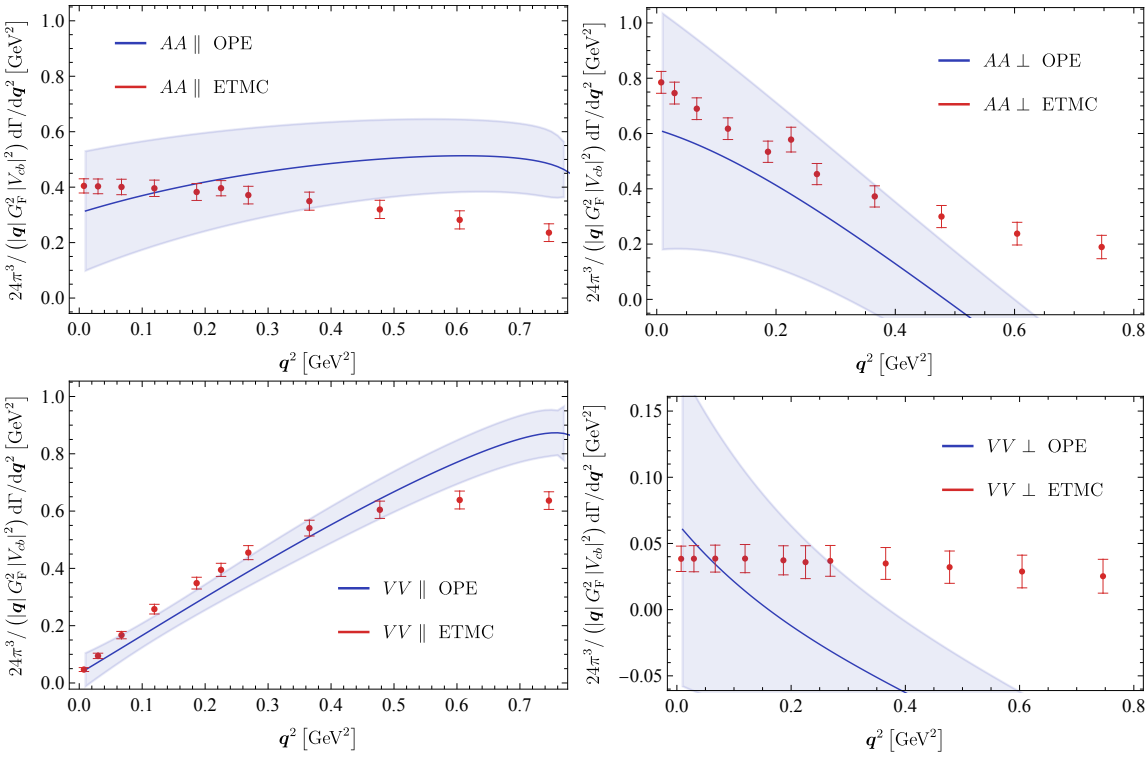

Figure 5.4.4: Differential $\boldsymbol{q}^2$ spectrum, divided by $|\boldsymbol{q}|$, in the various channels. The plots show the comparison between OPE and ETMC data.

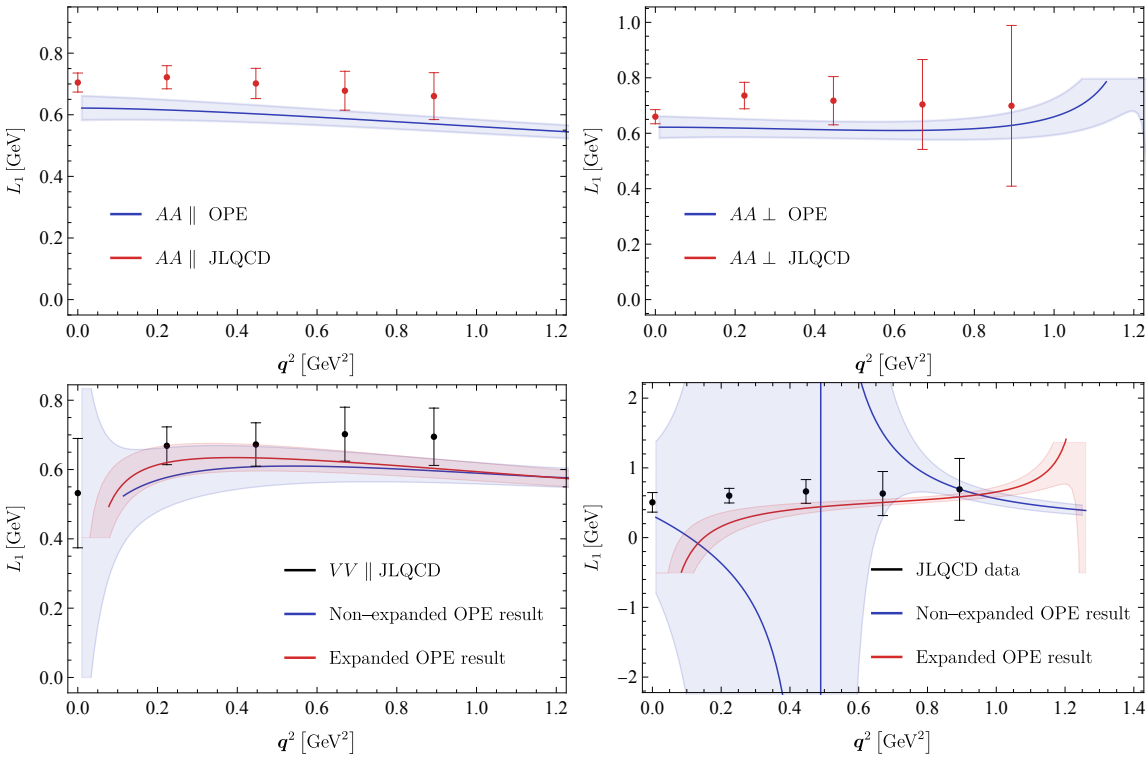

Figure 5.4.5: Differential first leptonic moment in the various channels. The plot shows the comparison between OPE and JLQCD data.

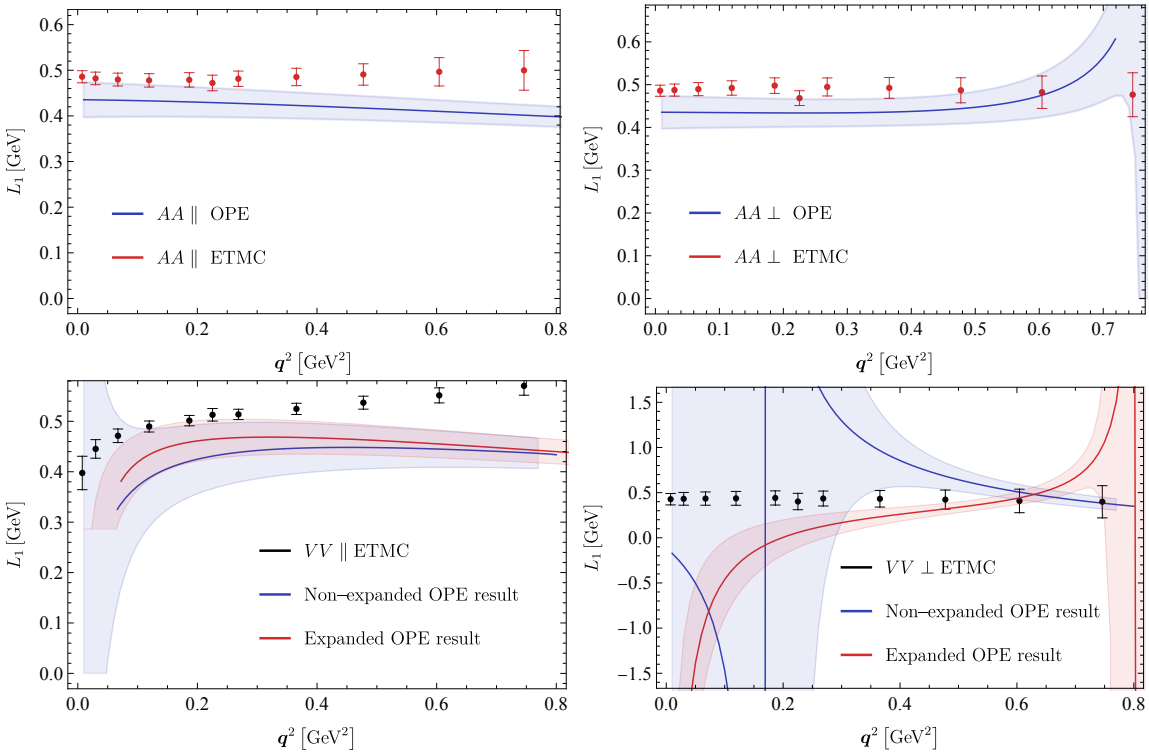

Figure 5.4.6: Differential moment $L_1(q^2)$ in the various channels. The plots show the comparison between OPE and ETMC data.

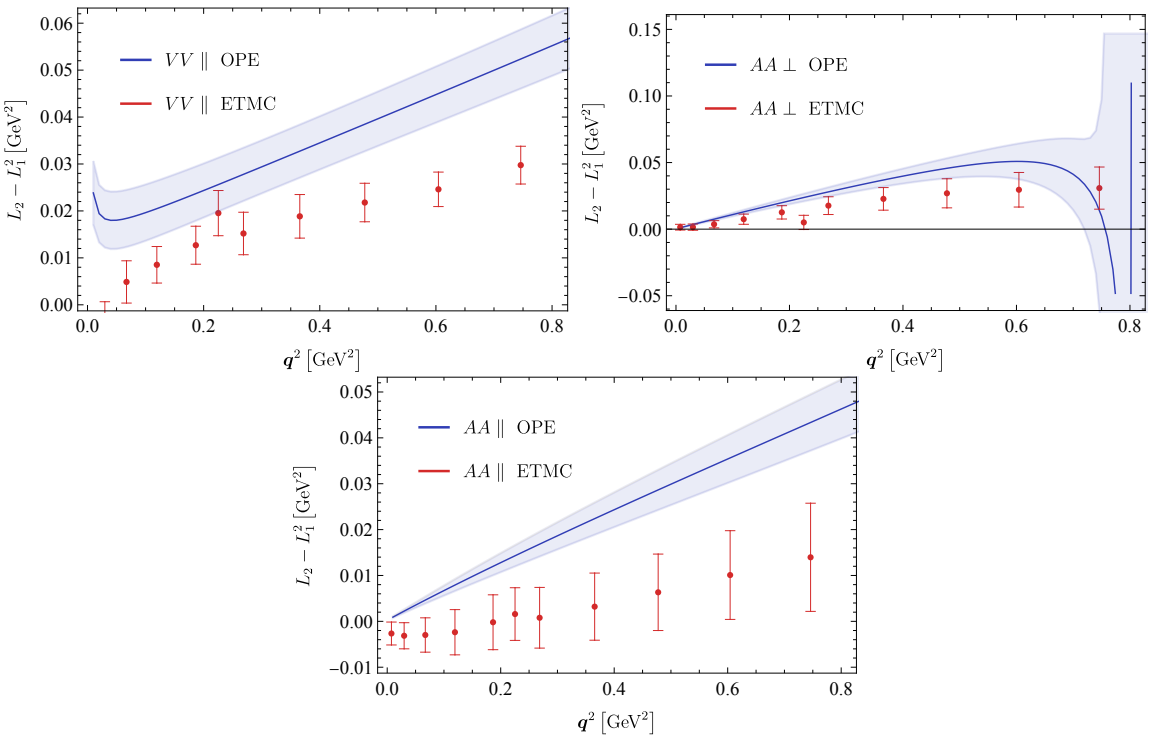

Figure 5.4.7: Differential moment $L_{2c} = L_2 - L_1^2$ in the various channels. The plots show the comparison between OPE and ETMC data.

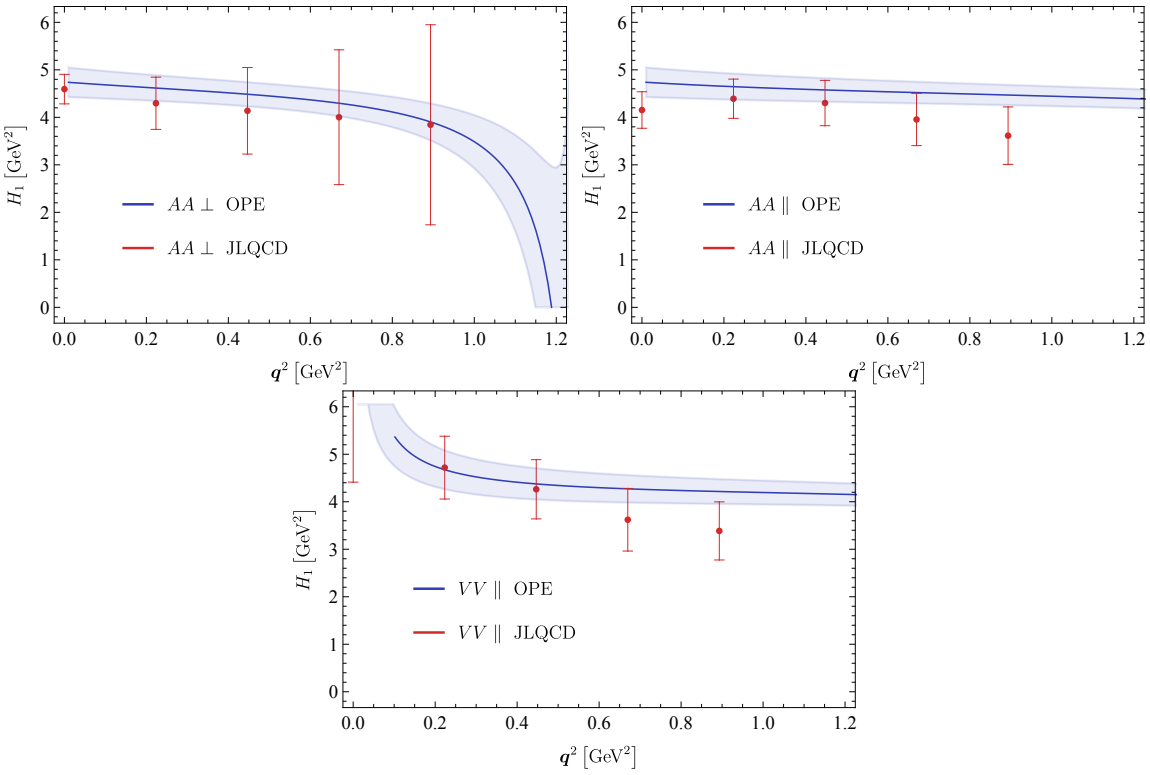

Figure 5.4.8: Differential moment $H_1(\boldsymbol{q}^2) = \langle M_X^2 \rangle(\boldsymbol{q}^2)$ in the various channels. The plots show the comparison between OPE and JLQCD data.

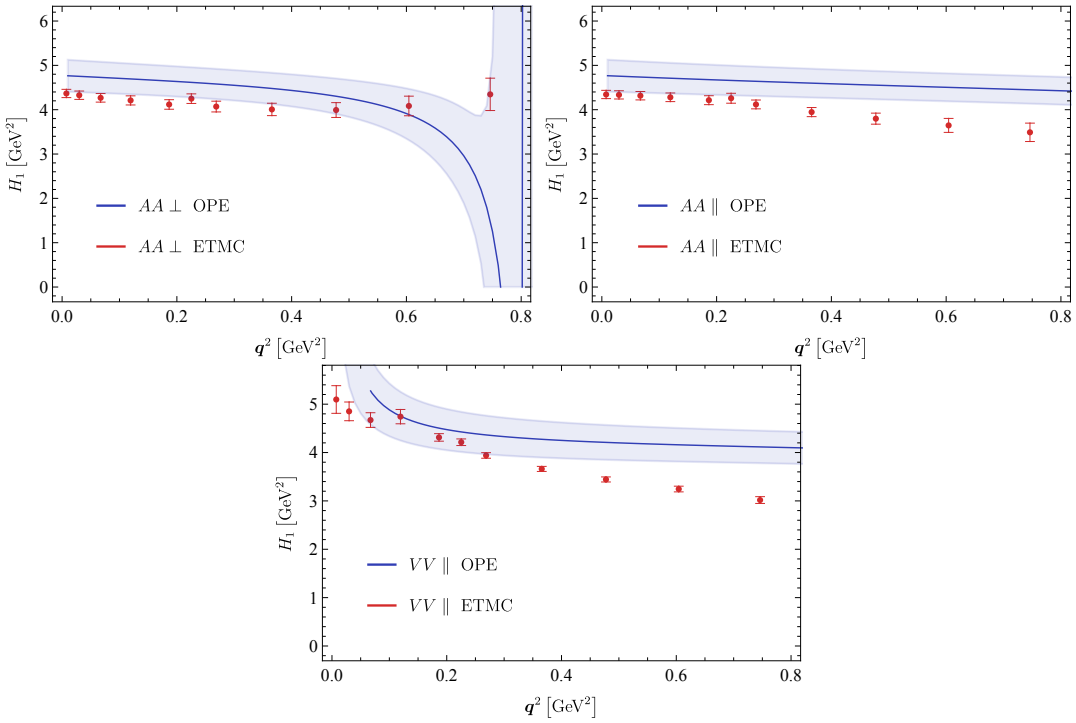

Figure 5.4.9: Differential moment $H_1(\boldsymbol{q}^2) = \langle M_X^2 \rangle(\boldsymbol{q}^2)$ in the various channels. The plots show the comparison between OPE and ETMC data.

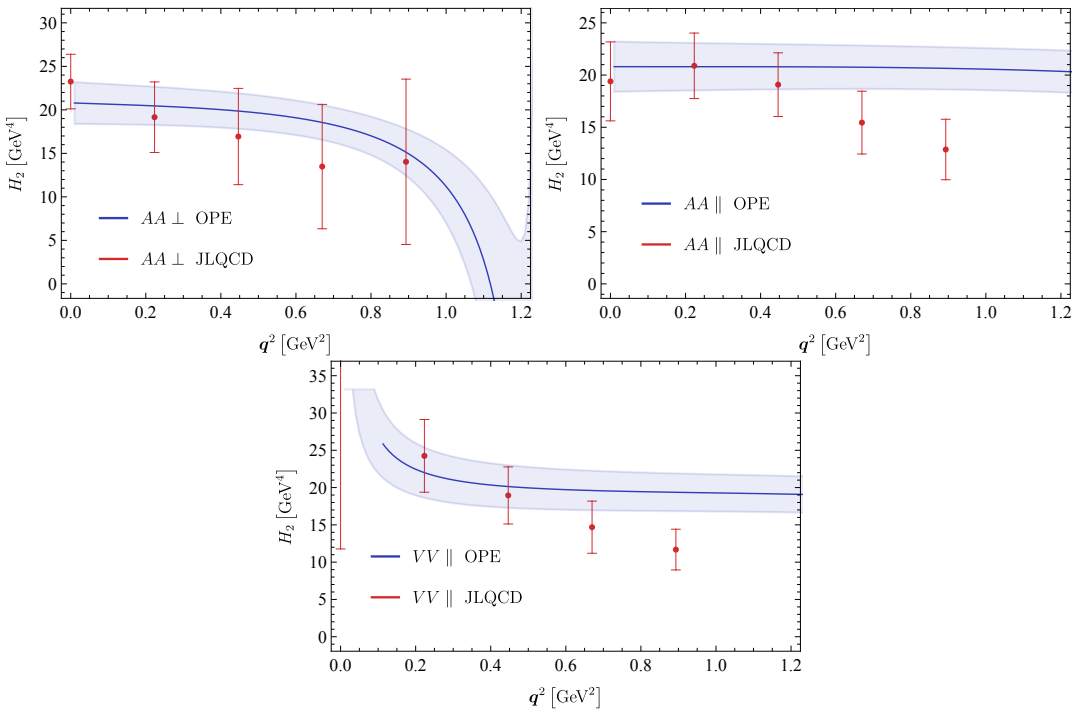

Figure 5.4.10: Differential moment $H_2(\boldsymbol{q}^2) = \langle M_X^4 \rangle(\boldsymbol{q}^2)$ in the various channels. The plots show the comparison between OPE and JLQCD data.

	JLQCD	OPE
$\Gamma/\lvert V_{cb}^2\rvert \times 10^{13}$ (GeV)	4.46(21)	5.7(9)
$\langle E_\ell \rangle$ (GeV)	0.650(40)	0.626(36)
$\langle M_X^2 \rangle$ (GeV^2)	3.75(31)	4.22(30)

Table 5.4.2: Total width and moments in the JLQCD case.

	ETMC	OPE
$\Gamma/\lvert V_{cb}^2\rvert \times 10^{13}$ (GeV)	0.987(60)	1.20(46)
$\langle E_\ell \rangle$ (GeV)	0.491(15)	0.441(43)
$\langle E_\ell^2 \rangle$ (GeV^2)	0.263(16)	0.207(49)
$\langle E_\ell^2 \rangle - \langle E_\ell \rangle^2$(GeV^2)	0.022(16)	0.020(8)
$\langle M_X^2 \rangle$ (GeV^2)	3.77(9)	4.32(56)

Table 5.4.3: Total width and moments in the ETMC case.

5.4.3 Total width and moments

We perform a comparison between OPE predictions and lattice results also in the case of the total semileptonic width and of the global moments introduced in eq. (5.2.37) and in eq. (5.2.38). In this case the OPE results are going to be slightly more accurate as we can take advantage of existing two- and even three-loop calculations [126]. We can also test the relevance of the singularity at $\boldsymbol{q}^2_{\rm max}$. The lattice results for the $\boldsymbol{q}^2$ spectrum can be interpolated by polynomials or piecewise polynomials, leading to the results shown in table 5.4.2 and in table 5.4.3. As the $\boldsymbol{q}^2$-spectrum is peaked near $\boldsymbol{q}^2_{\rm max}$, see figure 5.3.10, the total width is particularly sensitive to that region. In the JLQCD case the limited number of $\boldsymbol{q}^2$ points makes the extrapolation to the highest $\boldsymbol{q}^2$ values more uncertain, with clear implications on the estimate of the total width. On the other hand, it is difficult to estimate such uncertainty, hence table 5.4.2 shows only the statistic uncertainty.

In the OPE the total width receives large and concurring power and perturbative corrections, which reflect in a $\sim$ 20–40% uncertainty. This is at variance with what happens in the case of the physical b quark, for which a recent estimate of the total uncertainty is about 2% [88]. Indeed, the convergence of the OPE expansion deteriorates rapidly as m_b decreases approaching m_c, even from 2.7 to 2.4 GeV. To illustrate this point we show the various contributions to the semileptonic width in the ETMC case:

$$\frac{\Gamma}{|V_{cb}^2|} = \left[3.03 - 0.32_{pert} - 0.65_{\mu_G^2} - 0.09_{\mu_\pi^2} - 0.66_{\rho_D^3} - 0.10_{\rho_{LS}^3} + \dots\right] \times 10^{-13}\,\text{GeV}\,, \quad (5.4.6)$$

where the perturbative contribution includes $O(\alpha_s^3)$ and the non-perturbative contributions include the $O(\alpha_s)$ corrections to the Wilson coefficients. We estimate the perturbative uncertainty by varying the scale of α_s between 1.5 and 3.0 GeV. Notice that more than half of the uncertainty on the width reported in tables 5.4.2 and 5.4.3 is due to the large uncertainty on the heavy quark masses, in both the JLQCD and ETMC cases.

For what concerns the leptonic moments, only the $O(\alpha_s^2)$ corrections have been computed, either numerically for physical values of the heavy-quark masses [201], or analytically in an expansion up to $O(r^7)$ in powers of $r = m_c/m_b$ [205]. Unfortunately, this expansion converges

slowly and does not provide reliable results for $r \sim 0.5$, which is the value relevant in the ETMC case. We therefore show results computed to $O(\alpha_s)$ and include the $O(\alpha_s \mu^2_{\pi,G}/m_b^2)$ corrections discussed in ref. [34] as well. The first moment in the ETMC case is given by

$$\langle E_\ell \rangle = \Big[0.533 - 0.051_{\mu_G^2} + 0.021_{\mu_\pi^2} - 0.051_{\rho_D^3} - 0.003_{\rho_{LS}^3} - 0.008_{\alpha_s} + \dots\Big] \text{ GeV}, \qquad (5.4.7)$$

where both power and perturbative corrections are smaller than in the total width. Similarly, the second central moment $L_{2c} = \langle E_\ell^2 \rangle - \langle E_\ell \rangle^2$ is given by

$$L_{2c} = \Big[0.0297 - 0.0057_{\mu_G^2} + 0.0103_{\mu_\pi^2} - 0.0167_{\rho_D^3} + 0.0006_{\rho_{LS}^3} + 0.0021_{\alpha_s} + \dots\Big] \text{ GeV}. \quad (5.4.8)$$

As shown in tables 5.4.2 and 5.4.3, there is reasonable agreement between OPE and both JLQCD and ETMC data in all cases. As a general comment, we stress that the large contributions of ρ_D^3 are related to a kinematically enhanced Wilson coefficient and do not necessarily imply similarly large higher-power corrections.

Finally, the OPE prediction for the first hadronic mass moment in the JLQCD case is

$$\langle M_X^2 \rangle = \Big[3.84 - 0.36_{\mu_\pi^2} + 0.23_{\mu_G^2} + 0.41_{\rho_D^3} + 0.05_{\rho_{LS}^3} + 0.04_{\alpha_s} + \dots\Big] \text{ GeV}^2, \qquad (5.4.9)$$

where we do not include the $O(\alpha_s/m_b^2)$ corrections and consequently enlarge the uncertainty slightly. The OPE prediction for the first hadronic moment is in reasonable agreement with both the JLQCD and ETMC values, see table 5.4.2 and table 5.4.3.

5.4.4 Determination of the OPE parameters

As different physical quantities have a different dependence on the OPE parameters, it is possible to constrain their values using lattice data. The analytic expressions for the power corrections to the differential $\boldsymbol{q}^2$ distribution and for the moments, which encode this dependence, are rather lengthy and are provided in an ancillary Mathematica file.

To illustrate this point, let us consider a few examples using simpler approximate formulas, and focusing on the differential leptonic moments at moderately low $\boldsymbol{q}^2$, where the OPE is more reliable. We choose a $\boldsymbol{q}^2$ value for which we have lattice data, $\boldsymbol{q}_*^2 = 0.1865$ GeV^2. In the ETMC setup, the OPE prediction for $L_1(\boldsymbol{q}_*^2)$ can be approximated by

$$\begin{aligned}
L_1^{VV\|}(\boldsymbol{q}_*^2) &\simeq 0.5597 + \frac{1}{2}\delta_b - 0.47\delta_c + 0.056\mu_G^2 - 0.19\mu_\pi^2 - 0.094\rho_D^3 - 0.057\rho_{LS}^3 \,, \\
L_1^{AA\|}(\boldsymbol{q}_*^2) &\simeq 0.5455 + \frac{1}{2}\delta_b - 0.47\delta_c - 0.141\mu_G^2 - 0.074\mu_\pi^2 - 0.069\rho_D^3 + 0.043\rho_{LS}^3 \,, \\
L_1^{AA\perp}(\boldsymbol{q}_*^2) &\simeq 0.5448 + \frac{1}{2}\delta_b - 0.47\delta_c - 0.175\mu_G^2 - 0.033\mu_\pi^2 - 0.101\rho_D^3 + 0.039\rho_{LS}^3 \,,
\end{aligned}$$

where $\delta_b = m_b - 2.39$, $\delta_c = m_c - 1.19$, and all quantities are expressed in GeV to the appropriate power. Notice that the lowest order expression for the differential leptonic moments is universal, namely does not depend on the channel. We do not consider the $VV_\perp$ channel because, as discussed above, the expanded form does not provide a good approximation. The analogous expressions for the second central moments are

$$\begin{aligned}
L_{2c}^{VV\|}(\boldsymbol{q}_*^2) &\simeq 0.005 + 0.010\mu_\pi^2 + 0.052\rho_D^3 - 0.015\rho_{LS}^3 \,, \\
L_{2c}^{AA\|}(\boldsymbol{q}_*^2) &\simeq 0.009 + 0.010\mu_\pi^2 - 0.058\rho_D^3 + 0.011\rho_{LS}^3 \,, \\
L_{2c}^{AA\perp}(\boldsymbol{q}_*^2) &\simeq 0.019 + 0.010\mu_\pi^2 - 0.026\rho_D^3 - 0.002\rho_{LS}^3 \,.
\end{aligned}$$

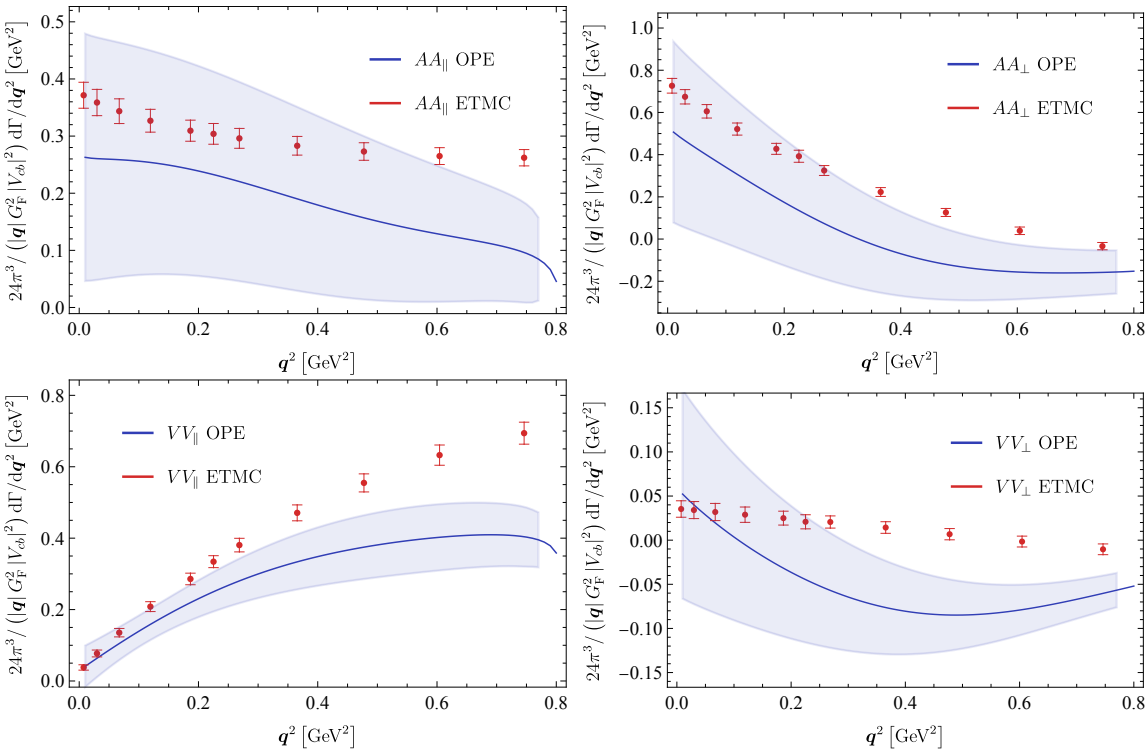

Figure 5.4.11: Differential $\boldsymbol{q}^2$ spectrum computed with a sigmoid approximation to the kernel with $\sigma = 0.12 m_B$. The plots show the comparison between OPE and ETMC data.

Each of these moments has a different dependence on the non-perturbative parameters and they can be used in a fit to the lattice ETMC results to obtain constraints on those parameters. In fact, using only these six inputs with their theoretical uncertainty does not lead to any improvement on the constraints given in table 5.4.1. Considering additional $\boldsymbol{q}^2$ points enhances the sensitivity to the non-perturbative parameters, but one has to estimate the correlation among the theoretical uncertainties at adjacent $\boldsymbol{q}^2$ points. One can also include in the fit the data for the $\boldsymbol{q}^2$ distribution in the different channels, as well as additional moments like the hadronic mass moments. A global fit to lattice data is however beyond the scope of this paper, especially because our estimate of the lattice systematic uncertainty is incomplete. We stress that the limiting factor here is not the statistical uncertainty of the present ETMC calculation, but the theoretical uncertainty we attach to the OPE predictions. In this respect the unphysical case we have considered, with the partonic energy release (of the order of $m_b - m_c$) about a factor 2 (JLQCD) or 3 (ETMC) smaller than in reality, is strongly penalising. At the physical point the OPE enjoys a much better convergence and the prospects for constraining the non-perturbative parameters are better than it appears from this exploratory study.

5.4.5 Computations with a smooth kernel

In sections 5.2 and 5.3 we have seen that the reconstruction of the discontinuous kernel is one of the main problems in the calculation of physical quantities. As far as the comparison with the OPE is concerned, however, the kernel does not need to be discontinuous. Indeed, one can compute inclusive (unphysical) quantities in the OPE employing a smooth kernel ($\sigma \neq 0$) and compare them directly with the analogous quantities computed on the lattice. In this way it is possible to check that the level of agreement between the two calculations is not affected by

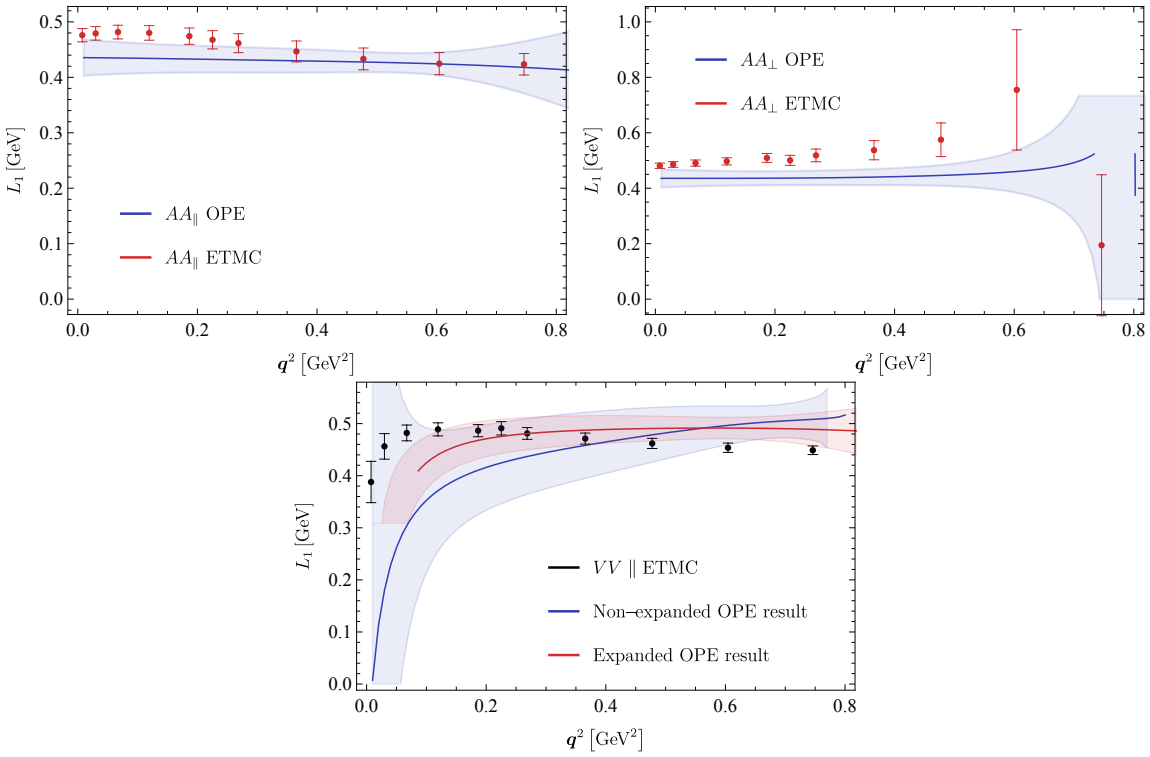

Figure 5.4.12: Differential first lepton moments computed with a sigmoid approximation to the kernel with $\sigma = 0.12 m_B$. The plots show the comparison between OPE and ETMC data.

the $\sigma \to 0$ limit, and to extract information on the non-perturbative parameters of the OPE, as well as on the heavy quark masses, from slightly more precise lattice data.

In figure 5.4.11 we show the $\boldsymbol{q}^2$ spectrum in the different channels computed on the lattice using the sigmoid approximation $\theta^{\mathrm{s}}_\sigma$ of eq. (5.2.36) for $\theta(\omega_{\max} - \omega)$ with $\sigma = 0.12 m_B$. In the OPE calculation, where the partonic kinematics holds, we replace $\theta(1 - \hat{\eta} - \sqrt{\boldsymbol{q}^2})$ by the sigmoid $\theta^{\mathrm{s}}_\sigma(1 - \hat{\eta} - \sqrt{\boldsymbol{q}^2})$ using $\sigma = 0.12 m_B$. At low $\boldsymbol{q}^2$ the agreement between OPE and ETMC data is similar to that in figure 5.4.4, while at large $\boldsymbol{q}^2$ there is marginal improvement, as expected because the smearing occurs over a larger ω range. In figure 5.4.12 we show the first differential leptonic moment $L_1(\boldsymbol{q}^2)$ in the different channels, excluding $VV_\perp$ because of the large uncertainties in the OPE calculation. With respect to figure 5.4.6 we observe a marked improvement of the agreement between OPE and ETMC data at large $\boldsymbol{q}^2$ in the $AA_\parallel$ and $VV_\parallel$ channels, while in the $AA_\perp$ channel the agreement is slightly worse. Finally, in figure 5.4.13 we show the $\boldsymbol{q}^2$ spectrum in the different channels computed from the JLQCD configurations using the sigmoid approximation $\theta^{\mathrm{s}}_\sigma$ with $\sigma = 0.1/a$. Here the overall agreement between lattice calculations and OPE is similar to figure 5.4.3, but now the $\boldsymbol{q}^2$ dependence of the lattice data is closer to the OPE result, obtained using $\theta^{\mathrm{s}}_\sigma(1 - \hat{\eta} - \sqrt{\boldsymbol{q}^2})$ with $\sigma = 0.1$.

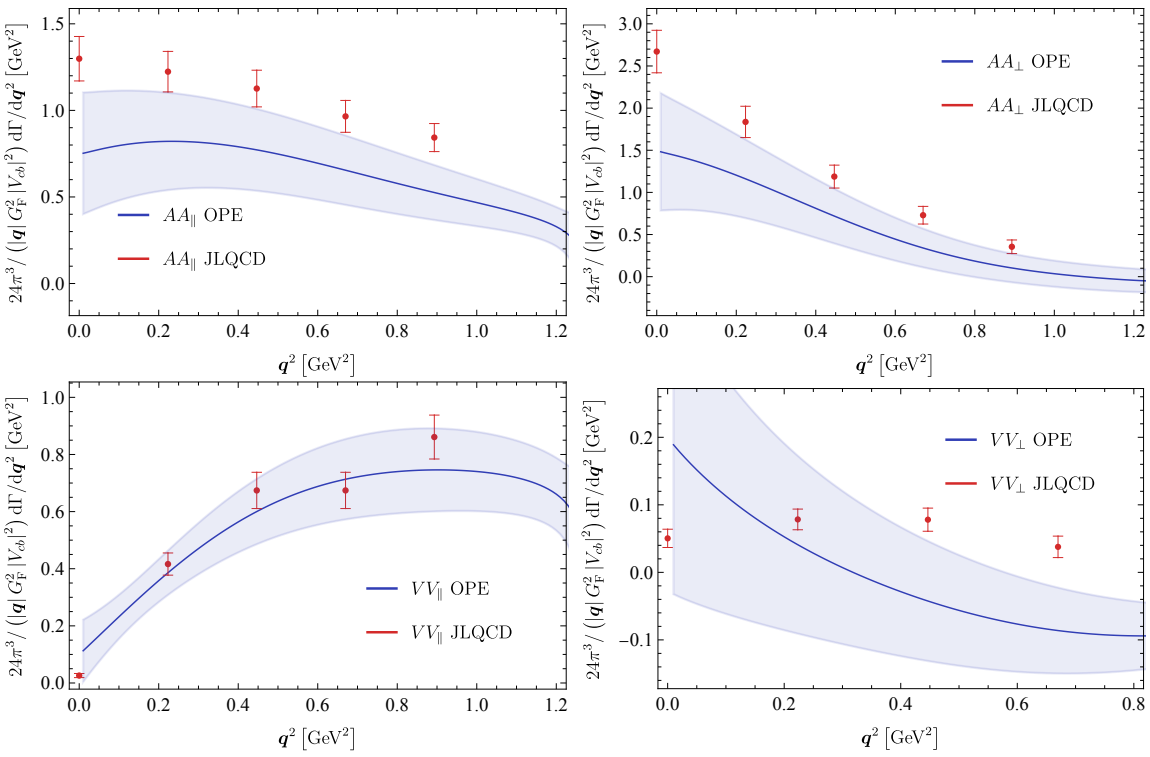

Figure 5.4.13: Differential $\boldsymbol{q}^2$ spectrum computed with a sigmoid approximation to the kernel with $\sigma = 0.1/a$. The plots show the comparison between OPE and JLQCD data.

5.5 Discussion and future prospects

In this article we have presented the first comprehensive investigation of inclusive semileptonic B-meson decays on the lattice. Using the method of ref. [143] we have computed various inclusive observables with gauge-field ensembles generated by the JLQCD and ETM collaborations for unphysically light values of the b quark mass (about 2.7 GeV and 2.4 GeV, respectively) and m_c close to its physical value. In this exploratory study we have not performed the continuum and infinite-volume limits.

An important feature of the method we have adopted is that it requires the approximation of the energy-integral kernel. The kinematics of the inclusive semileptonic decay involves a discontinuity at the boundary of the phase space, for which a reasonable approximation with the Euclidean correlator obtained on the lattice is impractical. The problem can be dealt with using a sequence of smooth kernels, parametrized by a smearing width σ, which converge to the physical phase space in the limit $\sigma \to 0$. As emphasized in section 5.2, the $\sigma \to 0$ limit does not commute with the infinite-volume limit that has to be taken first. Under the assumption that finite volume effects are negligible with respect to the statistical errors associated with our lattice results, we have studied the $\sigma \to 0$ extrapolation in detail and found that it does not induce a significant uncertainty.

We have compared the JLQCD results with the contributions of the charmed ground states, estimated from a JLQCD calculation of the $B_s \to D_s^{(*)}$ form factors for the same values of the heavy-quark masses (details are given in the appendix A.9). Due to the proximity between the charm and bottom masses and to the limited phase space available in the decay, the inclusive results are nearly saturated by the ground-state contributions. Although the correlator themselves show the presence of excited states, their contribution to the inclusive

rate is relatively small. The ETMC results obtained at even lower b quark mass are also expected to be largely dominated by the ground states.

While the JLQCD and ETMC results cannot be compared directly as they are obtained at different b quark masses, they can be both compared with the expectations from the OPE, assuming that discretisation and finite-volume effects are negligible. When the OPE can be considered reliable, the agreement with both JLQCD and ETMC results is generally good, while we observe possible indications of quark-hadron duality violation at large $\boldsymbol{q}^2$. The variance of the lepton energy distribution also shows a clear and unexpected deviation, which could be due to underestimated uncertainties in our OPE calculation or to non-negligible lattice systematics. To the best of our knowledge, this is the first time that the onset of quark-hadron duality is studied on the lattice. For $m_b \sim 2.4$ GeV, the OPE converges much more slowly than at the physical point, but the normalised moments allow us to perform a relatively clean comparison with the lattice data.

We have found that the calculation of the total width and of other global quantities like the moments of the lepton energy or of the hadronic invariant-mass distribution depends crucially on the number of $\boldsymbol{q}^2$ points that can be computed on the lattice. In the ETMC calculation the flexibility due to the use of twisted boundary conditions has allowed us to reach an accuracy of 6% on the total width and 3% on the first leptonic moment. These uncertainties do not yet include several lattice systematics that need to be considered, but are dominated by statistical uncertainties and could be improved with a dedicated effort. This is an aspect which will become important for future phenomenological applications, which should also focus on reaching the physical b mass.

Finally, we have shown that one can constrain the non-perturbative parameters in the OPE analysis from our results. We have not attempted a fit to the lattice data in the unphysical setup we have considered, as this is penalised by large uncertainties from higher-dimensional operators. With larger b-quark masses these uncertainties will be reduced and the data obtained at different values of m_b will provide an additional handle on the non-local matrix elements that appear in eq. (5.4.5).

There are certainly many issues to be improved or investigated in order to get results of direct phenomenological relevance. First, we have not yet studied the continuum and infinite-volume limits. Although we have presented a rather detailed discussion of the systematics associated with the reconstruction of the smearing kernels, including the required extrapolation at vanishing smearing radius, this last step is only permitted after having checked the onset of the infinite-volume limit. The continuum and infinite-volume limits can only be taken by performing calculations at different values of the lattice spacing and on different physical volumes, a task that is beyond the exploratory nature of this study and that we postpone to future work on this subject.

Second, the calculation has to be performed at the physical b and light quark masses. Simulations with physical pion masses are nowadays possible and, for instance, a collection of $N_f = 2 + 1 + 1$ ensembles with physical light, strange and charm quark masses has been produced by the ETM collaboration at different values of the lattice spacing and with different physical volumes. Although it is not possible to simulate directly a physical b quark on these ensembles (because of potentially dangerous cutoff effects), the problem can nevertheless be approached by using well-established techniques such as the ETMC ratio method [84], based on ratios of the observable of interest computed at nearby heavy-quark masses. The ratio method has been already applied to determine the mass of the b quark, the leptonic decay constants, the bag parameters of $B_{(s)}$ mesons and the matrix elements of dimension-four and

dimension-five operators appearing in the Heavy Quark Expansion of pseudoscalar and vector meson masses [98, 103, 121, 147, 148]. Its main advantages can be summarised as follows: *i*) B-physics computations can be carried out using the same relativistic action setup with which the lighter-quark computations are performed; *ii*) an extra simulation at the static point limit is not necessary, while the exact information about it is automatically incorporated in the construction of the ratios of the observable; *iii*) the use of ratios greatly helps in reducing the discretisation effects. However, there is an important subtlety. In order to apply the ratio method (or any other method based on extrapolations in the b-quark mass) in the case of the inclusive decay rates one has to cope with the fact that at unphysical (lighter) values of the b-quark mass the phase-space available to the decay shrinks. This implies that some of the hadronic channels that are open at the physical value of m_b are *totally* excluded from the phase-space integral at $m_h < m_b$. The important point to be noticed here is that this happens when the integration limits are imposed sharply, i.e. by using the exact Heaviside functions that implement the phase-space constraint. The problem is totally analogous to the ordered double-limit required in order to deal with the finite-volume distortion of the hadronic spectral density. Indeed, we envisage applying the ratio method to $\Gamma \equiv \Gamma(m_b)$ *before* taking the $\sigma \to 0$ extrapolation: while $\Gamma(m_h)$ is (at least in principle) a distribution in m_h, $\Gamma_\sigma(m_h)$ is certainly a smooth function that can safely be extrapolated at the physical value of m_b. Moreover, we already have simulations with $m_h \sim 0.8 m_b$, and it can be reasonably argued that for such large masses the missing (mostly continuum) states scale with m_h.

Although we have compared the lattice results with the OPE, a more direct and effective validation of our method would come from a comparison with experimental data, such as those for the branching ratio and for the electron energy spectrum in inclusive semileptonic decays of the D or D_s mesons [27, 50]. Here the challenge is to get accurate results at physical light-quark masses, while the charm quark can be simulated directly on present lattices. Beside validating the method without extrapolations in the heavy-quark mass, a calculation of charm decays might shed light on the following two open and phenomenologically relevant questions. *i*) To what extent is the OPE applicable to charm decays? *ii*) What is the role played by weak annihilation (WA) contributions? The first question refers to the onset of quark-hadron duality, and a detailed study of charm decays in connection with their OPE description may yield an insight on this conceptual issue. Answering the second question may help us quantifying the role played by WA contributions in charmless semileptonic B decays, hence improving the inclusive determination of $|V_{ub}|$. If one could reproduce the lepton energy spectrum of the D_s inclusive semileptonic decays that is measured experimentally, a more ambitious future application would be a direct calculation of $B \to X_u \ell \nu$.

Finally, one may wonder whether the foreseeable precision will be sufficient for a precision determination of $|V_{cb}|$ and for interesting phenomenology. Indeed, present experimental errors for $B \to X_c \ell \nu$ are 1.4% on the branching ratio and a few per mille on the first few moments of the lepton energy distribution. The lattice precision is unlikely to get close to that, at least initially. On the other hand, on a relatively short time-scale lattice calculations of inclusive semileptonic decays might be able to enhance the predictive power of the OPE by accessing other quantities that are inaccurate or beyond the reach of current experiments and are highly sensitive to the non-perturbative parameters, allowing us to validate and improve the results of the semileptonic fits on which the OPE predictions are based.

Chapter 6

Higher Dimensional Operator Corrections

This chapter presents the work published in [73].

6.1 Introduction

Over recent years the study of semileptonic decays of B mesons has been developing rapidly, with intriguing tensions between Standard Model (SM) predictions and experimental measurements appearing. One of the most persistent tensions in this field is the $\sim 3\sigma$ tension between the exclusive and inclusive determinations of the CKM matrix element V_{cb} [43, 141, 146, 225].

On the inclusive side the theoretical description relies on the Heavy Quark Expansion (HQE) [83, 105, 197], an expansion in powers of $\Lambda_{\rm QCD}/m_b$. By now the HQE is at a mature state with the corrections up to $\mathcal{O}\left(\Lambda^5_{\rm QCD}/m_b^5\right)$ known at tree-level [74, 145, 196], the one–loop correction fully known at $\mathcal{O}\left(\Lambda^2_{\rm QCD}/m_b^2\right)$ [33, 34, 62, 194, 195] and in the case of the lepton invariant mass spectrum even at $\mathcal{O}\left(\Lambda^3_{\rm QCD}/m_b^3\right)$ [192]. At the leading order in the HQE the three–loop corrections to the total decay rate and the semileptonic moments have been computed recently [126, 127].

The starting point of any HQE computation is the Weak Effective Theory (WET) with the W boson integrated out at the electroweak scale. The leading corrections to the limit of an infinitely heavy W boson are given by terms of $\mathcal{O}(q^2/m_W^2)$, where q^2 is the dilepton invariant mass. Being suppressed by the W boson mass, these corrections are expected to be small. Nonetheless, in principle they could have a sizeable effect on the moments of the dilepton invariant mass spectrum recently used to determine the CKM matrix element V_{cb} [68] due to an enhancement in the phase space integration, especially if it is constrained by a lower cut. In conjunction with the current theory precision this renders a computation of $\mathcal{O}\left(q^2/m_W^2\right)$ effects on the inclusive decay rate and moments timely. The purpose of this paper is the presentation of such a computation.

6.2 Triple differential decay width to $\mathcal{O}(q^2/m_W^2)$

We consider the inclusive decay $B(p) \to X_c(p-q)\ell(p_\ell)\nu_\ell(p_\nu)$ of a B meson into a charmed hadronic final state and lepton pair. As usual we start by integrating the W boson out of our description physics at the B scale. We do however keep terms of $\mathcal{O}(q^2/m_W^2)$ in the expansion

of the W propagator, leading to the effective Hamiltonian

$$\mathcal{H}_{\text{eff}} = \frac{G_{\text{F}}}{\sqrt{2}} V_{cb} \Big[g_{\mu\nu} \left(1 - \frac{D^2}{m_W^2}\right) J_q^\mu J_\ell^\nu - \frac{D_\mu D_\nu}{m_W^2} J_q^\mu J_\ell^\nu \Big], \tag{6.2.1}$$

where $J_q^\mu(x) = (\bar{c}\gamma^\mu(1-\gamma_5)b)$ and $J_\ell^\mu(x) = \left(\bar{\ell}\gamma^\nu(1-\gamma_5)\nu_\ell\right)$ are the hadronic and leptonic currents and the covariant derivative is given by

$$D_\mu = \partial_\mu + igT^a G_\mu^a + ieQA_\mu, \tag{6.2.2}$$

with the $\text{SU}(3)_c$ and $\text{U}(1)_Q$ gauge fields G_μ^a and A_μ. In the following we consider light leptons ($\ell \in \{e, \mu\}$). In this limit the last term of eq. (6.2.1) does not contribute.

Now we can write the triple differential decay rate as

$$\begin{aligned} &\frac{8\pi^3}{G_{\text{F}}^2 \left|V_{cb}\right|^2} \frac{\mathrm{d}\Gamma}{\mathrm{d}q^2 \mathrm{d}q^0 \mathrm{d}E_\ell} \\ &= L_{\mu\nu} g^{\mu\alpha} \left(1 + \frac{q^2}{m_W^2}\right) g^{\nu\beta} \left(1 + \frac{q^2}{m_W^2}\right) W_{\alpha\beta} \\ &= \left(1 + \frac{2q^2}{m_W^2}\right) L_{\mu\nu} W^{\mu\nu} + \mathcal{O}\left(\frac{q^4}{m_W^4}\right). \end{aligned} \tag{6.2.3}$$

Here

$$L^{\mu\nu} = p_\ell^\mu p_\nu^\nu - p_\ell \cdot p_\nu g^{\mu\nu} + p_\ell^\nu p_\nu^\mu + i\epsilon^{\mu\alpha\nu\beta} p_{\ell,\alpha} p_{\nu,\beta} \tag{6.2.4}$$

is the standard leptonic tensor and the hadronic tensor is defined as

$$\begin{aligned} &\frac{2m_B}{(2\pi)^3} W^{\mu\nu} = \\ &\sum_{X_c} \delta^{(4)}(p_B - q - p_X) \left\langle B \left| J_q^{\mu\dagger} \right| X_c \right\rangle \left\langle X_c \left| J_q^\nu \right| B \right\rangle. \end{aligned} \tag{6.2.5}$$

The hadronic tensor can be decomposed into Lorentz invariant structure functions as

$$W^{\mu\nu} = -g^{\mu\nu} W_1 + v^\mu v^\nu W_2 - i\epsilon^{\mu\nu\alpha\beta} v_\alpha \hat{q}_\beta W_3, \tag{6.2.6}$$

where $v = p/m_B$ is the B meson four velocity and $\hat{q} = q/m_b$. Then in the rest frame of the decaying B-meson we have $v \cdot p_\ell = E_\ell$ and $v \cdot q = q_0$. Consequently

$$\begin{aligned} L_{\mu\nu} W^{\mu\nu} =& q^2 W_1 + \left(2E_\ell q_0 - 2E_\ell^2 - \frac{q^2}{2}\right) W_2 \\ &+ q^2 \left(2E_\ell - q_0\right) W_3. \end{aligned} \tag{6.2.7}$$

The structure functions are computed in the HQE, resulting in a double expansion in terms of inverse powers of the b quark mass and powers of the strong coupling constant. The current state of the art of the HQE is summarized in table A.8.1.

6.3 Results

We study the impact of $\mathcal{O}(q^2/m_W^2)$ contributions on the total decay rate and the moments of the charged lepton energy E_ℓ, the hadronic invariant mass m_X and the invariant mass of the lepton pair q^2. The moments are defined as

$$\langle x^n \rangle = \frac{1}{\Gamma} \int_{E_\ell > E_\ell^{\text{cut}},\, q^2 > q^2_{\text{cut}}} \mathrm{d}q^2 \mathrm{d}q_0 \mathrm{d}E_\ell x^n \frac{\mathrm{d}\Gamma}{\mathrm{d}q^2 \mathrm{d}q_0 \mathrm{d}E_\ell} \tag{6.3.1}$$

with

$$\Gamma = \int_{E_\ell > E_\ell^{\text{cut}},\, q^2 > q^2_{\text{cut}}} \mathrm{d}q^2 \mathrm{d}q_0 \mathrm{d}E_\ell \frac{\mathrm{d}\Gamma}{\mathrm{d}q^2 \mathrm{d}q_0 \mathrm{d}E_\ell} \tag{6.3.2}$$

for $x \in \{E_\ell, m_X, q^2\}$. In the leptonic and hadronic moments a lower cut on the energy of the charged lepton, E_ℓ, is applied while in the case of the q^2 a lower cut on the invariant mass of the lepton pair is applied. For the lepton energy and q^2 moments these integrals can be evaluated directly. In the case of the hadronic mass moments however we compute the moments of $\hat{u} = ((p-q)^2 - m_c^2)/m_b^2$ and $\hat{\omega} = 1 - q_0/m_b$ and relate them to the hadronic final state mass through

$$\left\langle m_X^2 \right\rangle = m_c^2 + \Lambda^2 + 2\Lambda m_b \left\langle \hat{\omega} \right\rangle + m_b^2 \left\langle \hat{u} \right\rangle, \tag{6.3.3}$$

where $\Lambda = m_B - m_b$ is the mass difference between the B meson and the b quark. For $n > 1$ one usually considers the central moments $\langle (x - \langle x \rangle)^n \rangle$. We denote them as

$$\begin{aligned}
\ell_i &= \begin{cases} \langle E_\ell \rangle\,, & \text{for } i = 1 \\ \left\langle \left(E_\ell - \langle E_\ell \rangle\right)^i \right\rangle, & \text{for } i > 1 \end{cases} \\
h_i &= \begin{cases} \langle m_X^2 \rangle\,, & \text{for } i = 1 \\ \left\langle \left(m_X^2 - \langle m_X^2 \rangle\right)^i \right\rangle, & \text{for } i > 1 \end{cases} \\
\mathcal{Q}_i &= \begin{cases} \langle q^2 \rangle\,, & \text{for } i = 1 \\ \left\langle \left(q^2 - \langle q^2 \rangle\right)^i \right\rangle, & \text{for } i > 1. \end{cases}
\end{aligned} \tag{6.3.4}$$

By carrying out the integrations in eq. (6.3.1) and re-expanding the ratio in powers of $1/m_b$, α_s and $\xi = 2m_b^2/m_W^2$ we find the contributions of $\mathcal{O}(q^2/m_W^2)$. As the analytic expressions are lengthy they are attached to the arXiv submission in an ancillary file. Numerically we find the results in tables 6.3.2 to 6.3.4.

Parameter	Value
$m_b^{\text{kin}}(m_b)$	4.6 GeV
$\overline{m}_c(2\text{GeV})$	1.15 GeV
μ_π^2	0.4 GeV^2
μ_G^2	0.35 GeV^2
ρ_D^3	0.2 GeV^3
ρ_{LS}^3	-0.15 GeV^3

Table 6.3.1: Default input values

In appendix A.10 the full dependence of the moments on the experimental cuts is illustrated by the examples of the first moments of the charged lepton energy, the hadronic invariant mass

	$10^4 \times \mathcal{O}\left(\frac{q^2}{m_W^2}\right) \Big/ \text{LO}$			
E_{cut}	Γ	ℓ_1	ℓ_2	ℓ_3
0	14.3	1.134	−3.140	3.212
1 GeV	15.9	0.368	−1.53043	25.4

Table 6.3.2: $\mathcal{O}(q^2/m_W^2)$) contributions to the total decay rate and leptonic moments

	$10^4 \times \mathcal{O}\left(\frac{q^2}{m_W^2}\right) \Big/ \text{LO}$		
E_{cut}	h_1	h_2	h_3
0	−0.933	3.50	−21.0
1 GeV	−0.946	1.77	−46.2

Table 6.3.3: $\mathcal{O}(q^2/m_W^2)$) contributions to the hadronic moments

	$10^4 \times \mathcal{O}\left(\frac{q^2}{m_W^2}\right) \Big/ \text{LO}$		
q^2_{cut}	$\mathcal{Q}_1$	$\mathcal{Q}_2$	$\mathcal{Q}_3$
0	6.04	3.50	−21.0
3 GeV^2	2.47	2.87	−14.2

Table 6.3.4: $\mathcal{O}(q^2/m_W^2)$) contributions to the leptonic invariant mass moments

and the dilepton invariant mass. The charged lepton energy moments have been measured by the DELPHI [24], BaBar [51] and Belle [217] collaborations, the hadronic invariant mass moments have been measured by the BaBar [53,54], Belle [214], Belle II [28], CDF [29], CLEO [112] and DELPHI [24] collaborations and the q^2 moments have been measured by the Belle [218], Belle II [2] and CLEO [112] collaborations. The Belle II uncertainties are not plotted because they are larger than the ones of the older measurements. As can be seen in the plots the q^2/m_W^2 corrections decrease for higher cuts and they are multiple orders of magnitude smaller than the experimental uncertainties. Therefore they are unlikely to significantly impact the theory prediction of V_{cb}.

They are however of the same order of magnitude as the $\mathcal{O}(\alpha_s^3)$ for the total rate, the second central lepton energy moment and the first hadronic mass moment. Therefore they may also be considered if one keeps the three–loop corrections, in order to consistently treat contributions of their order of magnitude.

Intuitively the smallness of the q^2/m_W^2 corrections can be seen from the fact that the q^2-distribution decreases with increasing q^2 and the fact that the average dilepton mass is ~ 5 GeV^2. So even though q^2/m_W^2 is about 0.6% we obtain a 0.14% correction to the total decay rate. In the moments there is also a cancellation between numerator and denominator, suppressing the corrections even more.

6.4 Conclusions

We computed the corrections of $\mathcal{O}\left(q^2/m_W^2\right)$ to the inclusive total rate and moments in semileptonic B decays. In most kinematical distributions these effects are several orders of magnitude smaller than the current experimental uncertainties. However, they are of comparable size to the three–loop corrections, which are included in present analyses. Thanks to the results

presented in this paper, they can be consistently included in future studies.

Chapter 7

Exclusive Decays of B Mesons

In this chapter we shift our attention away from inclusive decays of B mesons to exclusive decays, in which we know the exact final state. In particular we study the decays which at the parton-level proceed via a $b \to s\ell\ell$ transition.

The structure of this chapter is the following. After motivating the study of $b \to s\ell\ell$ transitions in section 7.1 we introduce the necessary formalism in section 7.2 and apply it to a study of long-distance contributions to the decays $B^+ \to K^+\ell^+\ell^-$ and $B^0 \to K^*\ell^+\ell^-$ in section 7.5. Throughout this chapter q will denote the four-momentum of the lepton pair.

7.1 Why Study Exclusive $b \to s\ell\ell$ transitions?

In section 2.4 we found that there are no Flavour Changing Neutral Current (FCNC) interactions at tree-level in the SM. Thus in the SM processes which are mediated by FCNC are rare. This property makes them great probes of NP because even small effects can easily be distinguished from the tiny SM expectation.

Indeed there are intriguing tensions between the SM prediction and measured values in the branching ratios $\mathcal{B}(B \to K^+\mu^+\mu^-)$ [7, 208] and $\mathcal{B}(B^0 \to K^*\mu^+\mu^-)$ [16] and in the angular observables of $B \to K^*\ell^-\ell^+$ [21]. Especially the branching ratios consistently show a deficit in the $b \to s\mu\mu$ mode.

The SM predictions of the branching ratios and angular observables are plagued by hadronic contributions which can mimic a NP contribution to the Wilson coefficients however. In order to distinguish genuine NP effects from hadronic SM effects it is important to study these contributions. This problem arises because the leading contribution of the four-quark operators in the effective Hamiltonian involves a charm loop which can go on-shell. In the following section we will see this explicitly.

7.2 Generalities

The effective Hamiltonian for $b \to s\ell\ell$ decays is given by [85, 87]

$$\mathcal{H}_{\text{eff}}(b \to s\ell^+\ell^-) = \frac{4G_F}{\sqrt{2}} \left[\lambda_u^s \sum_{i=1}^{2} \mathcal{C}_i \mathcal{Q}_i^u + \lambda_c^s \sum_{i=1}^{2} \mathcal{C}_i \mathcal{Q}_i^c - \lambda_t^s \sum_{i=3}^{10} \mathcal{C}_i \mathcal{Q}_i \right], \tag{7.2.1}$$

where $\lambda_p^s = V_{pb}V_{ps}^*$, and

$$\begin{aligned}
\mathcal{Q}_1^c =& (\bar{s}_L^a\gamma_\mu c_L^b)(\bar{c}_L^b\gamma^\mu b_L^a), & \mathcal{Q}_2^c =& (\bar{s}_L\gamma_\mu c_L)(\bar{c}_L\gamma^\mu b_L),\\
\mathcal{Q}_1^u =& (\bar{s}_L^a\gamma_\mu u_L^b)(\bar{u}_L^b\gamma^\mu b_L^a), & \mathcal{Q}_2^u =& (\bar{s}_L\gamma_\mu u_L)(\bar{u}_L\gamma^\mu s_L),\\
\mathcal{Q}_3 =& (\bar{s}_L\gamma_\mu b_L)\sum_q(\bar{q}_L\gamma^\mu q_L) & \mathcal{Q}_4 =& \left(\bar{s}_L^a\gamma_\mu b_L^b\right)\sum_q\left(\bar{q}_L^b\gamma^\mu q_L^a\right)\\
\mathcal{Q}_5 =& (\bar{s}_L\gamma_\mu\gamma_\nu\gamma_\rho b_L)\sum_q(\bar{q}_R\gamma^\mu\gamma^\nu\gamma^\rho q_R) & \mathcal{Q}_6 =& \left(\bar{s}_L^a\gamma_\mu\gamma_\nu\gamma_\rho b_L^b\right)\sum_q\left(\bar{q}_R^b\gamma^\mu\gamma^\nu\gamma^\rho q_R^a\right)\\
\mathcal{Q}_7 =& \frac{e}{16\pi^2}m_b(\bar{s}_L\sigma^{\mu\nu}b_R)F_{\mu\nu}, & \mathcal{Q}_8 =& \frac{g_s}{16\pi^2}m_b(\bar{s}_L\sigma^{\mu\nu}T^a b_R)G^a_{\mu\nu},\\
\mathcal{Q}_9 =& \frac{e^2}{16\pi^2}(\bar{s}_L\gamma_\mu b_L)(\bar{\ell}\gamma^\mu\ell), & \mathcal{Q}_{10} =& \frac{e^2}{16\pi^2}(\bar{s}_L\gamma_\mu b_L)(\bar{\ell}\gamma^\mu\gamma_5\ell).
\end{aligned} \tag{7.2.2}$$

The only operators which have a non-vanishing matrix element in $b\to sll$ are $\mathcal{O}_7$, $\mathcal{Q}_9$ and $\mathcal{Q}_{10}$. The four-quark operators $Q_{1,\dots,6}$ have non-vanishing matrix elements only at the loop level, as shown in fig. 7.2.1. In the loop we can have a light quark (u, d or s) or a heavy quark (c or b).

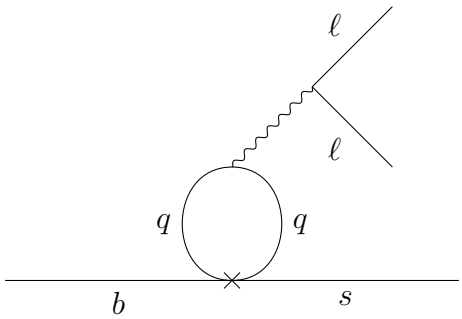

Figure 7.2.1: Leading order contribution of the operators $\mathcal{Q}_1,\dots\mathcal{Q}_6$. The cross denotes an insertion of the operator.

At this level of accuracy WC $C_1,\dots,C_6$ only appear in specific combinations, accompanied by C_9 or C_7 [97]. Therefore we define an effective C_7

$$C_7^{\text{eff}} = C_7 - \frac{1}{3}\left(C_3 + \frac{4}{3}C_4 + 20C_5 + \frac{80}{3}C_6\right) \tag{7.2.3}$$

and an effective C_9

$$C_9^{\text{eff}} = C_9 + Y\left(q^2\right) \tag{7.2.4}$$

with

$$\begin{aligned}
Y\left(q^2\right) = \frac{4}{3}C_3 + \frac{64}{9}C_5 + \frac{64}{27}C_6 &- \frac{1}{2}h\left(q^2,0\right)\left(C_3 + \frac{4}{3}C_4 + 16C_5 + \frac{64}{3}C_6\right)\\
&+ h\left(q^2,m_c\right)\left(\frac{4}{3}C_1 + C_2 + 6C_3 + 60C_5\right)\\
&- \frac{1}{2}h\left(q^2,m_b\right)\left(7C_3 + \frac{4}{3}C_4 + 76C_5 + \frac{64}{3}C_6\right),
\end{aligned} \tag{7.2.5}$$

where the function

$$h\left(q^2,m\right)=-\frac{4}{9}\left(\ln\frac{m^2}{\mu^2}-\frac{2}{3}-x\right)-\frac{4}{9}\left(2+x\right)\begin{cases}\sqrt{x-1}\arctan\frac{1}{\sqrt{x-1}}, & x>1\\ \sqrt{1-x}\left(\ln\frac{1+\sqrt{1-x}}{\sqrt{x}}-\frac{i\pi}{2}\right), & x\geq 1\end{cases} \tag{7.2.6}$$

with $x=4m^2/q^2$ corresponds to the fermion loop integral in fig. 7.2.1. The effective C_9 depends on q^2 due to the q^2 dependence of the loop function in fig. 7.2.1. In eq. (7.2.5) we have three quark loop contributions. The contribution proportional to $h\left(q^2,0\right)$ describes a loop containing light quarks while $h\left(q^2,m_b\right)$ and $h\left(q^2,m_c\right)$ describe bottom and charm loops, respectively.

The function $h\left(q^2,m\right)$ is not sufficient for modeling the q^2 dependence of C_9^{eff} [37,159]. This is due to the fact that in B decays there is enough energy for the charm quarks in the loop to go on-shell. In this case the decay proceeds via an intermediate $c\bar{c}$ resonance which is not described adequately by the function h, which misses the non-perturbative dynamics. Instead it has to be described by a non-perturbative framework. In section 7.3 we will estimate the resonance contributions from subtracted dispersion relations instead of using the h function defined above.

But first we turn to the computation of matrix elements of the effective Hamiltonian eq. (7.2.1). In section 7.2.1 we describe the semileptonic decay of a B meson to a vector meson V and in section 7.2.2 we describe the semileptonic decay of a B meson to a pseudoscalar meson P.

7.2.1 $B\to V\ell\ell$

We cannot analytically compute the hadronic matrix elements of the operators $\mathcal{Q}_i$ in eq. (7.2.1). Instead we parametrize them in terms of the seven form factors [41]

$$\begin{aligned}\left\langle V(k)\left|\bar{s}\gamma_\mu\left(1-\gamma_5\right)b\right|\overline{B}(p)\right\rangle =&-i\epsilon^*\left(m_B+m_V\right)A_1\left(q^2\right)+i\left(2p-q\right)_\mu\left(\epsilon^*\cdot q\right)\frac{A_2\left(q^2\right)}{m_B+m_V}\\ &+iq_\mu\left(\epsilon^*\cdot q\right)\frac{2m_V}{q^2}\left[A_3\left(q^2\right)-A_0\left(q^2\right)\right]+\epsilon_{\mu\nu\rho\sigma}\epsilon^{*\nu}p^\rho k^\sigma\frac{2V\left(q^2\right)}{m_B+m_V},\end{aligned} \tag{7.2.7}$$

$$\begin{aligned}\left\langle V(k)\left|\bar{s}\sigma_{\mu\nu}q^\nu\left(1+\gamma_5\right)b\right|\overline{B}(p)\right\rangle =&i\epsilon_{\mu\nu\rho\sigma}\epsilon^{*\nu}p^\rho k^\sigma 2T_1\left(q^2\right)+T_2\left(q^2\right)\left[\epsilon^*\left(m_B^2-m_V^2\right)-\left(\epsilon^*\cdot q\right)\left(2p-q\right)_\mu\right]\\ &+T_3\left(q^2\right)\left(\epsilon^*\cdot q\right)\left[q_\mu-\frac{q^2}{m_B^2-m_V^2}(2p-q)_\mu\right]\end{aligned} \tag{7.2.8}$$

where $A_0(0)=A_3(0)$, $T_1(0)=T_2(0)$ and one of the form factors $A_{1,2,3}$ is redundant because we have the relation

$$A_3\left(q^2\right)=\frac{m_B+m_V}{2m_V}A_1\left(q^2\right)-\frac{m_B-m_V}{2m_V}A_2\left(q^2\right). \tag{7.2.9}$$

In experiments the vector meson V is not directly observed. Instead it decays and its decay products are observed. In the cases of interest to us here one actually observes the decay $B\to K^*(\to K\pi)\ell^+\ell^-$ and $B_s\to\phi\left(\to K^+K^-\right)\ell^+\ell^-$. Assuming that the vector meson decays resonantly and has a small width, i.e. $\Gamma_V\ll m_V$ (corrections to this approximation can be found in [116]), and after summing over the lepton spins and integrating over the $K\pi$ or K^+K^-

invariant mass one finds the fully differential decay width

$$\begin{aligned}\frac{\mathrm{d}^4\Gamma}{\mathrm{d}q^2\mathrm{d}\cos\theta_\ell\mathrm{d}\cos\theta_V\mathrm{d}\phi} = \frac{9}{32\pi}&\left(J_1^s + J_2^s\cos 2\theta_\ell + J_6^s\cos\theta_\ell\right)\sin^2\theta_V \\ &+ \left(J_1^c + J_2^c\cos 2\theta_\ell + J_6^c\cos\theta_\ell\right)\cos^2\theta_V \\ &+ \left(J_3\cos 2\phi + J_9\sin 2\phi\right)\sin^2\theta_V\sin^2\theta_\ell \\ &+ \left(J_4\cos\phi + J_8\sin\phi\right)\sin 2\theta_V\sin 2\theta_\ell \\ &+ \left(J_5\cos\phi + J_7\sin\phi\right)\sin 2\theta_V\sin\theta_\ell. \end{aligned} \tag{7.2.10}$$

For the angles we use the LHCb basis described in detail in Appendix A of [4]. We define θ_ℓ as the angle between the flight direction of the μ^+ (μ^-) in the muon pair rest frame and the direction of the muon pair in the B ($\overline{B}$) rest frame, explicitly

$$\begin{aligned}\cos\theta_\ell &= \hat{p}_{\mu^+}^{(\mu^+\mu^-)}\cdot\hat{p}_{\mu^+\mu^-}^{(B)} = \hat{p}_{\mu^+}^{(\mu^+\mu^-)}\cdot\left(-\hat{p}_B^{(B)}\right), \\ \cos\theta_\ell &= \hat{p}_{\mu^-}^{(\mu^+\mu^-)}\cdot\hat{p}_{\mu^+\mu^-}^{(\overline{B})} = \hat{p}_{\mu^-}^{(\mu^+\mu^-)}\cdot\left(-\hat{p}_{\overline{B}}^{(\overline{B})}\right)\end{aligned} \tag{7.2.11}$$

for B and $\overline{B}$ decays, respectively. The angle θ_V is defined as the angle between the flight direction of the kaon in the kaon rest frame and the direction of the vector meson V in the B ($\overline{B}$) rest frame, explicitly

$$\begin{aligned}\cos\theta_V &= \hat{p}_{K^+}^{(V)}\cdot\hat{p}_V^{(B)} = \hat{p}_{K^+}^{V}\cdot\left(-\hat{p}_B^{(V)}\right) \\ \cos\theta_V &= \hat{p}_{K^-}^{(\overline{V})}\cdot\hat{p}_{\overline{V}}^{(\overline{B})} = \hat{p}_{K^-}^{\overline{V}}\cdot\left(-\hat{p}_{\overline{B}}^{(V)}\right),\end{aligned} \tag{7.2.12}$$

for the decays of a B meson and of a $\overline{B}$ meson, respectively. Last but not least we define the angle ϕ as the angle between the plane spanned by the muon pair and the plane spanned by the decay products of V, explicitly

$$\begin{aligned}\cos\phi &= \left(\hat{p}_{\mu^+}^{(B)}\times\hat{p}_{\mu^-}^{(B)}\right)\cdot\left(\hat{p}_{K^+}^{(B)}\times\hat{p}_{\pi^-(K^-)}^{(B)}\right) \\ \sin\phi &= \left[\left(\hat{p}_{\mu^+}^{(B)}\times\hat{p}_{\mu^-}^{(B)}\right)\times\left(\hat{p}_{K^+}^{(B)}\times\hat{p}_{\pi^-(K^-)}^{(B)}\right)\right]\cdot\hat{p}_V^{(B)}\end{aligned} \tag{7.2.13}$$

for the decay of a B meson and

$$\begin{aligned}\cos\phi &= \left(\hat{p}_{\mu^-}^{(\overline{B})}\times\hat{p}_{\mu^+}^{(\overline{B})}\right)\cdot\left(\hat{p}_{K^-}^{(\overline{B})}\times\hat{p}_{\pi^+(K^+)}^{(\overline{B})}\right) \\ \sin\phi &= -\left[\left(\hat{p}_{\mu^-}^{(\overline{B})}\times\hat{p}_{\mu^+}^{(\overline{B})}\right)\times\left(\hat{p}_{K^-}^{(\overline{B})}\times\hat{p}_{\pi^+(K^+)}^{(\overline{B})}\right)\right]\cdot\hat{p}_{\overline{V}}^{(\overline{B})}\end{aligned} \tag{7.2.14}$$

for a $\overline{B}$ meson.

This definition of θ_ℓ differs from the one in [41], where θ_ℓ is defined with respect to the positive muon in both cases. It is important to keep this in mind because we implement the angular observables based on [41] but use data from LHCb. We compensate for the different angular definitions by using the relation $\theta_\ell^{[41]} = \pi - \theta_\ell^{\mathrm{LHCb}}$ which amounts to a change of the sign of J_4 and J_6^s. A detailed comparison of the LHCb conventions to the conventions commonly used by theory groups can be found in Appendix C.2 of [152].

The angular coefficients J_i in eq. (7.2.10) can be computed in terms of the seven transversity amplitudes $A^{L,R}_{\parallel,\perp,0}$ and A_t [183]. In terms of the transversity amplitudes the angular observables are given by

$$
\begin{aligned}
J_1^s &= \frac{2+\beta^2}{4}\left(\left|A_\perp^L\right|^2+\left|A_\parallel\right|^2+(L\to R)\right)+\frac{4m_\ell^2}{q^2}\mathrm{Re}\left(A_\perp^L A_\perp^{R*}+A_\parallel^L A_\parallel^{R*}\right)\\
J_1^c &= \left|A_0^L\right|^2+\left|A_0^R\right|^2+\frac{4m_\ell^2}{q^2}\left(|A_t|^2+2\mathrm{Re}\left(A_0^L A_0^{R*}\right)\right)\\
J_2^s &= \frac{\beta^2}{4}\left(\left|A_\perp^L\right|^2+\left|A_\parallel^L\right|^2+(L\to R)\right)\\
J_2^c &= -\beta^2\left(\left|A_0^L\right|^2+(L\to R)\right)\\
J_3 &= \frac{1}{2}\beta^2\left(\left|A_\perp^L\right|^2-\left|A_\parallel^L\right|^2+(L\to R)\right)\\
J_4 &= \frac{1}{\sqrt{2}}\beta^2\left(\mathrm{Re}\left(A_0^L A_\parallel^{L*}\right)+(L\to R)\right)\\
J_5 &= \sqrt{2}\beta\left(\mathrm{Re}\left(A_0^L A_\perp^{L*}\right)-(L\to R)\right)\\
J_6^s &= 2\beta\left(\mathrm{Re}\left(A_\parallel^L A_\perp^{L*}\right)-(L\to R)\right)\\
J_6^c &= 0\\
J_7 &= \sqrt{2}\beta\left(\mathrm{Im}\left(A_0^L A_\parallel^{L*}\right)-(L\to R)\right)\\
J_8 &= \frac{1}{\sqrt{2}}\beta^2\left(\mathrm{Im}\left(A_0^L A_\perp^{L*}\right)+(L\to R)\right)\\
J_9 &= \beta^2\left(\mathrm{Im}\left(A_\parallel^{L*} A_\perp^L\right)+(L\to R)\right)
\end{aligned}
\tag{7.2.15}
$$

where $\beta=\sqrt{1-2m_\ell^2/q^2}$ and

$$
\begin{aligned}
A_{\perp L,R} &= N\sqrt{2\lambda}\left(\left(C_9^{\mathrm{eff}}\mp C_{10}\right)\frac{V\left(q^2\right)}{m_B+m_V}+\frac{2m_b}{q^2}C_7^{\mathrm{eff}}T_1\left(q^2\right)\right)\\
A_{\parallel L,R} &= -N\sqrt{2}\left(m_B^2-m_V^2\right)\left(\left(C_9^{\mathrm{eff}}\mp C_{10}\right)\frac{A_1\left(q^2\right)}{m_B-m_V}+\frac{2m_b}{q^2}C_7^{\mathrm{eff}}T_2\left(q^2\right)\right)\\
A_{0L,R} &= -\frac{N}{2m_V\sqrt{q^2}}\Bigg(\left(C_9^{\mathrm{eff}}\mp C_{10}\right)\left(\left(m_B^2-m_V^2-q^2\right)\left(m_B+m_V\right)A_1\left(q^2\right)-\lambda\frac{A_2\left(q^2\right)}{m_B+m_V}\right)\\
&\qquad +2m_bC_7^{\mathrm{eff}}\left(\left(m_B^2+3m_V^2-q^2\right)T_2\left(q^2\right)-\frac{\lambda}{m_B^2-m_V^2}\right)T_3\left(q^2\right)\Bigg)\\
A_t &= \frac{2N}{\sqrt{q^2}}\sqrt{\lambda}C_{10}A_0\left(q^2\right),
\end{aligned}
\tag{7.2.16}
$$

with $\lambda=m_B^4+m_V^4+q^4-2\left(m_B^2m_V^2+m_V^2q^2+m_B^2q^2\right)$ and the normalization factor

$$
N=V_{tb}V_{ts}^*\left(\frac{G_{\mathrm{F}}\alpha^2}{3\cdot 2^{10}\pi^5m_B^3}q^2\sqrt{\lambda}\beta\right)^{\frac{1}{2}},
\tag{7.2.17}
$$

where $\alpha=e^2/(4\pi)$ is the fine structure constant.

Now we can define the observables we will use to study the long-distance contributions to C_9^{eff} later on. We will need the differential branching ratio

$$\frac{\mathrm{d}\mathcal{B}\left(B\to V\ell^+\ell^-\right)}{\mathrm{d}q^2}=\frac{1}{\Gamma_B}\int \mathrm{d}\cos\theta_\ell \mathrm{d}\cos\theta_V \mathrm{d}\cos\phi \frac{\mathrm{d}^4\Gamma}{\mathrm{d}q^2 \mathrm{d}\cos\theta_\ell \mathrm{d}\cos\theta_V \mathrm{d}\cos\phi}, \tag{7.2.18}$$

where Γ_B denotes the total B meson decay rate and the CP-averaged angular observables introduced in [41]

$$S_i^{(a)}=\left(J_i^{(a)}+\overline{J}_i^{(a)}\right)\Big/\frac{\mathrm{d}\left(\Gamma+\overline{\Gamma}\right)}{\mathrm{d}q^2} \tag{7.2.19}$$

The CP conjugates $\overline{J}_i$ of the angular coefficients are found by conjugating all the weak phases in the transversity amplitudes, i.e. the phases of the Wilson coefficients and of the normalization factor. As $J_{7,8,9}$ are CP odd in the SM we have $S_{7,8,9}=0$, up to corrections of $\mathcal{O}\left(V_{us}/V_{ts}\right)$. Explicitly carrying out the integrations over the angles θ_ℓ, θ_V and ϕ in eq. (7.2.10) we find the q^2-spectrum

$$\frac{\mathrm{d}\Gamma}{\mathrm{d}q^2}=\frac{3}{4}\left(2J_1^s+J_1^c\right)-\frac{1}{4}\left(2J_2^s+J_2^c\right), \tag{7.2.20}$$

and due to the normalization of the angular observables this yields the relation

$$\frac{3}{4}\left(2S_1^s+S_1^c\right)-\frac{1}{4}\left(2S_2^s+S_2^c\right)=1 \tag{7.2.21}$$

which renders one of the observables $S_{(1,2)}^{(s,c)}$ redundant. If the final state leptons are massless, which is a good approximation for $q^2>1\text{GeV}^2$, additionally the relations $S_1^s=3S_2^s$ and $S_1^c=-S_2^c$ hold, reducing the number of independent angular observables from 12 to 8.

In experimental measurements the differential observables are averaged over bins of q^2 as

$$\left\langle\frac{\mathrm{d}\mathcal{B}\left(B\to V\ell^+\ell^-\right)}{\mathrm{d}q^2}\right\rangle_{\left[q^2_{\text{min}},q^2_{\text{max}}\right]}=\frac{1}{q^2_{\text{max}}-q^2_{\text{min}}}\int_{q^2_{\text{min}}}^{q^2_{\text{max}}}\mathrm{d}q^2\frac{\mathrm{d}\mathcal{B}\left(B\to V\ell^+\ell^-\right)}{\mathrm{d}q^2} \tag{7.2.22}$$

and

$$\left\langle S_i^{(a)}\right\rangle_{\left[q^2_{\text{min}},q^2_{\text{max}}\right]}=\int_{q^2_{\text{min}}}^{q^2_{\text{max}}}\mathrm{d}q^2\left(J_i^{(a)}+\overline{J}_i^{(a)}\right)\Big/\int_{q^2_{\text{min}}}^{q^2_{\text{max}}}\mathrm{d}q^2\frac{\mathrm{d}\left(\Gamma+\overline{\Gamma}\right)}{\mathrm{d}q^2}\,. \tag{7.2.23}$$

To match the LHCb conventions on the names of the observables we will refer to S_1^c as F_L from now on because it corresponds to the fraction of longitudinal polarization of the meson V and we replace S_6^s by the forward-backward asymmetry $A_{\text{FB}}=\frac{3}{4}S_6^s$ of the lepton pair [13].

This concludes the general treatment of $B\to V\ell\ell$ decays. In section 7.5 we implement the binned branching ratio and the angular observables $\{F_L,S_3,S_4,S_5,A_{\text{FB}},S_7,S_8,S_9\}$, employing a novel parametrization of the charm loop effects in a fit of the WC C_9. Another possibility would be to use the optimized observables $P_i^{(\prime)}$, which suffer from smaller form factor uncertainties.

7.2.2 $B\to P\ell\ell$

In this case we will focus on the decay $B^+\to K^+\mu^+\mu^-$. The hadronic matrix elements appearing in this decay are commonly parametrized in terms of three form factors as

$$\begin{aligned}\langle K(k)\left|\bar{s}\gamma_\mu b\right|B(p)\rangle&=\left((p+k)_\mu-\frac{m_B^2-m_K^2}{q^2}q_\mu\right)f_+\left(q^2\right)+\frac{m_B^2-m_K^2}{q^2}q_\mu f_0\left(q^2\right)\\ \langle K(k)\left|\bar{s}\sigma_{\mu\nu}b\right|B(p)\rangle&=-i\left(p_\mu k_\nu-p_\nu k_\mu\right)\frac{2f_T\left(q^2\right)}{m_B+m_K}.\end{aligned} \tag{7.2.24}$$

The fully differential $B \to K\ell^+\ell^-$ decay rate is given by [63]

$$\frac{\mathrm{d}^2\Gamma\left(B \to K\ell^+\ell^-\right)}{\mathrm{d}q^2 \mathrm{d}\cos\theta} = a_\ell\left(q^2\right) + b_\ell\left(q^2\right)\cos\theta + c_\ell\left(q^2\right)\cos^2\theta, \tag{7.2.25}$$

where θ is the angle between the flight direction of the B meson and and of ℓ^- in the rest frame of the lepton pair. Carrying out the integral over θ yields the q^2-spectrum

$$\frac{\mathrm{d}\Gamma\left(B \to K\ell^+\ell^-\right)}{\mathrm{d}q^2} = 2a_\ell + \frac{2}{3}c_\ell. \tag{7.2.26}$$

The angular coefficients a_ℓ and c_ℓ are given by

$$\begin{aligned} a_\ell &= N_K\left(q^2\left|F_P\right|^2 + \frac{\lambda_K}{4}\left(\left|F_A\right|^2 + \left|F_V\right|^2\right)\right) + 4m_\ell^2 m_B^2\left|F_A\right|^2 + 2m_\ell\left(m_B^2 - m_K^2 + q^2\right)\mathrm{Re}\left(F_P F_A^*\right) \\ c_\ell &= -\frac{N_K\lambda_K\beta^2}{4}\left(\left|F_A\right|^2 + \left|F_V\right|^2\right), \end{aligned} \tag{7.2.27}$$

where $\lambda_K = m_B^4 + m_K^4 + q^4 - 2\left(M_B^2 q^2 + M_K^2 q^2 + M_B^2 M_K^2\right)$ and the normalization constant N_K is given by

$$N_K = \left|V_{tb}V_{ts}^*\right|^2 \frac{G_\mathrm{F}\alpha^2}{2^9\pi^5 m_B^3}\beta\sqrt{\lambda_K}. \tag{7.2.28}$$

The quantities $F_{P,V,A}$ are constructed from the form factors as

$$\begin{aligned} F_P &= -m_\ell C_{10}\left(f_+ - \frac{m_B^2 - m_K^2}{q^2}\left(f_0 - f_+\right)\right) \\ F_V &= C_9^{\mathrm{eff}} f_+ + \frac{2m_b}{m_B + m_K}C_7^{\mathrm{eff}} f_T \\ F_A &= C_{10} f_+. \end{aligned} \tag{7.2.29}$$

Again the values of the branching ratio measured in experiments are averages over q^2-bins so we compute

$$\left\langle \frac{\mathrm{d}\mathcal{B}\left(B \to K\ell^+\ell^-\right)}{\mathrm{d}q^2} \right\rangle_{\left[q^2_{\mathrm{min}}, q^2_{\mathrm{max}}\right]} = \frac{1}{\left(q^2_{\mathrm{max}} - q^2_{\mathrm{min}}\right)\Gamma_B}\int_{q^2_{\mathrm{min}}}^{q^2_{\mathrm{max}}} \mathrm{d}q^2 \frac{\mathrm{d}\Gamma\left(B \to K\ell^+\ell^-\right)}{\mathrm{d}q^2}. \tag{7.2.30}$$

In section 7.5 we will use this observable to study the q^2-dependence of C_9^{eff} from experimental data. To this end we develop a new treatment of the charm loop contributions in the next section.

7.3 Long Distance Contributions from $c\bar{c}$ resonances

As already stated the contribution of intermediate $c\bar{c}$ states cannot be described by perturbation theory. We proceed with a formulation of the $c\bar{c}$ resonances following [90]. First we modify our effective C_9 and add a new term $Y_{c\bar{c}}^{(\lambda)}$. The label λ in parentheses stems from the fact that in the $B \to V\ell\ell$ case this term depends on the polarization of the vector meson V. So we introduce a new effective C_9

$$C_9^{\mathrm{eff}} \to C_9^{(\lambda),\mathrm{eff}}\left(q^2\right) = C_9 + \tilde{Y}\left(q^2\right) + Y_{c\bar{c}}^{(\lambda)}\left(q^2\right), \tag{7.3.1}$$

where $\tilde{Y}\left(q^2\right)$ is defined by eq. (7.2.5) with the replacement

$$h\left(q^2, m_c^2\right) \to \lim_{q^2\to 0} h\left(q^2, m_c^2\right) = \frac{4}{9}\left(\frac{2}{3} + 3\ln\frac{\mu^2}{q^2} + 3i\right). \tag{7.3.2}$$

This modification is necessary in order to not double count the charm loop contributions. For $B \to V\ell\ell$ we denote the form factor proportional to C_9 in the transversity amplitude A_λ as f_λ, i.e. $f_\perp = V$, $f_\parallel = A_1$ and $f_0 = A_{12}$. In the case of $B \to P\ell\ell$ C_9 is proportional to f_+ and therefore $f = f_+$ in this case. Then we express the functions $Y_{c\bar{c}}^{(\lambda)}$ as

$$Y_{c\bar{c}}^{(\lambda)}\left(q^2\right) = \frac{16\pi^2}{f_{(\lambda)}\left(q^2\right)}\mathcal{H}_{c\bar{c}}^{(\lambda)}(q^2)\,, \tag{7.3.3}$$

where [179]

$$\begin{aligned} & i\int d^4x e^{iqx}\langle P(k)|T\left\{j_\mu^{(\lambda),\mathrm{em}}(x), \sum_{i=1,2}\mathcal{C}_i^c\mathcal{O}_i^q(0)\right\}|\bar{B}(p)\rangle \\ & = \left[(p\cdot q)q_\mu - q^2 p_\mu\right]\mathcal{H}_{c\bar{c}}^{(\lambda)}\left(q^2\right)\,, \end{aligned} \tag{7.3.4}$$

with $j_\mu^{\mathrm{em}} = \sum_{q=u,d,s,c,b} Q_q \bar{q}\gamma_\mu q$. In practice, we are unable to evaluate these expressions from first principles and we estimate them from data using dispersion relations [81, 86, 110, 179, 190].

In full generality, we can write a subtracted dispersion relation for $\mathcal{H}_{c\bar{c}}(q^2)$

$$\Delta Y_{q\bar{q}}^{(\lambda)}(q^2) = \frac{16\pi^2}{f_{(\lambda)}\left(q^2\right)}\Delta\mathcal{H}_{q\bar{q}}^{(\lambda)}(q^2)\,, \tag{7.3.5}$$

with

$$\begin{aligned} \Delta\mathcal{H}_{q\bar{q}}^{(\lambda)}(q^2) &= \frac{q^2 - q_0^2}{\pi}\int_{s_0}^{\infty} ds \frac{\mathrm{Im}[\mathcal{H}_{q\bar{q}}^{(\lambda)}(s)]}{(s-q_0^2)(s-q^2)} \\ &\equiv \frac{q^2 - q_0^2}{\pi}\int_{s_0}^{\infty} ds \frac{\rho_{q\bar{q}}^{(\lambda)}(s)}{(s-q_0^2)(s-q^2)}\,, \end{aligned} \tag{7.3.6}$$

The function $\rho_{q\bar{q}}(s)$ is the spectral density for an intermediate hadronic state with valence quarks $q\bar{q}$ and invariant mass s, and the parameter s_0 is the energy threshold where the state can be created on-shell. The parameter q_0^2 is the subtraction point that we choose for the different $q\bar{q}$ states ($q_0^2 < s_0$).

The leading contribution to $\rho_{q\bar{q}}(s)$ is provided by single-particle intermediate states. We can describe them as a sum of Breit-Wigner distributions:

$$\begin{aligned} \Delta\mathcal{H}_{q\bar{q}}^{(\lambda),1\mathrm{P}} &= \sum_{V_j}\eta_{V_j}^{(\lambda)} e^{i\delta_{V_j}^{(\lambda)}}\frac{(q^2-q_0^2)}{(m_V^2-q_0^2)}A_{V_j}^{\mathrm{res}}\left(q^2\right)\,, \\ A_{V_j}^{\mathrm{res}}\left(q^2\right) &= \frac{m_{V_j}\Gamma_{V_j}}{m_{V_j}^2 - q^2 - i m_{V_j}\Gamma_{V_j}}\,, \end{aligned} \tag{7.3.7}$$

where the sum runs over all the possible vector states associated with the the $q\bar{q}$ valence quarks. The parameters η_j and δ_j have to be determined from data. For the charmonium resonances, which have a high invariant mass, we use dispersion relations subtracted at $q^2 = 0$, yielding

$$\Delta\mathcal{H}_{c\bar{c}}^{(\lambda),1\mathrm{P}} = \sum_{V_j = J/\psi,\psi(2S),\ldots}\eta_{V_j}^{(\lambda)} e^{i\delta_{V_j}^{(\lambda)}}\frac{q^2}{m_{V_j}^2}A_{V_j}^{\mathrm{res}}\left(q^2\right)\,. \tag{7.3.8}$$

Then we can write eq. (7.3.1) as

$$C_9^{(\lambda),\text{eff}}\left(q^2\right) = C_9 + \tilde{Y}\left(q^2\right) + \frac{16\pi^2}{f_{(\lambda)}\left(q^2\right)} \sum_{V_j = J/\psi, \psi(2S), \ldots} \eta_{V_j}^{(\lambda)} e^{i\delta_{V_j}^{(\lambda)}} \frac{q^2}{m_{V_j}} \frac{\Gamma_{V_j}}{m_{V_j}^2 - q^2 - i m_{V_j}\Gamma_{V_j}}. \quad (7.3.9)$$

7.4 Extraction of the resonance parameters from data

7.4.1 $B \to KV_j \to K\ell^+\ell^-$

For the decay chain $B^+ \to KV_j \to K^+\ell^+\ell^-$ we can determine the resonance parameters from the following expression [90]

$$\begin{aligned}&\mathcal{B}\left(B^+ \to K^+ V_j\right) \times \mathcal{B}\left(V_j \to \mu^+\mu^-\right) = \\ &\left|\eta_{V_j}\right|^2 \tau_{B^+} \frac{G_\text{F}^2 \alpha^2 \left|V_{cb}V_{cs}^*\right|^2}{1024\pi^5} \int_{4m_\mu^2}^{(m_B - m_K)^2} |\mathbf{k}|^3 \left[\beta - \frac{1}{3}\beta^3\right] \left(16\pi^2\right)^2 \left|A_{V_j}^\text{res}\left(q^2\right)\right|^2 \left|\frac{q^2}{m_{V_j}^2}\right|^2 \mathrm{d}q^2, \end{aligned} \quad (7.4.1)$$

where τ_B is the B^+ meson lifetime and $|\mathbf{k}| = \sqrt{\lambda\left(m_{B^+}, m_{K^+}, m_{V_j}\right)}/2m_B$ is the modulus of the kaon 3-momentum in the B^+ meson rest frame. The function $\left|A_{V_j}^\text{res}\left(q^2\right)\right|^2$, describing the resonance takes the form of a Breit-Wigner distribution:

$$A_V^\text{res}\left(q^2\right) = \frac{m_{V_j}\Gamma_{V_j}}{\left(m_{V_j}^2 - q^2\right) - i m_{V_j}\Gamma_{V_j}}. \quad (7.4.2)$$

After taking the modulus squared of the resonance function we can facilitate the integration by taking the narrow width approximation

$$\left|A_{V_j}^\text{res}\left(q^2\right)\right|^2 = \frac{m_{V_j}^2\Gamma_{V_j}^2}{\left(q^2 - m_{V_j}^2\right)^2 + m_{V_j}^2\Gamma_{V_j}^2} \overset{\frac{\Gamma_{V_j}}{m_{V_j}} \to 0}{\longrightarrow} m_{V_j}\Gamma_{V_j}\pi\delta\left(q^2 - m_{V_j}^2\right). \quad (7.4.3)$$

Then eq. (7.4.1) yields

$$\left|\eta_{V_j}\right|^2 = \frac{6m_{B^+}^3 \mathcal{B}\left(B^+ \to K^+ V_j\right) \mathcal{B}\left(V_j \to \mu^+\mu^-\right)}{\tau_{B^+} G_\text{F}^2 \alpha^2 \left|V_{cb}V_{cs}^*\right|^2 \Gamma_{V_j} m_{V_j} \lambda^{3/2}\left(m_{B^+}, m_{K^+}, m_{V_j}\right)}, \quad (7.4.4)$$

where $\lambda(a,b,c) = a^4 + b^4 + c^4 - 2\left(a^2b^2 + a^2c^2 + b^2c^2\right)$.

Using the the PDG result for the branching ratios, the LHCb results in [17] (we use the values in the upper right corner of Table 3) and the input values in table B.1.1, we then obtain the values reported in table B.2.1 for the J/ψ and $\psi(2s)$ resonances. The values for the higher resonances are taken from table 2 of [90].

7.4.2 $B \to VV_j \to V\ell^+\ell^-$

$B \to VV_j$

As a first step we determine the $B \to V\ell\ell$ amplitude from the measured values of the transversity amplitudes for $B_s \to J/\psi\phi$, $B_s \to \psi(2s)\phi$ and $B \to J/\psi K^*$. We can do this by treating

the decay as a sequential process $B \to VV_j \to V\ell^+\ell^-$. The first step of this process is where the measured non-leptonic amplitudes come in. Once we have expressed the matrix element

$$\left\langle V(k,\epsilon_V(\lambda))V_j^*(q,\epsilon_{V_j}(\lambda_j))\right|\mathcal{Q}_{1,2}^p\left|B_q(p_B)\right\rangle\,, \tag{7.4.5}$$

in terms of measured transversity amplitudes we relate it to the full decay and extract the resonance parameters $\eta_{V_j}^\lambda$ and $\delta_{V_j}^\lambda$. where $V_{1,2}$ are two vector states, characterized by mass $m_{1,2}$ and their momentum $p_{1,2}$ and polarization vector $\epsilon_{1,2}$. Following [119], we have:

$$\begin{aligned}&\left\langle V(k,\epsilon_V(\lambda))V_j^*(q,\epsilon_{V_j}(\lambda_j))\right|\mathcal{Q}_{1,2}^p\left|B_q(p_B)\right\rangle = \\ &\epsilon_{V\mu}^*(\lambda)\epsilon_{V_j\nu}^*(\lambda_j)\left[ag^{\mu\nu}+\frac{b}{m_V m_{V_j}}q^\mu k^\nu + i\frac{c}{m_V m_{V_j}}\epsilon^{\mu\nu\alpha\beta}k_\alpha q_\beta\right]\,,\end{aligned} \tag{7.4.6}$$

where the coefficients a, b and c encode the contributions to this decay due to all possible topologies. We can introduce 3 transversity amplitudes, which are related to the coefficients a, b and c as

$$\mathcal{A}_0 = -\,xa - (x^2-1)b\,, \tag{7.4.7}$$

$$\mathcal{A}_\parallel = +\,\sqrt{2}\,a\,, \tag{7.4.8}$$

$$\mathcal{A}_\perp = +\,\sqrt{2(x^2-1)}\,c\,. \tag{7.4.9}$$

With this definition, we have that

$$\Gamma(B_s\to J/\psi\phi) = (|\mathcal{A}_0|^2+|\mathcal{A}_\parallel|^2+|\mathcal{A}_\perp|^2)\frac{\sqrt{\lambda\left(m_B,m_V,m_{V_j}\right)}}{16\pi m_B^3}\,. \tag{7.4.10}$$

In order to extract the amplitudes from data, we need to compare the previous expression to the one used in experimental analysis, where

$$\frac{d\Gamma(B_s\to J/\psi\phi)}{dt} = \mathcal{N}(|A_0(t)|^2+|A_\parallel(t)|^2+|A_\perp(t)|^2)\,, \tag{7.4.11}$$

and for each amplitude we have:

$$\begin{aligned}|A_k(t)|^2 = |A_k(0)|^2 e^{-\Gamma_s t}\Bigg[&a_k\cosh\left(\frac{1}{2}\Delta\Gamma_s t\right)+b_k\sinh\left(\frac{1}{2}\Delta\Gamma_s t\right)\\ &+c_k\cos(\Delta m_s t)+d_k\sin(\Delta m_s t)\Bigg]\,,\end{aligned} \tag{7.4.12}$$

and the coefficients are

$$a_0 = a_\parallel = a_\perp = 1\,, \tag{7.4.13}$$

$$b_0 = b_\parallel = -b_\perp = -\,2\frac{|\lambda\left(m_B,m_V,m_{V_j}\right)|\cos\phi_s}{1+|\lambda\left(m_B,m_V,m_{V_j}\right)|^2}\,, \tag{7.4.14}$$

$$c_0 = c_\parallel = c_\perp = \frac{1-|\lambda\left(m_B,m_V,m_{V_j}\right)|^2}{1+|\lambda\left(m_B,m_V,m_{V_j}\right)|^2}\,, \tag{7.4.15}$$

$$d_0 = d_\parallel = -d_\perp = -\,2\frac{|\lambda\left(m_B,m_V,m_{V_j}\right)|\sin\phi_s}{1+|\lambda\left(m_B,m_V,m_{V_j}\right)|^2}\,. \tag{7.4.16}$$

In order to find the constant $\mathcal{N}$, we integrate eq. (7.4.11), in the approximation $\Delta\Gamma_s = 0$, $\Delta m_s = 0$ and $\lambda = 1$, obtaining:

$$\mathcal{N}_{V,V_j} = \Gamma_B^2 \times \mathcal{B}(B \to VV_j)\,. \tag{7.4.17}$$

Using the data in [44,227], we have for example $\mathcal{N}_{\phi,J/\psi} = 2.03 \times 10^{-28}\,\mathrm{GeV}^2$. In order to extract the amplitudes $\mathcal{A}_i$, we integrate eq. (7.4.11). Using the results in [42,228] we find:

$$\begin{aligned}
|\mathcal{A}_i\,(B_s \to \phi J/\psi)\,|^2 &= 2.13 \times 10^{-13} |A_i(0)|^2 \mathrm{GeV}^2\,,\\
|\mathcal{A}_i\,(B_s \to \phi\psi(2s))\,|^2 &= 1.46 \times 10^{-13} |A_i(0)|^2 \mathrm{GeV}^2\,,\\
|\mathcal{A}_i\,(B \to K^* J/\psi)\,|^2 &= 2.46 \times 10^{-13} |A_i(0)|^2 \mathrm{GeV}^2\,,\\
|\mathcal{A}_i\,(B \to K^* \psi(2s))\,|^2 &= 1.61 \times 10^{-13} |A_i(0)|^2 \mathrm{GeV}^2\,.
\end{aligned} \tag{7.4.18}$$

The amplitudes A_i are in principle complex valued numbers. They are usually parametrized as

$$A_i = |A_i| e^{-i\delta_i}\,, \tag{7.4.19}$$

where historically $\delta_0 = 0$. From [12], we extract for the decay $B_s \to J/\psi\phi$:

$$\begin{aligned}
|A_0|^2 &= 0.5241 \pm 0.0034 \pm 0.0067\,, \qquad \delta_\parallel = 3.26^{+0.10+0.06}_{-0.17-0.07}\,,\\
|A_\perp|^2 &= 0.2504 \pm 0.0049 \pm 0.0036\,, \qquad \delta_\perp = 3.08^{+0.14}_{-0.15} \pm 0.06\,,
\end{aligned} \tag{7.4.20}$$

where the phases are expressed in radians and the value of $A_\parallel$ can be extracted from the relation: $|A_0|^2 + |A_\parallel|^2 + |A_\perp|^2 = 1$. For the decay $B \to J/\psi K^*$ we use [6] and extract

$$\begin{aligned}
|A_0|^2 &= 0.227 \pm 0.004 \pm 0.011\,, \qquad \delta_\parallel = -2.94 \pm 0.02 \pm 0.03\,,\\
|A_\perp|^2 &= 0.201 \pm 0.004 \pm 0.008\,, \qquad \delta_\perp = 2.94 \pm 0.02 \pm 0.02\,.
\end{aligned} \tag{7.4.21}$$

Last but not least we use [15] for the decay $B \to \psi(2s)\phi$ and extract

$$\begin{aligned}
|A_\perp|^2 &= 0.264^{+0.024}_{-0.023} \pm 0.002\,, \qquad \delta_\perp = 3.29^{+0.43}_{-0.39} \pm 0.04,\\
|A_0|^2 &= 0.422 \pm 0.014 \pm 0.003\,, \qquad \delta_\parallel = 3.67^{+0.13}_{-0.18} \pm 0.03\,.
\end{aligned} \tag{7.4.22}$$

The amplitudes for the decay $B \to K^*\psi(2s)$ have not been measured so in the following we estimate them from $\mathrm{SU(3)_F}$ relations.

Estimation of the Polarization Amplitudes for $B \to \psi(2s)K^*$

In order to estimate the transversity amplitudes for the decay $B \to \psi(2s)K^*$ we build the ratios $A_i\,(B \to \psi(2s)\phi)\,/A_i\,(B \to J/\psi\phi)$ for $i \in \{0, \perp, \|\}$ and assume the corresponding ratios in the $B \to K^*$ case are the same. We find the ratios

$$\begin{aligned}
&\left|\frac{A_0\,(B_s \to \psi(2s)\phi)}{A_0\,(B_s \to J/\psi\phi)}\right| = 0.897 \pm 0.017,\\
&\left|\frac{A_\perp\,(B_s \to \psi(2s)\phi)}{A_\perp\,(B_s \to J/\psi\phi)}\right| = 1.03 \pm 0.33, \qquad \frac{\delta_\perp\,(B_s \to \psi(2s)\phi)}{\delta_\perp\,(B_s \to J/\psi\phi)} = 1.08 \pm 0.14,\\
&\left|\frac{A_\parallel\,(B_s \to \psi(2s)\phi)}{A_\parallel\,(B_s \to J/\psi\phi)}\right| = 1.18 \pm 0.32, \qquad \frac{\delta_\parallel\,(B_s \to \psi(2s)\phi)}{\delta_\parallel\,(B_s \to J/\psi\phi)} = 1.13 \pm 0.07.
\end{aligned} \tag{7.4.23}$$

From them we compute

$$\begin{aligned}
&\left|A_0\left(B\to\psi(2s)K^*\right)\right|^2 = 0.461\pm0.021,\\
&\left|A_\perp\left(B\to\psi(2s)K^*\right)\right|^2 = 0.21\pm0.13, \qquad \delta_\perp\left(B\to\psi(2s)K^*\right) = 3.2\pm0.4,\\
&\left|A_\parallel\left(B\to\psi(2s)K^*\right)\right|^2 = 0.32\pm0.17, \qquad \delta_\parallel\left(B\to\psi(2s)K^*\right) = -1.06\pm0.07.
\end{aligned} \tag{7.4.24}$$

As a quick sanity check we add the squared amplitudes and find

$$\left|A_0\left(B\to\psi(2s)K^*\right)\right|^2 + \left|A_\perp\left(B\to\psi(2s)K^*\right)\right|^2 + \left|A_\parallel\left(B\to\psi(2s)K^*\right)\right|^2 = 0.99\pm0.22 \tag{7.4.25}$$

which is compatible with 1, so the relation: $|A_0|^2+|A_\parallel|^2+|A_\perp|^2 = 1$ is satisfied by the estimated amplitudes.

$B \to VV_j \to V\ell^+\ell^-$

At this point we have the transversity amplitudes and an expression of the $B\to V_jV$ matrix element in terms of them. The next step is to relate this expression to the matrix element of the effective Hamiltonian eq. (7.2.1) in terms of $C_9^{\text{eff},\lambda}$,

$$\begin{aligned}
&\mathcal{M}\left(B\to V\ell^+\ell^-\right)\big|_{C_9} =\\
&\frac{G_F\alpha}{2\sqrt{2}\pi}V_{tb}V_{ts}^*C_9^{\text{eff},\lambda}\left(q^2\right)\Bigg(i\left(-\epsilon_{V,\mu}^*(\lambda)\left(m_B+m_V\right)+q_\mu\left(\epsilon_V^*(\lambda)\cdot q\right)\frac{m_B+m_V}{q^2}\right)A_1\left(q^2\right)\\
&\qquad + i\left(\left(2p-q\right)_\mu - q_\mu\frac{m_B-m_V}{q^2}\right)\left(\epsilon_V^*(\lambda)\cdot q\right)\frac{A_2\left(q^2\right)}{m_B+m_V}\\
&\qquad - iq_\mu\left(\epsilon_V^*(\lambda)\cdot q\right)\frac{2m_V}{q^2}A_0\left(q^2\right) + \epsilon_{\mu\nu\rho\sigma}\epsilon_V^{*,\nu}(\lambda)p^\rho k^\sigma\frac{2V\left(q^2\right)}{m_B+m_V}\Bigg).
\end{aligned} \tag{7.4.26}$$

Next we write the matrix element for the sequential decay via a resonance V_j as

$$\mathcal{M}\left(B\to V(\lambda)V_j\left(\lambda_j\right)\to V(\lambda)\ell^+\ell^-\right) = \sum_{\lambda_j}\mathcal{M}\left(B\to V(\lambda)V_j\left(\lambda_j\right)\right)\mathcal{M}\left(V_j\left(\lambda_j\right)\to\ell^+\ell^-\right), \tag{7.4.27}$$

where $\mathcal{M}\left(B\to V(\lambda)V_j\left(\lambda_j\right)\right)$ is given by writing eq. (7.4.6) in the form

$$\mathcal{M}\left(B\to V(\lambda)V_j\left(\lambda_j\right)\right) = \epsilon_{V,\mu}^*(\lambda)\epsilon_{V_j,\nu}^*(\lambda_j)M^{\mu\nu} \tag{7.4.28}$$

and

$$\mathcal{M}\left(V_j\left(\lambda_j\right)\to\ell^+\ell^-\right) = \epsilon_{V_j,\rho}\left(\lambda_j\right)\frac{2ef_{V_j}}{q^2-m_{V_j}^2-im_{V_j}\Gamma_{V_j}}\bar{\ell}\gamma^\rho\ell. \tag{7.4.29}$$

Details on the charmonium decay constant f_{V_j} can be found in appendix B.4. For evaluating the sum over the polarization λ_j of the vector resonance we use the completeness relation

$$\sum_{\lambda_j}\epsilon_{V_j,\nu}^*\left(\lambda_j\right)\epsilon_{V_j,\rho}\left(\lambda_j\right) = -g_{\nu\rho}+\frac{q_\nu q_\rho}{m_{V_j}^2}, \tag{7.4.30}$$

obtaining

$$\sum_{\lambda_j} \mathcal{M}\left(B \to V V_j\right) \mathcal{M}\left(V_j \to \ell^+\ell^-\right) =$$
$$\frac{2e f_{V_j}}{q^2 - m_{V_j}^2 - i m_{V_j}\Gamma_{V_j}} \left[\frac{A_\parallel}{\sqrt{2}} \left(-\epsilon_v^{*\rho}(\lambda) + \frac{\epsilon_V^*(\lambda)\cdot q}{m_{V_j}^2} q^\rho \right) + \frac{x \epsilon_V^*(\lambda)\cdot q}{x^2-1} \left(\frac{p_V^\rho}{m_V m_{V_j}} - \frac{(p_V\cdot q)\, q^\rho}{m_V m_{V_j}^3} \right) \right.$$
$$+ \frac{A_0}{x^2-1} \left(\epsilon_V^*(\lambda)\cdot q\right) \left(\frac{(p_V\cdot q)\, q^\rho}{m_V m_{V_j}^3} - \frac{p_V^\rho}{m_V m_{V_j}} \right)$$
$$\left. - \frac{i A_\perp}{\sqrt{2\left(x^2-1\right)} m_V m_{V_j}} \epsilon^{\mu\alpha\beta\rho} \epsilon_{V,\mu}^*(\lambda) p_{V,\alpha} q_\beta \right] \bar{\ell}\gamma_\rho \ell. \tag{7.4.31}$$

By equating eq. (7.4.26) and eq. (7.4.31) for $\lambda = (0, \parallel, \perp)$ (details on the polarization vectors in the V_j rest frame can be found in appendix B.3) we can now extract the parameters η_V^λ and δ_V^λ, finding

$$\begin{aligned}
\eta_{V_j}^0 e^{i\delta_{V_j}^0} &= \frac{f_{V_j}}{8\sqrt{2\pi\alpha} G_F V_{tb} V_{ts}^* m_B m_{V_j} \Gamma_{V_j}} A_0 \\
\eta_{V_j}^\parallel e^{i\delta_{V_j}^\parallel} &= \frac{f_{V_j}}{2\sqrt{\pi\alpha} G_F V_{tb} V_{ts}^* (m_B + m_V) m_{V_j} \Gamma_{V_j}} A_\parallel \\
\eta_{V_j}^\perp e^{i\delta_{V_j}^\perp} &= \frac{f_{V_j}(m_B + m_V)}{2\sqrt{\pi\alpha\lambda} G_F V_{tb} V_{ts}^* m_{V_j} \Gamma_{V_j}} A_\perp .
\end{aligned} \tag{7.4.32}$$

The phases in eq. (7.4.32) are composed of three contributions. There are the phases of the transversity amplitudes, given in eq. (7.4.20), the phase of $(V_{ts}^*)^{-1}$, shown in table B.1.1, and an overall phase between the short and long distance amplitudes measured in [17], for which we use the upper right corner of table 3.

7.5 Fit

In this section we perform multiple fits of the Wilson coefficient C_9 using the available experimental data on the differential branching ratios $\mathcal{B}\left(B^+ \to K^+\ell^+\ell^-\right)$ and $\mathcal{B}\left(B^0 \to K^{0*}\ell^+\ell^-\right)$, as well as on the set of angular observables defined in the end of section 7.2.1 in the case of $B^0 \to K^{0*}\ell^+\ell^-$. We use the input parameters reported in table B.1.2.

In the theory predictions we implement C_9^{eff} as defined in eq. (7.3.1) and perform fits to its constant part we called C_9, assuming a different value $C_9^{(i)}$ in each q^2-bin i. If our implementation of the $c\bar{c}$ resonances does a good job at modeling the q^2-dependence of $C_9^{(\lambda),\text{eff}}$ the fit should yield a flat distribution of $C_9^{(i)}$ across all bins.

The best-fit results are calculated by minimizing the χ^2 defined as follows for a generic observable O and N bins:

$$\chi^2\left(\left\{C_9^{(i)}\right\}_{i=1,\ldots,N}\right) = \vec{x}^{\,\mathrm{T}} V^{-1} \vec{x}, \tag{7.5.1}$$

where

$$x_i = \langle O_{\text{measured}} \rangle_i - \langle O_{\text{theory}} \rangle_i , \tag{7.5.2}$$

$\langle O\rangle_i$ is the observable O averaged over the bin i and V is the matrix of theoretical and experimental covariances between the bins:

$$V = V_{\text{theory}} + V_{\text{exp}}. \tag{7.5.3}$$

In principle also V_{theory} depends on C_9, but we neglect the higher-order terms in C_9 by evaluating it at the SM value.

Let us denote by χ^2_{min} the minimum value of the full $\chi^2\left(C_9^{(1)},\ldots,C_9^{(N)}\right)$. We profile the full χ^2 with respect to each coefficient $C_9^{(i)}$, obtaining N one-dimensional profiles $\chi^2_i\left(C_9^{(i)}\right)$. The uncertainty for each coefficient $C_9^{(i)}$ is then extracted from the interval in which

$$\left|\chi^2_i\left(C_9^{(i)}\right) - \chi^2_{\text{min}}\right| \leq 1, \tag{7.5.4}$$

the upper (lower) uncertainty being given by the distance between the best fit point and the upper (lower) end of this interval.

7.5.1 $B \to K$

We implement the differential branching ratio defined in eq. (7.2.30) for the decay $B^+ \to K^+\mu^+\mu^-$. For the form factors we employ the recent HPQCD results [207]. On the experimental side the differential branching ratio has been measured by the LHCb collaboration [7].

In fig. 7.5.1 the theory prediction we find after adding the $c\bar{c}$ resonances is shown. Let us

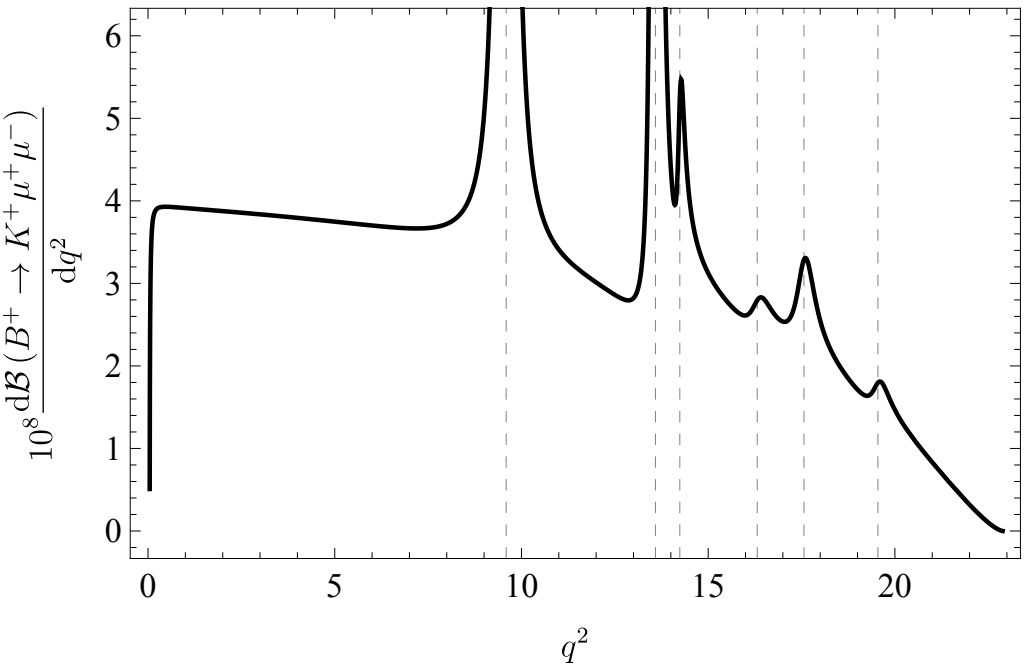

Figure 7.5.1: Theory prediction for the differential $B^+ \to K^+\ell^+\ell^-$ branching ratio including the $c\bar{c}$ resonances. The dashed lines indicate the squared resonance masses.

now turn to the covariance matrix. It is composed of 4 terms:

$$V = V^{\text{FF}}_{\text{theory}} + V^{\eta,\delta}_{\text{theory}} + V^{\text{stat}}_{\text{exp}} + V^{\text{syst}}_{\text{exp}}, \tag{7.5.5}$$

where the theory covariances are split up into a term coming from the uncertainties on the form factors and one from the uncertainties of the resonance parameters and the experimental ones are split into systematic and statistical contributions. The parametric uncertainties of the numerical inputs in table B.1.2 are neglected.

For any observable O given in terms of parameters μ_i with given covariances $\mathrm{cov}(\mu)$ we propagate the theory covariances according to the master formula

$$(V_{\text{theory}})_{ij} = \left\langle \frac{\partial O}{\partial \mu_k} \right\rangle_i \mathrm{cov}(\mu)_{kl} \left\langle \frac{\partial O}{\partial \mu_l} \right\rangle_j . \tag{7.5.6}$$

The form factors are supplied in the form of a series expansion in terms of

$$z = \frac{\sqrt{t_+ - q^2} - \sqrt{t_+ - t_0}}{\sqrt{t_+ - q^2} + \sqrt{t_+ - t_0}}, \tag{7.5.7}$$

where $t_+ = (m_B + m_K)^2$, $t_- = (m_B - m_K)^2$ and $t_0 = t_+ \left(1 - \sqrt{1 - t_-/t_+}\right)$. In order to find $V^{\text{FF}}_{\text{theory}}$ we therefore evaluate the derivatives of the branching ratio with respect to the coefficients in this z-expansion and plug them into eq. (7.5.6) together with the covariance matrix supplied in [207].

For finding the covariances originating in the uncertainties of the resonance parameters η_{V_j} and δ_{V_j} we assume that they are uncorrelated. Then their covariance matrix is diagonal and contains their squared standard deviations. We evaluate the derivatives of the branching ratio with respect to the resonance parameters and use eq. (7.5.6) to find $V^{\eta,\delta}_{\text{theory}}$. In figs. B.5.1 and B.5.2 the theory covariances can be found. As the covariance matrices have 72 rows and columns we show them as matrix plots.

The statistical and systematical uncertainties can be found in [7]. We treat the statistical ones as uncorrelated and assume the systematical ones to be fully correlated, finding the covariances using the relation

$$\left(V^{\text{syst}}_{\text{exp}}\right)_{ij} = \sigma_i \sigma_j, \tag{7.5.8}$$

where σ_i is the squared standard deviation of the value measured in bin i. Finally we have performed fits in 3 different ranges of q^2. First we considered the whole q^2 range from 0.1 GeV^2 to 22 GeV^2. In this range we want to compare different formulations of the charm-loop contributions. To this end performed fits for 3 scenarios:

(i) with C_9^{eff} defined as in eq. (7.2.4)

(ii) with C_9^{eff} defined in eq. (7.3.9)

(iii) with eq. (7.3.9) with $\tilde{Y}(q^2)$ replaced by $Y(q^2)$.

The result of these fits are presented in fig. 7.5.2. As one can see scenario (ii) shows the smallest residual q^2 dependence. This is why in the following we will consider this scenario for a q^2 independent determination of C_9 in the regions below and above the narrow resonances.

The result of a q^2 independent fit in the low-q^2 range from from 1.1 GeV^2 to 8 GeV^2 is shown in fig. 7.5.3. The result in the high-q^2 range from 15 GeV^2 to 22 GeV^2 is shown in fig. 7.5.4.

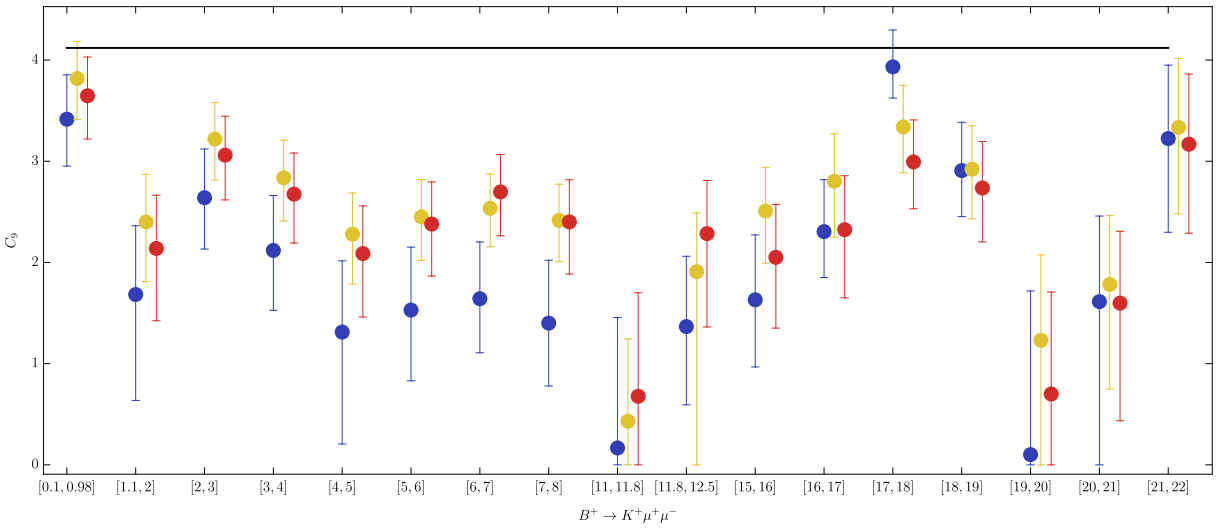

Figure 7.5.2: Results of the fits for $B^+ \to K^+\mu^+\mu^-$ in the whole q^2 range. The blue dots correspond to scenario (i), that is purely perturbative contributions, while the red and yellow dots correspond the the scenarios (ii) and (iii) respectively, which take into account the resonance contributions. The horizontal black line corresponds to the SM value of C_9.

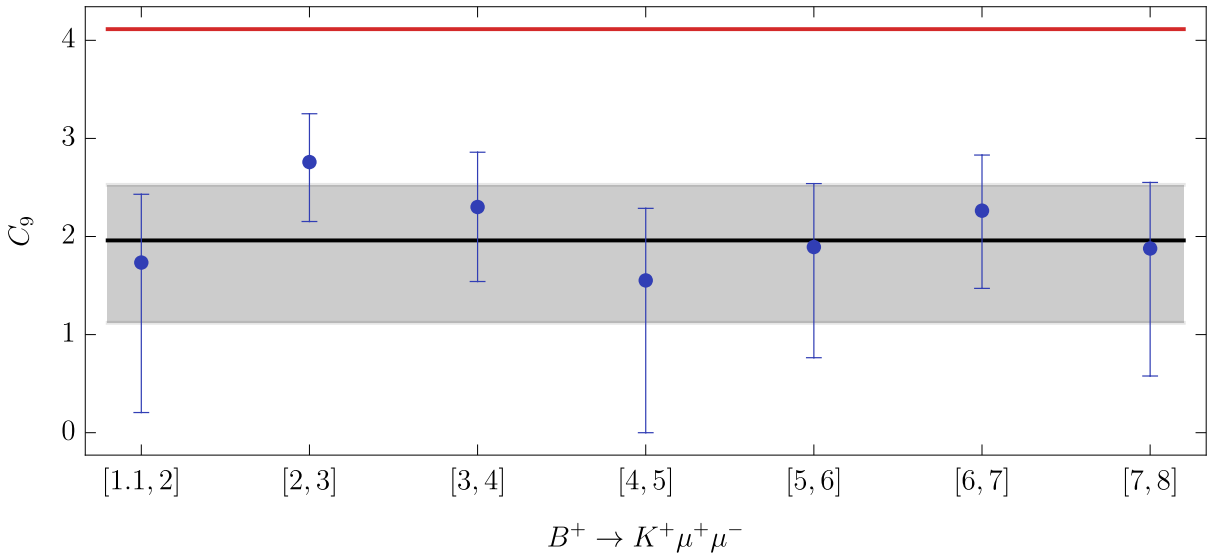

Figure 7.5.3: Results of the fits for $B^+ \to K^+\mu^+\mu^-$ in the low-q^2 range. The black line corresponds to the result of the fit assuming a constant shift in C_9 and the grey band shows its uncertainty. The red line shows the SM value of C_9.

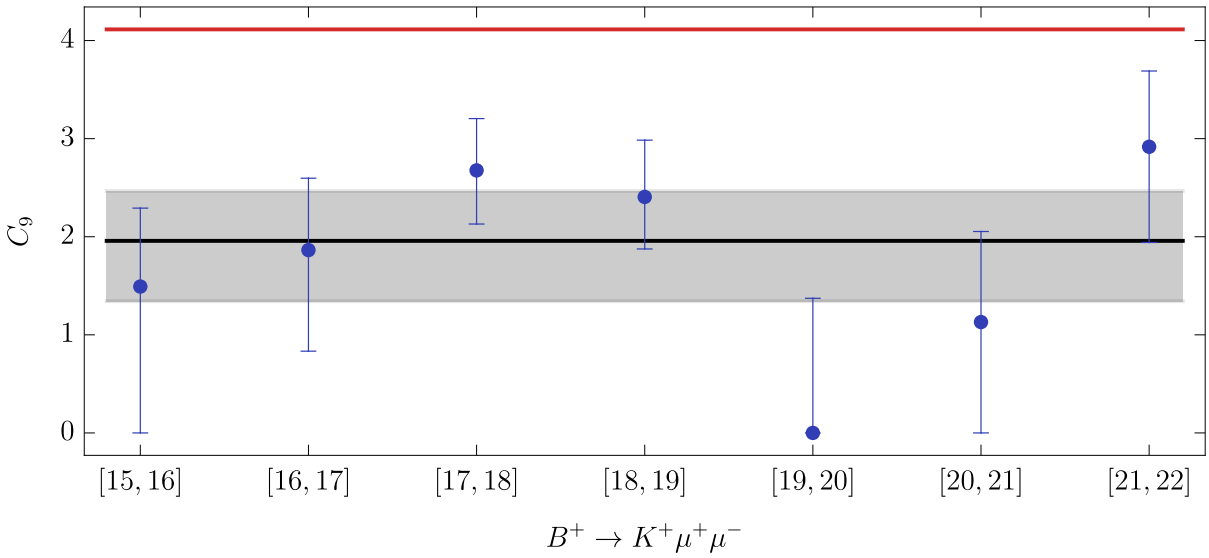

Figure 7.5.4: Results of the fits for $B^+ \to K^+\mu^+\mu^-$ in the high-q^2 range. The black line corresponds to the result of the fit assuming a constant shift in C_9 and the grey band shows its uncertainty. The red line shows the SM value of C_9.

7.5.2 $B \to K^*$

For the decay $B^0 \to K^{0*}\mu^+\mu^-$ we implement the branching ratio defined in eq. (7.2.22) and additionally the set of angular observables defined in the end of section 7.2.1, which are defined in eq. (7.2.23). We use the form factors computed in [69]. The differential branching ratio has been measured in [16] and the angular observables were measured in [21].

The theory prediction for the differential branching ratio including the $c\bar{c}$ resonances can be seen in fig. 7.5.5. Due to lack of data on the decays $B \to K^* V_j$ with V_j above the $\psi(2s)$ resonance only the first two $c\bar{c}$ resonances are implemented in this case. The treatment of the

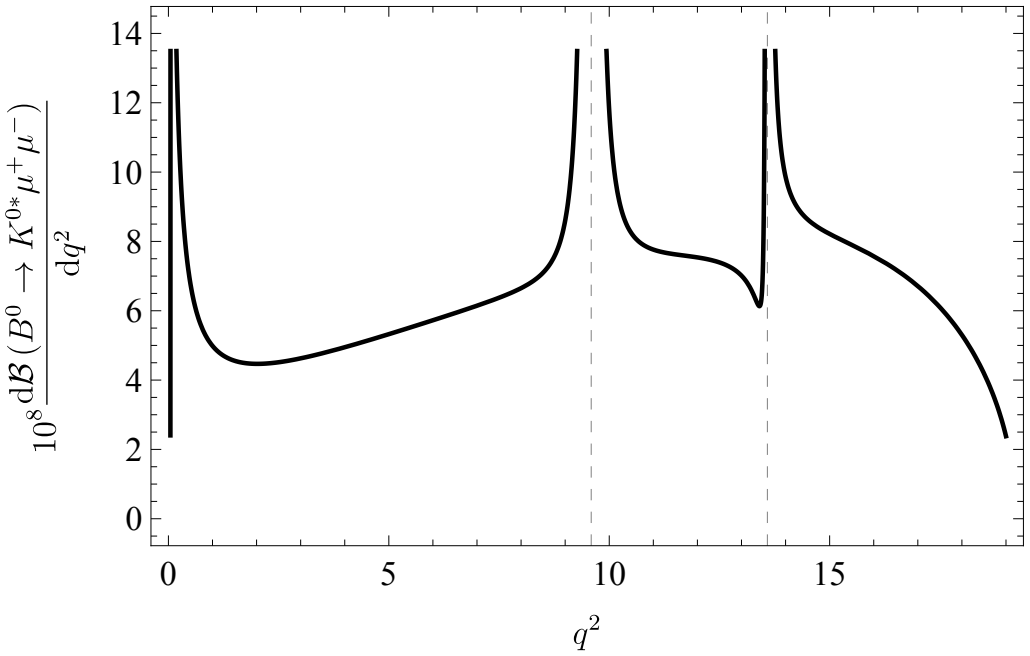

Figure 7.5.5: Theory prediction for the differential $B^0 \to K^{0*}\ell^+\ell^-$ branching ratio including the $c\bar{c}$ resonances. The dashed lines indicate the squared resonance masses.

theory covariances is exactly as described in the previous section. As we consider 9 observables here, which are all measured in 8 bins of q^2, the full covariance matrix is a 72×72 matrix. Again we treat the statistical uncertainties as uncorrelated. For the systematic uncertainties we assume

$$\text{corr}\left(\langle O_k \rangle_i, \langle O_l \rangle_j\right) = \delta_{kl}, \tag{7.5.9}$$

where $O_i \in \{\mathcal{B}, F_L, S_3, S_4, S_5, A_{\text{FB}}, S_7, S_8, S_9\}$ and $\langle\cdot\rangle_i$ denotes the average over the q^2-bin i. In other words we assume that the systematic uncertainties of a given observable are fully correlated between different bins but that they are independent from the uncertainties of different variables. So far the covariance matrix would be block diagonal. This is not case because the angular observables extracted by LHCb are correlated within a given bin, which induces nonzero off-block-diagonal entries in V. The full covariance matrix is too lengthy to write down explicitly but in fig. B.5.6 a plot of the size of its elements can be found.

As we saw in eq. (7.3.9) the long distance contributions from $c\bar{c}$ resonances depend on λ, the polarization of the K^*. Now we write the effective C_9 in the theory expressions as

$$C_9^{\lambda,\text{eff}}\left(q^2\right) = C_9^\lambda + \tilde{Y}\left(q^2\right) + Y_{c\bar{c}}^\lambda\left(q^2\right) \tag{7.5.10}$$

and extract C_9^λ for each polarization λ. This way we can see if the effective C_9 receives helicity dependent contributions beyond the ones from the resonances.

Again the fit is performed in ranges of q^2, the full one $[0.1, 19]$ GeV^2, the low-q^2 range $[1.1, 8]$ GeV^2 and the high-q^2 range $[12.5, 19]$ GeV^2 separately for each helicity. The results are shown in figs. 7.5.6 to 7.5.8.

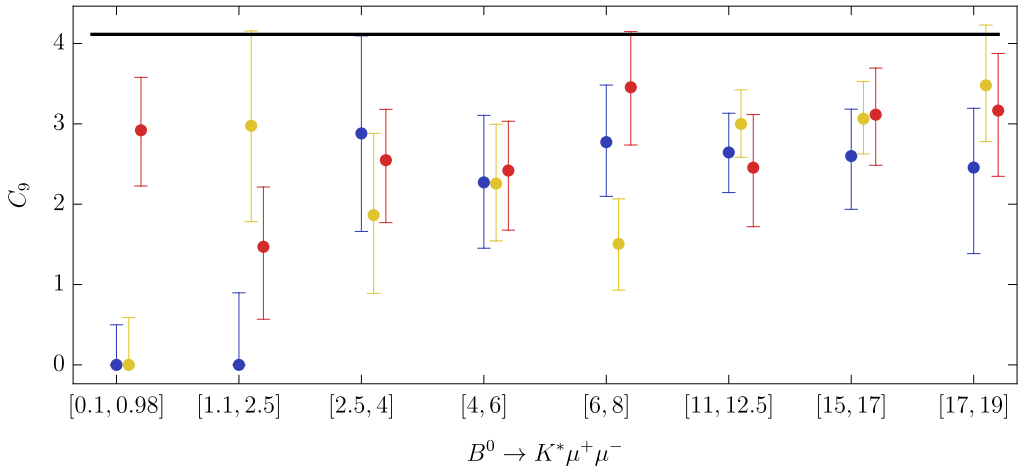

Figure 7.5.6: Fit results for $B^0 \to K^{0*}\mu^+\mu^-$ in the full q^2 range. The blue dots correspond to $C_9^{\parallel}$, the yellow dots correspond to $C_9^{\perp}$ and the red dots correspond to C_9^0, respectively. The black horizontal line indicates the SM value of C_9.

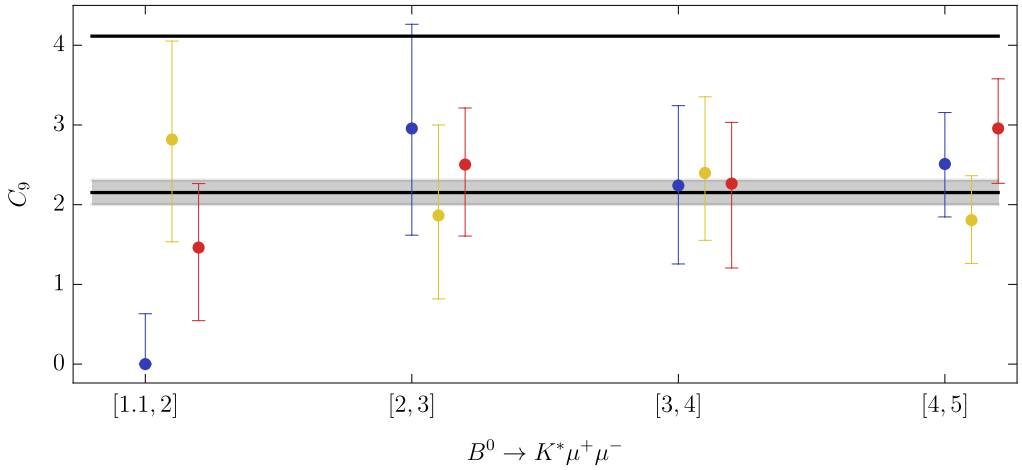

Figure 7.5.7: Fit results for $B^0 \to K^{0*}\mu^+\mu^-$ in the low-q^2 range. The blue dots correspond to $C_9^{\parallel}$, the yellow dots correspond to $C_9^{\perp}$ and the red dots correspond to C_9^0, respectively. The black horizontal line indicates the SM value of C_9.

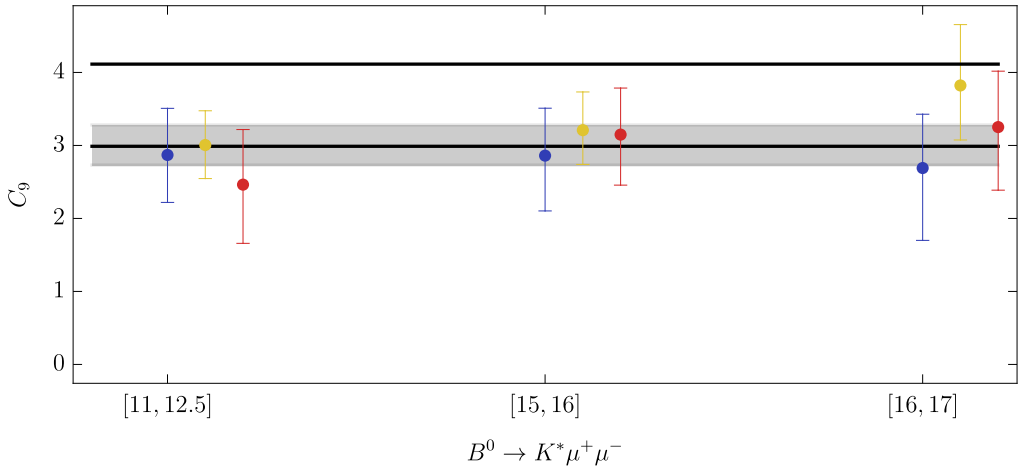

Figure 7.5.8: Fit results for $B^0 \to K^{0*}\mu^+\mu^-$ in the high-q^2 range. The blue dots correspond to $C_9^{\parallel}$, the yellow dots correspond to $C_9^{\perp}$ and the red dots correspond to C_9^0, respectively. The black horizontal line indicates the SM value of C_9.

7.6 Discussion

In order to assess how compatible the results of a given fit are with their average value we consider the squared deviations from their weighted average,

$$\chi^2 = \sum_i^N \frac{\overline{C}_9 - C_9^{(i)}}{\left(\delta C_9^{(i)}\right)^2}, \tag{7.6.1}$$

where N denotes the number of bins in a given fit, $C_9^{(i)} \pm \delta C_9^{(i)}$ denotes the value of C_9 in the i-th bin and

$$\overline{C}_9 \pm \delta\overline{C}_9 = \frac{\sum_i^N \frac{1}{\left(\delta C_9^{(i)}\right)^2} C_9^{(i)}}{\sum_i^N \frac{1}{\left(\delta C_9^{(i)}\right)^2}} \pm \left(\sum_i^N \frac{1}{\left(\delta C_9^{(i)}\right)^2}\right)^{-\frac{1}{2}} \tag{7.6.2}$$

is their weighted average. For the fits performed in fig. 7.5.2 we find for the different scenarios

(i) $\chi^2/(16) = 2.51$ and $\overline{C}_9 = 2.51 \pm 0.15$

(ii) $\chi^2/(16) = 1.15$ and $\overline{C}_9 = 2.63 \pm 0.14$

(iii) $\chi^2/(16) = 1.52$ and $\overline{C}_9 = 2.75 \pm 0.13$

where we scaled the uncertainties by a factor of $\sqrt{\chi^2/(N-1)}$. As anticipated the q^2-dependence of the effective C_9 is best modeled in scenario (ii). In the following we study this scenario more closely.

The results for scenario (ii) in the low and high-q^2 regions for both $B \to K$ and $B \to K^*$ (separated into different helicities) are reported in table 7.6.1. As can be seen in all cases we obtain a good χ^2, the only exception being $C_9^{\parallel}(B \to K^*)$ at low q^2. The eight independent determinations of C_9 thus obtained are also shown in fig. 7.6.1. Here the error of $C_9^{\parallel}(B \to K^*)$ is rescaled according to the PDG procedure.

We stress that these should be treated as independent determinations of C_9 coming from different kinematical regions and different hadronic amplitudes. The overall consistency of these eight independent determinations, and their difference from the SM value provide a significant indication of short-distance contributions to C_9 that is not accounted for in the present SM analysis.

		low q^2		high q^2	
X	λ	$\chi^2/(n-1)$	C_9	$\chi^2/(n-1)$	C_9
K		0.2	2.31 ± 0.35	0.87	2.23 ± 0.31
K^*	$\parallel$	3.2	1.5 ± 0.4	0.01	2.8 ± 0.4
K^*	$\perp$	0.24	2.0 ± 0.4	0.36	3.20 ± 0.32
K^*	0	0.58	2.4 ± 0.4	0.28	3.0 ± 0.4

Table 7.6.1: Summary of the averaged fit results for the decays $B \to X\mu^+\mu^-$.

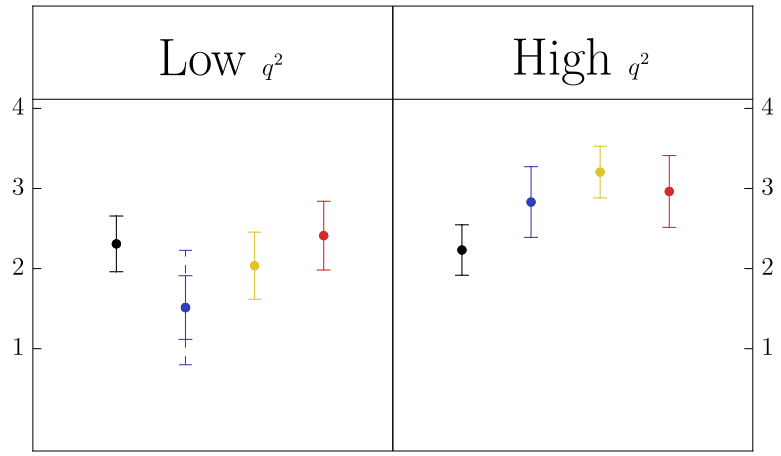

Figure 7.6.1: Averaged fit results. The black dots correspond to $C_9(B \to K)$ and the blue, yellow and red dots correspond to $C_9^\lambda(B \to K^*)$ in the ordering $(\parallel, \perp, 0)$. The dashed error band shows the uncertainty scaled by a factor of $\sqrt{\chi^2/(N-1)}$ in the case where $\chi^2/(N-1) > 1$ (see table 7.6.1). The black horizontal line indicates the SM value of C_9.

7.7 Conclusion

We have studied the long distance hadronic contributions to the effective Wilson coefficient C_9 in $B^+ \to K^+\mu^+\mu^-$ and $B^0 \to K^{0*}$ decays. The effects of $c\bar{c}$ resonances in the contributions of the operators $\mathcal{Q}_{1,\dots,6}$ were estimated via dispersion relations and using data from non-leptonic $B \to J/\psi\phi$, $B \to \psi(2s)\phi$ and $B \to J/\psi K^*$ decays. Additionally the polarization amplitudes for $B \to \psi(2s)K^*$ were estimated from $\mathrm{SU(3)_F}$ relations.

We implemented an effective Wilson coefficient C_9^{eff} including effects from the $c\bar{c}$ resonances $J/\psi, \psi(2s), \psi(3770), \psi(4040), \psi(4160), \psi(4450)$ for the $B \to K$ decay and including the resonances J/ψ and $\psi(2s)$ for the $B \to K^*$ decay.

Using this effective C_9 we have computed the differential branching ratios for both decay modes and a set of angular observables for $B \to K^*$, which were then employed in different fits to experimental data.

In the fits we extracted the q^2 dependence of C_9^{eff} in low and high regions of the squared lepton pair mass. In the low-q^2 region our results indicate that the resonances model its q^2-dependence well and we find consistent results across both decay modes. In the high-q^2 region we find consistent results within a given decay mode. The values extracted from $B \to K^*$ are a bit higher than the ones extracted from $B \to K$, however. In part this might be due to the missing contributions of the resonances above $\psi(2s)$ in the theory predictions for the $B \to K^*$ observables.

Overall the consistency of the eight independent determinations of C_9 shown in fig. 7.6.1 provide a significant indication for a missing short-distance contribution in the present description of $b \to sll$ amplitudes.

Chapter 8

Conclusions

The decays of B mesons exhibit several intriguing discrepancies between SM expectation and measured data, but also between different determinations of the same constant of nature.

In this thesis we presented 3 studies. The first two were concerned with inclusive $b \to c\ell\nu$ decays in which the hadronic part of the final state is not resolved and the third one was concerned with hadronic long-distance contributions in exclusive $b \to s\mu\mu$ decays.

The studies of inclusive B decays were motivated by a long standing 3σ tension between the inclusive and the exclusive determination of the CKM matrix element V_{cb}. This discrepancy calls for a careful check of the established framework based on the heavy quark expansion.

In chapter 5 we performed such a check by using lattice QCD simulations as a virtual laboratory. Inclusive observables were computed by two lattice collaborations at an unphysically low b quark mass and systematically compared to an OPE computation for the first time. As this is an exploratory study there are multiple issues to be addressed in future work. First of all the continuum and infinite-volume limits were not performed in the lattice computations. In order to take these limits the calculations have to be performed at different values of the lattice spacing and different physical volumes. This task goes beyond the exploratory nature of this study. Secondly the calculation should be performed at the physical value of the b quark mass. At a higher b quark mass the OPE converges more quickly, reducing the associated uncertainties and additionally a direct comparison of lattice results to experimental data becomes possible at the physical m_b. Despite these issues in general we found a good agreement between the lattice and OPE results and showed the possibility of determining OPE matrix matrix elements from lattice data.

In light of a recent determination of V_{cb} from q^2 moments we also studied the impact of order q^2/m_W^2 effects on inclusive observables. These effects were expected to be small, as $m_b^2/m_W^2 \sim 0.006$. In principle they could however receive enhancements in the phase space integration, especially if the phase space is constrained by a lower cut. We explicitly computed the q^2/m_W^2 corrections in chapter 6 and studied their dependence on lower cuts, finding that they are smaller than the current experimental uncertainties. Compared to the current theoretical precision, which goes up to three loops, they can be sizeable however.

The last work presented in this thesis dealt with the discrepancies between the SM predictions for the branching ratios of $B \to K^{(*)}\mu\mu$, the angular observables in $B \to K^*\mu\mu$ and their respective measured values. We implemented these observables, employing a dispersive formulation of the $c\bar{c}$ resonances, in chapter 7. After determining the resonance parameters from measurements of non-leptonic B decays we were able to determine the value of the Wilson coefficient C_9 from the decay channels $B \to K$ and $B \to K^*$, keeping the different helicities

separate, in two regions of q^2. The consistency of the eight independent determinations of C_9 we obtained in this way is a clear indication of a missing short-distance contribution in the present SM analysis of $b \to s\ell\ell$ decays.

In summary we have seen that the decays of B mesons remain a fascinating and active area of fundamental research. On one hand, the ongoing studies of inclusive B decays on the lattice might bring us closer to a resolution of the V_{cb} puzzle soon. This would drastically improve many NP physics searches, in which the leading uncertainty is V_{cb}. On the other hand, the presence of unknown short-distance effects in $b \to s\ell\ell$ decays points towards physics beyond the SM in B decays.

List of Scientific Publications

- P. Gambino, S. Hashimoto, S. Mächler, M. Panero, F. Sanfilippo, S. Simula, A. Smecca and N. Tantalo, "Lattice QCD study of inclusive semileptonic decays of heavy mesons," JHEP **07** (2022), 083 doi:10.1007/JHEP07(2022)083 [arXiv:2203.11762 [hep-lat]].
- P. Gambino, S. Hashimoto, S. Mächler, M. Panero, F. Sanfilippo, S. Simula, A. Smecca and N. Tantalo, "Inclusive semileptonic B-decays from lattice QCD," [arXiv:2211.11833 [hep-lat]].
- P. Gambino, S. Hashimoto, S. Mächler, M. Panero, F. Sanfilippo, S. Simula, A. Smecca and N. Tantalo, "Towards the computation of inclusive decay rates using lattice QCD," [arXiv:2209.15494 [hep-lat]].
- S. Mächler, P. Gambino and S. Hashimoto, "Comparison of lattice QCD results for inclusive semi-leptonic decays B mesons with the OPE," PoS **LATTICE2021** (2022), 512 doi:10.22323/1.396.0512 [arXiv:2111.02833 [hep-ph]].
- A. Smecca, P. Gambino, S. Hashimoto, S. Mächler, M. Panero, F. Sanfilippo, S. Simula and N. Tantalo, "Inclusive semileptonic B-decays from lattice QCD," PoS **LATTICE2022** (2023), 423 doi:10.22323/1.430.0423 [arXiv:2211.11833 [hep-lat]].
- D. Bigi and S. Mächler, "Finite W mass corrections to inclusive B decays," [arXiv:2305.04973 [hep-ph]], submitted
- M. Bordone, G. Isidori, S. Mächler, A. Tinari, "Long-distance contributions in $b \to s\ell\ell$" in preparation
- J. Aebischer, D. A. Faroughy, J. F. Kamenik, S. Mächler, "Machine learning and flavour fits" in preparation

Appendix A

Inclusive decays of B Mesons

A.1 Triple Differential Decay Rate for $B \to X_c \ell \overline{\nu}_\ell$

The general expression for the differential decay rate of a particle $\mathcal{A}$ to final states f is given by [209]

$$\mathrm{d}\Gamma = \frac{1}{2m_{\mathcal{A}}} \left(\prod_f \frac{\mathrm{d}^2}{(2\pi)^3} \frac{1}{2E_f} \right) |\mathcal{M}\left(m_{\mathcal{A}} \to \{p_f\}\right)|^2 (2\pi)^4 \, \delta^4 \left(p_{\mathcal{A}} - \sum p_f \right). \tag{A.1.1}$$

We consider semileptonic $\overline{B}$ decays with the effective Hamiltonian

$$\begin{aligned} \mathcal{L}_{\mathrm{int}} = -\mathcal{H}_{\mathrm{int}} &= -\frac{G_{\mathrm{F}}}{\sqrt{2}} V_{\mathrm{cb}} \left(\bar{c} \gamma_\mu \left(1 - \gamma_5\right) b \right) \left(\bar{\ell} \gamma^\mu \left(1 - \gamma_5\right) \nu_\ell \right) \\ &\equiv -\frac{G_{\mathrm{F}}}{\sqrt{2}} V_{\mathrm{cb}} J_{q,\mu} J_\ell^\mu . \end{aligned} \tag{A.1.2}$$

Then the matrix element for the inclusive process is given by

$$\mathcal{M}\left(\overline{B} \to X_c \ell \overline{\nu}_\ell\right) = \left\langle X_c \ell \overline{\nu}_\ell \left| \mathcal{H}_{\mathrm{int}} \right| \overline{B} \right\rangle = \frac{G_{\mathrm{F}}}{\sqrt{2}} V_{\mathrm{cb}} \left\langle X_c \ell \overline{\nu}_\ell \left| J_{q,\mu}(0) J_\ell^\mu(0) \right| \overline{B} \right\rangle . \tag{A.1.3}$$

The interaction is local because we integrated out the W–boson. Then we can write the differential decay rate as

$$\begin{aligned} \mathrm{d}\Gamma = \sum_{X_c} \sum_{\substack{\text{lepton} \\ \text{spins}}} \frac{1}{2M_B} \left(\frac{\mathrm{d}^3 p_\ell}{(2\pi)^3} \frac{1}{2E_\ell} \right) \left(\frac{\mathrm{d}^3 p_{\overline{\nu}}}{(2\pi)^3} \frac{1}{2E_{\overline{\nu}}} \right) \left| \mathcal{M}\left(\overline{B} \to X_c \ell \overline{\nu}_\ell\right) \right|^2 \\ \times (2\pi)^4 \, \delta^4 \left(p_B - \left(p_\ell + p_{\overline{\nu}} + p_X \right) \right) \end{aligned} \tag{A.1.4}$$

where

$$\begin{aligned} \left| \mathcal{M}\left(\overline{B} \to X_c \ell \overline{\nu}_\ell\right) \right|^2 &= \frac{G_{\mathrm{F}}^2}{2} |V_{\mathrm{cb}}|^2 \left\langle X_c \ell \overline{\nu}_\ell \left| J_{q,\mu}(0) J_\ell^\mu(0) \right| \overline{B} \right\rangle \\ &= \frac{G_{\mathrm{F}}^2}{2} |V_{\mathrm{cb}}|^2 \left\langle \overline{B} \left| J_{q,\mu}^\dagger \right| X_c \right\rangle \left\langle X_c \left| J_{q,\nu} \right| \overline{B} \right\rangle \left\langle 0 \left| J_\ell^{\mu\dagger} \right| \ell \overline{\nu}_\ell \right\rangle \left\langle \ell \overline{\nu}_\ell \left| J_\ell^\nu \right| 0 \right\rangle . \end{aligned} \tag{A.1.5}$$

As the hadronic and leptonic parts of the amplitude do not interfere they can be separated from each other and computed individually. To this end we define a leptonic tensor

$$L^{\mu\nu} = \frac{1}{8} \sum_{\substack{\text{lepton} \\ \text{spins}}} \left\langle 0 \left| J_\ell^{\mu\dagger} \right| \ell\overline{\nu}_\ell \right\rangle \left\langle \ell\overline{\nu}_\ell \left| J_\ell^\nu \right| 0 \right\rangle \tag{A.1.6}$$

describing the leptonic part of the interaction and a hadronic tensor

$$W_{\mu\nu} = \frac{1}{2M_B} \sum_{X_c} (2\pi)^3 \delta\left(p_B - (p_\ell + p_{\overline{\nu}} + p_X)\right) \left\langle \overline{B} \left| J_{q,\nu}^\dagger \right| X_c \right\rangle \left\langle X_c \left| J_{q,\mu} \right| \overline{B} \right\rangle \tag{A.1.7}$$

containing the non–perturbative hadronic dynamics. In terms of these objects we can write the differential decay rate as

$$\mathrm{d}\Gamma = 8\pi G_{\mathrm{F}}^2 \left|V_{\mathrm{cb}}\right|^2 \left(\frac{\mathrm{d}^3 p_\ell}{(2\pi)^3} \frac{1}{2E_\ell}\right) \left(\frac{\mathrm{d}^2 p_{\overline{\nu}}}{(2\pi)^3} \frac{1}{2E_{\overline{\nu}}}\right) W_{\mu\nu} L^{\mu\nu}. \tag{A.1.8}$$

For massless leptons the leptonic tensor evaluates to

$$L^{\mu\nu} = p_\ell^\mu p_{\overline{\nu}}^\nu + p_\ell^\nu p_{\overline{\nu}}^\mu - g^{\mu\nu} p_\ell \cdot p_{\overline{\nu}} + i\epsilon^{\mu\alpha\nu\beta} p_{\ell,\alpha} p_{\overline{\nu},\beta} \tag{A.1.9}$$

with the convention $\epsilon^{0123} = -\epsilon_{0123} = 1$. The hadronic tensor cannot be copmuted from first principles. It is computed in the context of the heavy quark expansion (HQE) using the heavy quark effective theory (HQET). By employing the optical theorem the hadronic tensor is connected to the forward scattering amplitude

$$T_{\mu\nu} = -\frac{i}{2M_B} \int \mathrm{d}^4 x e^{iqx} \left\langle \overline{B} \left| \mathcal{T}\left[J_{q,\mu}(x), J_{q,\nu}(0)\right] \right| \overline{B} \right\rangle \tag{A.1.10}$$

as

$$-\frac{1}{\pi} \mathrm{Im} T_{\mu\nu} = W_{\mu\nu}. \tag{A.1.11}$$

Let us now perform the phase space integration for the triple differential rate. The triple differential rate is obtained by differentiating the total decay rate

$$\Gamma = 8\pi G_{\mathrm{F}}^2 \left|V_{cb}\right|^2 \int \left(\frac{\mathrm{d}^3 p_\ell}{(2\pi)^3} \frac{1}{2E_\ell}\right) \left(\frac{\mathrm{d}^3 p_{\overline{\nu}}}{(2\pi)^3} \frac{1}{2E_{\overline{\nu}}}\right) W_{\mu\nu} L^{\mu\nu} \tag{A.1.12}$$

and given by

$$\begin{aligned}
&\frac{\mathrm{d}\Gamma}{\mathrm{d}q^2 \mathrm{d}E_\ell \mathrm{d}E_{\overline{\nu}}} \\
&= \left|\tilde{\mathcal{M}}\right| \int \frac{\mathrm{d}^3 p_\ell}{(2\pi)^3} \frac{1}{2E_\ell} \int \frac{\mathrm{d}^3 p_{\overline{\nu}}}{(2\pi)^3} \frac{1}{2E_{\overline{\nu}}} \delta\left(E_\ell - p_\ell^0\right) \delta\left(E_{\overline{\nu}} - p_{\overline{\nu}}^0\right) \delta\left(q^2 - (p_\ell + p_{\overline{\nu}})^2\right) \\
&= \left|\tilde{\mathcal{M}}\right| \int \frac{\mathrm{d}^3 p_\ell}{(2\pi)^3} \int \frac{\mathrm{d}^3 p_{\overline{\nu}}}{(2\pi)^3} \frac{1}{4E_\ell E_{\overline{\nu}}} \delta\left(E_\ell - p_\ell^0\right) \delta\left(E_{\overline{\nu}} - p_{\overline{\nu}}^0\right) \delta\left(q^2 - (p_\ell + p_{\overline{\nu}})^2\right)
\end{aligned} \tag{A.1.13}$$

As the integrand is symmetric we change to spherical coordinates $\mathrm{d}^2 p_{\ell,\overline{\nu}} = \left|\vec{p}_{\ell,\overline{\nu}}\right|^2 \mathrm{d}\left|\vec{p}_{\ell,\overline{\nu}}\right| \mathrm{d}\cos\theta_{\ell,\overline{\nu}} d\phi_{\ell,\overline{\nu}}$ and choose the three momentum $\vec{p}_\ell$ to be aligned with the z–direction. Then

$$\int \mathrm{d}\cos\theta_{\overline{\nu}} \mathrm{d}\phi_{\overline{\nu}} \mathrm{d}\phi_\ell = 2 \cdot 2\pi \cdot 2\pi = 8\pi^2. \tag{A.1.14}$$

For the phase space of the triple differential rate above this yields

$$\begin{aligned}
\mathrm{d}\varphi &= \int \frac{\mathrm{d}^3 p_\ell}{(2\pi)^3} \int \frac{\mathrm{d}^3 p_{\overline{\nu}}}{(2\pi)^3} \frac{1}{4E_\ell E_{\overline{\nu}}} \delta\left(E_\ell - |\vec{p}_\ell|\right) \delta\left(E_{\overline{\nu}} - |\vec{p}_{\overline{\nu}}|\right) \delta\left(q^2 - (p_\ell + p_{\overline{\nu}})^2\right) \\
&= \int_{-\infty}^{\infty} \Theta\left(|p_\ell|\right) |\vec{p}_\ell|^2 \,\mathrm{d}\,|\vec{p}_\ell| \int_{-\infty}^{\infty} \Theta\left(|p_{\overline{\nu}}|\right) |\vec{p}_{\overline{\nu}}|^2 \,\mathrm{d}\,|\vec{p}_{\overline{\nu}}| \int_{-1}^{1} \mathrm{d}\cos\theta \frac{8\pi^2}{4(2\pi)^6 E_\ell E_{\overline{\nu}}} \\
&\qquad \times \delta\left(E_\ell - |\vec{p}_\ell|\right) \delta\left(E_{\overline{\nu}} - |\vec{p}_{\overline{\nu}}|\right) \delta\left(q^2 - 2E_\ell E_{\overline{\nu}} + 2\,|\vec{p}_\ell|\,|\vec{p}_{\overline{\nu}}| \cos\theta\right) \\
&= \frac{1}{4(2\pi)^4} \Theta\left(E_\ell\right) \Theta\left(E_{\overline{\nu}}\right) \int_{-1}^{1} \mathrm{d}\cos\theta \delta\left(\cos\theta - \left(1 - \frac{q^2}{2E_\ell E_{\overline{\nu}}}\right)\right) \\
&= \frac{1}{4(2\pi)^4} \Theta\left(E_\ell\right) \Theta\left(E_{\overline{\nu}}\right) \int_{-\infty}^{\infty} \mathrm{d}\cos\theta \Theta\left(\cos\theta + 1\right) \Theta\left(1 - \cos\theta\right) \delta\left(\cos\theta - \left(1 - \frac{q^2}{2E_\ell E_{\overline{\nu}}}\right)\right) \\
&= \frac{1}{4(2\pi)^4} \Theta\left(E_\ell\right) \Theta\left(E_{\overline{\nu}}\right) \Theta\left(2 - \frac{q^2}{2E_\ell E_{\overline{\nu}}}\right) \Theta\left(\frac{q^2}{2E_\ell E_{\overline{\nu}}}\right) \\
&= \frac{1}{4(2\pi)^4} \Theta\left(4E_\ell E_{\overline{\nu}} - q^2\right) \Theta\left(q^2\right) \Theta\left(E_\ell\right) \Theta\left(E_{\overline{\nu}}\right). \qquad \text{(A.1.15)}
\end{aligned}$$

By plugging this result into the triple differential rate we obtain

$$\begin{aligned}
\frac{\mathrm{d}^3\Gamma}{\mathrm{d}q^2 \mathrm{d}E_{\overline{\nu}} \mathrm{d}E_\ell} &= \frac{1}{4(2\pi)^4} \left|\tilde{\mathcal{M}}\right|^2 \Theta\left(4E_\ell E_{\overline{\nu}} - q^2\right) \Theta\left(q^2\right) \Theta\left(E_\ell\right) \Theta\left(E_{\overline{\nu}}\right) \\
&= \frac{8\pi G_{\mathrm{F}}^2 \left|V_{\mathrm{cb}}\right|^2}{4(2\pi)^4} W_{\mu\nu} L^{\mu\nu} \Theta\left(4E_\ell E_{\overline{\nu}} - q^2\right) \Theta\left(q^2\right) \Theta\left(E_\ell\right) \Theta\left(E_{\overline{\nu}}\right) \qquad \text{(A.1.16)}
\end{aligned}$$

which becomes

$$\frac{\mathrm{d}^3\Gamma}{\mathrm{d}q^2 \mathrm{d}q^0 \mathrm{d}E_\ell} = \frac{G_{\mathrm{F}}^2 \left|V_{\mathrm{cb}}\right|^2}{8\pi^3} W_{\mu\nu} L^{\mu\nu} \Theta\left(4E_\ell \left(q_0 - E_\ell\right) - q^2\right) \Theta\left(q^2\right) \Theta\left(E_\ell\right) \Theta\left(q_0 - E_\ell\right) \qquad \text{(A.1.17)}$$

after changing variables from $E_{\overline{\nu}}$ to q^0.

A.2 Computation of the leptonic tensor

We use the following identities

$$\begin{aligned}
\overline{u}(p) &= u^\dagger(p)\gamma_0 \\
\overline{u}^\dagger(p) &= \gamma_0 u(p) \\
\sum_s u^s(p)\overline{u}^s(p) &= \not{p} + m \\
\sum_s v^s(p)\overline{v}^s(p) &= \not{p} - m \\
(\gamma^\mu)^\dagger &= \gamma^0 \gamma^\mu \gamma^0 \\
\gamma_5^\dagger &= \gamma_5 \\
\gamma_5^2 &= \mathbb{1} \\
\gamma_0^2 &= \mathbb{1}
\end{aligned}$$

$$\begin{aligned}\{\gamma_5, \gamma_\mu\} &= 0\\ \sigma^{\mu\nu} &= \frac{i}{2}[\gamma^\mu, \gamma^\nu]\\ \sigma^\dagger_{\mu\nu} &= \gamma_0\sigma_{\mu\nu}\gamma_0\\ \epsilon^{0123} &= +1\end{aligned} \tag{A.2.1}$$

First we evaluate the spin sums and obtain

$$L_{\Gamma\Gamma'} = \mathrm{Tr}\left(\left(\not{p}_\ell + m_\ell\right)(a_\Gamma\Gamma + b_\Gamma\Gamma\gamma_5)\not{p}_\nu\left(a^*_{\Gamma'}\Gamma' - b^*_{\Gamma'}\gamma_5\Gamma'\right)\right). \tag{A.2.2}$$

Then we compute this quantity for the cases $\Gamma^{(\prime)} \in \{\mathbb{1}, \gamma^\mu, \sigma^{\mu\nu}\}$.

1. $\Gamma = \Gamma' = \mathbb{1}$

$$\begin{aligned}L_{11} &= \mathrm{Tr}\left(\left(\not{p}_\ell + m_\ell\right)(a_\mathrm{S} + b_\mathrm{P}\gamma_5)\not{p}_\nu\left(a^*_\mathrm{S} + b^*_\mathrm{P}\gamma_5\right)\right)\\ &= 2\left(|a_s|^2 + |b_s|^2\right)p_\ell\cdot p_\nu\end{aligned} \tag{A.2.3}$$

2. $\Gamma = \gamma^\mu,\ \Gamma' = \gamma^\rho$

$$\begin{aligned}L_{\gamma^\mu\gamma^\rho} &= \mathrm{Tr}\left(\left(\not{p}_\ell + m_\ell\right)(a_\mathrm{V}\gamma^\mu + b_\mathrm{A}\gamma^\mu\gamma_5)\not{p}_\nu\left(a^*_\mathrm{V}\gamma^\rho + b^*_\mathrm{A}\gamma_5\gamma^\rho\right)\right)\\ &= 2\left(|a_\mathrm{V}|^2 + |b_\mathrm{A}|^2\right)\left(p^\mu_\ell p^\rho_\nu + p^\rho_\ell p^\mu_\nu - p_\ell\cdot p_\nu g^{\mu\rho}\right) + 4i\mathrm{Re}\left(a_\mathrm{V}b^*_\mathrm{A}\right)\epsilon^{\alpha\beta\mu\rho}p_{\ell,\alpha}p_{\nu,\beta}\end{aligned} \tag{A.2.4}$$

3. $\Gamma = \sigma^{\kappa\lambda},\ \Gamma' = \sigma^{\rho\tau}$

$$\begin{aligned}L_{\sigma^{\kappa\lambda}\sigma^{\rho\tau}} &= \mathrm{Tr}\left(\left(\not{p}_\ell + m_\ell\right)\left(a_\mathrm{T}\sigma^{\kappa\lambda} + b_{\mathrm{T}_5}\sigma^{\kappa\lambda}\gamma_5\right)\not{p}_\nu\left(a^*_\mathrm{T}\sigma^{\rho\tau} - b^*_{\mathrm{T}_5}\gamma_5\sigma\rho\tau\right)\right)\\ &= \left(|a_T|^2 + |b_{T_5}|^2\right)\mathrm{Tr}\left(\not{p}_\ell\sigma^{\kappa\lambda}\not{p}_\nu\sigma^{\rho\tau}\right) + 2\mathrm{Re}\left(a_T b^*_{T_5}\right)\mathrm{Tr}\left(\not{p}_\ell\sigma^{\kappa\lambda}\gamma^5\not{p}_\nu\sigma^{\rho\tau}\right)\end{aligned} \tag{A.2.5}$$

Using eqs. (A.3.2) and (A.3.3) we can evaluate the traces and find

$$\begin{aligned}L_{\sigma^{\kappa\lambda}\sigma^{\rho\tau}} = 4\left(|a_T|^2 + |b_{T_5}|^2\right)\Big(&\left(g^{\kappa\rho}g^{\lambda\tau} - g^{\kappa^\tau}g^{\lambda\rho}\right)p_\ell\cdot p_\nu\\ &+ g^{\kappa\tau}\left(p^\lambda_\ell p^\rho_\nu + p^\rho_\ell p^\lambda_\nu\right) - g^{\lambda\tau}\left(p^\kappa_\ell p^\rho_\nu + p^\rho_\ell p^\kappa_\nu\right)\\ &- g^{\kappa\rho}\left(p^\lambda_\ell p^\tau_\nu + p^\tau_\ell p^\lambda_\nu\right) + g^{\lambda\rho}\left(p^\kappa_\ell p^\tau_\nu + p^\tau_\ell p^\kappa_\nu\right)\Big)\\ - 4i\mathrm{Re}\left(a_T b^*_{T_5}\right)\Big(&\left(p^\kappa_\ell\epsilon^{\lambda\rho\tau\alpha} - p^\lambda_\ell\epsilon^{\kappa\rho\tau\alpha}\right)p_{\nu,\alpha} - \left(p^\rho_\nu\epsilon^{\kappa\lambda\tau\alpha} - p^\tau_\nu\epsilon^{\kappa\lambda\rho\alpha}\right)p_{\ell,\alpha}\Big)\end{aligned} \tag{A.2.6}$$

4. $\Gamma = \mathbb{1},\ \Gamma' = \gamma^\mu$

$$\begin{aligned}L_{1\gamma^\mu} &= \mathrm{Tr}\left(\left(\not{p}_\ell + m_\ell\right)(a_\mathrm{S} + b_\mathrm{P}\gamma_5)\not{p}_\nu\left(a^*_\mathrm{V}\gamma^\mu - b^*_\mathrm{A}\gamma^5\gamma^\mu\right)\right)\\ &= 2\left(a_\mathrm{S}a_{\mathrm{V}^*} + b_\mathrm{P}b^*_\mathrm{A}\right)m_\ell p^\mu_\nu\end{aligned} \tag{A.2.7}$$

5. $\Gamma = \mathbb{1},\ \Gamma' = \sigma^{\mu\rho}$

$$\begin{aligned}L_{1\sigma^{\mu\rho}} &= \mathrm{Tr}\left(\left(\not{p}_\ell + m_\ell\right)(a_\mathrm{S} + b_\mathrm{P}\gamma_5)\not{p}_\nu\left(a^*_\mathrm{T}\sigma^{\mu\rho} - b^*_{\mathrm{T}_5}\gamma^5\sigma^{\mu\rho}\right)\right)\\ &= 2i\left(a_\mathrm{S}a^*_\mathrm{T} + b_\mathrm{P}b^*_{\mathrm{T}_5}\right)\left(p^\rho_\ell p^\mu_\nu - p^\mu_\ell p^\rho_\nu\right) - 2\left(a_\mathrm{S}b^*_{\mathrm{T}_5} + b_\mathrm{P}a^*_\mathrm{T}\right)p_{\ell,\alpha}p_{\nu,\beta}\epsilon^{\alpha\beta\mu\nu}\end{aligned} \tag{A.2.8}$$

6. $\Gamma = \gamma^\mu,\ \Gamma' = \sigma^{\kappa\lambda}$

$$\begin{aligned} L_{\gamma^\mu\sigma^{\kappa\lambda}} &= \mathrm{Tr}\left(\left(\not{p}_\ell + m_\ell\right)\left(a_\mathrm{V}\gamma^\mu + b_\mathrm{a}\gamma^\mu\gamma_5\right)\not{p}_\nu\left(a_\mathrm{T}^*\sigma^{\kappa\lambda} - b_{\mathrm{T}_5}^*\gamma^5\sigma^{\kappa\lambda}\right)\right) \\ &= 2m_\ell\left(i\left(a_\mathrm{V}a_\mathrm{T}^* + b_\mathrm{A}b_{\mathrm{T}_5}^*\right)\left(g^{\mu\lambda}p_\nu^\kappa - g^{\mu\kappa}p_\nu^\lambda\right) - \left(a_\mathrm{V}b_{\mathrm{T}_5}^* + b_\mathrm{A}a_\mathrm{T}^*\right)p_{\nu,\alpha}\epsilon^{\kappa\lambda\mu\alpha}\right) \end{aligned} \tag{A.2.9}$$

By replacing $p_\nu = q - p_\ell$ we arrive at the following expressions for the leptonic tensors

$$\begin{aligned} L_{1,1} &= 2\left(|a_\mathrm{S}|^2 + |b_\mathrm{P}|^2\right)\left(q^2 - m_\ell^2\right) \\ L_{\gamma^\mu\gamma^\nu} &= 2\left(|a_\mathrm{V}|^2 + |b_\mathrm{A}|^2\right)\left(-g^{\mu\nu}\left(q^2 - m_\ell^2\right) - 4p_\ell^\mu p_\ell^\nu + 4\left(p_\ell^\mu q^\nu + p_\ell^\nu q^\mu\right)\right) \\ &\quad + 4i\mathrm{Re}\left(a_\mathrm{V}b_\mathrm{A}^*\right)\epsilon^{\mu\nu\alpha\beta}p_{\ell,\alpha}q_\beta \\ L_{\sigma^{\kappa\lambda}\sigma\rho\tau} &= \left(|a_\mathrm{T}|^2 + |b_{\mathrm{T}_5}|^2\right)\Big(\left(g^{\kappa\tau}g^{\lambda\rho} - g^{\kappa\rho}g^{\lambda\tau}\right)\left(m_\ell^2 + q^2\right) \\ &\qquad + 4\left(p_\ell^\kappa\left(p_\ell^\rho g^{\lambda\tau} - p_\ell^\tau g^\lambda\rho\right) + p_\ell^\lambda\left(p_\ell^\tau g^{\kappa\rho} - p_\ell^\rho g^{\kappa\tau}\right)\right) \\ &\qquad + 2g^{\kappa\tau}\left(p_\ell^\kappa q^\rho + p_\ell^\rho q^\lambda\right) - 2g^{\lambda\tau}\left(p_\ell^\kappa q^\rho + p_\ell^\rho q^\kappa\right) \\ &\qquad - 2g^{\kappa\rho}\left(p_\ell^\lambda q^\tau + p_\ell^\tau q^\lambda\right) + 2g^{\lambda\rho}\left(p_\ell^\kappa q^\tau + p_\ell^\tau q^\kappa\right)\Big) \\ &\quad - 4i\mathrm{Re}\left(a_\mathrm{T}b_{\mathrm{T}_5}^*\right)\Big(\left(p_\ell^\lambda\epsilon^{\kappa\rho\tau\alpha} - p_\ell^\kappa\epsilon^{\lambda\rho\tau\alpha} + p_\ell^\rho\epsilon^{\kappa\lambda\tau\alpha} - p_\ell^\tau\epsilon^{\kappa\lambda\rho\alpha}\right)p_{\ell,\alpha} \\ &\qquad + \left(q^\tau\epsilon^{\kappa\lambda\rho\alpha} - q^\rho\epsilon^{\kappa\lambda\tau\alpha}\right)p_{\ell,\alpha} + \left(p_\ell^\kappa\epsilon^{\lambda\rho\tau\alpha} - p_\ell^\lambda\epsilon^{\kappa\rho\tau\alpha}\right)q_\alpha\Big) \\ L_{1,\gamma^\mu} &= 2m_\ell\left(a_\mathrm{S}a_\mathrm{V}^* + b_\mathrm{P}b_\mathrm{A}^*\right)\left(q^\mu - p_\ell^\mu\right) \\ L_{\gamma^\mu,1} &= L_{1,\gamma^\mu}^* \\ L_{1,\sigma\kappa\lambda} &= 2i\left(a_\mathrm{S}a_\mathrm{T}^* + b_\mathrm{P}b_{\mathrm{T}_5}^*\right)\left(p_\ell^\lambda q^\kappa - p_\ell^\kappa q^\lambda\right) - 2\left(a_\mathrm{S}b_{\mathrm{T}_5}^* + b_\mathrm{P}a_\mathrm{T}^*\right)\epsilon^{\kappa\lambda\alpha\beta}p_{\ell,\alpha}q_\beta \\ L_{\sigma^{\kappa\lambda},1} &= L_{1,\sigma^{\kappa\lambda}}^* \\ L_{\gamma^\mu,\sigma^{\kappa\lambda}} &= 2m_\ell\Big(i\left(a_\mathrm{V}a_\mathrm{T}^* + b_\mathrm{A}b_{\mathrm{T}_5}^*\right)\left(g^{\mu\kappa}p_\ell^\lambda - g^{\mu\lambda}p_\ell^\kappa + g^{\mu\lambda}q^\kappa - g^{\mu\kappa}q^\lambda\right) \\ &\qquad + \left(a_\mathrm{V}b_{\mathrm{T}_5}^* + b_\mathrm{A}a_\mathrm{T}^*\right)\left(\epsilon^{\kappa\lambda\mu\alpha}p_{\ell,\alpha} - \epsilon^{\kappa\lambda\mu\alpha}q_\alpha\right)\Big) \\ L_{\sigma^{\kappa\lambda},\gamma^\mu} &= L_{\gamma^\mu,\sigma^{\kappa\lambda}}^* \end{aligned} \tag{A.2.10}$$

A.3 Traces of products of Dirac γ–matrices

One can easily show that any trace of a product of an odd number of γ–matrices vanishes by multiplying the string of γ–matrices by $\gamma_5^2 = \mathbb{1}$ and using the cyclicity of the trace.
For $N \in \mathbb{N}$ being an even number we can rewrite the trace of a product of N γ–matrices as a sum of traces of products of $(N-2)$ γ–matrices. By writing the trace as

$$\mathrm{Tr}\left(\gamma^{\mu_1}\cdots\gamma^{\mu_N}\right) = \frac{1}{2}\mathrm{Tr}\left[\{\gamma^{\mu_1}, \gamma^{\mu_2}\cdots\gamma^{\mu_N}\}\right] \tag{A.3.1}$$

and commuting γ^{μ_1} in the second term of the anticommutator to the left we find

$$\mathrm{Tr}\left(\gamma^{\mu_1}\cdots\gamma^{\mu_N}\right) = \sum_{k=2}^{N}(-1)^k g^{\mu_1\mu_k}\mathrm{Tr}\left[\prod_{\substack{l=2\\l\neq k}}^{N}\gamma^{\mu_l}\right]. \tag{A.3.2}$$

If the string of γ–matrices is multiplied by γ_5 we get an additional minus sign from commuting the γ^{μ_1} and γ_5 and obtain

$$\mathrm{Tr}\left(\gamma^{\mu_1}\cdots\gamma^{\mu_N}\gamma^5\right) = \sum_{k=2}^{N}(-1)^{k-1}g^{\mu_1\mu_k}\mathrm{Tr}\left[\prod_{\substack{l=2\\l\neq k}}^{N}\gamma^{\mu_l}\right]\gamma^5. \tag{A.3.3}$$

In particular this leads to

$$\begin{aligned}\mathrm{Tr}\left(\gamma^\alpha\sigma^{\kappa\lambda}\gamma^5\gamma^\beta\sigma^{\rho\tau}\right) = 4i\big(&g^{\alpha\beta}\epsilon^{\kappa\lambda\rho\tau} - g^{\alpha\kappa}\epsilon^{\beta\lambda\rho\tau} + g^{\alpha\lambda}\epsilon^{\beta\kappa\rho\tau}\\ &- g^{\alpha\rho}\epsilon^{\beta\kappa\lambda\tau} + g^{\alpha\tau}\epsilon^{\beta\kappa\lambda\rho}\big)\end{aligned} \tag{A.3.4}$$

A.4 Properties of the Dirac δ–function

The determination of the derivatives of the Dirac δ–function by partial integration is straightforward:

$$\int_{-\infty}^{\infty}\mathrm{d}z f(z)\delta'(z) = f(z)\delta(z)|_{-\infty}^{\infty} - \int_{-\infty}^{\infty}\mathrm{d}z f'(z)\delta(z) = -f'(0) \tag{A.4.1}$$

$$\int_{-\infty}^{\infty}\mathrm{d}z f(z)\delta''(z) = \int_{-\infty}^{\infty}\mathrm{d}z f''(z)\delta(z) = f''(z) \tag{A.4.2}$$

$$\int_{-\infty}^{\infty}\mathrm{d}z f(z)\frac{\mathrm{d}^n}{\mathrm{d}z^n}\delta(z) = (-1)^n f^{(n)}(0). \tag{A.4.3}$$

A.5 Hadronic Matrix Elements

Following [203] heavy quarks can be represented by a spinor $u_h(v,s)$ which satisfies

$$\not{v}u_h(v,s) = u_h(v,s) \tag{A.5.1}$$

while the cloud of light degrees of freedom in total transforms like an antiquark with spin–$\frac{1}{2}$ and as such can be represented by a spinor $\overline{v}_l$ which satisfies

$$\overline{v}_l(v,s)\not{v} = -\overline{v}_l(v,s). \tag{A.5.2}$$

The ground state hadron can then be represented by the composite object $\psi = u_h\overline{v}_l$ which under a connected Lorentz–transformation transforms as

$$\psi \to D(\Lambda)\,\psi D^{-1}(\Lambda) \tag{A.5.3}$$

where

$$D(\Lambda) = \exp\left(-\frac{i}{4}\omega_{\mu\nu}\sigma^{\mu\nu}\right) \tag{A.5.4}$$

is the spinor representation of Λ. While heavy–quark–spin transformations only act on the heavy quark:

$$\psi \to D\left(\tilde{\Lambda}\right)\psi \tag{A.5.5}$$

The composite object ψ is a linear combination of physical meson states. In the meson rest frame they can be identified as

$$\begin{aligned} P(\vec{v}=0) &= -\frac{1}{\sqrt{2}}\frac{1+\gamma^0}{2}\gamma_5 \\ V(\vec{v}=0,\epsilon) &= \frac{1}{\sqrt{2}}\frac{1+\gamma^0}{2}\not{\epsilon}. \end{aligned} \tag{A.5.6}$$

When we change to a moving frame of reference with velocity v in the above expressions the γ^0 matrix is replaced by $\not{v}$. In order to study hadronic matrix elements the meson wave function

$$\mathcal{M}(v) = \frac{1+\not{v}}{2}\begin{cases} -\gamma_5, \text{ pseudoscalar meson} \\ \not{\epsilon}, \text{ vector meson} \end{cases} \tag{A.5.7}$$

which has the useful property

$$P_+\mathcal{M}(v)P_- = \frac{1+\not{v}}{2}\mathcal{M}(v)\frac{1-\not{v}}{2} = \mathcal{M}(v) \tag{A.5.8}$$

and its conjugate

$$\begin{aligned} \overline{\mathcal{M}}(v) &= \gamma_0\mathcal{M}(v)^\dagger\gamma_0 \\ &= \gamma_0\left(-\gamma_5\right)\frac{1+\gamma_0\not{v}\gamma_0}{2}\gamma_0 \\ &= \gamma_5\frac{1+\not{v}}{2} \end{aligned} \tag{A.5.9}$$

are introduced. The last two equalities are true in the pseudoscalar case. The hadronic matrix element of a current $h'_v\Gamma h_v$, where h_v and h'_v are heavy quark fields, is then given by

$$\left\langle \overline{M}'(v')\left|h'_v\Gamma h_v\right|M(v)\right\rangle = -\xi(w,\mu)\mathrm{Tr}\left\{\overline{\mathcal{M}}'(v')\Gamma\mathcal{M}(v)\right\}. \tag{A.5.10}$$

Now we are ready to compute the matrix elements we need for our purposes. First we have to find the HQET currents corresponding to the currents $\bar{b}\gamma^\mu\gamma^\nu b$ and $\bar{b}\gamma^\mu\gamma^\nu\gamma_5 b$. As the relation between the b–quark spinor in the full theory and its counterpart in HQET is given by

$$b(x) = e^{-ip_B\cdot x}\left(1+\frac{i\not{D}_\perp}{2m_b}+\cdots\right)b_v \tag{A.5.11}$$

at leading order the transition to HQET is obtained by the replacement

$$\bar{b}\gamma^\mu\gamma^\nu\left(\gamma_5\right)b \to \overline{b_v}\gamma^\mu\gamma^\nu\left(\gamma_5\right)b_v. \tag{A.5.12}$$

Then finding the LO expression for their hadronic matrix elements is straightforward. Using the standard relativistic normalization they are given by

$$\begin{aligned} \left\langle \overline{B}\left|\bar{b}_v b_{v'}\right|\overline{B}\right\rangle &= -\xi(w,\mu)m_B\mathrm{Tr}\left(\gamma_5\frac{1+\not{v}}{2}\frac{1+\not{v}}{2}\left(-\gamma_5\right)\right) \\ &= m_B\left(v\cdot v'+1\right)\xi(w,\mu), \end{aligned} \tag{A.5.13}$$

$$\begin{aligned}\left\langle \overline{B}\left|\bar{b}_v b_{v'}\right|\overline{B}\right\rangle &= -\xi(w,\mu)m_B\mathrm{Tr}\left(\gamma_5\frac{1+\not{v}}{2}\gamma_5\frac{1+\not{v}}{2}\left(-\gamma_5\right)\right)\\ &= 0,\end{aligned} \tag{A.5.14}$$

$$\begin{aligned}\left\langle \overline{B}\left|\bar{b}_v\gamma^\mu\gamma^\nu b_v\right|\overline{B}\right\rangle &= -\xi(x,\mu)m_B\mathrm{Tr}\left\{\gamma_5\frac{1+\not{v}'}{2}\gamma^\mu\gamma^\nu\frac{1+\not{v}}{2}\left(-\gamma_5\right)\right\}\\ &= \xi(w,\mu)m_B\left(\left(v'\cdot v+1\right)g^{\mu\nu}-v^\mu v'^\nu+v^\nu v'^\mu\right)\end{aligned} \tag{A.5.15}$$

and

$$\begin{aligned}\left\langle \overline{B}\left|\bar{b}_v\gamma^\mu\gamma^\nu\gamma_5\bar{b}\right|\overline{B}\right\rangle &= -\xi(x,\mu)m_B\mathrm{Tr}\left\{\gamma_5\frac{1+\not{v}'}{2}\gamma^\mu\gamma^\nu\gamma_5\frac{1+\not{v}}{2}\left(-\gamma_5\right)\right\}\\ &= -i\xi(w,\mu)m_B\epsilon^{\mu\nu\alpha\beta}v_\alpha v'_\beta.\end{aligned} \tag{A.5.16}$$

where ξ is the Isgur–Wise function.

In the following we need the forward scattering amplitude. In this case $v = v'$ and the above expressions at LO simplify to

$$\begin{aligned}\left\langle \overline{B}\left|\bar{b}b\right|\overline{B}\right\rangle &= 2m_B\\ \left\langle \overline{B}\left|\bar{b}\gamma_5 b\right|\overline{B}\right\rangle &= 0\\ \left\langle \overline{B}\left|\bar{b}\gamma^\mu b\right|\overline{B}\right\rangle &= 2p_B^\mu = 2m_B v^\mu\\ \left\langle \overline{B}\left|\bar{b}\gamma^\mu\gamma_5 b\right|\overline{B}\right\rangle &= 0\\ \left\langle \overline{B}\left|\bar{b}\gamma^\mu\gamma^\nu b\right|\overline{B}\right\rangle &= 2m_B g^{\mu\nu}\\ \left\langle \overline{B}\left|\bar{b}_v\gamma^\mu\gamma^\nu\gamma_5\bar{b}\right|\overline{B}\right\rangle &= 0.\end{aligned} \tag{A.5.17}$$

A.6 Structure Functions

A.6.1 $T_{1,1}$

The time–ordered product of interest here is given by

$$-i\int d^4x e^{-iq\cdot x}T\left\{J_S^\dagger(x)J_S(0)\right\}. \tag{A.6.1}$$

At lowest order in α_S and $1/m_B$ its the forward scattering amplitude is given by

$$\begin{aligned}T_{1,1} &= \frac{1}{2m_B u}\left(p_{b,\alpha}-q_\alpha\right)\left(\left(\left|c_S\right|^2+\left|d_P\right|^2\right)\left\langle \overline{B}\left|\bar{b}\gamma^\alpha b\right|\overline{B}\right\rangle + 2\mathrm{Re}\left(c_S d_P\right)\left\langle \overline{B}\left|\bar{b}\gamma^\alpha\gamma_5\right|\overline{B}\right\rangle\right)\\ &\quad+\frac{m_c}{2m_B u}\left(\left(\left|c_S\right|^2-\left|d_P\right|^2\right)\left\langle \overline{B}\left|\bar{b}b\right|\overline{B}\right\rangle + 2i\mathrm{Im}\left(c_S^* d_P\right)\left\langle \overline{B}\left|\bar{b}\gamma_5 b\right|\overline{B}\right\rangle\right)\\ &= \frac{1}{2m_B u}\left(p_{b,\alpha}-q_\alpha\right)\left(\left|c_S\right|^2+\left|d_P\right|^2\right)\left\langle \overline{B}\left|\bar{b}\gamma^\alpha b\right|\overline{B}\right\rangle\\ &\quad+\frac{m_c}{2m_B u}\left(\left|c_S\right|^2-\left|d_P\right|^2\right)\left\langle \overline{B}\left|\bar{b}b\right|\overline{B}\right\rangle\\ &= \frac{1}{2m_B u}\left(p_{b,\alpha}-q_\alpha\right)\left(\left|c_S\right|^2+\left|d_P\right|^2\right)2p_B^\alpha\\ &\quad+\frac{m_c}{u}\left(\left|c_S\right|^2-\left|d_P\right|^2\right)\\ &= \frac{1}{u}\left(\left|c_S\right|^2+\left|d_P\right|^2\right)\left(m_b-q\cdot v\right)+\frac{m_c}{u}\left(\left|c_S\right|^2-\left|d_P\right|^2\right).\end{aligned} \tag{A.6.2}$$

Then the structure function t_0 is

$$t_0 = \frac{1}{u}\left(\left(|c_S|^2 + |d_P|^2\right)(m_b - q\cdot v) + \left(|c_S|^2 - |d_P|^2\right) m_c\right). \tag{A.6.3}$$

A.6.2 $T_{\gamma^\kappa,\gamma^\lambda}$

Here we are interested in the time–ordered product

$$\tilde{T}_{\gamma^\mu,\gamma^\nu} = -i\int d^4x e^{-iq\cdot x} T\left\{J_V^{\mu\dagger}(x) J_V^\nu(0)\right\}. \tag{A.6.4}$$

In the OPE we find that its matrix element between $\overline{B}$–meson states at leading order corresponds to

$$\begin{aligned}
T_{V,V}^{\mu\nu} &= \frac{(p_b - q)_\alpha}{2m_B u}\left\langle \overline{B}\left|\bar{b}\left(c_V^* - d_A^*\gamma^5\right)\gamma^\mu\gamma^\alpha\gamma^\nu\left(c_V + d_A\gamma^5\right) b\right|\overline{B}\right\rangle \\
&\quad + \frac{m_c}{2m_B u}\left\langle \overline{B}\left|\bar{b}\left(c_V^* - d_A^*\gamma^5\right)\gamma^\mu\gamma^\nu\left(c_V + d_A\gamma^5\right) b\right|\overline{B}\right\rangle \\
&= \frac{c_V c_V^* + d_A d_A^*}{2m_B u}(m_b v - q)^\mu\left\langle \overline{B}\left|\bar{b}\gamma^\nu b\right|\overline{B}\right\rangle \\
&\quad + \frac{c_V c_V^* + d_A d_A^*}{2m_B u}(m_b v - q)^\nu\left\langle \overline{B}\left|\bar{b}\gamma^\mu b\right|\overline{B}\right\rangle \\
&\quad - \frac{c_V c_V^* + d_A d_A^*}{2m_B u} g^{\mu\nu}(m_b v - q)_\alpha\left\langle \overline{B}\left|\bar{b}\gamma^\alpha b\right|\overline{B}\right\rangle \\
&\quad - \frac{i\left(c_V d_A^* + d_A c_V^*\right)}{2m_B u}\epsilon^{\mu\nu\alpha\beta}(m_b v - q)_\alpha\left\langle \overline{B}\left|\bar{b}\gamma_\beta b\right|\overline{B}\right\rangle \\
&\quad + \frac{m_c}{2m_b u}\left(|c_V|^2 - |d_A|^2\right)\left\langle \overline{B}\left|\bar{b}\gamma^\mu\gamma^\nu b\right|\overline{B}\right\rangle
\end{aligned} \tag{A.6.5}$$

where we used

$$\gamma^\mu\gamma^\alpha\gamma^\nu = g^{\mu\alpha}\gamma^\nu + g^{\alpha\nu}\gamma^\mu - g^{\mu\nu}\gamma^\alpha - i\epsilon^{\mu\nu\alpha\beta}\gamma_\beta \tag{A.6.6}$$

and the fact that the matrix elements containing one γ^5 matrix vanish by parity. Plugging in the result matrix element from the previous section then yields

$$\begin{aligned}
T_{V,V}^{\mu\nu} &= \frac{1}{u}\left(|c_V|^2 + |d_A|^2\right)\left[2m_b v^\mu v^\nu - q^\mu v^\nu - q^\nu v^\mu - (m_b - v\cdot q)\, g^{\mu\nu}\right] \\
&\quad + \frac{m_c}{u}\left(|c_V|^2 - |d_A|^2\right) g^{\mu\nu} + \frac{2im_B}{u}\mathrm{Re}\left(c_V d_A^*\right)\epsilon^{\mu\nu\alpha\beta} v_\alpha \hat{q}_\beta \\
&= \frac{1}{u}\left(|c_V|^2 + |d_A|^2\right)\left[2m_b v^\mu v^\nu - m_B\left(v^\mu\hat{q}^\nu + v^\nu\hat{q}^\mu\right)\right] \\
&\quad + \frac{1}{u}\left[\left(|c_V|^2 - |d_A|^2\right) m_c - \left(|c_V|^2 + |d_A|^2\right)(m_b - m_B v\cdot\hat{q})\right] g^{\mu\nu} \\
&\quad - \frac{2im_B}{u}\mathrm{Re}\left(c_V d_A^*\right)\epsilon^{\mu\nu\alpha\beta} v_\alpha\hat{q}_\beta
\end{aligned} \tag{A.6.7}$$

from which we obtain

$$
\begin{aligned}
t_1 &= \frac{1}{u}\left[\left(|c_V|^2+|d_A|^2\right)(m_b - v\cdot q) - \left(|c_V|^2-|d_A|^2\right)m_c\right] \\
t_2 &= \frac{2m_b}{u}\left(|c_V|^2+|d_A|^2\right) \\
t_3 &= \frac{2m_b}{u}\mathrm{Re}\left(c_V d_A^*\right) \\
t_4 &= 0 \\
t_5 &= -\frac{m_b}{u}\left(|c_V|^2+|d_A|^2\right).
\end{aligned} \tag{A.6.8}
$$

These results agree with the ones given in [83]

A.6.3 $T_{\sigma^{\kappa\lambda},\sigma^{\rho\tau}}$

$$
\tilde{T}^{\kappa\lambda\rho\tau}_{T,T} = -i\int d^4x e^{-iq\cdot x} T\left\{J_T^{\kappa\lambda\dagger}(x) J_T^{\rho\tau}(0)\right\} \tag{A.6.9}
$$

At lowest order in $\Lambda_{\mathrm{QCD}}/m_B$ and α_s:

$$
\begin{aligned}
T^{\kappa\lambda\rho\tau}_{T,T} &= -i\int d^4x e^{-iq\cdot x}\left\langle \overline{B}\left|T\left\{J_T^{\kappa\lambda\dagger}(x)J_T^{\rho\tau}(0)\right\}\right|\overline{B}\right\rangle \\
&= \frac{(p_b-q)_\alpha}{2m_B u}\left\langle\overline{B}\left|\left(c_T^* - d_{T_5}^*\gamma^5\right)\bar{b}\sigma^{\kappa\lambda}\gamma^\alpha\sigma^{\rho\tau}b\left(c_T + d_{T_5}\gamma^5\right)\right|\overline{B}\right\rangle \\
&= \frac{(p_b-q)_\alpha}{2m_B u}\Big(\left(c_T c_T^* + d_{T_5}d_{T_5}^*\right)\left\langle\overline{B}\left|\bar{b}\sigma^{\kappa\lambda}\gamma^\alpha\sigma^{\rho\tau}b\right|\overline{B}\right\rangle \\
&\qquad + 2\mathrm{Re}\left(c_T d_{T_5}^*\right)\left\langle\overline{B}\left|\bar{b}\sigma^{\kappa\lambda}\gamma^\alpha\sigma^{\rho\tau}\gamma^5 b\right|\overline{B}\right\rangle\Big) \\
&= \frac{1}{u}\left[\left(|c_T|^2+|d_{T_5}|^2\right)(m_b - m_B v\cdot\hat{q}) + \left(|c_T|^2-|d_{T_5}|^2\right)m_c\right]\left(g^{\kappa\rho}g^{\lambda\tau}-g^{\kappa\tau}g^{\lambda\rho}\right) \\
&\quad + \frac{1}{u}\left(|c_T|^2+|d_{T_5}|^2\right)\Big[2m_b\left(v^\lambda v^\rho g^{\kappa\tau} - v^\kappa v^\rho g^{\lambda\tau} + v^\kappa v^\tau g^{\lambda\rho} - v^\lambda v^\tau g^{\kappa\rho}\right) \\
&\qquad\qquad + m_B\Big(g^{\kappa\rho}\left(v^\lambda\hat{q}^\tau + v^\tau\hat{q}^\lambda\right) - g^{\kappa\tau}\left(v^\lambda\hat{q}^\rho + v^\rho\hat{q}^\lambda\right) \\
&\qquad\qquad\quad - g^{\lambda\rho}\left(v^\kappa\hat{q}^\tau + v^\tau\hat{q}^\kappa\right) + g^{\lambda\tau}\left(v^\kappa\hat{q}^\rho + v^\rho\hat{q}^\kappa\right)\Big)\Big] \\
&\quad + \frac{2i}{u}\mathrm{Re}\left(c_T d_{T_5}^*\right)\Big[m_b\left(v^\kappa\epsilon^{\lambda\rho\tau\alpha} - v^\lambda\epsilon^{\kappa\rho\tau\alpha} - v^\rho\epsilon^{\kappa\lambda\tau\alpha} + v^\tau\epsilon^{\kappa\lambda\rho\alpha}\right)v_\alpha \\
&\qquad\qquad + m_B\left(\left(v^\lambda\epsilon^{\kappa\rho\tau\alpha} - v^\kappa\epsilon^{\lambda\rho\tau\alpha}\right)\hat{q}_\alpha + \left(\hat{q}^\rho\epsilon^{\kappa\lambda\tau\alpha} - \hat{q}^\tau\epsilon^{\kappa\lambda\rho\alpha}\right)v_\alpha\right)\Big] \\
&\quad + \frac{2m_c}{u}\mathrm{Im}\left(c_T d_{T_5}^*\right)\epsilon^{\kappa\lambda\rho\tau}
\end{aligned} \tag{A.6.10}
$$

Where we used eq. (A.6.6) again and in the last line we used the Schouten identity

$$
\delta_{\mu\nu}\epsilon_{\alpha\beta\lambda\rho} + \delta_{\mu\alpha}\epsilon_{\beta\lambda\rho\nu} + \delta_{\mu\beta}\epsilon_{\lambda\rho\nu\alpha} + \delta_{\mu\lambda}\epsilon_{\rho\nu\alpha\beta} + \delta_{\mu\rho}\epsilon_{\nu\alpha\beta\lambda} \equiv 0 \tag{A.6.11}
$$

to rewrite the structure in the last line in a simpler form. From the above expression we can read off the leading order expressions for the structure functions

$$
\begin{aligned}
t_6 &= 0 \\
t_7 &= \frac{1}{u}\left[\left(|c_T|^2+|d_{T_5}|^2\right)(m_b - v\cdot q) + \left(|c_T|^2-|d_{T_5}|^2\right)m_c\right] \\
t_8 &= \frac{2m_b}{u}\left(|c_T|^2+|d_{T_5}|^2\right) \\
t_9 &= 0 \\
t_{10} &= -\frac{m_b}{u}\left(|c_T|^2+|d_{T_5}|^2\right) \\
t_{11} &= -\frac{2m_b}{u}\mathrm{Re}\left(c_T d_{T_5}^*\right) \\
t_{12} &= \frac{m_b}{u}\mathrm{Re}\left(c_T d_{T_5}^*\right) \\
t_{13} &= \frac{m_b}{u}\mathrm{Re}\left(c_T d_{T_5}^*\right) \\
t_{14} &= 0 \\
t_{15} &= \frac{2m_c}{u}\mathrm{Im}\left(c_T d_{T_5}^*\right)
\end{aligned}
\tag{A.6.12}
$$

A.6.4 T_{1,γ^μ}

$$
\tilde{T}^\mu_{S,V} = -i\int d^4x e^{-iq\cdot x} T\left\{J_S^\dagger(x) J_V^\mu(0)\right\} \tag{A.6.13}
$$

At lowest order in $\Lambda_{\mathrm{QCD}}/m_B$ and α_S:

$$
\begin{aligned}
T^\mu_{S,V} &= \frac{(p_b-q)_\alpha}{2m_B u}\left\langle \overline{B}\left|\left(c_S^* - d_P^*\gamma^5\right)\bar{b}\gamma^\alpha\gamma^\mu b\left(c_V + d_A\gamma^5\right)\right|\overline{B}\right\rangle \\
&\quad + \frac{m_c}{2m_B u}\left\langle \overline{B}\left|\left(c_S^* - d_P^*\gamma^5\right)\bar{b}\gamma^\mu b\left(c_V + d_A\gamma^5\right)\right|\overline{B}\right\rangle \\
&= \frac{(p_b-q)_\alpha}{2m_B u}\Big(\left(c_S^* c_V - d_P^* d_A\right)\left\langle \overline{B}\left|\bar{b}\gamma^\alpha\gamma^\mu b\right|\overline{B}\right\rangle \\
&\qquad\qquad + \left(c_S^* d_A - d_P^* c_V\right)\left\langle \overline{B}\left|\bar{b}\gamma^\alpha\gamma^\mu\gamma^5 b\right|\overline{B}\right\rangle\Big) \\
&\quad + \frac{m_c}{2m_B u}\Big(\left(c_S^* c_V + d_P^* d_A\right)\left\langle \overline{B}\left|\bar{b}\gamma^\mu b\right|\overline{B}\right\rangle \\
&\qquad\qquad + \left(c_S^* d_A + d_P^* c_V\right)\left\langle \overline{B}\left|\bar{b}\gamma^\mu\gamma_5 b\right|\overline{B}\right\rangle\Big) \\
&= \frac{1}{u}\left(\left(c_S^* c_V - d_P^* d_A\right)\left(m_b v^\mu - m_B\hat{q}^\mu\right) + \left(c_S^* c_V + d_P^* d_A\right)m_c v^\mu\right)
\end{aligned}
\tag{A.6.14}
$$

$$
\begin{aligned}
t_{16} &= \frac{m_b}{u}\left(d_P d_A^* - c_S c_V^*\right) \\
t_{17} &= \frac{1}{u}\left(\left(c_S c_V^* - d_P d_A^*\right)m_b + \left(c_S c_V^* + d_P d_A^*\right)m_c\right)
\end{aligned}
\tag{A.6.15}
$$

A.6.5 $T_{\mathbf{1},\sigma^{\kappa\lambda}}$

$$\tilde{T}^{\kappa\lambda}_{S,T} = -i\int d^4x e^{-iq\cdot x} T\left\{J^\dagger_S(x) J^{\kappa\lambda}_T(0)\right\} \tag{A.6.16}$$

At lowest order in $\Lambda_{\rm QCD}/m_B$ and α_S:

$$\begin{aligned}
T^{\kappa\lambda}_{S,T} &= \frac{(p_b-q)_\alpha}{2m_B u}\left\langle \overline{B}\left|\left(c^*_S - d^*_P\gamma^5\right)\bar{b}\gamma^\alpha\sigma^{\kappa\lambda}b\left(c_T + d_{T_5}\gamma^5\right)\right|\overline{B}\right\rangle \\
&\quad + \frac{m_c}{2m_B u}\left\langle \overline{B}\left|\left(c^*_S - d^*_P\gamma^5\right)\bar{b}\sigma^{\kappa\lambda}b\left(c_T + d_{T_5}\gamma^5\right)\right|\overline{B}\right\rangle \\
&= \frac{(p_b-q)_\alpha}{2m_B u}\Big(\left(c^*_S c_T + d^*_P d_{T_5}\right)\left\langle \overline{B}\left|\bar{b}\gamma^\alpha\sigma^{\kappa\lambda}b\right|\overline{B}\right\rangle \\
&\qquad\qquad + \left(c^*_S d_{T_5} + d^*_P c_T\right)\left\langle \overline{B}\left|\bar{b}\gamma^\alpha\sigma^{\kappa\lambda}\gamma^5 b\right|\overline{B}\right\rangle\Big) \\
&\quad + \frac{m_c}{2m_B u}\Big(\left(c^*_S c_T - d^*_P d_{T_5}\right)\left\langle \overline{B}\left|\bar{b}\sigma^{\kappa\lambda}b\right|\overline{B}\right\rangle \\
&\qquad\qquad + \left(c^*_S d_{T_5} - d^*_P c_T\right)\left\langle \overline{B}\left|\bar{b}\sigma^{\kappa\lambda}\gamma^5\right|\overline{B}\right\rangle\Big) \\
&= \frac{(p_b-q)_\alpha}{2m_B u}\Big(i\left(c^*_S c_T + d^*_P d_{T_5}\right)\left\langle \overline{B}\left|\bar{b}\left(g^{\alpha\kappa}\gamma^\lambda - g^{\alpha\lambda}\gamma^\kappa\right)b\right|\overline{B}\right\rangle \\
&\qquad\qquad - \left(c^*_S d_{T_5} + d^*_P c_T\right)\left\langle \overline{B}\left|\bar{b}\epsilon^{\alpha\kappa\lambda\beta}\gamma_\beta b\right|\overline{B}\right\rangle\Big) \\
&\quad + \frac{m_c}{4m_B u}\Big(i\left(c^*_S c_T - d^*_P d_{T_5}\right)\left\langle \overline{B}\left|\bar{b}\left(\gamma^\kappa\gamma^\lambda - \gamma^\lambda\gamma^\kappa\right)b\right|\overline{B}\right\rangle \\
&\qquad\qquad + i\left(c^*_S d_{T_5} - d^*_P c_T\right)\left\langle \overline{B}\left|\bar{b}\left(\gamma^\kappa\gamma^\lambda - \gamma^\lambda\gamma^\kappa\right)\gamma^5 b\right|\overline{B}\right\rangle\Big) \\
&= \frac{(p_b-q)_\alpha}{2m_B u}\Big(i\left(c^*_S c_T + d^*_P d_{T_5}\right)\left(g^{\alpha\kappa}\delta^\lambda_\beta - g^{\alpha\lambda}\delta^\kappa_\beta\right) \\
&\qquad\qquad - \left(c^*_S d_{T_5} + d^*_P c_T\right)\epsilon^{\alpha\kappa\lambda\eta}g_{\eta\beta}\Big)\left\langle \overline{B}\left|\bar{b}\gamma^\beta b\right|\overline{B}\right\rangle \\
&\quad + \frac{im_c}{2m_B u}\left(c^*_S c_T - d^*_P d_{T_5}\right)\left\langle \overline{B}\left|\bar{b}\left(\gamma^\kappa\gamma^\lambda - \gamma^\lambda\gamma^\kappa\right)b\right|\overline{B}\right\rangle \\
&= \frac{(p_b-q)_\alpha}{m_B u}\Big(i\left(c^*_S c_T + d^*_P d_{T_5}\right)\left(g^{\alpha\kappa}p^\lambda_B - g^{\alpha\lambda}p^\kappa_B\right) \\
&\qquad\qquad - \left(c^*_S d_{T_5} + d^*_P c_T\right)\epsilon^{\alpha\kappa\lambda\eta}p_{B,\eta}\Big) \\
&\quad + \frac{im_c}{u}\left(c^*_S c_T - d^*_P d_{T_5}\right)\left(g^{\kappa\lambda} - g^{\lambda\kappa}\right) \\
&= \frac{m_B}{u}\Big(i\left(c^*_S c_T + d^*_P d_{T_5}\right)\left(v^\kappa\hat{q}^\lambda - v^\lambda\hat{q}^\kappa\right) - \left(c^*_S d_{T_5} + d^*_P c_T\right)\epsilon^{\kappa\lambda\eta\alpha}v_\eta\hat{q}_\alpha\Big)
\end{aligned} \tag{A.6.17}$$

Then the structure functions t_{19}, t_{18} are given by

$$\begin{aligned}
t_{18} &= -\frac{m_b}{u}\left(c_S c^*_T + d_P d^*_{T_5}\right) \\
t_{19} &= -\frac{m_b}{u}\left(c_S d^*_{T_5} + d_P c^*_T\right).
\end{aligned} \tag{A.6.18}$$

A.6.6 $T_{\gamma^\mu,\sigma^{\kappa\lambda}}$

$$\tilde{T}^{\mu\kappa\lambda}_{V,T} = -i\int d^4x e^{-iq\cdot x} T\left\{J^{\mu\dagger}_V(x) J^{\kappa\lambda}_T(0)\right\} \tag{A.6.19}$$

At lowest order in $\Lambda_{\rm QCD}/m_B$ and α_S:

$$\begin{aligned}
T^{\mu\kappa\lambda}_{V,T} &= \frac{(p_b-q)_\alpha}{2m_B u}\left\langle \overline{B}\left|\left(c_V^* - d_A^*\gamma^5\right)\bar{b}\gamma^\mu\gamma^\alpha\sigma^{\kappa\lambda}b\left(c_T + d_{T_5}\gamma^5\right)\right|\overline{B}\right\rangle \\
&\quad + \frac{m_c}{2m_B u}\left\langle \overline{B}\left|\left(c_V^* - d_A^*\gamma^5\right)\bar{b}\gamma^\mu\sigma^{\kappa\lambda}b\left(c_T + d_{T_5}\gamma^5\right)\right|\overline{B}\right\rangle \\
&= \frac{(p_b-q)_\alpha}{2m_B u}\Big(\left(c_V^* c_T - d_A^* d_{T_5}\right)\left\langle \overline{B}\left|\bar{b}\gamma^\mu\gamma^\alpha\sigma^{\kappa\lambda}b\right|\overline{B}\right\rangle \\
&\qquad\qquad + \left(c_V^* d_{T_5} - d_A^* c_T\right)\left\langle \overline{B}\left|\bar{b}\gamma^\mu\gamma^\alpha\sigma^{\kappa\lambda}\gamma^5 b\right|\overline{B}\right\rangle \Big) \\
&\quad + \frac{m_c}{2m_B u}\Big(\left(c_V^* c_T + d_A^* d_{T_5}\right)\left\langle \overline{B}\left|\bar{b}\gamma^\mu\sigma^{\kappa\lambda}b\right|\overline{B}\right\rangle \\
&\qquad\qquad + \left(c_V^* d_{T_5} + d_A^* c_T\right)\left\langle \overline{B}\left|\bar{b}\gamma^\mu\sigma^{\kappa\lambda}\gamma^5 b\right|\overline{B}\right\rangle \Big) \\
&= \frac{i}{u}\left(c_V^* c_T - d_A^* d_{T_5}\right)\left[m_b\left(v^\kappa g^{\lambda\mu} - v^\lambda g^{\kappa\mu}\right) + m_B\left(\hat{q}^\lambda g^{\kappa\mu} - \hat{q}^\kappa g^{\lambda\mu}\right)\right] \\
&\quad - \frac{i}{u}\left(c_V^* c_T + d_A^* d_{T_5}\right) m_c\left(v^\kappa g^{\lambda\mu} - v^\lambda g^{\kappa\mu}\right) \\
&\quad + \frac{1}{u}\left(c_V^* d_{T_5} - d_A^* c_T\right)\left[\left(m_b - m_B v\cdot\hat{q}\right)\epsilon^{\kappa\lambda\mu\alpha}v_\alpha + m_B\left(v^\kappa\epsilon^{\lambda\mu\alpha\beta} - v^\lambda\epsilon^{\kappa\mu\alpha\beta} + v^\mu\epsilon^{\kappa\lambda\alpha\beta}\right)\hat{q}_\alpha v_\beta\right] \\
&\quad - \frac{1}{u}\left(c_V^* d_{T_5} + d_A^* c_T\right) m_c\epsilon^{\kappa\lambda\mu\alpha}v_\alpha \\
&= \frac{i}{u}\left[\left(c_V^* c_T - d_A^* d_{T_5}\right) m_b - \left(c_V^* c_T + d_A^* d_{T_5}\right) m_c\right]\left(v^\kappa g^{\lambda\mu} - v^\lambda g^{\kappa\mu}\right) \\
&\quad + \frac{im_B}{u}\left(c_V^* c_T - d_A^* d_{T_5}\right)\left(\hat{q}^\lambda g^{\kappa\mu} - \hat{q}^\kappa g^{\lambda\mu}\right) \\
&\quad + \frac{1}{u}\left[\left(\left(c_V^* d_{T_5} - d_A^* c_T\right) m_b - \left(c_V^* d_{T_5} + d_A^* c_T\right) m_c\right)\epsilon^{\mu\kappa\lambda\alpha}v_\alpha\right] \\
&\quad - \frac{m_B}{u}\left(c_V^* d_{T_5} - d_A^* c_T\right)\epsilon^{\mu\kappa\lambda\alpha}\hat{q}_\alpha
\end{aligned} \tag{A.6.20}$$

$$\begin{aligned}
t_{20} &= \frac{1}{u}\left[\left(c_V c_T^* - d_A d_{T_5}^*\right) m_b - \left(c_V c_T^* + d_A d_{T_5}^*\right) m_c\right] \\
t_{21} &= -\frac{m_b}{u}\left(c_V c_T^* - d_A d_{T_5}^*\right) \\
t_{22} &= 0 \\
t_{23} &= 0 \\
t_{24} &= \frac{1}{u}\left[\left(c_V d_{T_5}^* - d_A c_T^*\right) m_b - \left(c_V d_{T_5}^* + d_A c_T^*\right) m_c\right] \\
t_{25} &= \frac{m_b}{u}\left(d_A c_T^* - c_V d_{T_5}^*\right)
\end{aligned} \tag{A.6.21}$$

Therefore at the leading order the structure functions are given by

$$
\begin{aligned}
t_0 &= \frac{1}{u}\left(\left(|c_S|^2+|d_P|^2\right)(m_b - q\cdot v) + \left(|c_S|^2-|d_P|^2\right)m_c\right)\\
t_1 &= \frac{1}{u}\left[\left(|c_V|^2+|d_A|^2\right)(m_b - v\cdot q) - \left(|c_V|^2-|d_A|^2\right)m_c\right]\\
t_2 &= \frac{2m_b}{u}\left(|c_V|^2+|d_A|^2\right)\\
t_3 &= \frac{2m_b}{u}\mathrm{Re}\left(c_V d_A^*\right)\\
t_4 &= 0\\
t_5 &= -\frac{m_b}{u}\left(|c_V|^2+|d_A|^2\right)\\
t_6 &= 0\\
t_7 &= \frac{1}{u}\left[\left(|c_T|^2+|d_{T_5}|^2\right)(m_b - v\cdot q) + \left(|c_T|^2-|d_{T_5}|^2\right)m_c\right]\\
t_8 &= \frac{2m_b}{u}\left(|c_T|^2+|d_{T_5}|^2\right)\\
t_9 &= 0\\
t_{10} &= -\frac{m_b}{u}\left(|c_T|^2+|d_{T_5}|^2\right)\\
t_{11} &= -\frac{2m_b}{u}\mathrm{Re}\left(c_T d_{T_5}^*\right)\\
t_{12} &= \frac{m_b}{u}\mathrm{Re}\left(c_T d_{T_5}^*\right)\\
t_{13} &= \frac{m_b}{u}\mathrm{Re}\left(c_T d_{T_5}^*\right)\\
t_{14} &= 0\\
t_{15} &= \frac{2m_c}{u}\mathrm{Im}\left(c_T d_{T_5}^*\right)\\
t_{16} &= \frac{m_b}{u}\left(d_P d_A^* - c_S c_V^*\right)\\
t_{17} &= \frac{1}{u}\left(\left(c_S c_V^* - d_P d_A^*\right)m_b + \left(c_S c_V^* + d_P d_A^*\right)m_c\right)\\
t_{18} &= -\frac{m_b}{u}\left(c_S c_T^* + d_P d_{T_5}^*\right)\\
t_{19} &= -\frac{m_b}{u}\left(c_S d_{T_5}^* + d_P c_T^*\right)\\
t_{20} &= \frac{1}{u}\left[\left(c_V c_T^* - d_A d_{T_5}^*\right)m_b - \left(c_V c_T^* + d_A d_{T_5}^*\right)m_c\right]\\
t_{21} &= -\frac{m_b}{u}\left(c_V c_T^* - d_A d_{T_5}^*\right)\\
t_{22} &= 0\\
t_{23} &= 0\\
t_{24} &= \frac{1}{u}\left[\left(c_V d_{T_5}^* - d_A c_T^*\right)m_b - \left(c_V d_{T_5}^* + d_A c_T^*\right)m_c\right]\\
t_{25} &= \frac{m_b}{u}\left(d_A c_T^* - c_V d_{T_5}^*\right)
\end{aligned}
\tag{A.6.22}
$$

A.7 Double Differential Decay Rate Including General NP

In order to present the double differential decay rate in a concise form we define $y = 2\hat{E}_\ell$, $\rho_\ell = m_\ell^2/m_b^2$, $\rho_c = m_c^2/m_b^2$ and new Wilson coefficients as $c_{V_{L,R}} = c_V \mp d_A$, $c_{S_{L,R}} = c_S \mp d_P$, $\tilde{c}_T = 2c_T = -2d_{T_5}$. Additionally we only consider left-handed neutrinos. Thus we set

$$a_V = a_S = a_T = -b_A = -b_P = -b_{T_5} = \frac{1}{2}. \tag{A.7.1}$$

Thanks to the Dirac delta function we can directly integrate the triple differential decay rate found from eq. (4.2.15) over the neutrino energy, obtaining

$$\begin{aligned}
\frac{d^2\Gamma}{\mathrm{d}\hat{q}^2\mathrm{d}y} = \frac{G_F^2 \left|V_{cb}\right|^2 m_b^5}{192\pi^3}\Big\{ & 12\left|c_{V_L}\right|^2 \left(y-\rho_\ell-\hat{q}^2\right)\left(1+\hat{q}^2-\rho_c-y\right) \\
& +12\left|c_{V_R}\right|^2 y\left(1+\rho_\ell-\rho_c-y\right) \\
& +24\mathrm{Re}\left(c_{V_L}c_{V_R}^*\right)\sqrt{\rho_c}\left(\rho_\ell-\hat{q}^2\right) \\
& +3\left(\left|c_{S_L}\right|^2+\left|c_{S_R}\right|^2\right)\left(\hat{q}^2-\rho_\ell\right)\left(1-\hat{q}^2+\rho_c\right) \\
& +12\mathrm{Re}\left(c_{S_L}c_{S_R}^*\right)\sqrt{\rho_c}\left(\hat{q}^2-\rho_\ell\right) \\
& +48\left|\tilde{c}_T\right|^2\left(\rho_c\left(3\rho_\ell+\hat{q}^2-4y\right)-\rho_\ell\left(3\hat{q}^2-4y+1\right)\right. \\
& \qquad \left. +4y\left(\hat{q}^2+1\right)-\hat{q}^2\left(\hat{q}^2+3\right)-4y^2\right) \\
& +12\left(\mathrm{Re}\left(c_{S_L}c_{V_L}^*\right)+\mathrm{Re}\left(c_{S_R}c_{V_R}^*\right)\right)\sqrt{\rho_\ell\rho_c}\left(1+\hat{q}^2-\rho_c-y\right) \\
& +12\left(\mathrm{Re}\left(c_{S_L}c_{V_R}^*\right)+\mathrm{Re}\left(c_{S_R}c_{V_L}^*\right)\right)\sqrt{\rho_\ell}\left(1+\rho_\ell-\rho_c-y\right) \\
& +24\mathrm{Re}\left(c_{S_L}\tilde{c}_T^*\right)\left(\rho_\ell\left(\hat{q}^2+1\right)+\hat{q}^2\left(\hat{q}^2-2y+1\right)-\rho_c\left(\rho_\ell+\hat{q}^2\right)\right) \\
& +144\mathrm{Re}\left(c_{V_L}\tilde{c}_T^*\right)\sqrt{\rho_c\rho_\ell}\left(\rho_c+y-\hat{q}^2-1\right) \\
& +144\mathrm{Re}\left(c_{V_R}\tilde{c}_T^*\right)\sqrt{\rho_\ell}\left(1+\rho_\ell-\rho_c-y\right)\Big\}.
\end{aligned} \tag{A.7.2}$$

A.8 Currently available corrections

In table A.8.1 we list the currently available corrections and where to find them. Note that in different references different input values for the quark masses, HQE matrix elements, the strong coupling constant and the kinematic cut are used so these numbers can not be directly compared to each other. Nonetheless, their respective orders of magnitude are informative and having them all collected in one place might be useful to someone who is not yet familiar with the HQE.

The values in the first two columns, i.e. the corrections of $\mathcal{O}\left(\Lambda_{\mathrm{QCD}}^2/m_b^2\right)$ and $\mathcal{O}\left(\Lambda_{\mathrm{QCD}}^3/m_b^3\right)$ are computed from the triple differential decay rates given in [83] and [156] respectively.

The $\mathcal{O}\left(\Lambda_{\mathrm{QCD}}^2/m_b^2\right)$ and $\mathcal{O}\left(\Lambda_{\mathrm{QCD}}^3/m_b^3\right)$ corrections to the central moments of q^2 are computed from the expressions of the ancillary file supplied with [123] using the default input values given in table 6.3.1 with a cut of $q_{\mathrm{cut}}^2 = 3\mathrm{GeV}^2$. While for the $\mathcal{O}\left(\Lambda_{\mathrm{QCD}}^4/m_b^4\right)$ the results of the results of the fit including all $1/m_b^4$ parameters in [68] are used for the input parameters and a cut of $q_{\mathrm{cut}} = 3\mathrm{GeV}^2$ is applied.

Table A.8.1: Available contributions. The input parameters can be found in the respective references. In the radiative corrections the reference values in the kinetic scheme with a cutoff of $\mu_{\text{kin}} = 1\text{GeV}$ and charm mass defined in the $\overline{\text{MS}}$ scheme evaluated at 2 GeV are cited.

	$\frac{\Lambda^2_{\text{QCD}}}{m_b^2}$	$\frac{\Lambda^3_{\text{QCD}}}{m_b^3}$	$\frac{\Lambda^4_{\text{QCD}}}{m_b^4}$	$\frac{\Lambda^5_{\text{QCD}}}{m_b^5}$	α_s	$\beta_0\alpha_s^2$	α_s^2	α_s^3	$\alpha_s\frac{\Lambda^2_{\text{QCD}}}{m_b^2}$	$\alpha_s\frac{\Lambda^3_{\text{QCD}}}{m_b^3}$	$\frac{q^2}{m_W^2}$
$\mathrm{d}\Gamma/\mathrm{d}x^3$	[83]	[156]			[49]	[49]		[126]	[34]		
Γ	-4%	-3%	$\mathcal{O}(1\%)$ [196]	$\mathcal{O}(0.5\%)$ [196]	-8.7% [126]	-12% [49]	-1.8% [126]	-0.03% [126]	0.3% [34]	–	0.14%
ℓ_1	-0.5%	-1.1%	$\mathcal{O}(0.5\%)$ [196]	$\mathcal{O}(0.25)\%$ [196]	-0.2% [140]	0.24% [140]	-0.1% [140]	-0.2% [127]	0.5% [34]	–	0.01%
ℓ_2	9.7%	-11.5%	$\mathcal{O}(5\%)$ [196]	$\mathcal{O}(1\%)$ [196]	-0.5% [140]	1.7% [140]	-0.6% [140]	0.02% [127]	-2% [34]	–	-0.03%
ℓ_3	-255%	191%	$\mathcal{O}(-30)\%$ [196]	$\mathcal{O}(10\%)$ [196]	-3% [140]	3.1% [140]	-6% [140]	1.4% [127]	-1.5% [34]	–	0.03%
$\langle m_X^2\rangle$	-2.81%	5.3%	$\mathcal{O}(-2\%)$ [196]	$\mathcal{O}(-1\%)$ [196]	1.3% [140]	-1.2% [140]	0.6% [140]	0.03% [127]	0.6% [34]	–	-0.01%
h_2	788%	-628%	$\mathcal{O}(100\%)$ [196]	$\mathcal{O}(50\%)$ [196]	99% [140]	85% [140]	-34% [140]	51% [127]	-143% [34]	–	0.04%
h_3	-6633.5%	-22448.2%	$\mathcal{O}(6000\%)$ [196]	$\mathcal{O}(600\%)$ [196]	1761% [140]	2020% [140]	155% [140]	-2000% [127]	-8475% [34]	–	-0.2%
$\langle q^2\rangle$	-3.4%	-4%	0.6%	–	1.4% [192]	–	–	-0.5% [127]	-0.7% [192]	-1.8% [192]	0.06%
$q^2_{\text{central},2}$	-14.4%	-23.5%	4%	–	2.8% [192]	–	–	-1.1% [127]	-2.7% [192]	-9.8% [192]	0.04%
$q^2_{\text{central},3}$	-32.2%	-87.2%	18%	–	-5.8% [192]	–	–	-1.9% [127]	-3.8% [192]	-33% [192]	-0.2%
$q^2_{\text{central},4}$	-31.9%	-71.1%	16%	–	4.8% [192]	–	–	-2.4% [127]	-5.5% [192]	-27% [192]	0.02%

A.9 Contributions from the ground states

Among the complete set of states inserted in eq. (5.2.4), we consider the contribution of the lowest-lying states, which are the S-wave states, i.e. D and D^* mesons. (Here and in the following, we omit the subscript s for brevity.) The corresponding matrix elements can be parametrized by the form factors as

$$\begin{aligned}
\langle D(v')|V^\mu|B(v)\rangle &= h_+(w)(v+v')^\mu + h_-(w)(v-v')^\mu \,, && \text{(A.9.1)}\\
\langle D^*(v',\epsilon)|V^\mu|B(v)\rangle &= -h_V(w)\epsilon^{\mu\nu\rho\sigma}v_\nu v'_\rho \epsilon^*_\sigma \,, && \text{(A.9.2)}\\
\langle D^*(v',\epsilon)|A^\mu|B(v)\rangle &= -ih_{A_1}(w)(1+w)\epsilon^{*\mu} \\
&\quad +i\left[h_{A_2}(w)v^\mu + h_{A_3}(w)v'^\mu\right]\epsilon^*\cdot v \,, && \text{(A.9.3)}
\end{aligned}$$

where ϵ^* denotes the polarization vector of the vector D^* meson. We use the HQET definition of the meson states, so that the kinematics is parametrized by the velocities v and v' (with $p = m_B v$ and $p' = m_{D^{(*)}}v'$) and $w = v\cdot v'$. In the rest frame of the B meson $\vec{v}' = -\vec{q}/m_{D^{(*)}}$.

From a separate calculation of the $B \to D^{(*)}$ from factors on the lattice with the same setup as we use for the inclusive decays, we numerically obtain the form factors of the form

$$h_X(w) = c_X^{(0)} + c_X^{(1)}(w-1) + c_X^{(2)}(w-1)^2 \qquad \text{(A.9.4)}$$

after fitting the lattice data. The fit is shown in fig. A.9.1, and the numerical coefficients $c_X^{(0)}$, $c_X^{(1)}$, $c_X^{(2)}$ are listed in table A.9.1.

Now, we insert the parametrizations given in eqs. (A.9.1), (A.9.2), and (A.9.3) into eq. (5.2.4) and perform the ω integral, which merely picks the ground state through $\delta(p_0 - q_0 - E_{D^{(*)}}) = \delta(\omega - E_{D^{(*)}})$. For $\bar{X} \equiv \sum_{l=0}^{2} X^{(l)}$, we obtain

$$\bar{X}^{VV\|} = \frac{\boldsymbol{q}^2}{4m_D E_D}\left((m_B+m_D)h_+ - (m_B-m_D)h_-\right) \qquad \text{(A.9.5)}$$

for the D meson contribution, which corresponds to the partial decay rate

$$\begin{aligned}
\Gamma^{B\to D} &= \frac{G_F^2|V_{cb}|^2}{8\pi^3}\int d\boldsymbol{q}^2 \frac{|\boldsymbol{q}|}{3}\cdot\frac{\boldsymbol{q}^2(m_B+m_D)^2}{4m_D E_D}\left[h_+ - \frac{m_B-m_D}{m_B+m_D}h_-\right]^2 \\
&= \frac{G_F^2|V_{cb}|^2 m_B^5}{48\pi^3}\int dw\,(w^2-1)^{3/2}r^3(1+r)^2\left[h_+ - \frac{1-r}{1+r}h_-\right]^2 , \qquad \text{(A.9.6)}
\end{aligned}$$

X	$c_X^{(0)}$	$c_X^{(1)}$	$c_X^{(2)}$
$+$	1.0082(26)	−1.40(12)	1.0(1.2)
$-$	−0.057(11)	−0.01(17)	
A_1	0.9143(34)	−1.17(15)	0.4(1.6)
A_2	−0.354(75)	0.5(1.2)	
A_3	0.999(75)	−1.0(1.2)	
V	1.243(13)	−1.78(20)	

Table A.9.1: Numerical coefficients $c_X^{(i)}$ to parametrize the form factors of $B \to D$ ($X = +$ and $-$) and $B \to D^*$ (A_1, A_2, A_3 and V) decays. A polynomial expansion of the form $h_X(w) = c_X^{(0)} + c_X^{(1)}(w-1) + c_X^{(2)}(w-1)^2$ is introduced.

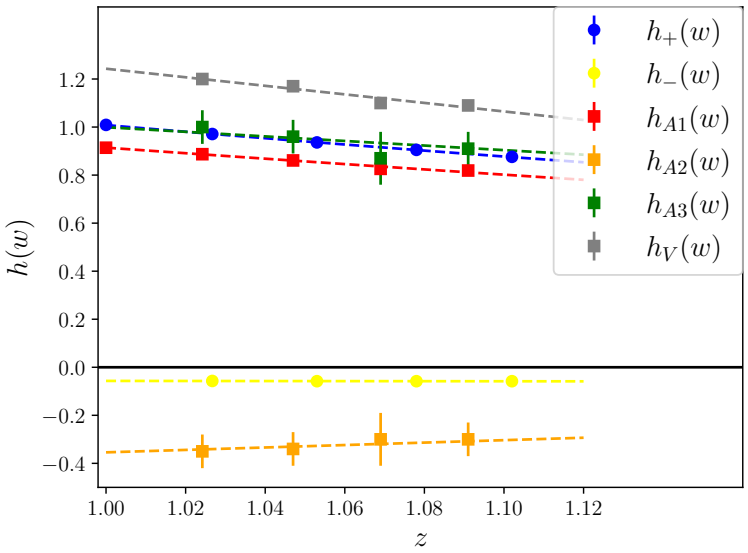

Figure A.9.1: Form factors computed from three-point functions.

where $w = v \cdot v' = \sqrt{1 + \boldsymbol{q}^2/m_D^2} = E_D/m_D$. The last line is a well-known formula for the $B \to D\ell\nu$ decay rate.

The vector meson D^* contributes in three channels: $AA_\parallel$, $AA_\perp$, $VV_\perp$. The contributions are

$$\begin{aligned}
\bar{X}^{AA\parallel} &= \frac{1}{4m_{D^*}E_{D^*}}\Bigg[(m_B - E_{D^*})E_{D^*}h_{A1}(1+w) \\
&\quad + \boldsymbol{q}^2\left(h_{A1}(1+w) - h_{A2} - \frac{m_B}{m_{D^*}}h_{A3}\right)\Bigg]^2 , \qquad \text{(A.9.7)} \\
\bar{X}^{AA\perp} &= \left[(m_B - m_{D^*})^2 - 2m_B(E_{D^*} - m_{D^*})\right]\frac{(1+w)^2}{2w}h_{A1}^2 , \qquad \text{(A.9.8)} \\
\bar{X}^{VV\perp} &= \left[(m_B - m_{D^*})^2 - 2m_B(E_{D^*} - m_{D^*})\right]\frac{\boldsymbol{q}^2}{2m_{D^*}E_{D^*}}h_V^2 . \qquad \text{(A.9.9)}
\end{aligned}$$

Adding them together, we obtain

$$\begin{aligned}
\Gamma^{B\to D^*} &= \frac{G_F^2|V_{cb}|^2}{8\pi^3}\int d\boldsymbol{q}^2\frac{|\boldsymbol{q}|}{3}\Bigg\{(q_0^2 - \boldsymbol{q}^2)\left[\frac{(1+w)^2}{2w}h_{A1}^2 + \frac{\boldsymbol{q}^2}{2m_{D^*}E_{D^*}}h_V^2\right] \\
&\quad + \frac{1}{4m_{D^*}E_{D^*}}\Bigg[(m_B - E_{D^*})E_{D^*}h_{A1}(1+w) \\
&\quad + \boldsymbol{q}^2\left(h_{A1}(1+w) - h_{A2} - \frac{m_B}{m_{D^*}}h_{A3}\right)\Bigg]^2\Bigg\} , \qquad \text{(A.9.10)}
\end{aligned}$$

where $r = m_{D^*}/m_B$ and $E_{D^*} = m_{D^*}w = m_B r w$, while $\boldsymbol{q}^2 = m_{D^*}^2(w^2-1) = m_B^2 r^2(w^2-1)$, and $q_0^2 - \boldsymbol{q}^2 = (m_B - m_{D^*})^2 - 2m_B(E_{D^*} - m_{D^*}) = m_B[(1-r)^2 - 2r(w-2)]$. Eq. (A.9.10) can then

be rewritten as

$$\Gamma^{B\to D^*} = \frac{G_F^2|V_{cb}|^2 m_B^5}{48\pi^3}\int dw\,(w^2-1)^{1/2} r^3 (1-r)^2 (w+1)^2 |h_{A1}|^2 \times\left\{2\frac{r^2-2rw+1}{(1-r)^2}\left[1+\frac{w-1}{w+1}R_1^2\right]+\left[1+\frac{w-1}{1-r}(1-R_2)\right]^2\right\}, \quad \text{(A.9.11)}$$

with $R_1 \equiv h_V/h_{A1}$ and $R_2 \equiv (h_{A3}+rh_{A2})/h_{A1}$, which confirms a well-known formula.

From this analysis, the contributions of the S-wave ground states, D and D^*, to the integrands $\bar{X}^{VV\parallel}$, $\bar{X}^{VV\perp}$, $\bar{X}^{AA\perp}$, and $\bar{X}^{AA\parallel}$ can be identified.

The contribution of the VA and AV insertions vanishes for the total decay rate as well as for the hadronic mass moments, but it is non-zero for the lepton energy moments. In the SM the contribution of the AV interference from the ground state $B \to D^*$ to the first leptonic moment can be written as

$$\bar{X}^{AV} = -\left[(m_B - E_{D^*})^2 - \boldsymbol{q}^2\right]\frac{\boldsymbol{q}^2}{4E_{D^*}}(1+w)h_V h_{A1}\,. \quad \text{(A.9.12)}$$

A.10 Cut dependence

In figs. A.10.1 to A.10.3 we present the dependencies of the moments on the phase space cuts applied in experiments.

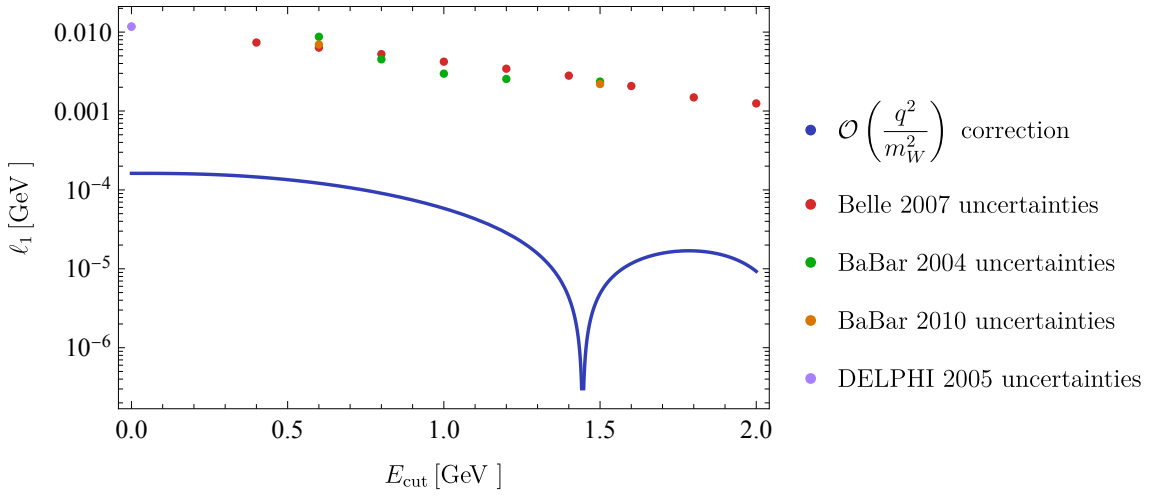

Figure A.10.1: Cut dependence of the first lepton energy moment

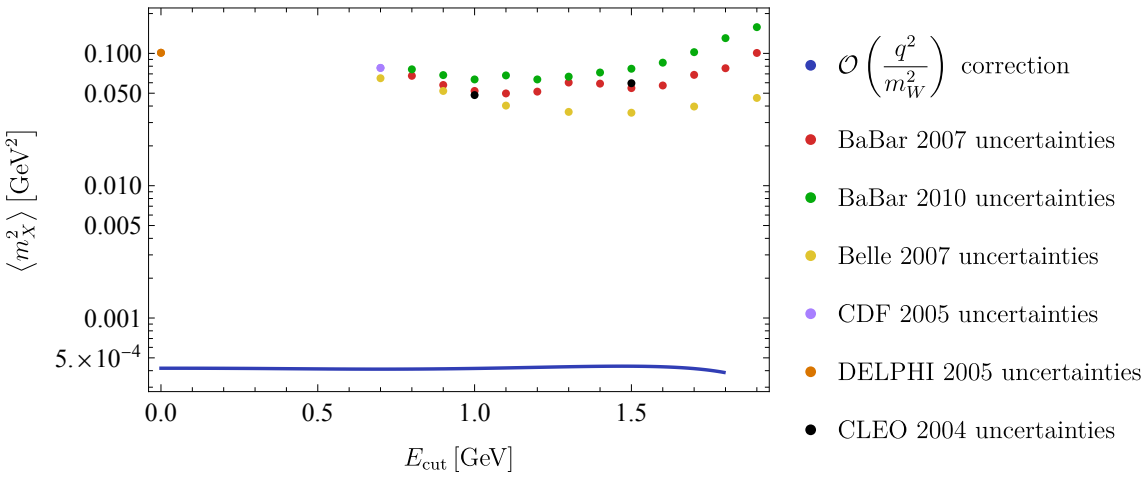

Figure A.10.2: Cut dependence of the first hadronic mass moment

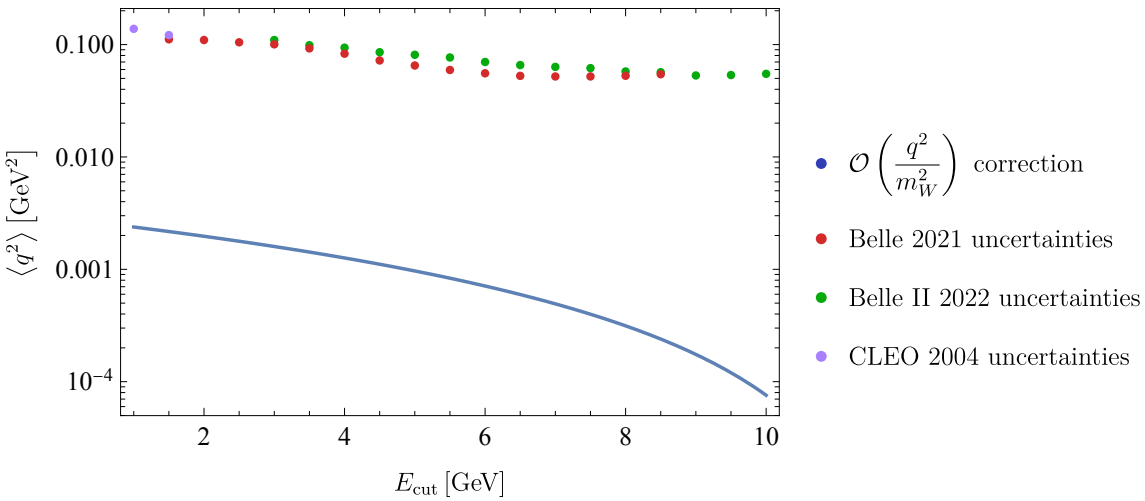

Figure A.10.3: Cut dependence of the first leptonic invariant mass moment

Appendix B

Exclusive Decays of B Mesons

B.1 Summary of input values

$G_{\rm F}$	$(1.1663787 \pm 0.0000006) \times 10^{-5}$ GeV^{-2}
α	$1/133.48$
$\lvert V_{cb}V_{cs}\rvert$	$(41.0 \pm 0.5) \times 10^{-3}$
m_{B_s}	5.36688 ± 0.00014 GeV
m_B	5.27966 ± 0.00014 GeV
m_{B^+}	5.27934 ± 0.00012 GeV
m_ϕ	1.019461 ± 0.000016 GeV
m_{K^*}	0.89555 ± 0.0002 GeV
m_{K^+}	0.493677 ± 0.000016 GeV
τ_{B^+}	$(2.489 \pm 0.006) \times 10^{12}$ GeV^{-1}
$m_{J/\psi}$	3.096900 ± 0.000006 GeV
$m_{\psi(2s)}$	3.6861 ± 0.00006 GeV
$\Gamma_{J/\psi}$	0.0000926 ± 0.0000017 GeV
$\Gamma_{\psi(2s)}$	0.000294 ± 0.000008 GeV
$\mathcal{B}(B^+ \to J/\psi K^+)$	$(1.020 \pm 0.019) \times 10^{-3}$
$\mathcal{B}(J/\psi \to \mu^+\mu^-)$	$(5.961 \pm 0.033) \times 10^{-2}$

Table B.1.1: Experimental inputs for the determination of the constants η_j^λ and δ_j^λ

$m_c^{\overline{\rm MS}}(m_c^{\overline{\rm MS}})$	1.2719 ± 0.0078 GeV
$m_b^{\overline{\rm MS}(\mu_b)}$	4.209 ± 0.021 GeV
m_c	1.68 ± 0.2GeV
m_b	4.87 ± 0.2GeV
m_μ	0.106 GeV
$1/\alpha_{\rm EW}$	133
$\lvert V_{tb}V_{ts}^*\rvert$	0.04185 ± 0.00093
$C_1(\mu_b)$	-0.294 ± 0.009
$C_2(\mu_b)$	1.017 ± 0.001
$C_3(\mu_b)$	-0.0059 ± 0.0002
$C_4(\mu_b)$	-0.087 ± 0.001
$C_5(\mu_b)$	$0.0004\pm$
$C_7^{\rm eff,0}(\mu_b)$	-0.2957 ± 0.0005
$C_8^{\rm eff}(\mu_b)$	-0.1630 ± 0.0006
$C_9(\mu_b)$	4.114 ± 0.014
$C_9^{\rm eff,0}(\mu_b)$	$C_9(\mu_b) + Y(q^2)$
$C_{10}(\mu_b)$	-4.193 ± 0.033
$\Gamma(B^+)$	$(4.018 \pm 0.010) \times 10^{-13}$
$\Gamma(B^0)$	$(4.333 \pm 0.011) \times 10^{-13}$
μ	$m_b^{\overline{\rm MS}(\mu_b)}$
V_{ts}	$(-0.041233 - 0.00056)\, e^{i(1.056\pm0.032)\frac{\pi}{180}}$
V_{tb}	(0.999112 ± 0.000024)

Table B.1.2: Input parameters

B.2 Summary of the resonance parameters

V	η_V	δ_V
J/ψ	32.3 ± 0.6	-1.50 ± 0.05
$\psi(2s)$	7.12 ± 0.32	2.08 ± 0.11
$\psi(3770)$	$(1.3 \pm 0.1) \times 10^{-2}$	-2.89 ± 0.19
$\psi(4040)$	$(4.8 \pm 0.8) \times 10^{-3}$	-2.69 ± 0.52
$\psi(4160)$	$(1.5 \pm 0.1) \times 10^{-2}$	-2.13 ± 0.33
$\psi(4415)$	$(1.1 \pm 0.2) \times 10^{-2}$	-2.43 ± 0.43

Table B.2.1: Resonance amplitudes and phases for $B^+ \to K^+\mu^+\mu^-$

V	Polarization	η_V	δ_V
J/ψ	$\perp$	26.6 ± 1.1	1.46 ± 0.06
	$\parallel$	12.3 ± 0.5	-4.42 ± 0.06
	longitudinal	13.9 ± 0.5	-1.48 ± 0.05
$\psi(2s)$	$\perp$	3.0 ± 0.9	3.2 ± 0.4
	$\parallel$	1.11 ± 0.30	-3.32 ± 0.22
	longitudinal	1.14 ± 0.06	2.10 ± 0.11

Table B.2.2: Resonance amplitudes and phases for $B \to K^* \mu^+ \mu^-$

V	Polarization	η_V	δ_V
J/ψ	$\perp$	27.8 ± 1.3	1.59 ± 0.16
	$\parallel$	11.0 ± 0.6	1.74 ± 0.16
	longitudinal	10.7 ± 0.5	-1.48 ± 0.05
$\psi(2s)$	$\perp$	3.2 ± 1.0	5.4 ± 0.4
	$\parallel$	1.02 ± 0.28	5.74 ± 0.19
	longitudinal	0.90 ± 0.05	2.10 ± 0.11

Table B.2.3: Resonance amplitudes and phases for $B_S \to \phi \mu^+ \mu^-$

B.3 The V_j rest frame

In the J/ψ rest frame, we have $\tilde{p}_{J/\psi} = (m_{J/\psi}, 0, 0, 0)$, while in the B rest frame $p_{J/\psi} = (E_{J/\psi}, 0, 0, -p)$, where $E_{J/\psi}$ and p are defined by the kinematics of the process. We can hence define a Lorentz transformation along the $\hat{z}$ axis as

$$\tilde{p}_{J/\psi} = \Lambda p_{J/\psi} \,, \tag{B.3.1}$$

where the parameter of the Lorentz transformation are

$$\gamma = \frac{E_{J/\psi}}{m_{J/\psi}} \,, \qquad \beta\gamma = \frac{p}{m_{J/\psi}} \,. \tag{B.3.2}$$

We can use these findings to boost the polarization vectors in the J/ψ rest frame. We find:

$$\tilde{\epsilon}_{J/\psi}(L) = (0,0,0,1) \,, \qquad \tilde{\epsilon}_{\phi}(L) = \left(\frac{\sqrt{\lambda}}{2 m_{J/\psi} m_\phi}, 0, 0, \frac{m_{J/\psi}^2 + m_\phi^2 - m_B^2}{2 m_{J/\psi} m_\phi} \right) , \tag{B.3.3}$$

$$\tilde{\epsilon}_{J/\psi}(+1) = \frac{1}{\sqrt{2}}(0,+1,-i,0) \,, \qquad \tilde{\epsilon}_{\phi}(+1) = \frac{1}{\sqrt{2}}(0,-1,-i,0) \,, \tag{B.3.4}$$

$$\tilde{\epsilon}_{J/\psi}(-1) = \frac{1}{\sqrt{2}}(0,-1,-i,0) \,, \qquad \tilde{\epsilon}_{\phi}(-1) = \frac{1}{\sqrt{2}}(0,1,-i,0) \,. \tag{B.3.5}$$

For completeness, we also report the momenta of the ϕ

$$\tilde{p}_\phi = -\left(\frac{m_{J/\psi}^2 + m_\phi^2 - m_B^2}{2 m_{J/\psi}}, 0, 0, \frac{\sqrt{\lambda}}{2 m_{J/\psi}} \right) \tag{B.3.6}$$

We define 3-momenta in bold characters. We further define a unit vector $\hat{\boldsymbol{p}} = (0, 0, -1)$. In the notation of [120], we get

$$\tilde{\boldsymbol{\epsilon}}^{*L}_{J/\psi}\tilde{\boldsymbol{\epsilon}}^{*L}_{\phi} = \frac{m_B^2 - m_{J/\psi}^2 - m_\phi^2}{2m_{J/\psi}m_\phi}\,, \tag{B.3.7}$$

$$\tilde{\boldsymbol{\epsilon}}^{*T}_{J/\psi} \cdot \tilde{\boldsymbol{\epsilon}}^{*T}_{\phi} = -\,2\,, \tag{B.3.8}$$

$$\tilde{\boldsymbol{\epsilon}}^{*}_{J/\psi} \times \tilde{\boldsymbol{\epsilon}}^{*}_{\phi} \cdot \hat{\boldsymbol{p}} = +\,2i\,. \tag{B.3.9}$$

We then redefine the amplitudes as

$$\mathcal{A}_0 = A_0 \times \sqrt{\frac{\sqrt{\lambda}}{16\pi m_B^3}}\frac{m_B^2 - m_{J/\psi}^2 - m_\phi^2}{2m_{J/\psi}m_\phi}\,, \tag{B.3.10}$$

$$\mathcal{A}_\parallel = A_\parallel \times (-2)\sqrt{\frac{\sqrt{\lambda}}{16\pi m_B^3}}\,, \tag{B.3.11}$$

$$\mathcal{A}_\perp = A_\perp \times (2i)\sqrt{\frac{\sqrt{\lambda}}{16\pi m_B^3}}\,. \tag{B.3.12}$$

B.4 Charmonium decay

The electromagnetic decay $V \to e^+e^-$ probes the matrix element of the electromagnetic current. We parametrize it as

$$\langle V(p)|j^\mu_{em}|0|V(p)|j^\mu_{em}|0\rangle = 2f_V(p^2)\varepsilon_V^{\mu*}(p)\,. \tag{B.4.1}$$

Then the decay matrix element is given by

$$\begin{aligned}\mathcal{M}\left(V(p,k) \to e^+(q_1)e^-(q_2)\right) &= \langle V(p,k)|j^\mu_{em}|0|V(p,k)|j^\mu_{em}|0\rangle \left\langle 0|j_{em,\mu}|e^+(q_1)e^-(q_2)\right|0|j_{em,\mu}|e^+(q_1)e^-(q_2)\rangle \\ &= f_V(p^2)\varepsilon_V^{\mu*}(p,k)(-ie)\overline{u}(q_2)\gamma_\mu u(q_1),\end{aligned} \tag{B.4.2}$$

from which we obtain the spin-averaged matrix element

$$\begin{aligned}\frac{1}{3}\sum_{k,s,s'}\left|\mathcal{M}\left(V(p,k) \to e^+(q_1)e^-(q_2)\right)\right|^2 &= \frac{1}{3}e^2 f_V^2(p^2)\sum_k \varepsilon_V^{\mu*}\varepsilon_V^{\nu}\mathrm{Tr}\left[\not{q}_2\gamma_\mu\left(1-\gamma^5\right)\not{q}_1\gamma_\nu\left(1-\gamma^5\right)\right] \\ &= \frac{1}{3}e^2 f_V^2(p^2)\left(-g^{\mu\nu} + \frac{p^\mu p^\nu}{m_V^2}\right)\mathrm{Tr}\left[\not{q}_2\gamma_\mu\left(1-\gamma^5\right)\not{q}_1\gamma_\nu\left(1-\gamma^5\right)\right] \\ &= \frac{64\pi}{3}\alpha_{\mathrm{em}} f_V(m_V^2)m_V^2,\end{aligned} \tag{B.4.3}$$

where we neglected the electron mass and set $p^2 = m_V^2$ in the last line. The differential $V(p) \to e^+(q_1)e^-(q_2)$ decay rate is then given by

$$\begin{aligned}\Gamma\left(V \to e^+e^-\right) &= \frac{1}{32\pi^2}\int_{\mathrm{PS}}\frac{1}{3}\sum_{k,s,s'}|\mathcal{M}|^2\,\frac{\mathbf{q_1}}{m_V^2}\mathrm{d}\Omega \\ &= \frac{4}{3}\alpha_{\mathrm{em}} f_V^2(m_V^2)m_V\end{aligned} \tag{B.4.4}$$

We can therefore extract $f_V(m_V^2)$ from the experimental measurement of $\mathcal{B}(V \to \ell^+\ell^-)$,

$$\mathcal{B}(V \to \ell^+\ell^-) = \frac{4\alpha_{\mathrm{em}} f_V^2(m_V^2)m_V}{3\Gamma_V}\,, \tag{B.4.5}$$

which yields $f_{\psi(2s)} = (4.87 \pm 0.07) \times 10^{-3}$ and $f_{J/\psi} = (1.36 \pm 0.02) \times 10^{-2}$.

B.5 Covariance Matrices

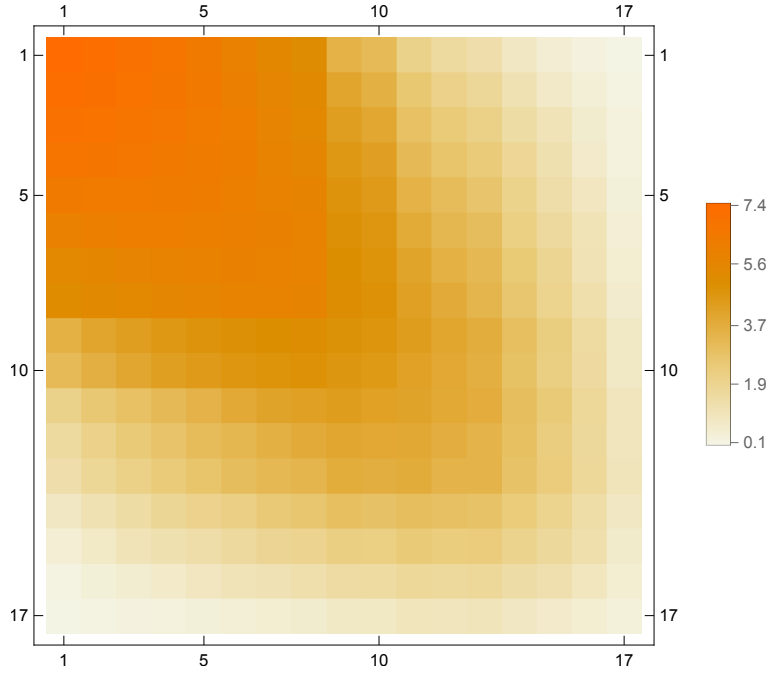

Figure B.5.1: Theory covariances for $B^+ \to K^+\mu^+\mu^-$ from the form factors.

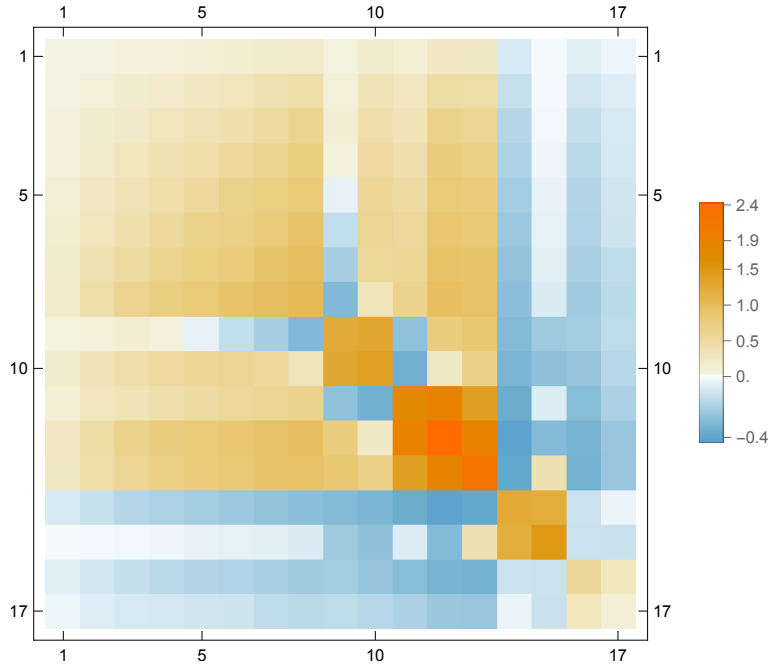

Figure B.5.2: Theory covariances for $B^+ \to K^+\mu^+\mu^-$ from the resonance parameters.

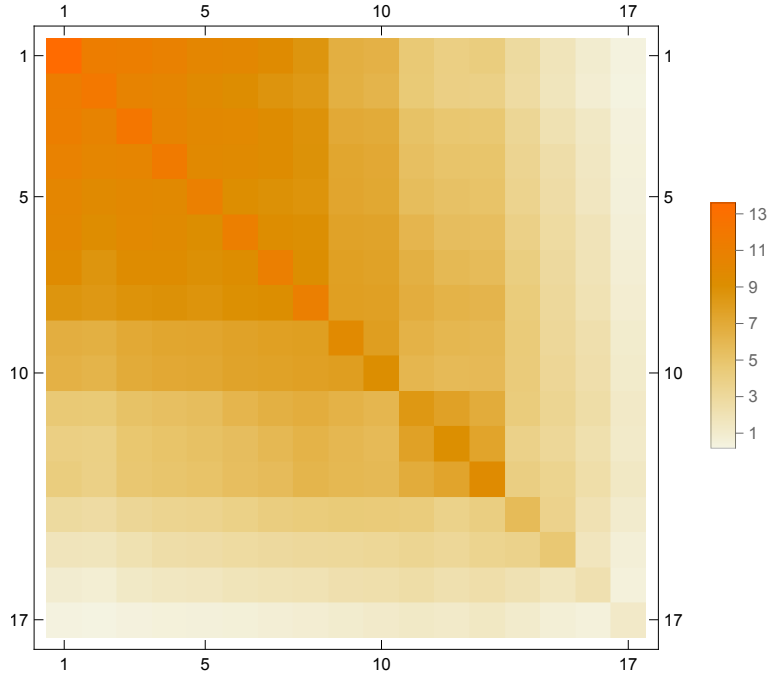

Figure B.5.3: Full covariances for $B^+ \to K^+\mu^+\mu^-$.

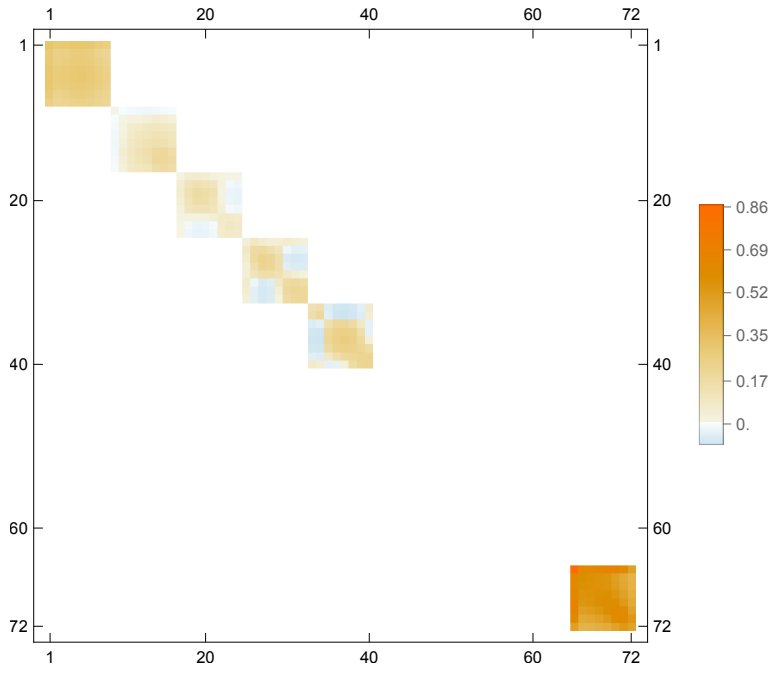

Figure B.5.4: Theory covariances for $B^0 \to K^{0*}\mu^+\mu^-$ from the form factors.

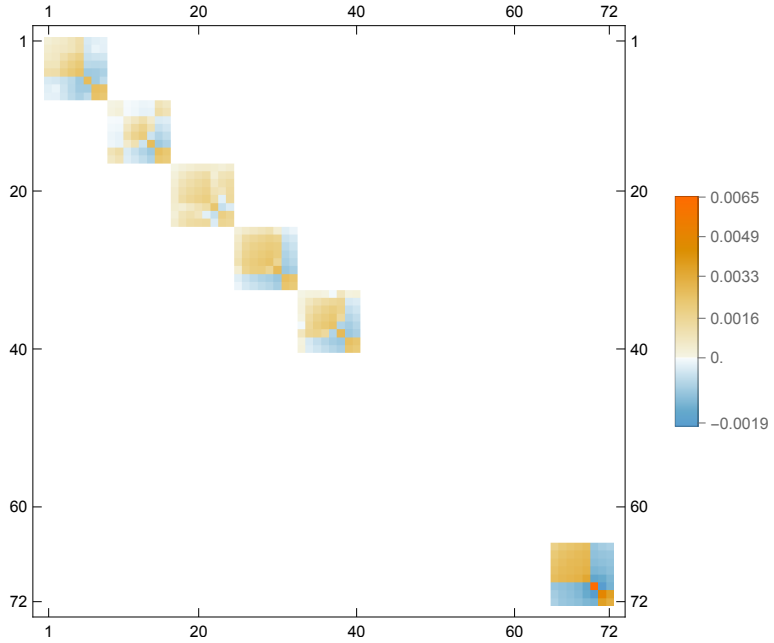

Figure B.5.5: Theory covariances for $B^0 \to K^{0*}\mu^+\mu^-$ from the resonance parameters.

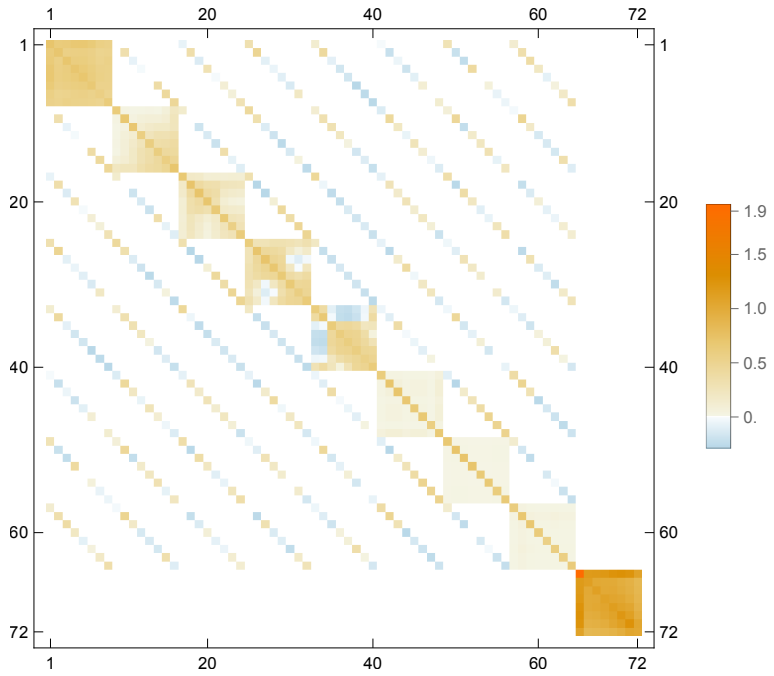

Figure B.5.6: Full covariances matrix for $B^0 \to K^{0*}\mu^+\mu^-$.

Bibliography

[1] Combination of the ATLAS, CMS and LHCb results on the $B^0_{(s)} \to \mu^+\mu^-$ decays.

[2] Measurement of Lepton Mass Squared Moments in $B \to X_c \ell \bar{\nu}_\ell$ Decays with the Belle II Experiment.

[3] Aaij, R., et al. Physics case for an LHCb Upgrade II - Opportunities in flavour physics, and beyond, in the HL-LHC era.

[4] Aaij, R., et al. Differential branching fraction and angular analysis of the decay $B^0 \to K^{*0}\mu^+\mu^-$. *JHEP 08* (2013), 131.

[5] Aaij, R., et al. Measurement of CP violation and the B^0_s meson decay width difference with $B^0_s \to J/\psi K^+K^-$ and $B^0_s \to J/\psi \pi^+\pi^-$ decays. *Phys. Rev. D 87*, 11 (2013), 112010.

[6] Aaij, R., et al. Measurement of the polarization amplitudes in $B^0 \to J/\psi K^*(892)^0$ decays. *Phys. Rev. D 88* (2013), 052002.

[7] Aaij, R., et al. Differential branching fractions and isospin asymmetries of $B \to K^{(*)}\mu^+\mu^-$ decays. *JHEP 06* (2014), 133.

[8] Aaij, R., et al. Measurement of *CP* asymmetries in the decays $B^0 \to K^{*0}\mu^+\mu^-$ and $B^+ \to K^+\mu^+\mu^-$. *JHEP 09* (2014), 177.

[9] Aaij, R., et al. Test of lepton universality using $B^+ \to K^+\ell^+\ell^-$ decays. *Phys. Rev. Lett. 113* (2014), 151601.

[10] Aaij, R., et al. First measurement of the differential branching fraction and *CP* asymmetry of the $B^\pm \to \pi^\pm\mu^+\mu^-$ decay. *JHEP 10* (2015), 034.

[11] Aaij, R., et al. Measurement of the ratio of branching fractions $\mathcal{B}(\bar{B}^0 \to D^{*+}\tau^-\bar{\nu}_\tau)/\mathcal{B}(\bar{B}^0 \to D^{*+}\mu^-\bar{\nu}_\mu)$. *Phys. Rev. Lett. 115*, 11 (2015), 111803. [Erratum: Phys.Rev.Lett. 115, 159901 (2015)].

[12] Aaij, R., et al. Precision measurement of *CP* violation in $B^0_s \to J/\psi K^+K^-$ decays. *Phys. Rev. Lett. 114*, 4 (2015), 041801.

[13] Aaij, R., et al. Angular analysis of the $B^0 \to K^{*0}\mu^+\mu^-$ decay using 3 fb^{-1} of integrated luminosity. *JHEP 02* (2016), 104.

[14] Aaij, R., et al. Angular analysis of the $B^0 \to K^{*0}\mu^+\mu^-$ decay using 3 fb^{-1} of integrated luminosity. *JHEP 02* (2016), 104.

[15] Aaij, R., et al. First study of the CP -violating phase and decay-width difference in $B_s^0 \to \psi(2S)\phi$ decays. *Phys. Lett. B 762* (2016), 253–262.

[16] Aaij, R., et al. Measurements of the S-wave fraction in $B^0 \to K^+\pi^-\mu^+\mu^-$ decays and the $B^0 \to K^*(892)^0\mu^+\mu^-$ differential branching fraction. *JHEP 11* (2016), 047. [Erratum: JHEP 04, 142 (2017)].

[17] Aaij, R., et al. Measurement of the phase difference between short- and long-distance amplitudes in the $B^+ \to K^+\mu^+\mu^-$ decay. *Eur. Phys. J. C 77*, 3 (2017), 161.

[18] Aaij, R., et al. Test of lepton universality with $B^0 \to K^{*0}\ell^+\ell^-$ decays. *JHEP 08* (2017), 055.

[19] Aaij, R., et al. Test of Lepton Flavor Universality by the measurement of the $B^0 \to D^{*-}\tau^+\nu_\tau$ branching fraction using three-prong τ decays. *Phys. Rev. D 97*, 7 (2018), 072013.

[20] Aaij, R., et al. Search for lepton-universality violation in $B^+ \to K^+\ell^+\ell^-$ decays. *Phys. Rev. Lett. 122*, 19 (2019), 191801.

[21] Aaij, R., et al. Measurement of CP-Averaged Observables in the $B^0 \to K^{*0}\mu^+\mu^-$ Decay. *Phys. Rev. Lett. 125*, 1 (2020), 011802.

[22] Aaij, R., et al. Measurement of CP-Averaged Observables in the $B^0 \to K^{*0}\mu^+\mu^-$ Decay. *Phys. Rev. Lett. 125*, 1 (2020), 011802.

[23] Aaij, R., et al. Branching Fraction Measurements of the Rare $B_s^0 \to \phi\mu^+\mu^-$ and $B_s^0 \to f_2'(1525)\mu^+\mu^-$- Decays. *Phys. Rev. Lett. 127*, 15 (2021), 151801.

[24] Abdallah, J., et al. Determination of heavy quark non-perturbative parameters from spectral moments in semileptonic B decays. *Eur. Phys. J. C 45* (2006), 35–59.

[25] Abdesselam, A., et al. Measurement of $\mathcal{R}(D)$ and $\mathcal{R}(D^*)$ with a semileptonic tagging method.

[26] Abdesselam, A., et al. Test of lepton flavor universality in $B \to K^*\ell^+\ell^-$ decays at Belle.

[27] Ablikim, M., et al. Measurement of the absolute branching fraction of inclusive semielectronic D_s^+ decays. *Phys. Rev. D 104*, 1 (2021), 012003.

[28] Abudinén, F., et al. Measurement of Hadronic Mass Moments $\langle M_X^n \rangle$ in $B \to X_c\ell\nu$ Decays at Belle II.

[29] Acosta, D., et al. Measurement of the moments of the hadronic invariant mass distribution in semileptonic B decays. *Phys. Rev. D 71* (2005), 051103.

[30] Aebischer, J., Altmannshofer, W., Guadagnoli, D., Reboud, M., Stangl, P., and Straub, D. M. B-decay discrepancies after Moriond 2019. *Eur. Phys. J. C 80*, 3 (2020), 252.

[31] Albanese, M., et al. Glueball Masses and String Tension in Lattice QCD. *Phys. Lett. B 192* (1987), 163–169.

[32] Alberti, A. *Higher order corrections to inclusive semileptonic B decays*. PhD thesis, Turin U., 3 2015.

[33] Alberti, A., Ewerth, T., Gambino, P., and Nandi, S. Kinetic operator effects in $\bar{B} \to X_c l\nu$ at $O(\alpha_s)$. *Nucl. Phys. B 870* (2013), 16–29.

[34] Alberti, A., Gambino, P., and Nandi, S. Perturbative corrections to power suppressed effects in semileptonic B decays. *JHEP 01* (2014), 147.

[35] Albrecht, J. Lepton Flavour Universality tests with B decays at LHCb. In *53rd Rencontres de Moriond on QCD and High Energy Interactions* (2018), pp. 89–92.

[36] Albrecht, J., Reichert, S., and van Dyk, D. Status of rare exclusive B meson decays in 2018. *Int. J. Mod. Phys. A 33*, 18n19 (2018), 1830016.

[37] Algueró, M., Biswas, A., Capdevila, B., Descotes-Genon, S., Matias, J., and Novoa-Brunet, M. To (b)e or not to (b)e: No electrons at LHCb.

[38] Algueró, M., Capdevila, B., Crivellin, A., Descotes-Genon, S., Masjuan, P., Matias, J., Novoa Brunet, M., and Virto, J. Emerging patterns of New Physics with and without Lepton Flavour Universal contributions. *Eur. Phys. J. C 79*, 8 (2019), 714. [Addendum: Eur.Phys.J.C 80, 511 (2020)].

[39] Ali, A., Parkhomenko, A. Y., and Rusov, A. V. Precise Calculation of the Dilepton Invariant-Mass Spectrum and the Decay Rate in $B^{\pm} \to \pi^{\pm}\mu^{+}\mu^{-}$ in the SM. *Phys. Rev. D 89*, 9 (2014), 094021.

[40] Alonso, R., Grinstein, B., and Martin Camalich, J. Lepton universality violation and lepton flavor conservation in B-meson decays. *JHEP 10* (2015), 184.

[41] Altmannshofer, W., Ball, P., Bharucha, A., Buras, A. J., Straub, D. M., and Wick, M. Symmetries and Asymmetries of $B \to K^{*}\mu^{+}\mu^{-}$ Decays in the Standard Model and Beyond. *JHEP 01* (2009), 019.

[42] Amhis, Y., et al. Averages of b-hadron, c-hadron, and τ-lepton properties as of 2021.

[43] Amhis, Y. S., et al. Averages of b-hadron, c-hadron, and τ-lepton properties as of 2018. *Eur. Phys. J. C 81*, 3 (2021), 226.

[44] Amhis, Y. S., et al. Averages of b-hadron, c-hadron, and τ-lepton properties as of 2018. *Eur. Phys. J. C81* (2021), 226. updated results and plots available at https://hflav.web.cern.ch/.

[45] Aoki, S., et al. FLAG Review 2019: Flavour Lattice Averaging Group (FLAG). *Eur. Phys. J. C 80*, 2 (2020), 113.

[46] Aoki, S., et al. FLAG Review 2019: Flavour Lattice Averaging Group (FLAG). *Eur. Phys. J. C 80*, 2 (2020), 113.

[47] Aoki, Y., et al. FLAG Review 2021. *Eur. Phys. J. C 82*, 10 (2022), 869.

[48] Appelquist, T., and Carazzone, J. Infrared Singularities and Massive Fields. *Phys. Rev. D 11* (1975), 2856.

[49] Aquila, V., Gambino, P., Ridolfi, G., and Uraltsev, N. Perturbative corrections to semileptonic b decay distributions. *Nucl. Phys. B 719* (2005), 77–102.

[50] Asner, D. M., et al. Measurement of absolute branching fractions of inclusive semileptonic decays of charm and charmed-strange mesons. *Phys. Rev. D 81* (2010), 052007.

[51] Aubert, B., et al. Measurement of the electron energy spectrum and its moments in inclusive $B \to Xe\nu$ decays. *Phys. Rev. D 69* (2004), 111104.

[52] Aubert, B., et al. Measurements of branching fractions, rate asymmetries, and angular distributions in the rare decays $B \to K\ell^+\ell^-$ and $B \to K^*\ell^+\ell^-$. *Phys. Rev. D 73* (2006), 092001.

[53] Aubert, B., et al. Measurement of moments of the hadronic-mass and energy spectrum in inclusive semileptonic anti-B —> X(c) l- anti-nu decays. In *2007 Europhysics Conference on High Energy Physics* (7 2007).

[54] Aubert, B., et al. Measurement and interpretation of moments in inclusive semileptonic decays anti-B —> X(c) l- anti-nu. *Phys. Rev. D 81* (2010), 032003.

[55] Bailas, G., Hashimoto, S., and Ishikawa, T. Reconstruction of smeared spectral function from Euclidean correlation functions. *PTEP 2020*, 4 (2020), 043B07.

[56] Bailey, J. A., et al. $|V_{ub}|$ from $B \to \pi\ell\nu$ decays and (2+1)-flavor lattice QCD. *Phys. Rev. D 92*, 1 (2015), 014024.

[57] Barbieri, R., Buttazzo, D., Sala, F., and Straub, D. M. Flavour physics from an approximate $U(2)^3$ symmetry. *JHEP 07* (2012), 181.

[58] Barbieri, R., Isidori, G., Jones-Perez, J., Lodone, P., and Straub, D. M. $U(2)$ and Minimal Flavour Violation in Supersymmetry. *Eur. Phys. J. C 71* (2011), 1725.

[59] Barbieri, R., Isidori, G., Pattori, A., and Senia, F. Anomalies in B-decays and $U(2)$ flavour symmetry. *Eur. Phys. J. C 76*, 2 (2016), 67.

[60] Baron, R., et al. Light hadrons from lattice QCD with light (u,d), strange and charm dynamical quarks. *JHEP 06* (2010), 111.

[61] Baron, R., et al. Light hadrons from $N_f = 2+1+1$ dynamical twisted mass fermions. *PoS LATTICE2010* (2010), 123.

[62] Becher, T., Boos, H., and Lunghi, E. Kinetic corrections to $B \to X_c\ell\bar{\nu}$ at one loop. *JHEP 12* (2007), 062.

[63] Becirevic, D., Kosnik, N., Mescia, F., and Schneider, E. Complementarity of the constraints on New Physics from $B_s \to \mu^+\mu^-$ and from $B \to Kl^+l^-$ decays. *Phys. Rev. D 86* (2012), 034034.

[64] Bedaque, P. F. Aharonov-Bohm effect and nucleon nucleon phase shifts on the lattice. *Phys. Lett. B 593* (2004), 82–88.

[65] Bedaque, P. F., and Chen, J.-W. Twisted valence quarks and hadron interactions on the lattice. *Phys. Lett. B 616* (2005), 208–214.

[66] Beneke, M., Bobeth, C., and Szafron, R. Enhanced electromagnetic correction to the rare B-meson decay $B_{s,d} \to \mu^+\mu^-$. *Phys. Rev. Lett. 120*, 1 (2018), 011801.

[67] Beneke, M., Bobeth, C., and Szafron, R. Power-enhanced leading-logarithmic QED corrections to $B_q \to \mu^+\mu^-$. *JHEP 10* (2019), 232.

[68] Bernlochner, F., Fael, M., Olschewsky, K., Persson, E., van Tonder, R., Vos, K. K., and Welsch, M. First extraction of inclusive V_{cb} from q^2 moments. *JHEP 10* (2022), 068.

[69] Bharucha, A., Straub, D. M., and Zwicky, R. $B \to V\ell^+\ell^-$ in the Standard Model from light-cone sum rules. *JHEP 08* (2016), 098.

[70] Bhattacharya, B., Datta, A., London, D., and Shivashankara, S. Simultaneous Explanation of the R_K and $R(D^{(*)})$ Puzzles. *Phys. Lett. B 742* (2015), 370–374.

[71] Bhom, J., and Chrzaszcz, M. HEPLike: an open source framework for experimental likelihood evaluation. *Comput. Phys. Commun. 254* (2020), 107235.

[72] Bigi, D., Gambino, P., and Schacht, S. A fresh look at the determination of $|V_{cb}|$ from $B \to D^*\ell\nu$. *Phys. Lett. B 769* (2017), 441–445.

[73] Bigi, D., and Mächler, S. Finite W mass corrections to inclusive B decays.

[74] Bigi, I., Mannel, T., Turczyk, S., and Uraltsev, N. The Two Roads to 'Intrinsic Charm' in B Decays. *JHEP 04* (2010), 073.

[75] Bigi, I. I., Mannel, T., and Uraltsev, N. Semileptonic width ratios among beauty hadrons. *JHEP 09* (2011), 012.

[76] Bigi, I. I. Y., Shifman, M. A., Uraltsev, N., and Vainshtein, A. I. High power n of m(b) in beauty widths and n=5 —> infinity limit. *Phys. Rev. D 56* (1997), 4017–4030.

[77] Bigi, I. I. Y., Shifman, M. A., Uraltsev, N. G., and Vainshtein, A. I. QCD predictions for lepton spectra in inclusive heavy flavor decays. *Phys. Rev. Lett. 71* (1993), 496–499.

[78] Bigi, I. I. Y., Shifman, M. A., Uraltsev, N. G., and Vainshtein, A. I. Sum rules for heavy flavor transitions in the SV limit. *Phys. Rev. D 52* (1995), 196–235.

[79] Bigi, I. I. Y., Uraltsev, N. G., and Vainshtein, A. I. Nonperturbative corrections to inclusive beauty and charm decays: QCD versus phenomenological models. *Phys. Lett. B 293* (1992), 430–436. [Erratum: Phys.Lett.B 297, 477–477 (1992)].

[80] Biswas, S., and Melnikov, K. Second order QCD corrections to inclusive semileptonic $b \to X_c l \bar{\nu}_l$ decays with massless and massive lepton. *JHEP 02* (2010), 089.

[81] Blake, T., Egede, U., Owen, P., Petridis, K. A., and Pomery, G. An empirical model to determine the hadronic resonance contributions to $\overline{B}^0 \to \overline{K}^{*0}\mu^+\mu^-$ transitions. *Eur. Phys. J. C 78*, 6 (2018), 453.

[82] Blankenburg, G., Isidori, G., and Jones-Perez, J. Neutrino Masses and LFV from Minimal Breaking of $U(3)^5$ and $U(2)^5$ flavor Symmetries. *Eur. Phys. J. C 72* (2012), 2126.

[83] Blok, B., Koyrakh, L., Shifman, M. A., and Vainshtein, A. I. Differential distributions in semileptonic decays of the heavy flavors in QCD. *Phys. Rev. D 49* (1994), 3356. [Erratum: Phys.Rev.D 50, 3572 (1994)].

[84] Blossier, B., et al. A Proposal for B-physics on current lattices. *JHEP 04* (2010), 049.

[85] Bobeth, C., Buras, A. J., Kruger, F., and Urban, J. QCD corrections to $\bar{B} \to X_{d,s}\nu\bar{\nu}$, $\bar{B}_{d,s} \to \ell^+\ell^-$, $K \to \pi\nu\bar{\nu}$ and $K_L \to \mu^+\mu^-$ in the MSSM. *Nucl. Phys. B 630* (2002), 87–131.

[86] Bobeth, C., Chrzaszcz, M., van Dyk, D., and Virto, J. Long-distance effects in $B \to K^*\ell\ell$ from analyticity. *Eur. Phys. J. C 78*, 6 (2018), 451.

[87] Bobeth, C., Misiak, M., and Urban, J. Photonic penguins at two loops and m_t dependence of $BR[B \to X_s l^+ l^-]$. *Nucl. Phys. B574* (2000), 291–330.

[88] Bordone, M., Capdevila, B., and Gambino, P. Three loop calculations and inclusive Vcb. *Phys. Lett. B 822* (2021), 136679.

[89] Bordone, M., Cornella, C., Fuentes-Martin, J., and Isidori, G. A three-site gauge model for flavor hierarchies and flavor anomalies. *Phys. Lett. B 779* (2018), 317–323.

[90] Bordone, M., Cornella, C., Isidori, G., and König, M. The LFU ratio R_π in the Standard Model and beyond. *Eur. Phys. J. C 81*, 9 (2021), 850.

[91] Bordone, M., and Gambino, P. The semileptonic B_s and Λ_b widths. In *11th International Workshop on the CKM Unitarity Triangle* (3 2022).

[92] Bordone, M., Isidori, G., and Pattori, A. On the Standard Model predictions for R_K and R_{K^*}. *Eur. Phys. J. C 76*, 8 (2016), 440.

[93] Bouchard, C., Lepage, G. P., Monahan, C., Na, H., and Shigemitsu, J. $B_s \to K\ell\nu$ form factors from lattice QCD. *Phys. Rev. D 90* (2014), 054506.

[94] Buchalla, G., Buras, A. J., and Lautenbacher, M. E. Weak decays beyond leading logarithms. *Rev. Mod. Phys. 68* (1996), 1125–1144.

[95] Bulava, J., and Hansen, M. T. Scattering amplitudes from finite-volume spectral functions. *Phys. Rev. D 100*, 3 (2019), 034521.

[96] Bulava, J., Hansen, M. T., Hansen, M. W., Patella, A., and Tantalo, N. Inclusive rates from smeared spectral densities in the two-dimensional O(3) non-linear σ-model.

[97] Buras, A. J., and Munz, M. Effective Hamiltonian for B —¿ X(s) e+ e- beyond leading logarithms in the NDR and HV schemes. *Phys. Rev. D52* (1995), 186–195.

[98] Bussone, A., et al. Mass of the b quark and B-meson decay constants from $N_f = 2+1+1$ twisted-mass lattice QCD. *Phys. Rev. D 93*, 11 (2016), 114505.

[99] Buttazzo, D., Greljo, A., Isidori, G., and Marzocca, D. B-physics anomalies: a guide to combined explanations. *JHEP 11* (2017), 044.

[100] Cabibbo, N. Unitary Symmetry and Leptonic Decays. *Phys. Rev. Lett. 10* (1963), 531–533.

[101] Calibbi, L., Crivellin, A., and Ota, T. Effective Field Theory Approach to $b \to s\ell\ell^{(')}$, $B \to K^{(*)}\nu\overline{\nu}$ and $B \to D^{(*)}\tau\nu$ with Third Generation Couplings. *Phys. Rev. Lett. 115* (2015), 181801.

[102] Callan, Jr., C. G. Broken scale invariance in scalar field theory. *Phys. Rev. D 2* (1970), 1541–1547.

[103] Carrasco, N., et al. B-physics from $N_f = 2$ tmQCD: the Standard Model and beyond. *JHEP 03* (2014), 016.

[104] Carrasco, N., et al. Up, down, strange and charm quark masses with $N_f = 2+1+1$ twisted mass lattice QCD. *Nucl. Phys. B 887* (2014), 19–68.

[105] Chay, J., Georgi, H., and Grinstein, B. Lepton energy distributions in heavy meson decays from QCD. *Phys. Lett. B 247* (1990), 399–405.

[106] Ciuchini, M., Fedele, M., Franco, E., Paul, A., Silvestrini, L., and Valli, M. Lessons from the $B^{0,+} \to K^{*0,+}\mu^+\mu^-$ angular analyses.

[107] Colangelo, P., De Fazio, F., and Loparco, F. Inclusive semileptonic Λ_b decays in the Standard Model and beyond. *JHEP 11* (2020), 032.

[108] Colquhoun, B., Hashimoto, S., Kaneko, T., and Koponen, J. Form factors of $B \to \pi\ell\nu$ and a determination of $|V_{ub}|$ with Möbius domain-wall-fermions.

[109] Cornella, C., Fuentes-Martin, J., and Isidori, G. Revisiting the vector leptoquark explanation of the B-physics anomalies. *JHEP 07* (2019), 168.

[110] Cornella, C., Isidori, G., König, M., Liechti, S., Owen, P., and Serra, N. Hunting for $B^+ \to K^+\tau^+\tau^-$ imprints on the $B^+ \to K^+\mu^+\mu^-$ dimuon spectrum. *Eur. Phys. J. C 80*, 12 (2020), 1095.

[111] Crivellin, A., and Pokorski, S. Can the differences in the determinations of V_{ub} and V_{cb} be explained by New Physics? *Phys. Rev. Lett. 114*, 1 (2015), 011802.

[112] Csorna, S. E., et al. Moments of the B meson inclusive semileptonic decay rate using neutrino reconstruction. *Phys. Rev. D 70* (2004), 032002.

[113] Czarnecki, A., Melnikov, K., and Uraltsev, N. Non-Abelian dipole radiation and the heavy quark expansion. *Phys. Rev. Lett. 80* (1998), 3189–3192.

[114] Dassinger, B. M., Feger, R., and Mannel, T. Testing the left-handedness of the b —> c transition. *Phys. Rev. D 75* (2007), 095007.

[115] de Divitiis, G. M., Petronzio, R., and Tantalo, N. On the discretization of physical momenta in lattice QCD. *Phys. Lett. B 595* (2004), 408–413.

[116] Descotes-Genon, S., Khodjamirian, A., and Virto, J. Light-cone sum rules for $B \to K\pi$ form factors and applications to rare decays. *JHEP 12* (2019), 083.

[117] Descotes-Genon, S., Matias, J., Ramon, M., and Virto, J. Implications from clean observables for the binned analysis of $B- > K * \mu^+\mu^-$ at large recoil. *JHEP 01* (2013), 048.

[118] Di Luzio, L., Fuentes-Martin, J., Greljo, A., Nardecchia, M., and Renner, S. Maximal Flavour Violation: a Cabibbo mechanism for leptoquarks. *JHEP 11* (2018), 081.

[119] Dighe, A. S., Dunietz, I., and Fleischer, R. Extracting CKM phases and $B_s - \bar{B}_s$ mixing parameters from angular distributions of nonleptonic B decays. *Eur. Phys. J. C 6* (1999), 647–662.

[120] Dighe, A. S., Dunietz, I., Lipkin, H. J., and Rosner, J. L. Angular distributions and lifetime differences in $B_s \to J/\psi\phi$ decays. *Phys. Lett. B 369* (1996), 144–150.

[121] Dimopoulos, P., et al. Lattice QCD determination of m_b, f_B and f_{B_s} with twisted mass Wilson fermions. *JHEP 01* (2012), 046.

[122] Dimopoulos, P., Frezzotti, R., Michael, C., Rossi, G. C., and Urbach, C. $O(a^2)$ cutoff effects in lattice Wilson fermion simulations. *Phys. Rev. D 81* (2010), 034509.

[123] Fael, M., Mannel, T., and Keri Vos, K. V_{cb} determination from inclusive $b \to c$ decays: an alternative method. *JHEP 02* (2019), 177.

[124] Fael, M., Schönwald, K., and Steinhauser, M. Kinetic Heavy Quark Mass to Three Loops. *Phys. Rev. Lett. 125*, 5 (2020), 052003.

[125] Fael, M., Schönwald, K., and Steinhauser, M. Relation between the $\overline{\text{MS}}$ and the kinetic mass of heavy quarks. *Phys. Rev. D 103*, 1 (2021), 014005.

[126] Fael, M., Schönwald, K., and Steinhauser, M. Third order corrections to the semileptonic b→c and the muon decays. *Phys. Rev. D 104*, 1 (2021), 016003.

[127] Fael, M., Schönwald, K., and Steinhauser, M. A first glance to the kinematic moments of B $\to$ X$_c\ell\nu$ at third order. *JHEP 08* (2022), 039.

[128] Falk, A. F. Hadrons of arbitrary spin in the heavy quark effective theory. *Nucl. Phys. B 378* (1992), 79–94.

[129] Falk, A. F. The Heavy quark expansion of QCD. In *24th Annual SLAC Summer Institute on Particle Physics: The Strong Interaction, From Hadrons to Protons* (10 1996), pp. 43–66.

[130] Falk, A. F., and Luke, M. E. Hadronic spectral moments in semileptonic b decays with a lepton energy cut. *Phys. Rev. D 57* (1998), 424–430.

[131] Foster, M., and Michael, C. Quark mass dependence of hadron masses from lattice QCD. *Phys. Rev. D 59* (1999), 074503.

[132] Frezzotti, R., Grassi, P. A., Sint, S., and Weisz, P. Lattice QCD with a chirally twisted mass term. *JHEP 08* (2001), 058.

[133] Frezzotti, R., Martinelli, G., Papinutto, M., and Rossi, G. C. Reducing cutoff effects in maximally twisted lattice QCD close to the chiral limit. *JHEP 04* (2006), 038.

[134] Frezzotti, R., and Rossi, G. C. Chirally improving Wilson fermions. 1. $O(a)$ improvement. *JHEP 08* (2004), 007.

[135] Frezzotti, R., and Rossi, G. C. Chirally improving Wilson fermions. II. Four-quark operators. *JHEP 10* (2004), 070.

[136] Frezzotti, R., and Rossi, G. C. Twisted mass lattice QCD with mass nondegenerate quarks. *Nucl. Phys. B Proc. Suppl. 128* (2004), 193–202.

[137] Fuentes-Martín, J., Isidori, G., König, M., and Selimović, N. Vector Leptoquarks Beyond Tree Level. *Phys. Rev. D 101*, 3 (2020), 035024.

[138] Fuentes-Martin, J., Isidori, G., Pagès, J., and Stefanek, B. A. Flavor Non-universal Pati-Salam Unification and Neutrino Masses.

[139] Fuentes-Martín, J., Isidori, G., Pagès, J., and Yamamoto, K. With or without U(2)? Probing non-standard flavor and helicity structures in semileptonic B decays. *Phys. Lett. B 800* (2020), 135080.

[140] Gambino, P. B semileptonic moments at NNLO. *JHEP 09* (2011), 055.

[141] Gambino, P., et al. Challenges in semileptonic B decays. *Eur. Phys. J. C 80*, 10 (2020), 966.

[142] Gambino, P., and Giordano, P. Normalizing inclusive rare B decays. *Phys. Lett. B 669* (2008), 69–73.

[143] Gambino, P., and Hashimoto, S. Inclusive Semileptonic Decays from Lattice QCD. *Phys. Rev. Lett. 125*, 3 (2020), 032001.

[144] Gambino, P., Hashimoto, S., Mächler, S., Panero, M., Sanfilippo, F., Simula, S., Smecca, A., and Tantalo, N. Lattice QCD study of inclusive semileptonic decays of heavy mesons. *JHEP 07* (2022), 083.

[145] Gambino, P., Healey, K. J., and Turczyk, S. Taming the higher power corrections in semileptonic B decays. *Phys. Lett. B 763* (2016), 60–65.

[146] Gambino, P., Jung, M., and Schacht, S. The V_{cb} puzzle: An update. *Phys. Lett. B 795* (2019), 386–390.

[147] Gambino, P., Lubicz, V., Melis, A., and Simula, S. Masses, decay constants and HQE matrix elements of pseudoscalar and vector heavy-light mesons in LQCD. *J. Phys. Conf. Ser. 1137*, 1 (2019), 012005.

[148] Gambino, P., Melis, A., and Simula, S. Extraction of heavy-quark-expansion parameters from unquenched lattice data on pseudoscalar and vector heavy-light meson masses. *Phys. Rev. D 96*, 1 (2017), 014511.

[149] Gambino, P., and Uraltsev, N. Moments of semileptonic B decay distributions in the $1/m_b$ expansion. *Eur. Phys. J. C 34* (2004), 181–189.

[150] Glashow, S. L. Partial Symmetries of Weak Interactions. *Nucl. Phys. 22* (1961), 579–588.

[151] Gorbahn, M., and Haisch, U. Effective Hamiltonian for non-leptonic $|\Delta F| = 1$ decays at NNLO in QCD. *Nucl. Phys. B 713* (2005), 291–332.

[152] Gratrex, J., Hopfer, M., and Zwicky, R. Generalised helicity formalism, higher moments and the $B \to K_{J_K}(\to K\pi)\bar{\ell}_1\ell_2$ angular distributions. *Phys. Rev. D 93*, 5 (2016), 054008.

[153] Graverini, E. Flavour anomalies: a review. *J. Phys. Conf. Ser. 1137*, 1 (2019), 012025.

[154] Greljo, A., Isidori, G., and Marzocca, D. On the breaking of Lepton Flavor Universality in B decays. *JHEP 07* (2015), 142.

[155] Greljo, A., and Stefanek, B. A. Third family quark–lepton unification at the TeV scale. *Phys. Lett. B 782* (2018), 131–138.

[156] Gremm, M., and Kapustin, A. Order 1/m(b)**3 corrections to B –> X(c) lepton anti-neutrino decay and their implication for the measurement of Lambda-bar and lambda(1). *Phys. Rev. D 55* (1997), 6924–6932.

[157] Guadagnoli, D., Mescia, F., and Simula, S. Lattice study of semileptonic form-factors with twisted boundary conditions. *Phys. Rev. D 73* (2006), 114504.

[158] Gubernari, N., Kokulu, A., and van Dyk, D. $B \to P$ and $B \to V$ Form Factors from B-Meson Light-Cone Sum Rules beyond Leading Twist. *JHEP 01* (2019), 150.

[159] Gubernari, N., Reboud, M., van Dyk, D., and Virto, J. Improved theory predictions and global analysis of exclusive $b \to s\mu^+\mu^-$ processes. *JHEP 09* (2022), 133.

[160] Gusken, S. A Study of smearing techniques for hadron correlation functions. *Nucl. Phys. B Proc. Suppl. 17* (1990), 361–364.

[161] Hambrock, C., Khodjamirian, A., and Rusov, A. Hadronic effects and observables in $B \to \pi\ell^+\ell^-$ decay at large recoil. *Phys. Rev. D 92*, 7 (2015), 074020.

[162] Hansen, M., Lupo, A., and Tantalo, N. Extraction of spectral densities from lattice correlators. *Phys. Rev. D 99*, 9 (2019), 094508.

[163] Hansen, M. T., Meyer, H. B., and Robaina, D. From deep inelastic scattering to heavy-flavor semileptonic decays: Total rates into multihadron final states from lattice QCD. *Phys. Rev. D 96*, 9 (2017), 094513.

[164] Hashimoto, S. Inclusive semi-leptonic B meson decay structure functions from lattice QCD. *PTEP 2017*, 5 (2017), 053B03.

[165] Heinonen, J., and Mannel, T. Improved Estimates for the Parameters of the Heavy Quark Expansion. *Nucl. Phys. B 889* (2014), 46–63.

[166] Herren, F., and Steinhauser, M. Version 3 of RunDec and CRunDec. *Comput. Phys. Commun. 224* (2018), 333–345.

[167] Hiller, G., and Kruger, F. More model-independent analysis of $b \to s$ processes. *Phys. Rev. D 69* (2004), 074020.

[168] Hiller, G., and Schmaltz, M. R_K and future $b \to s\ell\ell$ physics beyond the standard model opportunities. *Phys. Rev. D 90* (2014), 054014.

[169] Hirose, S., et al. Measurement of the τ lepton polarization and $R(D^*)$ in the decay $\bar{B} \to D^*\tau^-\bar{\nu}_\tau$. *Phys. Rev. Lett. 118*, 21 (2017), 211801.

[170] Horgan, R. R., Liu, Z., Meinel, S., and Wingate, M. Lattice QCD calculation of form factors describing the rare decays $B \to K^*\ell^+\ell^-$ and $B_s \to \phi\ell^+\ell^-$. *Phys. Rev. D89*, 9 (2014), 094501.

[171] Horgan, R. R., Liu, Z., Meinel, S., and Wingate, M. Rare B decays using lattice QCD form factors. *PoS LATTICE2014* (2015), 372.

[172] Hou, G. W.-S. Perspectives and Outlook from HEP Window on the Universe. *Int. J. Mod. Phys. A 34*, 02 (2019), 1930002.

[173] Hou, W.-S., Kohda, M., and Xu, F. Rates and asymmetries of B$\to\pi\ell^+\ell^-$ decays. *Phys. Rev. D 90*, 1 (2014), 013002.

[174] Isgur, N., and Wise, M. B. WEAK TRANSITION FORM-FACTORS BETWEEN HEAVY MESONS. *Phys. Lett. B 237* (1990), 527–530.

[175] Isidori, G., Nabeebaccus, S., and Zwicky, R. QED corrections in $\overline{B} \to \overline{K}\ell^+\ell^-$ at the double-differential level. *JHEP 12* (2020), 104.

[176] Isidori, G., Wilsch, F., and Wyler, D. The Standard Model effective field theory at work.

[177] Iwasaki, Y. Renormalization Group Analysis of Lattice Theories and Improved Lattice Action: Two-Dimensional Nonlinear $O(N)$ Sigma Model. *Nucl. Phys. B 258* (1985), 141–156.

[178] Kadanoff, L. P. Operator Algebra and the Determination of Critical Indices. *Phys. Rev. Lett. 23* (1969), 1430–1433.

[179] Khodjamirian, A., Mannel, T., and Wang, Y. $B \to K\ell^+\ell^-$ decay at large hadronic recoil. *JHEP 02* (2013), 010.

[180] Khodjamirian, A., and Rusov, A. V. $B_s \to K\ell\nu_\ell$ and $B_{(s)} \to \pi(K)\ell^+\ell^-$ decays at large recoil and CKM matrix elements. *JHEP 08* (2017), 112.

[181] Kobayashi, M., and Maskawa, T. CP Violation in the Renormalizable Theory of Weak Interaction. *Prog. Theor. Phys. 49* (1973), 652–657.

[182] Koenig, M., and Neubert, M. Exclusive Radiative Higgs Decays as Probes of Light-Quark Yukawa Couplings. *JHEP 08* (2015), 012.

[183] Kruger, F., and Matias, J. Probing new physics via the transverse amplitudes of $B^0 \to K^{*0}(\to K^-\pi^+)l^+l^-$ at large recoil. *Phys. Rev. D 71* (2005), 094009.

[184] Kruger, F., and Sehgal, L. Lepton polarization in the decays b —> X(s) mu+ mu- and B —> X(s) tau+ tau-. *Phys. Lett. B 380* (1996), 199–204.

[185] Kruger, F., and Sehgal, L. M. CP violation in the decay B —¿ X(d) e+ e-. *Phys. Rev. D55* (1997), 2799–2805.

[186] Langenbruch, C. Lepton Flavour Universality tests in B decays as a probe for New Physics. In *53rd Rencontres de Moriond on Electroweak Interactions and Unified Theories* (2018), pp. 53–58.

[187] Lees, J., et al. Measurement of an Excess of $\bar{B} \to D^{(*)}\tau^-\bar{\nu}_\tau$ Decays and Implications for Charged Higgs Bosons. *Phys. Rev. D 88*, 7 (2013), 072012.

[188] Leibovich, A. K., Ligeti, Z., Stewart, I. W., and Wise, M. B. Semileptonic B decays to excited charmed mesons. *Phys. Rev. D 57* (1998), 308–330.

[189] Luke, M. E. Effects of subleading operators in the heavy quark effective theory. *Phys. Lett. B 252* (1990), 447–455.

[190] Lyon, J., and Zwicky, R. Resonances gone topsy turvy - the charm of QCD or new physics in $b \to s\ell^+\ell^-$?

[191] Mannel, T. Operator product expansion for inclusive semileptonic decays in heavy quark effective field theory. *Nucl. Phys. B 413* (1994), 396–412.

[192] Mannel, T., Moreno, D., and Pivovarov, A. A. NLO QCD corrections to inclusive $b \to c\ell\bar{\nu}$decay spectra up to $1/m_Q^3$. *Phys. Rev. D 105*, 5 (2022), 054033.

[193] Mannel, T., and Pivovarov, A. A. QCD corrections to inclusive heavy hadron weak decays at $\Lambda_{\rm QCD}^3/m_Q^3$. *Phys. Rev. D 100*, 9 (2019), 093001.

[194] Mannel, T., Pivovarov, A. A., and Rosenthal, D. Inclusive semileptonic B decays from QCD with NLO accuracy for power suppressed terms. *Phys. Lett. B 741* (2015), 290–294.

[195] Mannel, T., Pivovarov, A. A., and Rosenthal, D. Inclusive weak decays of heavy hadrons with power suppressed terms at NLO. *Phys. Rev. D 92*, 5 (2015), 054025.

[196] Mannel, T., Turczyk, S., and Uraltsev, N. Higher Order Power Corrections in Inclusive B Decays. *JHEP 11* (2010), 109.

[197] Manohar, A. V., and Wise, M. B. Inclusive semileptonic B and polarized Lambda(b) decays from QCD. *Phys. Rev. D 49* (1994), 1310–1329.

[198] Manohar, A. V., and Wise, M. B. *Heavy quark physics*, vol. 10. 2000.

[199] Marquard, P., Smirnov, A. V., Smirnov, V. A., Steinhauser, M., and Wellmann, D. $\overline{\text{MS}}$-on-shell quark mass relation up to four loops in QCD and a general SU(N) gauge group. *Phys. Rev. D 94*, 7 (2016), 074025.

[200] McNeile, C., and Michael, C. Decay width of light quark hybrid meson from the lattice. *Phys. Rev. D 73* (2006), 074506.

[201] Melnikov, K. $O(\alpha_s^2)$ corrections to semileptonic decay $b \to cl\bar{\nu}_l$. *Phys. Lett. B 666* (2008), 336–339.

[202] Nakayama, K., Fahy, B., and Hashimoto, S. Determination of charm quark mass from temporal moments of charmonium correlator with Möbius domain-wall fermion. *PoS LATTICE2016* (2017), 192.

[203] Neubert, M. Heavy quark symmetry. *Phys. Rept. 245* (1994), 259–396.

[204] Osterwalder, K., and Seiler, E. Gauge Field Theories on the Lattice. *Annals Phys. 110* (1978), 440.

[205] Pak, A., and Czarnecki, A. Heavy-to-heavy quark decays at NNLO. *Phys. Rev. D 78* (2008), 114015.

[206] Pak, A., and Czarnecki, A. Mass effects in muon and semileptonic $b \to c$ decays. *Phys. Rev. Lett. 100* (2008), 241807.

[207] Parrott, W. G., Bouchard, C., and Davies, C. T. H. B→K and D→K form factors from fully relativistic lattice QCD. *Phys. Rev. D 107*, 1 (2023), 014510.

[208] Parrott, W. G., Bouchard, C., and Davies, C. T. H. Standard Model predictions for B→Kℓ+ℓ-, B→Kℓ1-ℓ2+ and B→K$\nu\nu^-$ using form factors from Nf=2+1+1 lattice QCD. *Phys. Rev. D 107*, 1 (2023), 014511. [Erratum: Phys.Rev.D 107, 119903 (2023)].

[209] Peskin, M. E., and Schroeder, D. V. *An Introduction to quantum field theory*. Addison-Wesley, Reading, USA, 1995.

[210] Pokorski, S. *GAUGE FIELD THEORIES*. Cambridge University Press, 1 2005.

[211] Rubbia, A. *Phenomenology of Particle Physics*. Cambridge University Press, Cambridge, UK, 6 2022.

[212] Sachrajda, C. T., and Villadoro, G. Twisted boundary conditions in lattice simulations. *Phys. Lett. B 609* (2005), 73–85.

[213] Salam, A. Weak and Electromagnetic Interactions. *Conf. Proc. C 680519* (1968), 367–377.

[214] Schwanda, C., et al. Moments of the Hadronic Invariant Mass Spectrum in $B \to X_c\ell\nu$ Decays at BELLE. *Phys. Rev. D 75* (2007), 032005.

[215] Shifman, M. A., and Voloshin, M. B. Preasymptotic Effects in Inclusive Weak Decays of Charmed Particles. *Sov. J. Nucl. Phys. 41* (1985), 120.

[216] Symanzik, K. Small distance behavior in field theory and power counting. *Commun. Math. Phys. 18* (1970), 227–246.

[217] Urquijo, P., et al. Moments of the electron energy spectrum and partial branching fraction of B —> X(c) e nu decays at Belle. *Phys. Rev. D 75* (2007), 032001.

[218] van Tonder, R., et al. Measurements of q^2 Moments of Inclusive $B \to X_c \ell^+ \nu_\ell$ Decays with Hadronic Tagging. *Phys. Rev. D 104*, 11 (2021), 112011.

[219] Wei, J.-T., et al. Measurement of the Differential Branching Fraction and Forward-Backword Asymmetry for $B \to K^{(*)} \ell^+ \ell^-$. *Phys. Rev. Lett. 103* (2009), 171801.

[220] Weinberg, S. A Model of Leptons. *Phys. Rev. Lett. 19* (1967), 1264–1266.

[221] Wilson, K. G. Nonlagrangian models of current algebra. *Phys. Rev. 179* (1969), 1499–1512.

[222] Wilson, K. G. Confinement of Quarks. *Phys. Rev. D 10* (1974), 2445–2459.

[223] Wilson, K. G., and Kogut, J. B. The Renormalization group and the epsilon expansion. *Phys. Rept. 12* (1974), 75–199.

[224] Wolfenstein, L. Parametrization of the Kobayashi-Maskawa Matrix. *Phys. Rev. Lett. 51* (1983), 1945.

[225] Workman, R. L., et al. Review of Particle Physics. *PTEP 2022* (2022), 083C01.

[226] Zimmermann, W. Normal products and the short distance expansion in the perturbation theory of renormalizable interactions. *Annals Phys. 77* (1973), 570–601.

[227] Zyla, P., et al. Review of Particle Physics. *PTEP 2020*, 8 (2020), 083C01.

[228] Zyla, P. A., et al. Review of Particle Physics. *PTEP 2020*, 8 (2020), 083C01.